

The influence of mucin glycans on microbial virulence and competition

By

Kelsey M. Wheeler

B.A. Biological Science / B.S. Geophysical Science

The University of Chicago, 2014

Submitted to the Microbiology Graduate Program in partial fulfillment of the requirements for the Degree of Philosophy at the Massachusetts Institute of Technology

February 2021

© 2021 Massachusetts Institute of Technology. All Rights Reserved.

The author hereby grants to MIT permission to reproduce and to distribute publicly paper and electronic copies of this thesis document in whole or in part in any medium now known or hereafter created.

Author

Kelsey M. Wheeler
Microbiology Graduate Program
November 9, 2020

Certified By.

Katharina Ribbeck
Associate Professor of Biological Engineering
Thesis Supervisor

Accepted By.

Jacquin C. Niles
Professor of Biological Engineering
Chair of Microbiology Program

The influence of mucin glycans on microbial virulence and competition

By

Kelsey M. Wheeler

Submitted to the Microbiology Graduate Program in partial fulfillment of the requirements for the degree of Doctor of Philosophy at the Massachusetts Institute of Technology

Abstract

The human body is colonized by trillions of microbes, many of which reside in a layer of mucus that covers all wet epithelia in the body. In this way, mucus serves as the first line of defense to the host, simultaneously protecting against pathogens while providing a habitat where commensal microbes thrive. It has long been known that defects in mucus production or biochemistry are associated with opportunistic infections; however, few studies have focused on how components of the intact mucus barrier interact with resident microbes to promote health. In this thesis, I fill this gap using a clinically relevant 3-dimensional model of the mucus environment based on mucin glycoproteins, the major structural component of mucus. This *in vitro* culturing system mimics the natural mucus environment, where mucin polymer domains interact and entangle into a flexible hydrogel, as opposed to 2-dimensional surface coatings, which can create artificially concentrated amounts of surface mucins. I apply this system to answer three major conceptual questions, separated into three projects. In the first project, I study the ability of mucin and their attached glycans to regulate interactions between a clinically-important opportunistic pathogen, *Pseudomonas aeruginosa*, and its host. I then investigate the underlying genetic mechanisms that enable *P. aeruginosa* to sense and respond to the mucus environment, and explore how mucin glycan-sensing in turn impacts microbe-microbe interactions in the mucosal niche. I end by investigating how mucin glycan-mediated microbial regulation modulates the composition of complex microbial communities isolated from the human oral cavity. Collectively, the work presented in this thesis lays the framework for characterizing the therapeutic nature of mucin and how specific mucin glycan moieties modulate the behavior, pathogenicity, and competitive interactions of host-associated microbes.

Thesis Supervisor: Katharina Ribbeck

Title: Hyman Career Development Professor of Biological Engineering

Acknowledgements

First and foremost, I would like to thank my thesis advisor Prof. Katharina Ribbeck. She has been the best mentor I could ever imagine. Striking the perfect balance of supportive and critical, Katharina has pushed me to the edge of my comfort zone and in doing so has helped me become a more creative, confident, and independent scientist. Her infectious love of the scientific process and mucus biology has inspired me to ask questions that I find exciting, regardless of how intractable they may seem.

I would also like to thank my committee members, Profs. Otto Cordero, Becky Lamason, and Dennis Kim for their guidance, support, and time over the past five years. To my external committee member, Prof. Daniel Wozniak, thank you for sharing your expertise.

To the Ribbeckers, thank you for your support, collaboration, and friendship. In particular, I have to thank Benjamin Wang who has been an amazing lab mate and friend. It has been such a blessing to go through each step of graduate school with you. Even though we'll be doing our postdocs on opposite sides of the country, I hope this is just the beginning of our collaborations. To Gerardo Cárcamo-Oyarce, it has been such a wonderful experience working so closely with you. You have been a great mentor to me and have taught me a lot, especially in the early days when I was first learning to develop an independent project. Thank you, Bradley Turner and Chloe Wu, I have thoroughly enjoyed working with both of you. Thank you to Julia Co and Erica Shapiro Frenkel, who did foundational work for the studies in this thesis, and to Christine Slocombe for always going above and beyond to keep the Ribbeck lab running so smoothly. And to my lab mates, past and present, Jade Bath, Wesley Chen, Kate DuPont, Michaela Gold, Jeff Hsiao, Miri Kupkrin, Tahoura Samad, Caroline Wagner, Aggi Walsh, Caroline Werlang, and Jacob Witten, thank you for creating a wonderful lab environment that I look forward to going to every day.

To my fellow Micros, thank you for your support and friendship over the past five years. Thank you to Jacquie Carota and Bonnielee Whang for keeping the program running.

I am also grateful to my undergraduate mentor Prof. Rima McLeod at the University of Chicago, who taught me to be a scientist. It was Prof. McLeod's support and encouragement that convinced me to apply to graduate school.

I am thankful for the love I've received from family and friends. Mom, Dad, Mallory, and Ryan, thank you for your continued support throughout my life. To my new Boston family, Ryan, Cassie, and Abzug Witthaus, I am so happy that you decided to move across the country. Life is a lot more fun with you around. I am also grateful to Suryalekha Rajan for her support, friendship, coffee dates, and willingness to sit through countless practice talks over the years, from my qualifying exam to my defense.

And, of course, I am immensely grateful to my husband Miles. Thank you for your love, encouragement, and support over the last ten years. I am so lucky to have found a partner who can challenge me to be a better scientist and person.

Table of Contents

ABSTRACT	2
ACKNOWLEDGEMENTS.....	3
CHAPTER 1: INTRODUCTION	6
STRUCTURE AND BIOCHEMISTRY OF THE MUCUS LAYER.....	6
MUCUS-MICROBE INTERACTIONS IN HEALTH AND DISEASE.....	7
MECHANISMS OF MUCIN-MICROBE INTERACTIONS.....	10
REFERENCES.....	14
ACKNOWLEDGEMENTS	18
FIGURES.....	19
CHAPTER 2: MUCIN GLYCANS ATTENUATE THE VIRULENCE OF <i>PSEUDOMONAS AERUGINOSA</i> IN INFECTION.....	23
ABSTRACT	23
INTRODUCTION	24
RESULTS.....	24
DISCUSSION.....	29
MATERIALS AND METHODS.....	31
REFERENCES.....	40
ACKNOWLEDGEMENTS	42
FIGURES.....	44
CHAPTER 3: MUCIN GLYCANS SIGNAL THROUGH THE SENSOR KINASE RETS TO INHIBIT VIRULENCE-ASSOCIATED TRAITS IN <i>PSEUDOMONAS AERUGINOSA</i>.....	51
ABSTRACT	51
INTRODUCTION	51
RESULTS.....	53
DISCUSSION.....	61
MATERIALS AND METHODS.....	65
REFERENCES.....	76
ACKNOWLEDGEMENTS	80
FIGURES.....	81
CHAPTER 4: MUCIN GLYCANS RESIST DYSBIOSIS IN COMPLEX MICROBIAL COMMUNITIES	89
ABSTRACT	89
INTRODUCTION	89
RESULTS.....	91
DISCUSSION.....	101
MATERIALS AND METHODS.....	104
REFERENCES.....	108
ACKNOWLEDGEMENTS	111
FIGURES.....	112
CHAPTER 5: CONCLUSIONS.....	121
LIMITATIONS AND EXTENSIONS	121
TRACTABLE MUCIN-BASED MODELS OF THE HOST ENVIRONMENT FOR <i>EX VIVO</i> BACTERIAL STUDIES.....	125
MUCIN GLYCANS AS THERAPEUTIC MOLECULES	125
REFERENCES.....	127
APPENDIX A: SUPPLEMENTARY INFORMATION FOR CHAPTER 2.....	129
SUPPLEMENTARY FIGURES.....	130
SUPPLEMENTARY TABLES	144

SUPPLEMENTARY REFERENCES.....	157
APPENDIX B: SUPPLEMENTARY INFORMATION FOR CHAPTER 3.....	158
SUPPLEMENTARY FIGURES.....	159
SUPPLEMENTARY TABLES.....	167
SUPPLEMENTARY REFERENCES.....	178
APPENDIX C: SUPPLEMENTARY INFORMATION FOR CHAPTER 4.....	179
SUPPLEMENTARY INFORMATION.....	180
SUPPLEMENTARY FIGURES.....	181
SUPPLEMENTARY REFERENCES.....	185

Chapter 1: Introduction

Text from this chapter has been adapted from: Wagner CE*, Wheeler KM*, Ribbeck K. Mucins and Their Role in Shaping the Functions of Mucus Barriers. *Annu Rev Cell Dev Biol.* 34.1 (2018):189-215.

doi: 10.1146/annurev-cellbio-100617-062818.

Structure and biochemistry of the mucus layer

Mucus is a biological hydrogel that coats every wet epithelial surface of the body including the eyes, lungs, and stomach (Figure 1.1; adapted from Frenkel & Ribbeck (2015a)). Mucus serves as a lubricant to protect host tissues against shear-induced damage from mechanical forces associated with processes such as digestion and blinking (Argüeso & Gipson 2001; Nordgård & Draget 2015; Sellers et al. 1988), and also acts as a selective physicochemical barrier by excluding foreign or harmful molecules while permitting the passage of desirable agents such as nutrients (Bansil & Turner 2006; Linden et al. 2008).

The primary structural components of mucus are mucin glycoproteins (Figure 1.2). To date 21 mucin-type glycoproteins, belonging to the MUC gene family, have been identified in the human body and are recognized by the Human Genome Organization (HUGO) gene nomenclature committee (<http://www.genenames.org>). The protein backbone of the mucin molecule is composed of a variable number of tandem repeats (VNTR) rich in proline, threonine, and/or serine (PTS domains), as well as cysteine-rich regions at the amino terminal, carboxy terminal, and interspersed between the PTS domains (Bansil & Turner 2006; Dekker et al. 2002). These PTS domains are modified with dense O-linked glycosylation and structurally resemble bottle brushes, with branched oligosaccharide chains (i.e., glycans) arranged radially from the protein core (Bansil & Turner 2006). Approximately 80% of the mass of these molecules is derived from carbohydrates, with the protein backbone making up the remaining 20% (Bansil & Turner 2006). Attempts to catalogue the diversity of mucin glycans have identified hundreds of distinct structures, representing a wealth of biochemical information in a minimum of space. Mucin-attached glycans provide the immense water-holding capacity and offer myriad interactions sites for particles, immune cells and molecules, and microbes.

Within the mucin family, there are two distinct sub-groups: 1) secreted mucins and 2) tethered, cell surfaced associated mucins. Within the secreted mucins, there exist five oligomeric, gel-

forming mucins (MUC2, MUC5AC, MUC5B, MUC6, and MUC19) (Thornton et al. 2008), as well as two non-polymeric glycoproteins (MUC7 and MUC8) (Thornton et al. 2008). The gel-forming mucins (Figure 1.2a) reside outside the epithelial cell layer (Hatrup & Gendler 2008), and the individual mucin subunits polymerize via end-to-end disulfide bonds to form even larger macromonomer chains which are arranged in a linear fashion (Kesimer et al. 2010; Taylor et al. 2005), although some studies have suggested the possibility of branched, trimer structures for specific mucins (Ambort et al. 2012; Godl et al. 2002; Nilsson et al. 2014). By contrast, the 11 tethered mucins (MUC1, MUC3A, MUC3B, MUC4, MUC12, MUC13, MUC15, MUC16, MUC17, MUC20, MUC21) have short cytoplasmic domains that reside inside of the cell, as well as extensive extracellular domains (Hatrup & Gendler 2008) (Figure 1.2b). The three remaining mucins are oviductal glycoprotein 1 (OVGP1, previously known as MUC9), endomucin (EMCN, also known as MUC14), and MUC22. Mucins are generated in and secreted from specialized cells in the surface epithelium known as goblet cells and mucous cells in submucosal glands (Hatrup & Gendler 2008; Thornton et al. 2008).

In this thesis, I focus on the secreted gel-forming mucins that form the mucosal niche encasing and interacting most directly with microbial cells. In aqueous solution, these high molecular weight mucin molecules form a network mediated by a complex series of reversible physical bonds including hydrophobic interactions and chain entanglements, and stabilized by electrostatic repulsion between the negatively charged oligosaccharide side chains (Schipper et al. 2007). Mucin molecule configuration and network interaction strength are sensitive to variations in pH as well as concentration of ions and small molecules across the organ systems (Figure 1.1) (Wagner et al. 2017). Consequently, mucus layers possess different mechanical and biochemical properties depending on their location and intended physiological function. For instance, the eyes have a thin, watery mucin solution on the surface for hydration and lubrication (Argüeso & Gipson 2001). By contrast, the stationary mucus lining the stomach is a stiffer mucin gel that protects the epithelial lining against acidic gastric juices (pH \approx 1-2) (Celli et al. 2007). Altered mechanical and biochemical properties of mucus can also indicate disease or pathological manipulation, such as the increased bacterial load and thick mucus associated with cystic fibrosis (Lai et al. 2009).

Mucus-microbe interactions in health and disease

The mucus barrier is one of the first lines of defense to the wet epithelial linings across the human

body. The secreted mucus layers accommodate trillions of microbes within the human microbiota, while simultaneously preventing mechanical and chemical damage from the external environment and protecting against infection by potentially harmful microbes. As such, alterations to the mucosal layer can result in serious pathologies and susceptibility to opportunistic infection. For example, the diseased mucus in the cystic fibrosis lung does not provide the same protection against microbes such as *Pseudomonas aeruginosa* (Singh et al. 2000).

A growing body of evidence suggests that healthy intact mucins are, at least in part, responsible for the ability of mucus to prevent virulence of opportunistic microbes. Mucin expression is often differentially regulated in response to infection. For example, middle ear epithelia overexpress the genes encoding the gel-forming mucins MUC2, MUC5AC, and MUC5B in response to three bacteria associated with otitis media, *Streptococcus pneumoniae*, *Haemophilus influenzae*, and *Moraxella catarrhalis* (Kerschner et al. 2014). Similarly, infection of the lung is generally associated with mucin overproduction. Specifically, the expression of MUC2 and MUC5AC is induced in cells exposed to wide variety of Gram-negative and Gram-positive bacteria including *P. aeruginosa* and *Staphylococcus aureus* (Dohrman et al. 1998; Li et al. 1997; McNamara et al. 2001), suggesting that mucin secretion may be a host defense response to infection.

Mucins have also been demonstrated to be directly involved in preventing pathogenicity in the respiratory tract and gastric niche. The lower airways of the healthy lung have traditionally been viewed as effectively sterile, owing to the efficiency of the mucus barrier at trapping and removing particulates and pathogens by mucociliary clearance. The structurally related mucin glycoproteins MUC5AC and MUC5B are the principal gel-forming macromolecules in airway mucus (Thornton et al. 2008) and play an important role in controlling the pathogenicity of opportunistic microbes. MUC5B is required for mucociliary clearance, controlling respiratory infections, and maintaining immune homeostasis in mice (Roy et al. 2014). Muc5b knockout mice had an accumulation of and chronic infection by multiple bacterial species that are normally absent in MUC5B-rich mucus, including the pneumonia-causing pathogen *S. aureus*. In the epithelial lining of the stomach, secreted MUC5AC and surface-attached MUC1 similarly protect against microbes like *Helicobacter pylori*, which can bind to these mucins via fucosylated and sialylated glycans (Mahdavi et al. 2002). In the rhesus monkey, mucins that efficiently bind *H. pylori* can aid in the removal of bacteria from the gastric niche (Lindén et al. 2008). MUC1 limits the density of *H. pylori* in mice and also limits adhesion to the cell surface in humans (Lindén et al. 2009). MUC1

can also protect the epithelium by acting as a physical barrier to other non-MUC1 binding bacteria (Lindén et al. 2009), further illustrating the capability of this polymer to protect the host from a broad range of bacteria.

In vitro studies using purified mucins have begun to elucidate the specific role of mucins in directly suppressing microbial virulence. The key innovation of the following selected *in vitro* experiments is the native purification of mucins and their presentation as a three dimensional network, which allows for the study of both direct mucin-microbe interactions and the consequences of the physicochemical properties of the surrounding matrix on the inhabiting cells. For example, the purified mucin MUC5B isolated from human saliva has been shown to protect surfaces from biofilm formation by the pathogen *Streptococcus mutans* (Frenkel & Ribbeck 2015b), which is one of the causative agents of the disease dental caries. While MUC5AC was not found to be essential for mucociliary clearance (Roy et al. 2014), *in vitro* studies with natively purified mucins have implicated this polymer in suppressing *P. aeruginosa* biofilm formation by promoting a more disperse planktonic lifestyle (Caldara et al. 2012). Since bacterial growth was not inhibited in either of these studies, mucin-mediated defense against microbes likely results from modulation of pathogen behavior rather than direct antimicrobial interactions.

Notably, the protective capacity of mucins extends beyond bacterial pathogens. *Candida albicans* is an important opportunistic fungal pathogen that is typically part of the healthy microbiota, but can cause infections like oral thrush and vaginitis. *C. albicans* pathogenicity is associated with virulence traits including surface adhesion, biofilm formation, filamentation, and the production of secreted proteases. The secreted gel-forming mucins MUC5AC, MUC5B, and MUC2 were all found to suppress filamentation, and MUC5AC was able to suppress expression of virulence-associated genes and prevent *C. albicans* from forming biofilms on synthetic surfaces and human epithelial cells (Kavanaugh et al. 2014). This ability to manipulate *C. albicans* physiology implicates mucins as key host signals for retaining *C. albicans* and other microbial pathogens in a host-compatible state.

These *in vitro* systems with purified mucins can also be used to study how mucosal environments influence multi-species interactions to support stable microbial communities. In the oral cavity, for example, saliva protects the underlying mucosa and structures an oral microbial community comprised of more than 500 microbial species including the dental pathogen *S. mutans* (Kroes et

al. 1999), which is often considered to be antagonistic to other bacterial species in co-culture because it generates large amounts of lactic acid. While *S. mutans* will generally outcompete the commensal bacteria *Streptococcus sanguinis* in standard growth media, a recent study has demonstrated that solutions containing the native salivary mucin MUC5B can support prolonged coexistence of these two bacteria (Frenkel & Ribbeck 2017). This result suggests that mucins may play a specific role in suppressing interspecific competition and promoting stable assembly of multispecies communities. Collectively, these studies indicate that healthy mucin production and function limit the virulence of microbial pathogens and prevent disease progression. Furthermore, these studies highlight how simple native mucin networks are capable of reconstituting important microbial interactions that cannot be captured with other *in vitro* models such as growing cells in media alone, or with commercially available mucins that have lost part of their native configuration (Figure 1.3).

Mechanisms of mucin-microbe interactions

The mechanisms that potentially permit mucins to suppress virulence traits in opportunistic pathogens and promote stability of microbial communities are numerous. In a first instance, mucus can influence microbial behavior and community structure by forming a 3-dimensional matrix that acts as a physical barrier (Figure 1.4a). As an example, in the stomach and large intestine, there is evidence that mucus provides the spatial structure necessary to protect the underlying epithelia from microbial damage and house a community of beneficial microorganisms (Johansson et al. 2011). The 3-dimensional meshwork of mucus may spatially segregate microbes to some extent, affecting their ability to compete with each other and for nutrient sources. Mucins may also create heterogeneity by binding certain nutrients, which can lead to gradient formation and spatial niche partitioning as can be observed along the gastrointestinal tract (Lu et al. 2014). Furthermore, by influencing the transport of small signaling molecules, mucins also have the potential to interfere with intercellular communication and thereby regulate interactions within microbial communities. Many microbes rely on the production of signaling molecules to control traits that affect community structure such as biofilm formation, toxin and antibiotic production, DNA transfer, and various forms of motility. Thus, through their rich biochemistry, mucin polymers may selectively bind and reduce the diffusion of certain signaling molecules and toxins, thereby promoting the formation of discrete microenvironments capable of supporting the coexistence of

otherwise antagonistic species.

Mucins also may protect against epithelial adhesion and cytotoxicity of pathogenic microbes by interacting directly with microbes. Specifically, the mucin backbone is grafted with over 200 unique glycan structures (Jin et al. 2017) that could serve as potential interaction sites for microbes. Many pathogens, including the malaria parasite *Plasmodium falciparum* (Beeson et al. 2000) and the bacterium *H. pylori* (Simon et al. 1997), initiate infection by binding host cell glycans. Cell surface glycans can also act as highly specific receptors for viral hemagglutinins, such as in influenza virus (Kastner et al. 2017; Varki 1993) and human immunodeficiency virus (HIV) (Bode et al. 2012), as well as microbial cytotoxins, such as cholera toxin (Fishman & Atikkan 1980; Varki 1993). The glycans of secreted glycoconjugates like mucin are postulated to act as decoys for such pathogens, diverting the binding of the pathogen or toxin away from target cell surfaces (Varki 1993, 2006) or agglutinating pathogens for mucus clearance, thereby protecting the underlying epithelial cells. Mucins isolated from porcine gastric mucus have already been shown to prevent the infection of epithelial cells by a broad range of small mucosotropic viruses such as human papilloma virus type 16, Merkel cell polyoma-virus, and a strain of influenza A virus by trapping the viruses in the biopolymer matrix (Lieleg et al. 2012). Similarly, submandibular-sublingual mucin is able to agglutinate the oral bacteria *S. sanguinis* and *S. mutans* (Levine et al. 1978). This study also found that removing terminal sialic acid residues from salivary mucin glycoproteins prevented their ability to agglutinate *S. sanguinis*, but not *S. mutans*, suggesting that mucin-bacterial interactions involve specific, distinct carbohydrate moieties.

In addition to its barrier and binding properties, mucins may regulate microbial interactions and promote a stable microbiota by serving as a source of nutrients for certain microbes (Figure 1.4b). While most microbes lack the complete machinery required to degrade and use host-derived substrates, growth of commensal bacteria is linked to the metabolism of host-derived limiting nutrients (Tailford et al. 2015). In the oral cavity, for example, consortia of bacteria are capable of using mucin-derived glycans as a primary carbon source (Bradshaw et al. 1994; van der Hoeven et al. 1990; Wickström & Svensäter 2008). Similarly, mucus in the gut is composed of mucin glycoproteins that may serve as a nutrient source to certain commensal bacteria (Png et al. 2010; Sonnenburg et al. 2005). This metabolic advantage to commensal bacteria can prevent the establishment of enteric pathogens by competitive exclusion (Bergstrom & Xia 2013; Buffie & Pamer 2013; Malago 2014) and promote stable community assembly. The current understanding

of the molecular mechanisms employed by mucin-degrading bacteria to use host glycans and adapt to the mucosal environment has been previously reviewed (Tailford et al. 2015), but remains a largely open area of research.

Lastly, mucins, and in particular their associated glycans, may also influence the behavior and composition of the microbiota by presenting biochemical signals that influence cell physiology (Figure 1.4c). Metabolic cues help pathogens coordinate the expression of virulence factors (Rohmer et al. 2011) and the great structural diversity of glycans makes them well-suited to encode a wealth biological information. In fact, glycans are known to serve many biological functions in other contexts. Dietary prebiotic glycans can promote stability of the microbiome (Preidis & Versalovic 2009) and protect against virulence by enteric pathogens (Macfarlane et al. 2008), and cell surface sugar chains are important for cell-cell signaling (Kobata 1992; Varki 1993). In plants, oligosaccharide signals regulate important processes including host cell defense, growth, and development, even at extremely low concentrations (John et al. 1997). Similarly, glycosylation is important in signal transduction for mammalian systems. For example, deglycosylation of glycoprotein hormones such as human β chorionic gonadotrophin prevents intracellular signaling (Varki 1993). Covalently linked sugar chains on the surface of mammalian cells are also known to help communication and recognition through cell-cell adhesion (Fukuda et al. 1999; Varki 1993). In immune cell function, the selectin family of receptor proteins mediates the adhesion of leukocytes to endothelial cells via recognition of sialylated, fucosylated, sulfated glycans (Fukuda et al. 1999). It is not yet clear which specific receptors or signaling pathways in microbial cells are regulated by glycans; however, promising candidates for mucin-glycan sensing include two component systems or second messenger systems, many of which have sugar binding sites (reviewed in (Mascher et al. 2006; Postma et al. 1993)).

The large diversity of mucin glycans provides many potential recognition sites for microbes, which may each have a distinct signaling potential and role in regulating microbial behavior, but it has so far been intractable to assess their individual bioactivities. A class of structurally similar sugars found in human breast milk, known as human milk oligosaccharides (HMO), may provide important insight to the function of complex mucin glycans. HMO have garnered significant attention due to their ability to regulate the infant microbiota (Bode et al. 2012; Pudlo et al. 2015; Tailford et al. 2015; Yu et al. 2013). These oligosaccharides modulate immune responses (Eiwegger et al. 2004), alter global transcriptional profiles of commensal microorganisms (Garrido

et al. 2015), and protect against virulence of opportunistic pathogens. For example, α 1–2-fucosylated HMO prevented epithelial adhesion of the pathogen *Campylobacter jejuni in vitro* (Ruiz-Palacios et al. 2003), and pooled HMO blocked *Entamoeba histolytica* attachment to the surface of human intestinal epithelial cells, protecting host cells from cytotoxicity (Jantscher-Krenn et al. 2012). Systematic analysis of mucins and their associated glycans as decoy binding sites and as signaling molecules may reveal specific protective functions not dissimilar to what has recently been observed with HMO (Yu et al. 2012, 2014).

Together, mucin-microbe interactions are multifaceted, with both physicochemical properties and glycosylation patterns playing important roles. Figure 1.4 presents three important, understudied mechanisms for how the mucin gel may interact with microbes to influence community assembly and behavior. Specifically, the ability of mucins to impose geometric and diffusive constraints (Figure 1.4a), present complex nutritional substrates (Figure 1.4b), and display instructive signals via associated glycans (Figure 1.4c), all have strong potential to regulate microbial behavior and virulence.

In this thesis, I evaluate the influence of each of these mechanisms by developing tractable model systems. In Chapter 2, I investigate the relative importance of mucin-imposed geometric constraints and glycan-mediated signaling function using the opportunistic pathogen, *P. aeruginosa*, as a model organism. In Chapter 3, I identify the molecular mechanisms by which mucin-associated glycans suppress the expression of the bacteria-killing type VI secretion system in *P. aeruginosa*. I further test how this glycan-mediated signaling influences competitive interactions between *P. aeruginosa* and *Burkholderia cenocepacia* or *Escherichia coli*. In Chapter 4, I extend the *in vitro* model of the mucus environment to study how mucin glycans influence the composition of a complex microbial community derived from saliva. Taken together, this thesis demonstrates that mucins glycans modulate microbial behavior and, in turn, microbial interactions with the host and the surrounding microbial community. By better understanding how alterations to the biochemistry of mucins and mucus impacts their protective capacity, it may be possible to repair these barriers in disease and restore healthy mucosal function.

References

- Ambort D, Johansson MEV, Gustafsson JK, Nilsson HE, Ermund A, et al. 2012. Calcium and pH-dependent packing and release of the gel-forming MUC2 mucin. *Proc. Natl. Acad. Sci.* 109(15):5645–50
- Argüeso P, Gipson IK. 2001. Epithelial mucins of the ocular surface: structure, biosynthesis and function. *Exp. Eye Res.* 73(3):281–89
- Bansil R, Turner BS. 2006. Mucin structure, aggregation, physiological functions and biomedical applications. *Curr. Opin. Colloid Interface Sci.* 11:164–70
- Beeson JG, Rogerson SJ, Cooke BM, Reeder JC, Chai W, et al. 2000. Adhesion of *Plasmodium falciparum*-infected erythrocytes to hyaluronic acid in placental malaria. *Nat. Med.* 6(1):86–90
- Bergstrom KSB, Xia L. 2013. Mucin-type O-glycans and their roles in intestinal homeostasis. *Glycobiology.* 23(9):1026–1037
- Bode L, Kuhn L, Kim H-Y, Hsiao L, Nissan C, et al. 2012. Human milk oligosaccharides and postnatal transmission of HIV through breastfeeding. *Am. J. Clin. Nutr.* 96(4):831–39
- Bradshaw DJ, Homer KA, Marsh PD, Beighton D. 1994. Metabolic cooperation in oral microbial communities during growth on mucin. *Microbiology.* 140(12):3407–12
- Buffie CG, Pamer EG. 2013. Microbiota-mediated colonization resistance against intestinal pathogens. *Nat Rev Immunol.* 13(11):790–801.
- Caldara M, Friedlander RS, Kavanaugh NL, Aizenberg J, Foster KR, Ribbeck K. 2012. Mucin biopolymers prevent bacterial aggregation by retaining cells in the free-swimming state. *Curr. Biol.* 22(24):2325–30
- Celli JP, Turner BS, Afdhal NH, Ewoldt RH, McKinley GH, et al. 2007. Rheology of gastric mucin exhibits a pH-dependent sol-gel transition. *Biomacromolecules* 8(5):1580–86
- Dekker J, Rossen JWA, Büller HA, Einerhand AWC. 2002. The MUC family: an obituary. *Trends Biochem. Sci.* 27(3):126–31
- Dohrman A, Miyata S, Gallup M, Li J-D, Chapelin C, et al. 1998. Mucin gene (MUC 2 and MUC 5AC) upregulation by Gram-positive and Gram-negative bacteria. *Biochim. Biophys. Acta Mol. Basis Dis.* 1406(3):251–59
- Eiwegger T, Stahl B, Schmitt J, Boehm G, Gerstmayr M, et al. 2004. Human milk-derived oligosaccharides and plant-derived oligosaccharides stimulate cytokine production of cord blood T-cells in vitro. *Pediatr. Res.* 56(4):536–40
- Fishman PH, Atikkan EE. 1980. Mechanism of action of cholera toxin: Effect of receptor density and multivalent binding on activation of adenylate cyclase. *J. Membr. Biol.* 54:51–60
- Frenkel ES, Ribbeck K. 2015a. Salivary mucins in host defense and disease prevention. *J. Oral Microbiol.* 7(1):29759
- Frenkel ES, Ribbeck K. 2015b. Salivary mucins protect surfaces from colonization by cariogenic bacteria. *Appl. Environ. Microbiol.* 81(1):332–38

- Frenkel ES, Ribbeck K. 2017. Salivary mucins promote the coexistence of competing oral bacterial species. *ISME J.* 11:1286-1290
- Fukuda M, Hiraoka N, Yeh J-C. 1999. C-type lectins and sialyl Lewis X oligosaccharides: versatile roles in cell-cell interaction. *J. Cell Biol.* 147(3):467–70
- Garrido D, Ruiz-Moyano S, Lemay DG, Sela DA, German JB, Mills DA. 2015. Comparative transcriptomics reveals key differences in the response to milk oligosaccharides of infant gut-associated bifidobacteria. *Sci. Rep.* 5:13517
- Godl K, Johansson ME, Lidell ME, Mörgelin M, Karlsson H, et al. 2002. The N terminus of the MUC2 mucin forms trimers that are held together within a trypsin-resistant core fragment. *J. Biol. Chem.* 277(49):47248–56
- Hatrup CL, Gendler SJ. 2008. Structure and function of the cell surface (tethered) mucins. *Annu. Rev. Physiol.* 70:431–57
- Jantscher-Krenn E, Lauwaet T, Bliss LA, Reed SL, Gillin FD, Bode L. 2012. Human milk oligosaccharides reduce *Entamoeba histolytica* attachment and cytotoxicity in vitro. *Br. J. Nutr.* 108(10):1839–46
- Jin C, Kenny DT, Skoog EC, Padra M, Adamczyk B, et al. 2017. Structural diversity of human gastric mucin glycans. *Mol. Cell. Proteom.* 16(5):743–58
- Johansson MEV, Larsson JMH, Hansson GC. 2011. The two mucus layers of colon are organized by the MUC2 mucin, whereas the outer layer is a legislator of host-microbial interactions. *Proc. Natl. Acad. Sci.* 108:4659-4665
- John M, Röhrig H, Schmidt J, Walden R, Schell J. 1997. Cell signaling by oligosaccharides. *Trends Plant Sci.* 2(3):111–15
- Kastner M, Karner A, Zhu R, Huang Q, Zhang D, et al. 2017. Relevance of host cell surface glycan structure for cell specificity of influenza A virus. *bioRxiv.* <https://doi.org/10.1101/203349>
- Kavanaugh NL, Zhang AQ, Nobile CJ, Johnson AD, Ribbeck K. 2014. Mucins suppress virulence traits of *Candida albicans*. *mBio.* 5(6):e01911-14
- Kerschner JE, Hong W, Khampang P, Johnston N. 2014. Differential response of gel-forming mucins to pathogenic middle ear bacteria. *Int. J. Pediatr. Otorhinolaryngol.* 78(8):1368–73
- Kesimer M, Makhov AM, Griffith JD, Verdugo P, Sheehan JK. 2010. Unpacking a gel-forming mucin: a view of MUC5B organization after granular release. *Am. J. Physiol. Lung Cell. Mol. Physiol.* 298(1):L15–22
- Kobata A. 1992. Structures and functions of the sugar chains of glycoproteins. *Eur. J. Biochem.* 209(2):483–501
- Kroes I, Lepp PW, Relman DA. 1999. Bacterial diversity within the human subgingival crevice. *Proc. Natl. Acad. Sci.* 96(25):14547-14552
- Lai SK, Wang Y-Y, Wirtz D, Hanes J. 2009. Micro- and macrorheology of mucus. *Proc. Natl. Acad. Sci.* 61(2):86–100
- Levine MJ, Herzberg MC, Levine MS, Ellison SA, Stinson MW, et al. 1978. Specificity of salivary-

- bacterial interactions: role of terminal sialic acid residues in the interaction of salivary glycoproteins with *Streptococcus sanguis* and *Streptococcus mutans*. *Infect. Immun.* 19(1):107–15
- Li J-D, Dohrman AF, Gallup M, Miyata S, Gum JR, et al. 1997. Transcriptional activation of mucin by *Pseudomonas aeruginosa* lipopolysaccharide in the pathogenesis of cystic fibrosis lung disease. *Proc. Natl. Acad. Sci.* 94(3):967–72
- Lieleg O, Lieleg C, Bloom J, Buck CB, Ribbeck K. 2012. Mucin biopolymers as broad-spectrum antiviral agents. *Biomacromolecules.* 13(6):1724–32
- Lindén S, Mahdavi J, Semino-Mora C, Olsen C, Carlstedt I, et al. 2008. Role of ABO secretor status in mucosal innate immunity and *H. pylori* infection. *PLOS Pathog.* 4(1):0006–0013
- Linden SK, Sutton P, Karlsson NG, Korolik V, McGuckin MA. 2008. Mucins in the mucosal barrier to infection. *Mucosal Immunol.* 1(3):183–97
- Lindén SK, Sheng YH, Every AL, Miles KM, Skoog EC, et al. 2009. MUC1 limits *Helicobacter pylori* infection both by steric hindrance and by acting as a releasable decoy. *PLOS Pathog.* 5(10):e1000617
- Lu HP, Lai YC, Huang SW, Chen HC, Hsieh CH, Yu HT. 2014. Spatial heterogeneity of gut microbiota reveals multiple bacterial communities with distinct characteristics. *Sci. Rep.* 4:6185
- Macfarlane GT, Steed H, Macfarlane S. 2008. Bacterial metabolism and health-related effects of galacto-oligosaccharides and other prebiotics. *J. Appl. Microbiol.* 104(2):305–44
- Mahdavi J, Sondén B, Hurtig M, Olfat FO, Forsberg L, et al. 2002. *Helicobacter pylori* SabA adhesin in persistent infection and chronic inflammation. *Science.* 297(5581):573–78
- Malago JJ. 2014. Contribution of microbiota to the intestinal physicochemical barrier. *Beneficial Microbes.* 6(3):295–311
- Mascher T, Helmann JD, Uden G. 2006. Stimulus perception in bacterial signal-transducing histidine kinases. *Microbiol. Mol. Biol. Rev.* 70(4):910–38
- McNamara N, Khong A, McKemy D, Caterina M, Boyer J, et al. 2001. ATP transduces signals from ASGM1, a glycolipid that functions as a bacterial receptor. *Proc. Natl. Acad. Sci.* 98(16):9086–91
- Nilsson HE, Ambort D, Bäckström M, Thomsson E, Koeck PJB, et al. 2014. Intestinal MUC2 mucin supramolecular topology by packing and release resting on D3 domain assembly. *J. Mol. Biol.* 426(14):2567–79
- Nordgård CT, Draget KI. 2015. Dynamic responses in small intestinal mucus: relevance for the maintenance of an intact barrier. *Eur. J. Pharm. Biopharm.* 95:144–50
- Png CW, Lindén SK, Gilshenan KS, Zoetendal EG, McSweeney CS, et al. 2010. Mucolytic bacteria with increased prevalence in IBD mucosa augment in vitro utilization of mucin by other bacteria. *Am. J. Gastroenterol.* 105:2420–2428
- Postma PW, Lengeler JW, Jacobson GR. 1993. Phosphoenolpyruvate: carbohydrate phosphotransferase systems of bacteria. *Microbiol. Rev.* 57(3):543–94
- Preidis GA, Versalovic J. 2009. Targeting the human microbiome with antibiotics, probiotics, and prebiotics: Gastroenterology enters the metagenomics era. *Gastroenterology.* 136(6):2015–31

- Pudlo NA, Urs K, Kumar SS, German JB, Mills DA, Martens EC. 2015. Symbiotic human gut bacteria with variable metabolic priorities for host mucosal glycans. *MBio*. 6(6):e01282–15
- Rohmer L, Hocquet D, Miller SI. 2011. Are pathogenic bacteria just looking for food? Metabolism and microbial pathogenesis. *Trends Microbiol*. 19(7):341–48
- Roy MG, Livraghi-Butrico A, Fletcher AA, Melissa M, Evans SE, et al. 2014. MUC5B is required for airway defense. *Nature*. 505(7483):412–16
- Ruiz-Palacios GM, Cervantes LE, Ramos P, Chavez-Munguia B, Newburg DS. 2003. Campylobacter jejuni binds intestinal H(O) antigen (Fuc α 1, 2Gal β 1, 4GlcNAc), and fucosyloligosaccharides of human milk inhibit its binding and infection. *J. Biol. Chem*. 278(16):14112–20
- Schipper RG, Silletti E, Vingerhoeds MH. 2007. Saliva as research material: biochemical, physicochemical and practical aspects. *Arch. Oral Biol*. 52(12):1114–35
- Sellers LA, Allen A, Morris ER, Ross-Murphy SB. 1988. Mucus glycoprotein gels. Role of glycoprotein polymeric structure and carbohydrate side-chains in gel-formation. *Carbohydr. Res*. 178(1):93–110
- Simon PM, Goode PL, Mobasser A, Zopf D. 1997. Inhibition of Helicobacter pylori binding to gastrointestinal epithelial cells by sialic acid-containing oligosaccharides. *Infect. Immun*. 65(2):750–757
- Singh PK, Schaefer AL, Parsek MR, Moninger TO, Welsh MJ, Greenberg EP. 2000. Quorum-sensing signals indicate that cystic fibrosis lungs are infected with bacterial biofilms. *Nature*. 407(6805):762–64
- Sonnenburg JL, Xu J, Leip DD, Chen C-H, Westover BP, et al. 2005. Glycan Foraging in Vivo by an Intestine-Adapted Bacterial Symbiont. *Science*. 307(5717):1955–1959
- Tailford LE, Crost EH, Kavanaugh D, Juge N. 2015. Mucin glycan foraging in the human gut microbiome. *Front. Genet*. 6:81
- Taylor C, Draget KI, Pearson JP, Smidsrød O. 2005. Mucous systems show a novel mechanical response to applied deformation. *Biomacromolecules*. 6(3):1524–30
- Thornton DJ, Rousseau K, McGuckin MA. 2008. Structure and function of the polymeric mucins in airways mucus. *Annu. Rev. Physiol*. 70:459–86
- van der Hoeven JS, van den Kieboom CWA, Camp PJM. 1990. Utilization of mucin by oral Streptococcus species. *Antonie Van Leeuwenhoek*. 57(3):165–72
- Varki A. 1993. Biological roles of oligosaccharides: All of the theories are correct. *Glycobiology*. 3(2):97–130
- Varki A. 2006. Nothing in glycobiology makes sense, except in the light of evolution. *Cell*. 126(5):841–45
- Wagner CE, Turner BS, Rubinstein M, McKinley GH, Ribbeck K. 2017. A rheological study of the association and dynamics of MUC5AC gels. *Biomacromolecules*. 18(11):3654–64
- Wickström C, Svensäter G. 2008. Salivary gel-forming mucin MUC5B—a nutrient for dental plaque bacteria. *Oral Microbiol. Immunol*. 23(3):177–82

- Yu Y, Lasanajak Y, Song X, Hu L, Ramani S, et al. 2014. Human milk contains novel glycans that are potential decoy receptors for neonatal rotaviruses. *Mol. Cell. Proteom.* 13(11):2944–60
- Yu Y, Mishra S, Song X, Lasanajak Y, Bradley KC, et al. 2012. Functional glycomic analysis of human milk glycans reveals the presence of virus receptors and embryonic stem cell biomarkers. *J. Biol. Chem.* 287(53):44784–99
- Yu Z-T, Chen C, Newburg DS. 2013. Utilization of major fucosylated and sialylated human milk oligosaccharides by isolated human gut microbes. *Glycobiology.* 23(11):1281–92

Acknowledgements

We thank N. Kavanaugh for the SEM images in Figure 1.3, as well as J. Witten, J. Takagi, T. Samad, and the rest of the Ribbeck lab for their helpful discussions and careful editorial assistance. This work was supported by the National Institutes of Health under award NIH R01-EB017755, the National Science Foundation under award PHY-1454673, and the MRSEC Program of the National Science Foundation under award DMR-14-19807. C.E.W. thanks NSERC (Canada) for a PGS D award. K.M.W. thanks the MIT/National Institute of General Medical Sciences Biotechnology Training Program (grant 5T32GM008334-28) and the National Science Foundation for a Graduate Research Fellowship under grant 1122374.

Figures

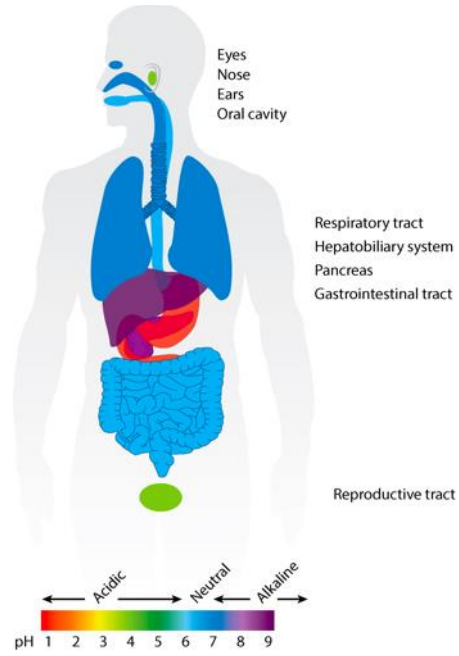


Figure 1.1 Epithelial surfaces of the body coated by mucus, with characteristic pH levels.

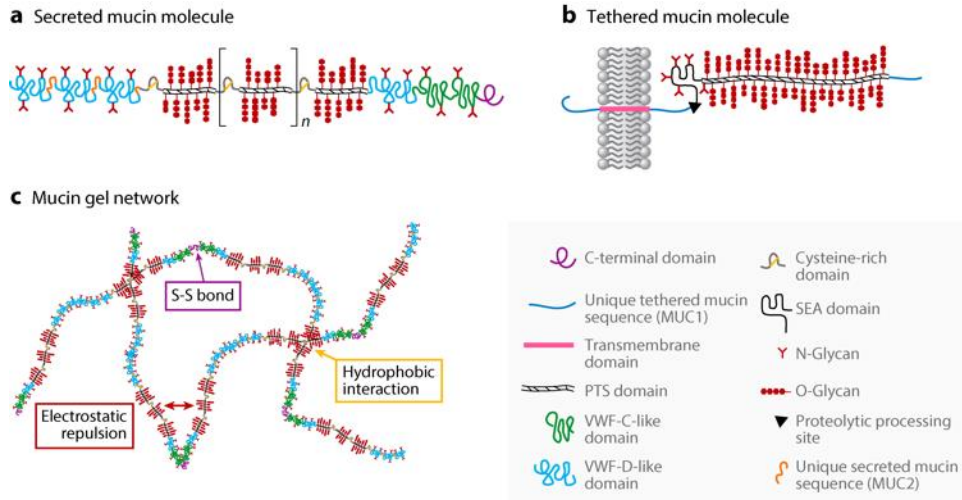


Figure 1.2 (a,b) Schematics of the general structure of (a) secreted and (b) tethered mucin molecules. (c) An illustration of the network established by the gel-forming, secreted mucins. Individual mucin subunits associate via end-to-end disulfide bonds to form even larger macromonomer chains. The network is formed from reversible associations such as hydrophobic interactions between the non-glycosylated, cysteine-rich regions of the molecules and is stabilized by electrostatic repulsion between the charged sugar side chains. Abbreviation: PTS domain, proline, threonine, and/or serine domain.

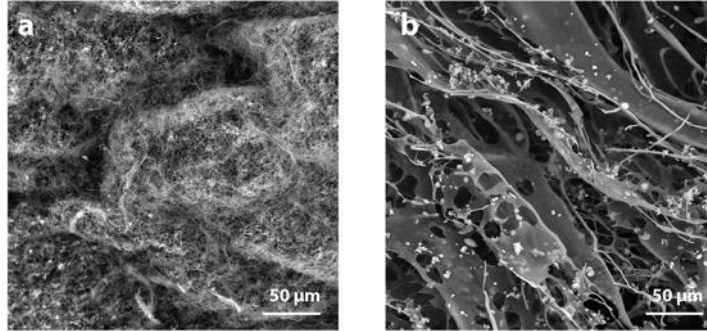


Figure 1.3 Scanning electron microscopy (SEM) reveals structural changes to mucins associated with different purification processes. **(a)** MUC5AC mucin purified from pig gastric mucus by the Ribbeck lab entangles to form the characteristic mesh-like network of the mucus gel. **(b)** Industrially purified porcine gastric mucin supplied by Sigma-Aldrich is degraded and deglycosylated.

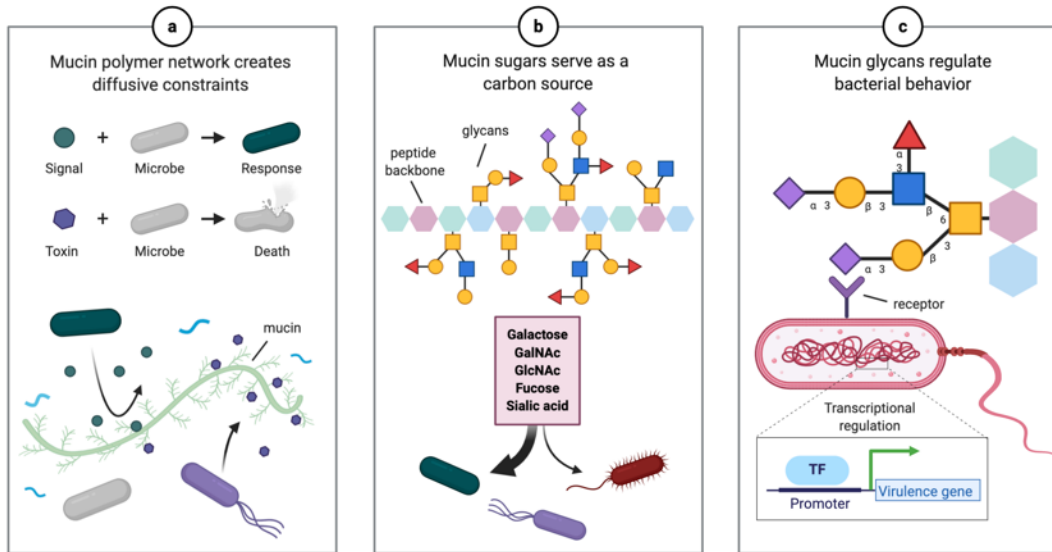


Figure 1.4 Microbial interactions with mucins influence pathogenicity and community-level behaviors, which may ultimately influence the composition or function of the microbiota. **(a)** Barrier properties of mucus can limit the diffusion of microbial signaling molecules, toxins, or nutrients through an environment. This can result in signal gradients that promote or interfere with intercellular communication, toxin sequestration that limits antagonism between competing microbes, or nutrient gradients that facilitate niche partitioning. **(b)** Mucin-derived sugars may serve as a carbon source to select microbes with glycan degradation machinery. **(c)** Mucin-associated glycans may serve as chemical signals that attenuate microbial virulence or competition. **(a-c)** Not drawn to scale. Created with BioRender.com

Chapter 2: Mucin glycans attenuate the virulence of *Pseudomonas aeruginosa* in infection

Work presented in this chapter is published in: Wheeler KM, Cárcamo-Oyarce G, Turner BS, Dellos-Nolan S, Co JY, Lehoux S, Cummings RD, Wozniak DJ, Ribbeck K. Mucin glycans attenuate the virulence of *Pseudomonas aeruginosa* in infection. *Nature microbiology*. (2019). doi: 10.1038/s41564-019-0581-8

Supplementary information is provided in Appendix A.

Abstract

A slimy, hydrated mucus gel lines all wet epithelia in the human body, including the eyes, lungs, gastrointestinal and urogenital tracts. Mucus forms the first line of defense while housing trillions of microbes that constitute the microbiota. Rarely do these microbes cause infections in healthy mucus, suggesting mechanisms exist in the mucus layer that regulate virulence. Using the bacterium *Pseudomonas aeruginosa* and a 3-dimensional (3D) laboratory model of native mucus, we determined that exposure to mucus triggers the downregulation of virulence genes involved in quorum sensing, siderophore biosynthesis, and toxin secretion, and rapidly disintegrates biofilms, a hallmark of mucosal infections. This phenotypic switch is triggered by mucins, polymers densely grafted with *O*-linked glycans that form the 3D scaffold inside mucus. Here we show isolated mucins act at various scales, suppressing distinct virulence pathways, promoting a planktonic lifestyle, reducing cytotoxicity to human epithelia *in vitro*, and attenuating infection in a porcine burn model. Other viscous polymer solutions lack the same effect, indicating that mucin's regulatory function is not a result of its polymeric structure alone. We identify that interactions with *P. aeruginosa* are mediated by mucin-associated glycans. By isolating glycans from the mucin backbone, we assessed the collective activity of hundreds of complex structures in solution. Like their grafted counterparts, free mucin glycans potently regulate bacterial phenotypes even at relatively low concentrations. This regulatory function likely depends on glycan complexity, as monosaccharides do not attenuate virulence. Thus, mucin glycans are potent host signals that “tame” microbes, rendering them less harmful to the host.

Introduction

Mucus is a biological hydrogel that coats all wet epithelia in the human body. These mucus layers represent the largest interface for host-microbe interactions and one of the first environments encountered by invading bacteria like *Pseudomonas aeruginosa* (Figure 2.1a). Although this opportunistic pathogen employs several virulence traits and can cause severe morbidity or even death in people with compromised immunity, burn wounds, or defects in mucus production (Figure 2.1b) (Sadikot et al. 2005; Parsek & Singh 2003), mucosal infections are uncommon in most healthy individuals exposed to this microbe (Parsek & Singh 2003). This lack of infection suggests the presence of host defense mechanisms within the mucus environment that enable the body to tolerate continued exposure to *P. aeruginosa*.

Growing evidence suggests that the major gel-forming components of mucus, the mucin glycopolymers, may have a role in protecting against opportunistic microbes. For instance, mucin genes are often up-regulated in response to infection by microbes (Kerschner et al. 2014; Dohrman et al. 1998; Li et al. 1997, McNamara et al. 2001), and media containing natively purified mucins are sufficient to prevent surface attachment and the formation of antibiotic-resistant cellular aggregates, known as biofilms, by several microbes (Caldara et al. 2012; Kavanaugh et al. 2014; Frenkel & Ribbeck 2015). These observations suggest that mucins may help promote host-compatibility by regulating virulence, but specific pathways altered by this host-produced factor remain poorly understood.

Results

To identify mechanisms in native mucus that control pathogens, we tested whether exposure to native intestinal mucus alters biofilm integrity. Mature *P. aeruginosa* biofilms were exposed to buffer or native intestinal mucus. While buffer alone did not affect biofilm integrity (Figure 2.1c), biofilms exposed to mucus dissociated from the surface and 70% of cells shifted into the planktonic phase (Figure 2.1d). Since the growth rate was not altered in mucus relative to buffer alone (Figure S2.1), the shift to planktonic growth may arise from phenotypic regulation by mucus. Mucus-mediated biofilm dispersal is dependent on an intact flagellum (Figure 2.1c), indicating that mucin triggers an active, motility-driven escape, as opposed to mechanical disruption. To test whether mucus only affects biofilms or more broadly regulates virulence traits, we measured the expression of genes important for establishing infection (Sadikot et al. 2005). This revealed intestinal mucus

transcriptionally suppresses quorum sensing (*lasR*), siderophore biosynthesis (*pvdA*), and type-three secretion (*pcrV*) (Figure 2.1e). Native gastric and salivary mucus similarly suppressed major infection-related genes (Figure 2.1e), suggesting that virulence suppression is conserved across various mucosal surfaces. Together, these findings demonstrate that mucus contains factors that modulate bacterial behaviors at the levels of gene expression and phenotype.

To identify specific regulatory factors within complex mucus, we tested mucus fractions separated according to molecular weight. The primary bioactive component of whole mucus was larger than 100 kDa (Figure 2.1f), pointing to mucin polymers as possible candidates. Mucins are a major high molecular-weight component of mucus that disperse cells in isolation (Co et al. 2018). Adding purified mucins back into depleted mucus was sufficient to restore biofilm dispersal and virulence gene suppression (Figure 2.1f-h), providing strong evidence that mucin glycopolymers constitute key regulatory cues inside mucus. Here, using natively purified mucins was critical because commercially available mucins harbor reduced chemical complexity due to the harsh purification process (Wagner et al. 2018).

To directly test whether mucins trigger a global transcriptional response, we performed RNA sequencing on *P. aeruginosa* grown with or without (0.5% w/v) MUC5AC or MUC5B, the most abundant gel-forming mucins secreted in niches colonized by *P. aeruginosa*, including the nasal and oral cavities, respiratory tract, eyes, and middle ear (Figure 2.2a, b). Both mucins triggered a genome-wide response (Figure 2.2c) and suppressed many virulence pathways, including type 1, 2, 3, and 6 secretion systems, siderophore biosynthesis (pyoverdine and pyochelin), and quorum sensing (Figure 2.2d). While we found no enrichment in virulence pathways among the upregulated genes, we detected enrichment in the denitrification genes, consistent with previous findings that this pathway is inversely regulated by quorum sensing (Toyofuku et al. 2007). There were differences in the exact genes that were differentially regulated, as well as differences in the magnitudes of those changes after exposure to MUC5AC or MUC5B (Figure 2.2c, S2.2, Table S2.1), suggesting that differences in mucin biochemistry influence specific regulatory function. We replicated this effect with various media, time points, and bacterial strains (Figure S2.3), demonstrating that mucin suppresses virulence gene expression across a range of experimental conditions.

Transcriptional regulation of virulence was validated by qPCR (Figure S2.4). To confirm the

phenotypic relevance of these changes, we combined functional biochemical assays and infection models (Figure 2.2e, i). Protease activity and siderophore production were lower in supernatants from *P. aeruginosa* exposed to mucin than in supernatants from bacteria grown in medium alone (Figure S2.5). Consistent with downregulation of biofilm formation, MUC5AC suppressed *P. aeruginosa* PAO1 association to surfaces made of glass (Figure S2.6) and plastic (Figure S2.7), and reduced attachment to live HT-29 human epithelial cells in a concentration dependent manner (Figure 2.2f). Mucins promoted a larger vertical distribution of *P. aeruginosa* cells than those grown in medium alone, shifting them to a suspended and less-aggregated planktonic-like state with cells still detectable ≥ 50 μm from the glass surface (Figure S2.6). Collectively, these data highlight two facets of mucin regulatory function: one in which mucins induce a global transcriptional response that “disarms” *P. aeruginosa* by downregulating important virulence genes, and another in which mucins suppress aggregation and bacterial attachment to surfaces. Mucin-mediated changes were sufficient to neutralize antagonistic interactions between *P. aeruginosa* and human cells. By monitoring survival of human epithelial cells over time, we determined that MUC5AC reduced *P. aeruginosa*-mediated epithelial cell death in a dose-dependent manner (Figure 2.2g), while maintaining the morphology and confluency of the epithelial cell monolayer (Figure 2.2h).

To better understand the relevance of mucin’s regulatory function in a complex biological system of multiple cell types and an active immune system, we exposed *P. aeruginosa*-infected porcine burn wounds to a wound dressing containing MUC5AC and quantified the bacterial burden over time by counting colony-forming units (CFU, Figure 2.2i, S2.8). Exposure to MUC5AC resulted in two-log reductions in CFU in wounds 1-week post-infection, compared to no reduction in the mucin-free mock treatment (Figure 2.2j). The sustained clearance of *P. aeruginosa* detected here is likely not due to direct killing by MUC5AC, as viability was not inhibited by mucins in isolation (Figure 2.2k). Rather, mucin likely mediates bacterial clearance through regulation of microbial phenotypes, which attenuates pathogens and thereby facilitates host-mediated clearance.

It is tempting to speculate that mucin triggers this phenotypic switch by maintaining cells in the planktonic, non-aggregate form. To test this hypothesis, we evaluated whether mucins still suppressed virulence genes in mutants lacking flagellar motility ($\Delta\text{motABCD}$) or the ability to aggregate (Δpslpel) (Figure 2.3a). Both mutants responded to mucins (Figure 2.3b), indicating that mucin’s virulence-attenuating function is not a downstream consequence of changes to motility or

aggregation, but rather a parallel effect. Integrating our RNA-seq results with the major genetic components of the *P. aeruginosa* virulence network (Jimenez et al. 2012, Balasubramanian et al. 2013, Figure 2.3c) revealed that mucin's broad virulence-attenuating effect likely involves multiple regulatory systems.

Polymer solutions like mucin have complex structural and biochemical properties that could directly or indirectly trigger signaling events through many sensory systems in *P. aeruginosa*. One possibility is that mucins may trigger a general response through their electrostatic or hydrophobic properties or by creating geometric constraints. An alternative hypothesis is that the observed response is triggered by sensing specific biochemical moieties that are presented on secreted mucins. To distinguish between these two possibilities, we tested whether carboxymethylcellulose (CMC), a well-established mucin mimetic with charge and viscoelastic properties similar to those of native mucins (Van Der Reijden et al. 1994), could elicit changes in *P. aeruginosa* virulence. Importantly, exposure to CMC did not differentially regulate signature virulence genes (Figure 2.3d), prevent surface attachment (Figure S2.9), or protect epithelial cells from *P. aeruginosa*-induced death (Figure S2.9). These results suggest that mucin's polymeric structure is not sufficient to mediate these virulence-attenuating effects. Rather, specific biochemistry present in mucins, but not CMC, is necessary to attenuate *P. aeruginosa* virulence.

Native mucins display a plethora of complex glycan structures covalently linked to serine/threonine (Jin et al. 2017, Karlsson et al. 1997, Holmen Larsson et al. 2013), creating a wealth of biochemical information with the potential to influence microbial gene expression. *P. aeruginosa* employs many strategies to sense and respond to host signals, allowing it to coordinate the switch between its pathogenic and host-compatible states (Jimenez et al. 2012, Balasubramanian et al. 2013). Sensing signature mucin-glycan motifs may be an effective mechanism to limit production of metabolically costly virulence factors in niches where virulence would not be advantageous. The potential of complex mucin glycans to regulate microbial behavior has been largely overlooked owing to fundamental technical limitations, including the difficulty of purifying intact mucins, non-standard methods for isolating *O*-linked glycans, and the analytical complexity of predicting glycan structures (Cummings and Pierce 2014). To determine whether glycans contribute to mucin's virulence-neutralizing capability, we assessed the degree to which glycans isolated from the MUC5AC protein backbone recapitulate the mucin response in *P. aeruginosa*. We isolated mucin glycans via alkaline β -elimination, which preserved the unique

sequences in the oligosaccharide chains and yielded a pooled library of *O*-linked glycans (Figure 2.4a, b). We then analyzed glycans via matrix-assisted laser desorption/ionization time-of-flight (MALDI-TOF). After processing for annotation and assignment based on mass and known core structures, we identified >90 glycan structures (Figure 2.4c, Table S2.2), not including distinct isomeric forms, which likely would increase the library diversity to several hundred structures. The diversity of our glycan library is comparable to those of published libraries for mammalian gastric and respiratory mucins (Jin et al. 2017, Karlsson et al. 1997, Holmen Larsson et al. 2013, Xia et al. 2005). Specifically, glycans in our library were predominantly built on core-2 [Gal β 1-3(GlcNAc β 1-6)GalNAc α 1-] and, to a lesser extent, core-1 (Gal β 1-3GalNAc α 1-) structures, with a high level of fucosylation and relatively little sialylation.

Like native mucus and intact mucins, mucin glycans triggered an active, motility-dependent dispersal of bacterial cells from mature biofilms (Figure 2.4d, S2.10) into the planktonic state (Figure 2.4e). Mucin glycans also prevented bacterial attachment to glass surfaces (Figure S2.11) and to human cells (Figure 2.4f) and yielded bacterial aggregates smaller than those formed in medium alone or with monosaccharides (Figure 2.4g). To determine which mucin-regulated pathways were specifically altered in response to mucin glycans, we exposed *P. aeruginosa* to a pool of potential glycan cues and monitored changes in gene expression. RNA-seq revealed that *P. aeruginosa* exposed to relatively low concentrations (0.01% w/v) of free MUC5AC glycans undergo a transcriptional response that mirrors that associated with exposure to 0.5% (w/v) whole native mucin comprised of up to 0.4% (w/v) grafted-glycans (Figure 2.4h). Functional enrichment analyses confirmed that the same virulence pathways suppressed by intact MUC5AC were also suppressed by MUC5AC glycans (Figure 2.4i), further indicating that an integral part of mucin rather than another mucus-associated factor is the primary virulence-neutralizing agent in mucus. We anticipate that increasing the glycan concentration to levels present on mucin will improve the dynamic range of the transcriptional response. Importantly, *P. aeruginosa* viability was not altered by the presence of monosaccharides represented in mucin glycans (Figure 2.4j). Exposure of *P. aeruginosa* to a pool of these monosaccharides did not trigger dispersal (Figure 2.4d), prevent attachment to glass (Figure S2.11) or human cells (Figure 2.4e), or differentially regulate quorum sensing (*lasR*), siderophore production (*pvdA*), or type-three secretion (*pcrV*) genes (Figure 2.4k). Monosaccharide exposure also did not suppress virulence-factor production, even with increasing concentrations (Figure S2.12), although a non-significant effect on bacterial burden *in vivo* was

detected (Figure 2.41). Based on these data, we conclude that the complex arrangement and particular stereochemistry of these sugar residues is critical to their function as regulatory signals.

Discussion

The diversity of *O*-glycans on mucins exceeds even that on tissue surfaces (Nakano et al. 2011, Lee et al. 2010, Yamada and Kinoshita 2009), and their complexity makes them ideal for encoding biological information with a high degree of specificity. In this way, mucins present and retain myriad potential regulatory cues. We propose that microbes likely evolved mechanisms to recognize, process, uptake, and respond to specific moieties within the complex array of mucin glycans (Varki 2017). The question remains how mucin glycans interact with, and are sensed by, *P. aeruginosa* at a molecular level. One possibility is that glycans may directly serve as signal through a carbohydrate binding site in a global regulatory system, such as those affecting the secondary messenger c-di-GMP or the non-coding RNAs *rsmY* and *rsmZ* (Jimenez et al. 2012, Balasubramanian et al. 2013). Potential glycan sensors have been identified in *P. aeruginosa* that are thought to feed into regulatory virulence pathways and have annotated carbohydrate binding sites, such as the two-component sensor LadS and the diguanylate cyclase NicD (Ventre et al. 2006, Basu Roy & Sauer 2014). Mucin glycans may also trigger metabolic changes by serving as a nutritional substrate or regulate signaling pathways through interactions with specific *P. aeruginosa* lectins or surface adhesins. We speculate that the structural diversity of mucins and mucin-associated glycans permits them to interact with several bacterial receptors and mediate distinct functions.

Collectively, our findings reveal a previously unrecognized role for mucin glycans as potent host-derived regulators of bacterial phenotype, which has broad implications for how the body prevents mucosal infections while maintaining a diverse microbiota. Why diseased mucus no longer retains the ability to attenuate virulence (Landry et al. 2006, Secor et al. 2018, Cattoir et al. 2012, Duan & Surette 2007, Arora et al. 1998) remains an open question. Based on our findings that glycans trigger a switch in bacterial phenotype, we postulate that changes to mucin glycosylation patterns in disease, such as increased sialylation (Xia et al. 2005), will alter both mucin's binding properties with microbes and its protective function. By isolating mucin glycan library, we have established the conceptual and technical framework to systematically address these open questions about the glycan regulatory code. We posit that cracking this code will elucidate the influence of glycans on

the virulence of microbes that interact with the host via mucosal surfaces. Identification of specific bioactive glycans will likely reveal a class of therapeutics for treating intractable bacterial infections and may inspire treatment strategies that tune host glycan signals to attenuate virulence and stabilize the healthy microbiota.

Materials and Methods

Strains and growth conditions. Batch cultivation of *Pseudomonas aeruginosa* strains (Table S2.3) was carried out shaking at 37 °C in LB (Difco). Thirty µg/mL gentamicin was added to the medium for strains with gentamicin-resistant plasmids.

For whole-mucus experiments, overnight cultures of PAO1 were diluted 10-fold into ABTGC, which is comprised of ABT minimal medium (Chua et al. 2015) supplemented with 5 g glucose and 5 g casamino acids, and grown for 4 h. Seventy-five microliters of these cultures were exposed to 75 µL of solubilized mucus or solubilization buffer (described in “preparation of whole mucus”) for 1 h at 37 °C in a static 96-well microtiter plate (CellStar).

For experiments involving liquid culture, overnight cultures of PAO1 were diluted to an OD₆₀₀ of 0.01 into 150 µL ABTGC with or without (0.01-0.5%) MUC5AC, (0.5%) MUC5B, 0.5% carboxymethylcellulose (CMC, Sigma), (0.01%) MUC5AC glycans, or (0.01%) monosaccharide mixture and grown for 5 h at 37 °C in a static 96-well microtiter plate. Note that based on the data in Figure 2.4b, the monosaccharide mixture contained equal weights of galactose, N-acetylglucosamine [GlcNAc], N-acetylgalactosamine [GalNAc], fucose, and sialic acid (all sugars purchased from Sigma). The concentration of glycans was selected based on the mucin dose response curves in Figure 2.2. In these experiments, we found that 0.01% was the lowest mucin concentration with measurable effects (Figure 2.2f). Due to the technical challenges of preparative-scale purification of mucin glycans, we used the minimal inhibitory concentration in this work.

Human saliva collection. Submandibular saliva was collected from human volunteers using a custom vacuum pump, pooled, centrifuged at 2500 x g for 5 minutes, and protease inhibitors were added as previously described (Frenkel & Ribbeck 2015). Human saliva samples were collected after explaining the nature and possible consequences of the studies, obtaining informed consent, and receiving approval from the institutional review board and Massachusetts Institute of Technology’s Committee on the Use of Humans as Experimental Subjects under protocol #1312006096.

Preparation of whole mucus. Mucus was scraped from fresh pig stomachs and intestines, and solubilized (1 g scrapings to 5 mL) in 0.2 M sodium chloride buffer with protease inhibitors (5

mM Benzamidine HCl, 1 mM dibromoacetophenone, 1 mM phenylmethylsulfonylfluoride (PMSF), and 5mM EDTA at pH 7) and 0.04% sodium azide (Sigma). Cellular debris and food waste was removed via low-speed centrifugation, 8000 x g, (7,000 rpm Sorvall GS-3 rotor), for 30 minutes at 4 °C.

Mucin purification. This study used native porcine gastric mucins (MUC5AC), porcine intestinal mucins (MUC2), and human salivary mucins (MUC5B). Native mucins were purified as previously reported (Caldara et al. 2012, Kavanaugh et al. 2014, Frenkel & Ribbeck 2015, Co et al. 2018, Lieleg et al. 2012). Briefly, mucus was scraped from fresh pig stomachs and intestines, solubilized in sodium chloride buffer (described above), and insoluble material was removed by ultracentrifugation at 190,000 x g RCF for 1 h at 4 °C (40,000 rpm, Beckman 50.2 Ti rotor with polycarbonate bottles). Submandibular saliva was collected from human volunteers using a custom vacuum pump, pooled, centrifuged, and protease inhibitors were added (Frenkel & Ribbeck 2015). Mucins were purified using size-exclusion chromatography on separate Sepharose CL-2B columns. Mucin fractions were then desalted, concentrated, and lyophilized for storage at -80°C. Lyophilized mucins were reconstituted by shaking them gently at 4°C overnight in the desired medium. Mass spectrometry is routinely used to monitor the composition of purified mucin extracts (Caldara et al. 2012, Lieleg et al. 2012). This type of analysis has shown that mucin extracts purified from porcine stomach mucus, for example, are composed predominantly of MUC5AC, with small quantities of MUC2, MUC5B, and MUC6, as well as histones, actin, and albumin (Caldara et al. 2012, Lieleg et al. 2012).

Isolation of mucin oligosaccharides. This study applied non-reductive alkaline β -elimination ammonolysis to dissociate non-reduced glycans from mucins (Huang et al. 2001). Purified mucins were dissolved in ammonium hydroxide saturated with ammonium carbonate and incubated at 60 °C for 40 h to release oligosaccharide glycosylamines and partially deglycosylated mucins. Volatile salts were removed via repeated centrifugal evaporation and the oligosaccharide glycosylamines were separated from residual deglycosylated mucins via centrifugal filtration through 3-5 kDa molecular weight cut-off membranes in accordance with the manufacturer's instructions (Amicon Ultracel). The resulting oligosaccharide glycosylamines were converted to reducing oligosaccharide hemiacetals via treatment with boric acid. Residual boric acid was removed via repeated centrifugal evaporation from methanol. Oligosaccharides were further

purified via solid-phase extraction through Hypercarb mini-columns (ThermoFisher) and residual solvents were removed through centrifugal evaporation (Packer et al. 1998).

Capillary electrophoresis of oligosaccharides. Reducing oligosaccharides released from mucins were labeled via reductive amination with the fluorescent tag 8-aminopyrene-1,3,6-trisulfonic acid, sodium cyanoborohydride, and citric acid. Labeled oligosaccharides were analyzed with polyvinyl alcohol coated N-CHO capillaries in accordance with the manufacturer's (SciEx/Beckman) protocol using a PA800 (Beckman) capillary electrophoresis instrument, detected with laser-induced fluorescence, and analyzed with 32Karat software. The relative sizes of separated oligosaccharides were determined by comparison with migration times of glucose polymer standards. Chromatograms were constructed in GraphPad Prism (v7.04).

Capillary electrophoresis of monosaccharides. The monosaccharide composition of released mucin glycans was determined through established methods (Chen & Evangelista 1998, Guttman 1997). Briefly, neutral monosaccharides were obtained by hydrolysis in trifluoroacetic acid for 1 h at 80 °C. The liberated monosaccharides were labeled with 8-aminopyrene-1,3,6-trisulfonic acid via reductive amination as described for oligosaccharides. Monosaccharides were analyzed with capillary electrophoresis on a bare silica column and detected via laser-induced fluorescence. Monosaccharides were identified and quantified by comparison to a maltose internal standard and migration times and standard curves were generated using purified standard sugars. Chromatograms were constructed in GraphPad Prism (v7.04).

Matrix-assisted laser desorption/ionization time-of-flight (MALDI-TOF) and prediction of mucin-glycan structure. β -eliminated glycans were permethylated and analyzed at the Glycomics Core at Beth Israel Deaconess Medical Center as previously described (Taniguchi et al. 2017). Mass spectrometry data were acquired on an UltraFlex II MALDI-TOF Mass Spectrometer (Bruker Daltonics). Reflective positive mode was used, and data were recorded between 500 m/z and 6000 m/z . The mass spectrometry *O*-glycan profile was acquired by aggregating at least 20,000 laser shots. Mass peaks were manually annotated and assigned to a particular *O*-glycan composition based on known core structures.

RNA preparation. Total RNA was extracted using the MasterPure RNA Purification kit (Lucigen) and residual DNA was removed using the Turbo DNA-free kit (Ambion). The integrity

of the total RNA was assessed with an Agilent 2100 Bioanalyzer (Agilent Technologies). 16S, 23S, and 5S rRNA were removed using the Ribo-Zero Magnetic Kit (Bacteria) (Epicentre).

RNA sequencing. Gene expression analysis was conducted via Illumina RNA sequencing (RNA-seq). RNA-seq was conducted for three biological replicates. Libraries were produced using the KAPA RNA HyperPrep kit (Kapa Biosystems). Libraries were sequenced using the Illumina HiSeq platform with a single-end protocol and read lengths of 40 nt or 50 nt.

Analysis of sequencing data. Sequence reads were mapped onto the *P. aeruginosa* PAO1 reference genome, which is available for download from the Pseudomonas Genome Database (<http://www.pseudomonas.com>) using the Galaxy server (Afgan et al. 2018). Gene expression values were normalized based on library size and differentially expressed genes were identified using a negative binomial test with a false discovery rate (FDR) less than 0.05. Expression changes in signature virulence genes identified by RNA-seq were validated with quantitative PCR (qPCR), which revealed strong concordance between the two methods (Figure S2.4).

Functional category (pathway) assignments were downloaded from the Pseudomonas Genome Database. Pathway enrichment analysis was performed in MATLAB (R2016b) using the one-sided Mann-Whitney U test, where ranking was based on the log₂-transformed fold change.

Heatmaps and scatter plots of gene expression data were constructed in GraphPad Prism. Principle component analysis was performed in R (3.4.0) using the DESeq 2 workflow (Love et al. 2014). For all analyses of sequencing data, *p*-values were adjusted for multiple comparisons with the Benjamini-Hochberg correction to obtain the FDR.

High-throughput sequencing data presented in Figures 2.1 and 2.4 are deposited in the Gene Expression Omnibus (GEO) under accession number GSE136097.

qRT-PCR analysis. Primers used in this study are listed in Table S2.3. Quantitative reverse transcriptase PCR (qRT-PCR) was performed using a two-step method. First-strand cDNA was synthesized from total RNA using the ProtoScript II First Strand cDNA Synthesis kit (NEB). The cDNA was used as a template for qRT-PCR with a SYBR PowerUp Master Mix kit (Applied Biosystems by Life Technologies) on a Roche LightCycler 480 Real-Time PCR System. Primers for qRT-PCR were designed based on previously published literature or using the NCBI Primer-

BLAST tool (<https://www.ncbi.nlm.nih.gov/tools/primer-blast/>). The genes *rpoD* and *proC* were used as endogenous controls. The elimination of contaminating DNA was confirmed via qPCR amplification of *rpoD* on control samples that did not have reverse transcriptase added during cDNA synthesis. Melting-curve analyses were employed to verify single-product amplification. Change in gene expression was calculated based on mean change in qPCR cycle threshold (dCt) using the $\Delta\Delta\text{Ct}$ method (Fold change = $2^{-\Delta\Delta\text{Ct}}$).

Dispersal of static *P. aeruginosa* biofilms. Biofilm dispersal under static conditions *P. aeruginosa* biofilm dispersal was assayed as previously described (Co et al. 2018), with slight modification. Briefly, an overnight culture of PAO1-GFP or PAO1-GFP ΔfliD was diluted in ABTGC medium to an initial OD₆₀₀ of 0.01, added to a glass-bottom or plastic 96-well plate, and incubated for 48 h at 37 °C under static conditions. The supernatant containing non-adherent cells was removed from the plate and the biofilm remaining in each well was washed at least three times with 0.9% NaCl. Biofilms were exposed to whole mucus, the solubilization buffer, ABTGC medium alone, or ABTGC medium + 0.01% mucin glycans or monosaccharides. Biofilms were statically incubated at 37 °C for 3 h. Plates were washed three times with 0.9% NaCl and resuspended in ABTGC medium, then examined via microscopy to determine the remaining biofilm biomass. Viable dispersed cells were quantified via CFU counts on LB agar plates. Image acquisition was performed using a confocal laser scanning microscope (LSM 800; Zeiss) equipped with a 63×/1.4 NA oil immersion or a 100×/1.4 NA oil immersion objective. The excitation wavelength for GFP was 488 nm. At least five stacks were recorded for each well and at least three independent wells. Biofilm quantification was performed using COMSTAT (1.66).

Measurement of protease activity. Bacterial cultures were pelleted via centrifugation (13,200 × *g* for 3 min at room temperature), and supernatants were filtered-sterilized using a 0.2 μm filter.

Protease IV activity. The activity of protease IV in cell-free culture supernatants was measured via breakdown of the chromogenic substrate Chromozym PL (Roche), which reacts specifically with protease IV in *P. aeruginosa* culture supernatants (Caballero et al. 2004). Briefly, 10 μL pre-treated sample and 3 μL Chromozym PL (7 mM) were combined in reaction buffer (20 mM Tris/HCl, pH 8.0) to a total volume of 100 μL in a microwell plate. Plates were assayed on a SpectraMax M Series Multi-Mode Microplate Reader (Molecular Devices) pre-equilibrated to 30

°C by measuring the rate of increase in absorbance at 405 nm at 3-min intervals for 30 min. Protease IV activity was calculated using the following equation:

$$F \times E \times d \times \Delta A/\text{min},$$

where F is the dilution factor, E is the extinction coefficient (at 405 nm = 10.4), d is the path length (at 100 μL volume in a microtiter plate ≈ 0.53 cm), and $\Delta A/\text{min}$ is the maximum change in absorbance per min. The protease activity was normalized to account for variation in bacterial cell growth based on the optical density (absorbance at 600 nm) of the culture at 5 h. Relative changes were calculated based on the protease activity in medium alone.

Alkaline protease activity. Alkaline protease activity was tested using a modified method previously described (Howe and Iglewski 1984). Samples containing 1 mg of Hide powder azure (Sigma) dissolved in buffer (0.075 mL) consisting of 20 mM Tris/HCl, pH 8.0 and 1 mM CaCl_2 were mixed with 0.025 mL of the culture supernatants. The reaction mixtures (0.1 mL) were incubated at 37 °C for 1 h. Undissolved substrate was removed via centrifugation at $4000 \times g$ for 5 min. The absorbance of the reaction mixtures was determined at 595 nm on a SpectraMax M Series Multi-Mode Microplate Reader (Molecular Devices). Protease activity was expressed in terms of protease units per milliliter (U/mL), where one unit is equivalent to an increase in OD_{595} of 1.0 per hour at 37 °C. Protease activity was normalized to account for variation in bacterial cell growth based on the OD_{600} of the culture at 5 h. Relative changes were calculated based on the protease activity in medium alone.

Measurement of siderophore fluorescence. Pyoverdine and pyochelin levels were simultaneously quantified based on characteristic fluorescence spectra, as previously described (Dumas et al. 2013). Briefly, fluorescence was measured on a SpectraMax M Series Multi-Mode Microplate Reader (Molecular Devices). Pyoverdine production was quantified using an excitation wavelength of 400 nm and an emission wavelength of 460 nm. Pyochelin fluorescence was quantified using an excitation wavelength of 350 nm and an emission wavelength of 410 nm. To account for the background fluorescence of pyoverdine, pyochelin production was calculated using the equation:

$$z = w - 3\text{E-}7 \times y^2 - 0.0413 \times y,$$

where z is the actual value of pyochelin production, w is the fluorescence measured at excitation/emission 350/410, and y is the pyoverdine fluorescence measured at excitation/emission 400/460.

Quantification of bacterial growth and polystyrene-attached biomass. Growth curves were measured in microtiter plates on a SpectraMax M Series Multi-Mode Microplate Reader (Molecular Devices) by measuring the absorbance at 600 nm and by CFU counts. Adherent biomass was quantified using crystal violet (Junker & Clardy 2007). Cells attached to the wells of the plate were washed three times with 0.9% NaCl and stained with 0.01% crystal violet for 15 min at room temperature. Wells were washed three times with 0.9% NaCl. Ethanol was added to each well and the absorbance at 595 nm was measured after 15 min. The absorbance in each well was normalized based on the optical density of the culture at 5 h.

Human cell culture. Authenticated, mycoplasma-free HT-29 cells (ATCC® HTB38™), a human carcinoma cell line with epithelial morphology were obtained directly from the American Type Culture Collection (ATCC). Morphology was routinely monitored to verify cell line authenticity and cells were periodically tested for contamination by PCR. Cells were cultured in Dulbecco's Modified Eagle Medium GlutaMAX (DMEM) (Gibco) supplemented with 10% fetal bovine serum (FBS) (Gibco) at 37 °C in 5% CO₂–95% air. Cells were split 1:12 and passaged as the culture reached confluence. To prepare for co-culture with bacteria, HT-29 cells were detached from the growth surface with 0.25% trypsin–1 mM EDTA (Gibco), resuspended in DMEM+FBS, counted, diluted to the appropriate density in DMEM+FBS, and seeded in 96-well plates to confluence (approximately 5×10^5 HT-29 cells).

Examination of bacterial interactions with epithelial cells. In all experiments, control and experimental HT-29 cells were identically treated except that co-culture medium did not contain bacteria in the uninfected controls. Bacteria were co-cultured with HT-29 cell monolayers at an initial multiplicity of infection (MOI) of 20 (1×10^7 CFU) for 1-8 h. Subsequently, HT-29 cells were processed and assayed in the cell-function assays described below.

Analysis of bacterial attachment. After 1 h of co-culture, non-adherent bacteria in the supernatant were aspirated and quantified by serial dilution as CFUs. HT-29 cell monolayers were washed three times with phosphate-buffered saline (PBS) (Gibco), and cells were lysed with 1% Triton X-

100 (Sigma) and removed from the growth surface. Attached bacteria were serially diluted in PBS and quantified as CFUs.

Epithelial cytotoxicity assay. HT-29 cell killing by *P. aeruginosa* was measured using the membrane impermeable nuclear stain propidium iodide (PI), which allows continuous quantitative measurement of cell viability over time, owing to its optimal linear DNA-binding, without background from bacterial cell death (Figure S2.14). After co-culture of 1-10 h, PI fluorescence (excitation/emission 535/617 nm) was measured on a SpectraMax M Series Multi-Mode Microplate Reader (Molecular Devices). Between measurements, plates were kept in an incubator at 37 °C, 5% CO₂-95% air. At the end of the experiment, maximal fluorescence was measured following treatment of each well with 1% Triton X-100 to permeabilize all cells and label all nuclei with PI, which corresponds to 100% cell death. Background fluorescence of PI was measured in uninfected control cells (exposed to medium alone or the appropriate concentration of MUC5AC) at the beginning of the experiment. Percentage cytotoxicity was calculated as:

$$(f - f_0) / (M - f_0) \times 100,$$

where f_0 is the initial fluorescence, M is the maximum fluorescence after addition of Triton X-100, and f is the fluorescence at any given time. Mucin dose response curves were assessed at 7.5 h.

Confocal imaging. Image acquisition was performed using a confocal laser scanning microscope (LSM 800; Zeiss) equipped with a 63×/1.4 NA oil immersion or a 100×/1.4 NA oil immersion objective. Images were analyzed with Zeiss ZEN 2.1 imaging software. The excitation wavelengths for GFP and PI were 488 nm and 535 nm, respectively. 3D images of attached and non-attached cells were created with IMARIS 7.7.2. Plots were generated in GraphPad Prism. Quantification of bacterial aggregate volume was performed using COMSTAT (1.66).

Examination of bacterial interactions with porcine burn wounds. Interactions between *P. aeruginosa* and full-thickness burn wounds were assessed as previously described (Roy et al. 2014). Briefly, Female Yorkshire pigs ($n = 4$) weighing between 70 and 80 pounds were anesthetized and the dorsal trunk was shaved and surgically prepared. Under aseptic conditions, six 2”x2” inch full-thickness burn wounds were created on the back of the pig using an electrically heated burn device with controlled pressure delivery for 50 s. One day after the thermal injury,

mid-log phase cultures of *P. aeruginosa* were topically inoculated onto the wound site at a concentration of 1×10^5 CFU in 250 μ L of 20% PF-127 (Sigma) prepared in phosphate-buffered saline with 0, 0.05% (0.5 mg/mL), or 0.5% (5.0 mg/mL) MUC5AC or 0.01% (0.1 mg/mL) MUC5AC glycans or monosaccharides. The inoculated and treated wound was rubbed with a sterile spatula for 30 s. On days 1 and 4 after inoculation, treatment was reapplied to the wound. On days 1 and 7 after inoculation, full-thickness wound-tissue biopsies were collected for microbiological analysis using a 6 mm sterile disposable punch biopsy tool. Treatments for each wound site were randomized, and not blinded.

Viable bacterial counts were determined from three randomly selected 6 mm punch biopsies from each wound site. Biopsies were weighed and placed in separate sterile polypropylene culture test tubes containing 1 mL of PBS. All samples were homogenized with a Pro Scientific Bio-Gen Series Pro200 hand-held homogenizer for 45 s. The resulting solutions were serially diluted and plated on Pseudomonas Isolation Agar PIA-rifampicin (100 μ g/mL) in at least triplicate and incubated at 37 °C overnight. CFU were calculated per gram of tissue. Since the data were not normally distributed, non-parametric Kruskal-Wallis one-way analysis of variance was used.

All care of laboratory animals was in accordance with institutional guidelines, and approved by the Ohio State University Institutional Laboratory Animal Care and Use Committee (ILACUC) under protocol 2008A0012-R1.

Statistical analysis. Unless noted otherwise, experiments were done with at least three biological replicates consisting of at least three technical replicates and results are presented as mean \pm standard error. Statistical significance was assessed by an ordinary one-way ANOVA, followed by Dunnett's multiple comparisons test, or a one-sample Student's *t* test for normalized data unless otherwise noted. Adjusted *p*-values <0.05 were considered significant.

References

- Afgan E, Baker D, van den Beek M, Blankenberg D, Bouvier D, et al. 2016. The Galaxy platform for accessible, reproducible and collaborative biomedical analyses: 2016 update. *Nucleic Acids Res.* 44(W1):W3–10
- Arora SK, Ritchings BW, Almira EC, Lory S, Ramphal R. 1998. The *Pseudomonas aeruginosa* flagellar cap protein, FliD, is responsible for mucin adhesion. *Infect. Immun.* 66(3):1000–1007
- Balasubramanian D, Schneper L, Kumari H, Mathee K. 2013. A dynamic and intricate regulatory network determines *Pseudomonas aeruginosa* virulence. *Nucleic Acids Res.* 41(1):1–20
- Basu Roy A, Sauer K. 2014. Diguanylate cyclase NicD-based signalling mechanism of nutrient-induced dispersion by *Pseudomonas aeruginosa*. *Mol. Microbiol.* 94(4):771–93
- Caballero A, Thibodeaux B, Marquart M, Traidej M, O’Callaghan R. 2004. *Pseudomonas* Keratitis: Protease IV Gene Conservation, Distribution, and Production Relative to Virulence and Other *Pseudomonas* Proteases. *Investig. Ophthalmol. Vis. Sci.* 45(2):522–30
- Caldara M, Friedlander RS, Kavanaugh NL, Aizenberg J, Foster KR, Ribbeck K. 2012. Mucin biopolymers prevent bacterial aggregation by retaining cells in the free-swimming state. *Curr. Biol.* 22(24):2325–30
- Cattoir V, Narasimhan G, Skurnik D, Aschard H, Roux D, et al. 2012. Transcriptional response of mucoid *Pseudomonas aeruginosa* to human respiratory mucus. *MBio.* 3(6):1–10
- Chen F-TA, Evangelista RA. 1998. Profiling glycoprotein N-linked oligosaccharide by capillary electrophoresis. *Electrophoresis.* 19(15):2639–44
- Chua SL, Hultqvist LD, Yuan M, Rybtke M, Nielsen TE, et al. 2015. In vitro and in vivo generation and characterization of *Pseudomonas aeruginosa* biofilm-dispersed cells via c-di-GMP manipulation. *Nat. Protoc.* 10(8):1165–80
- Cummings RD, Pierce JM. 2014. The challenge and promise of glycomics. *Chem. Biol.* 21(1):1–15
- Dohrman A, Miyata S, Gallup M, Li JD, Chapelin C, et al. 1998. Mucin gene (MUC 2 and MUC 5AC) upregulation by Gram-positive and Gram-negative bacteria. *Biochim. Biophys. Acta - Mol. Basis Dis.* 1406(3):251–59
- Duan K, Surette MG. 2007. Environmental regulation of *Pseudomonas aeruginosa* PAO1 las and Rhl quorum-sensing systems. *J. Bacteriol.* 189(13):4827–36
- Dumas Z, Ross-Gillespie A, Kümmerli R. 2013. Switching between apparently redundant iron-uptake mechanisms benefits bacteria in changeable environments. *Proc. R. Soc. B Biol. Sci.* 280(1764):20131055
- Frenkel ES, Ribbeck K. 2015. Salivary mucins protect surfaces from colonization by cariogenic bacteria. *Appl. Environ. Microbiol.* 81(1):332–38
- Guttman A. 1997. Analysis of monosaccharide composition by capillary electrophoresis. *J. Chromatogr. A.* 763(1–2):271–77

- Holmen Larsson JM, Thomsson KA, Rodriguez-Pineiro AM, Karlsson H, Hansson GC. 2013. Studies of mucus in mouse stomach, small intestine, and colon. III. Gastrointestinal Muc5ac and Muc2 mucin O-glycan patterns reveal a regiospecific distribution. *AJP Gastrointest. Liver Physiol.* 305(5):G357–63
- Howe TR, Iglewski BH. 1984. Isolation and characterization of alkaline protease-deficient mutants of *Pseudomonas aeruginosa* in vitro and in a mouse eye model. *Infect. Immun.* 43(3):1058–63
- Huang Y, Mechref Y, Novotny M V. 2001. Microscale nonreductive release of O-linked glycans for subsequent analysis through MALDI mass spectrometry and capillary electrophoresis. *Anal. Chem.* 73(24):6063–69
- Jimenez PN, Koch G, Thompson JA, Xavier KB, Cool RH, Quax WJ. 2012. The multiple signaling systems regulating virulence in *Pseudomonas aeruginosa*. *Microbiol. Mol. Biol. Rev.* 76(1):46–65
- Jin C, Kenny DT, Skoog EC, Padra M, Adamczyk B, et al. 2017. Structural diversity of human gastric mucin glycans. *Mol. Cell. Proteomics.* 16(5):743–58
- Junker LM, Clardy J. 2007. High-throughput screens for small-molecule inhibitors of *Pseudomonas aeruginosa* biofilm development. *Antimicrob. Agents Chemother.* 51(10):3582–90
- Karlsson NG, Nordman H, Karlsson H, Carlstedt I, Hansson GC. 1997. Glycosylation differences between pig gastric mucin populations: a comparative study of the neutral oligosaccharides using mass spectrometry. *Biochem. J.* 326:911–17
- Kavanaugh NL, Zhang AQ, Nobile CJ, Johnson AD, Ribbeck K. 2014. Mucins suppress virulence traits of *Candida albicans*. *MBio.* 5(6):1–8
- Kerschner J, Hong W, Khampang P, Johnston N. 2014. Differential response of gel-forming mucins to pathogenic middle ear bacteria. *Int J Pediatr Otorhinolaryngol.* 78(8):1368–73
- Landry RM, An D, Hupp JT, Singh PK, Parsek MR. 2006. Mucin-*Pseudomonas aeruginosa* interactions promote biofilm formation and antibiotic resistance. *Mol. Microbiol.* 59(1):142–51
- Lee SH, Yu SY, Nakayama J, Khoo KH, Stone EL, et al. 2010. Core2 O-glycan structure is essential for the cell surface expression of sucrose isomaltase and dipeptidyl peptidase-IV during intestinal cell differentiation. *J. Biol. Chem.* 285(48):37683–92
- Li JD, Dohrman a F, Gallup M, Miyata S, Gum JR, et al. 1997. Transcriptional activation of mucin by *Pseudomonas aeruginosa* lipopolysaccharide in the pathogenesis of cystic fibrosis lung disease. *Proc. Natl. Acad. Sci. U. S. A.* 94(3):967–72
- Lieleg O, Lieleg C, Bloom J, Buck CB, Ribbeck K. 2012. Mucin biopolymers as broad-spectrum antiviral agents. *Biomacromolecules.* 13(6):1724–32
- Love MI, Huber W, Anders S. 2014. Moderated estimation of fold change and dispersion for RNA-seq data with DESeq2. *Genome Biol.* 15(12):
- McNamara N, Khong A, McKemy D, Caterina M, Boyer J, et al. 2001. ATP transduces signals from ASGM1, a glycolipid that functions as a bacterial receptor. *Proc. Natl. Acad. Sci. U. S. A.* 98(16):9086–91

- Nakano M, Saldanha R, Göbel A, Kavallaris M, Packer NH. 2011. Identification of Glycan Structure Alterations on Cell Membrane Proteins in Desoxyepothilone B Resistant Leukemia Cells. *Mol. Cell. Proteomics*. 10(11):M111.009001
- Packer NH, Lawson MA, Jardine DR, Redmond JW. 1998. A general approach to desalting oligosaccharides released from glycoproteins. *Glycoconj. J.* 15(8):737–47
- Parsek MR, Singh PK. 2003. Bacterial Biofilms: An Emerging Link to Disease Pathogenesis. *Annu. Rev. Microbiol.* 57(1):677–701
- Roy S, Elgharably H, Sinha M, Ganesh K, Chaney S, et al. 2014. Mixed-species biofilm compromises wound healing by disrupting epidermal barrier function. *J. Pathol.* 233(4):331–43
- Sadikot RT, Blackwell TS, Christman JW, Prince AS. 2005. Pathogen-host interactions in pseudomonas aeruginosa pneumonia. *Am. J. Respir. Crit. Care Med.* 171(11):1209–23
- Secor PR, Michaels LA, Ratjen A, Jennings LK, Singh PK. 2018. Entropically driven aggregation of bacteria by host polymers promotes antibiotic tolerance in *Pseudomonas aeruginosa*. *Proc. Natl. Acad. Sci.* 115(42):10780-10785
- Taniguchi T, Woodward AM, Magnelli P, McColgan NM, Lehoux S, et al. 2017. N-Glycosylation affects the stability and barrier function of the MUC16 mucin. *J. Biol. Chem.* 292(26):11079–90
- Toyofuku M, Nomura N, Fujii T, Takaya N, Maseda H, et al. 2007. Quorum sensing regulates denitrification in *Pseudomonas aeruginosa* PAO1. *J. Bacteriol.* 189(13):4969–72
- Van Der Reijden WA, Veerman ECI, van Nieuw Amerongen A. 1994. Rheological Properties of Commercially Available Polysaccharides With Potential Use in Saliva Substitutes. *Biorheology*. 31(6):631–42
- Varki A. 2017. Biological roles of glycans. *Glycobiology*. 27(1):3–49
- Ventre I, Goodman AL, Vallet-Gely I, Vasseur P, Soscia C, et al. 2006. Multiple sensors control reciprocal expression of *Pseudomonas aeruginosa* regulatory RNA and virulence genes. *Proc. Natl. Acad. Sci.* 103(1):171-6
- Wagner CE, Wheeler KM, Ribbeck K. 2018. Mucins and Their Role in Shaping the Functions of Mucus Barriers. *Annu Rev Cell Dev Biol.* 34(1):189-215
- Xia B, Royall JA, Damera G, Sachdev GP, Cummings RD. 2005. Altered O-glycosylation and sulfation of airway mucins associated with cystic fibrosis. *Glycobiology*. 15(8):747–75
- Yamada K, Kinoshita M. 2009. Comparative studies on the structural features of O-glycans between leukemia and epithelial cell lines. *J Proteome Res.* 8:521–37

Acknowledgements

We thank S. Lory for comments and Life Science Editors for editing assistance. This research was supported by NIBIB/NIH grant R01 EB017755-04 (OSP 6940725), the National Science

Foundation Career award PHY-1454673, funding from the Deshpande Center for Technological Innovation and the MRSEC Program of the National Science Foundation under award DMR-1419807 (to K.R.), NIH grant P41GM103694 (to R.D.C.) and NIEHS/NIH grant P30-ES002109. D.J.W. is supported by NIH grants R01AI34895 and R01AI097511. This material is based on research supported by the National Science Foundation Graduate Research Fellowship under grant no. 1745302 and the MIT/NIGMS Biotechnology Training Program grant 5T32GM008334-28 (to K.M.W.). G.C.-O. is supported by the Early Postdoc Mobility Fellowship of the Swiss National Science Foundation (grant no. P2ZHP3_164844).

Figures

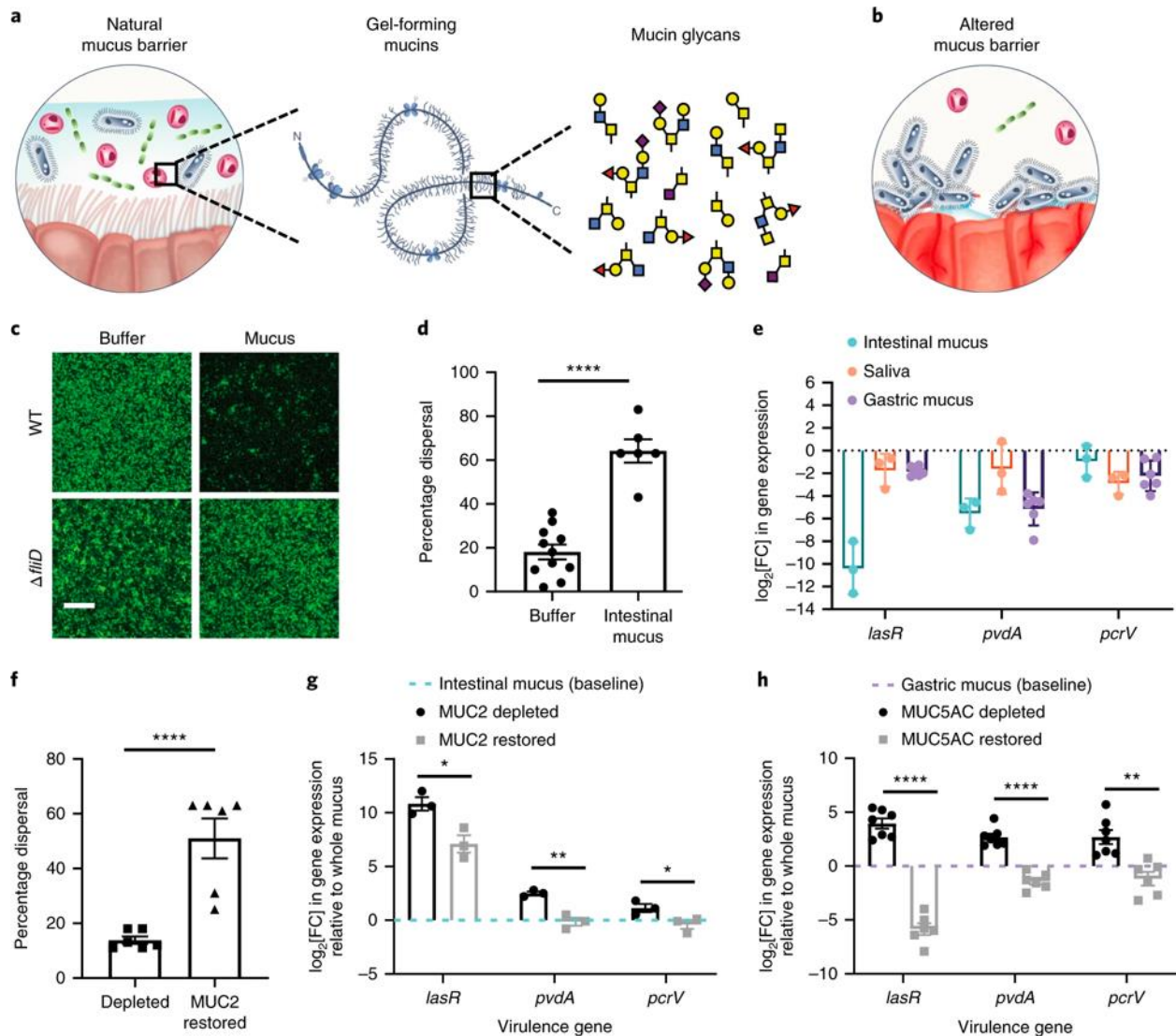


Figure 2.1. Native whole mucus suppresses virulence traits in the opportunistic pathogen *P. aeruginosa*. **a**, The natural mucus barrier (left) hosts a diverse range of microorganisms while limiting infections at the mucosa. Mucins (middle) are the major structural component of mucus and are densely grafted with complex glycans (right). **b**, Defects in mucus production are associated with disease and biofilm formation. **c**, Representative images of green fluorescent protein (GFP)-expressing *P. aeruginosa* biofilms after 3 h treatment with either buffer or native mucus reveal that native intestinal mucus reduces the biomass of biofilm in the wild-type (WT) strain, but not in the flagellar mutant ($\Delta fliD$). Similar results were observed in different fields of view across three independent replicates. Scale bar, 20 μm . **d**, Native intestinal mucus solutions disperse biofilm biomass into the planktonic state. Percentage dispersal is based on the ratio of planktonic cells to total biomass (planktonic cells + remaining biofilm cells). Data are from $n = 12$ (buffer) and $n = 6$ (intestinal mucus) biologically independent replicates. Data are mean \pm s.e.m.; significance was assessed using two-sided

Student's *t*-tests; **** $P < 0.0001$. **e**, Native mucus solutions suppress key virulence traits relative to mucus solubilization buffer. **f**, The depletion of intestinal mucus components of ≥ 100 kDa prevents biofilm dispersal. Supplementation of mucus filtrates with exogenous purified MUC2 partially restores biofilm dispersal. Data are mean \pm s.e.m. and were calculated from six biologically independent replicates. **g**, The depletion of intestinal mucus components of ≥ 100 kDa results in increased expression of virulence genes. Supplementation of mucus filtrates with exogenous purified MUC2 partially restores the downregulation of virulence genes. * $P < 0.05$, ** $P < 0.01$. **h**, The depletion of gastric mucus components of ≥ 100 kDa increases the expression of virulence genes. Supplementation of mucus filtrates with exogenous purified MUC5AC restores the downregulation of virulence genes. For **e,g,h**, data are \log_2 -transformed qPCR measurements of relative gene expression (fold change (FC)); data are mean \pm s.e.m. and were calculated from $n = 6$ (gastric mucus), $n = 3$ (intestinal mucus) and $n = 3$ (saliva) biologically independent replicates. For **g,h**, significance was assessed using two-sided Student's *t*-tests followed by multiple comparison correction using the Holm–Sidak method.

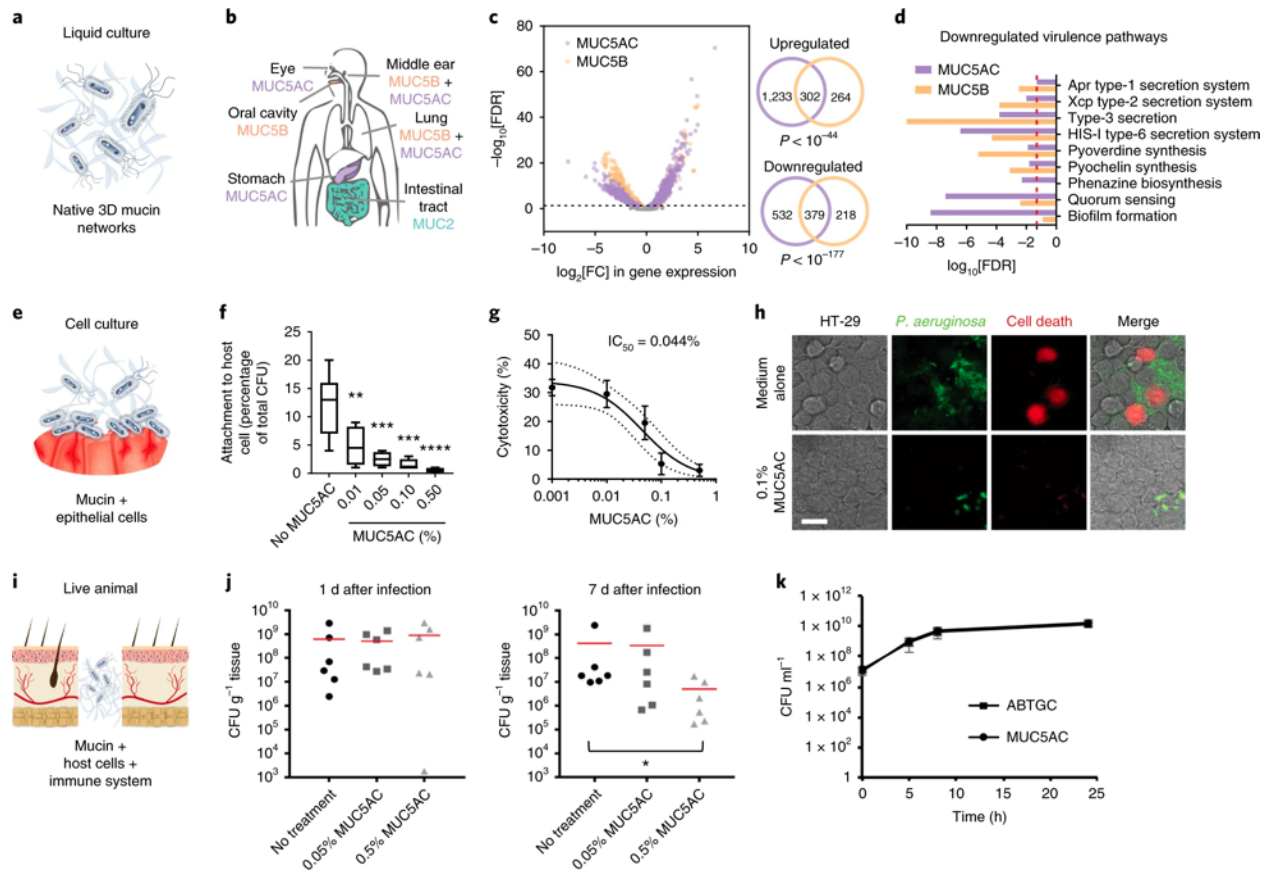


Figure 2.2. Mucins are sufficient to attenuate *P. aeruginosa* virulence *in vitro* and *in vivo*. **a**, Gene expression was evaluated in liquid culture with or without the native mucin network. **b**, The predominant gel-forming mucins secreted into mucosal niches throughout the body. The sources of mucin used in this study are highlighted. **c**, MUC5AC and MUC5B elicit global transcriptional responses in *P. aeruginosa* PAO1. Fold-change data are average measurements. FDR-adjusted *P* values were determined using the Benjamini–Hochberg *P*-value adjustment method. Data are from $n=6$ (no mucin treatment), $n=3$ (MUC5AC-treated) and $n=3$ (MUC5B-treated) biologically independent replicates. Correspondence plots of the fold-change values are provided in Figure S2.2. Principal component analysis of expression data is provided in Figure S2.13. The Venn diagrams contain the total number of genes that are differentially expressed (FDR-adjusted $P < 0.05$) after exposure to 0.5% w/v MUC5AC (purple) or MUC5B (orange). The significance of overlap was assessed using a hypergeometric test. Functional enrichment analysis of the non-overlapping regions of the Venn diagrams is provided Figure S2.2. **d**, Functional enrichment analyses identify key virulence pathways among downregulated genes. Significance of enrichment was assessed using one-sided Mann–Whitney *U*-tests, for which ranking was calculated on the basis of mean \log_2 -transformed fold changes from $n=6$ (no mucin treatment), $n=3$ (MUC5AC-treated) and $n=3$ (MUC5B-treated) biologically independent replicates. Bars, FDR-adjusted *P* values. The red dashed line indicates FDR-adjusted $P = 0.05$. **e**, *P. aeruginosa* pathogenicity was evaluated in cell culture (containing a single human epithelial cell type, HT-29). **f**, Exposure to increasing MUC5AC concentrations inhibited *P. aeruginosa* attachment to HT-29 cells. The centre line indicates the

median, the box limits indicate the upper and lower quartiles and the whiskers indicate 1.5× the interquartile range. Data are from $n = 7$ (no MUC5AC), $n = 4$ (0.01% MUC5AC), $n = 4$ (0.05% MUC5AC), $n = 4$ (0.1% MUC5AC) and $n = 7$ (0.5% MUC5AC) biologically independent replicates. Significance was assessed in relation to the medium-alone control using ordinary one-way analysis of variance (ANOVA), followed by Dunnett's multiple comparisons test; *** $P < 0.001$. **g**, MUC5AC protects HT-29 epithelial cells from death in a concentration-dependent manner. Dotted lines indicate the 95% confidence interval for the dose-response curve. Data are based on bulk measurements of propidium iodide fluorescence 7.5 h after infection. Data are mean \pm s.e.m.; $n = 4$ biologically independent replicates. IC_{50} , half-maximum inhibitory concentration. **h**, MUC5AC maintains the intact epithelial cell monolayer and prevents the onset of HT-29 cellular rounding, bacterial attachment and HT-29 death. Representative confocal microscopy of HT-29 epithelial cells (bright field), GFP-expressing *P. aeruginosa* PAO1 cells (green) and propidium iodide staining (red) after exposing HT-29 cells to *P. aeruginosa* for 5 h (top, medium alone) or 6 h (bottom, medium with MUC5AC) as indicated. Similar results were observed in different fields of view across three independent replicates. Scale bar, 20 μ m. **i**, Bacterial viability was monitored in a live dermal wound model (containing living tissue, immune cells and secreted factors). **j**, Bacterial burden on porcine burn wounds decreases after treatment with 0.5% MUC5AC for 7 d. Symbols represent *P. aeruginosa* PAO1 burden on six individual biopsies collected from two pigs following no treatment (circle), treatment with 0.05% MUC5AC (square) or treatment with 0.5% MUC5AC (triangle). The centre bars indicate the mean bacterial burden. Significance was assessed using Kruskal–Wallis tests followed by Dunn's multiple comparisons test. **k**, MUC5AC in isolation does not alter *P. aeruginosa* viability relative to medium alone. Data are mean CFU \pm s.e.m., $n = 3$ biologically independent replicates.

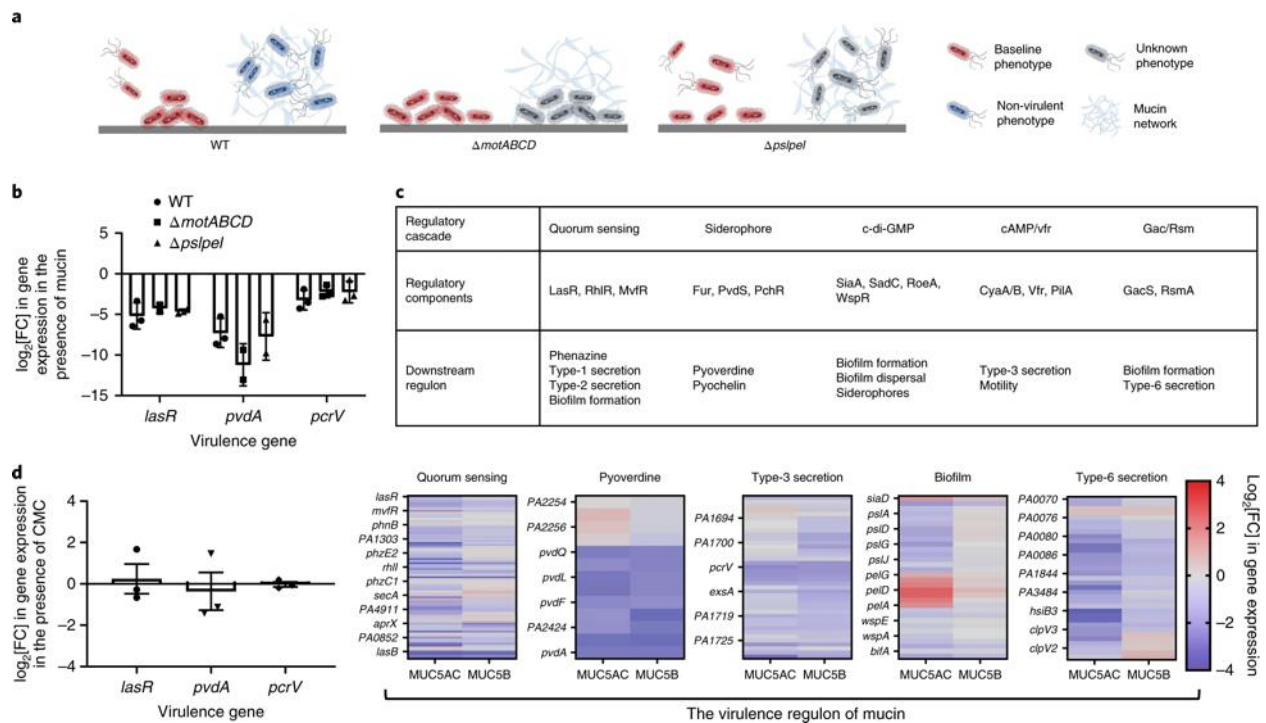


Figure 2.3. The virulence systems suppressed by mucin are downstream of multiple distinct regulatory cascades, and regulation of these systems is independent of bacterial motility and aggregation. **a**, Mucin promotes a motile non-aggregated phenotype and suppresses virulence in *P. aeruginosa* PAO1. To determine whether the changes to virulence are caused by a shift in motility or aggregation, we monitored the virulence phenotype of non-motile ($\Delta motABCD$) and non-aggregative ($\Delta pslpel$) mutants after exposure to mucin. **b**, Downregulation of the expression of virulence genes by mucin does not require a shift in motility or aggregation, indicating that it is a parallel effect of mucin. Data are \log_2 -transformed qPCR measurements of relative gene expression \pm s.e.m.; $n = 3$ biologically independent replicates. Significance was assessed using two-tailed t -tests followed by Holm–Sidak correction for multiple comparisons; no significant difference in \log_2 [fold change] was found between the WT and mutants. **c**, The virulence regulon of mucin is downstream of multiple interconnected regulatory cascades. **d**, CMC does not differentially regulate virulence genes. Data are \log_2 -transformed qPCR measurements of relative gene expression \pm s.e.m.; $n = 3$ biologically independent replicates. Significance was assessed using one-sample two-tailed t -tests followed by Bonferroni correction for multiple comparisons; no significant difference in \log_2 [fold change] was found between CMC and medium alone.

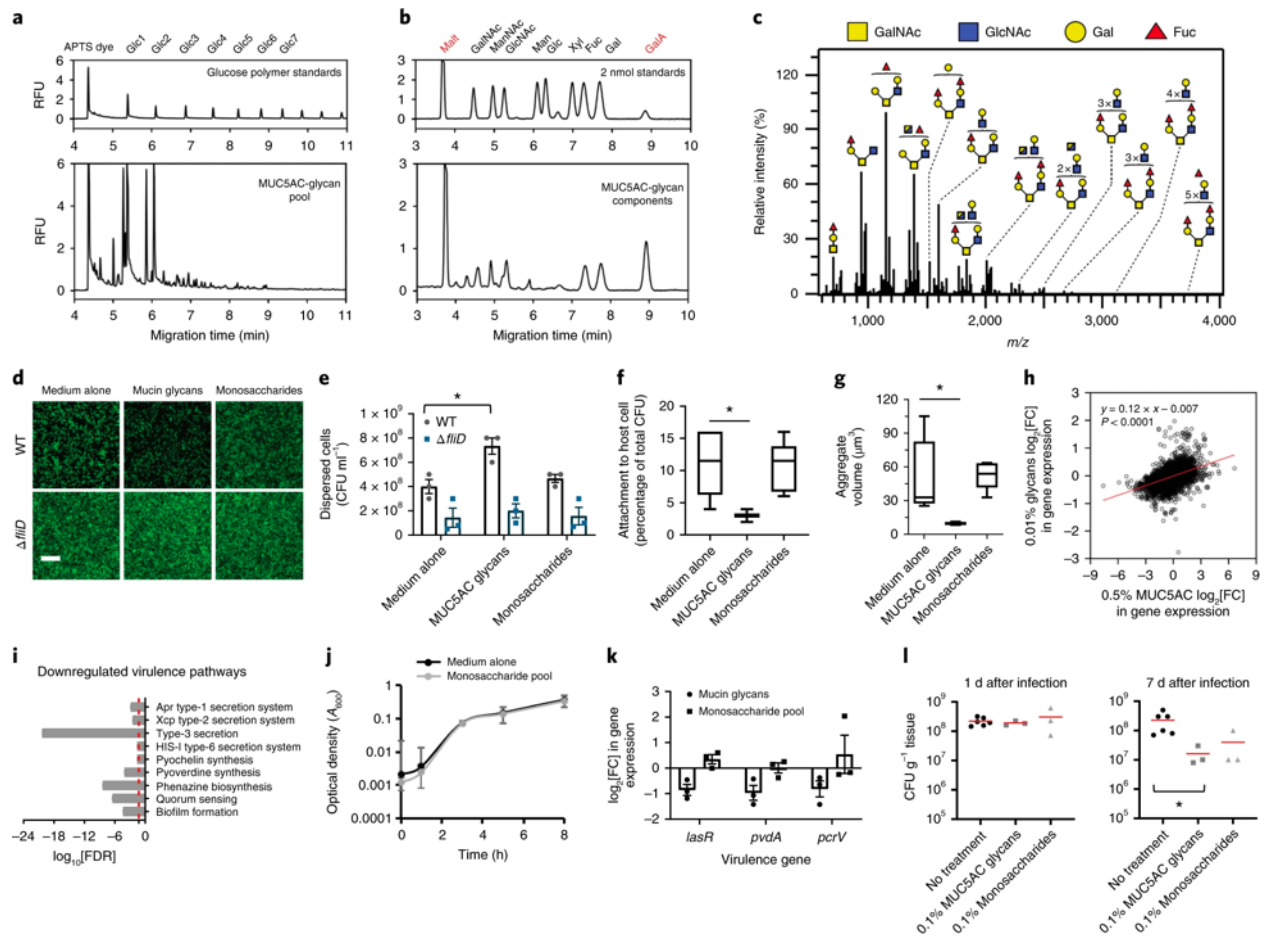


Figure 2.4. Complex *O*-linked glycans are the major regulatory component of MUC5AC. **a**, Oligosaccharides released by alkaline β -elimination were resolved using capillary electrophoresis. The mucin glycan pool includes extended chains consisting of >7 residues (bottom). Top, glucose (Glc) polymer standards. **b**, Monosaccharide composition of mucin glycans was assessed using capillary electrophoresis (bottom). These mucin oligosaccharides are predominantly *O*-linked, as evidenced by the ratio of mannose (Man; *N*-linked) to *N*-acetylgalactosamine (GalNAc; *O*-linked). The red labels indicate the quantification standard maltose (Malt) and the migration standard galacturonic acid (GalA). Migration times for monosaccharide standards (top) were as follows: *N*-acetylgalactosamine, 4.5 min; *N*-acetylmannosamine (ManNAc) from *N*-acetylneuraminic acid, 4.95 min; *N*-acetylglucosamine (GlcNAc), 5.26 min; mannose, 6.08 min; glucose (Glc), 6.33 min; xylose (Xyl), 6.99 min; fucose (Fuc), 7.29 min; and galactose (Gal), 7.67 min. **c**, MALDI-TOF spectrum of *O*-linked glycans from MUC5AC. The complete list of *O*-linked glycan structures with experimental and theoretical masses is provided in Table S2.2. For **a–c**, similar results were observed in three independent replicates. **d**, Representative images of GFP-expressing *P. aeruginosa* biofilms after a 3 h treatment with medium alone, 0.01% mucin glycans or a 0.01% pool of monosaccharides. Glycan solutions reduce biofilm biomass in the WT strain, but not the flagellar mutant ($\Delta fliD$). Similar results were observed in different fields of view across three independent replicates. Scale bar, 20 μm . **e**, Mucin glycans, but not monosaccharides,

disperse biofilm biomass into the planktonic state for the WT strain, but not the flagellar mutant (*ΔfliD*). Data are mean \pm s.e.m.; $n = 3$ biologically independent replicates. Significance was assessed in relation to the medium-alone control using ordinary one-way ANOVA followed by Dunnett's multiple comparisons test. **f**, Mucin glycans inhibit bacterial attachment to human epithelial HT-29 cells. The centre line indicates the median, the box limits indicate the upper and lower quartiles and the whiskers indicate 1.5 \times the interquartile range. Data are from $n = 6$ (medium alone), $n = 3$ (MUC5AC glycans) and $n = 6$ (monosaccharides) biologically independent replicates. Significance was assessed in relation to the medium-alone control using ordinary one-way ANOVA, followed by Dunnett's multiple comparisons test. **g**, Relative size distributions of aggregates were identified using live 3D confocal microscopy and analysed using IMARIS. In medium alone and medium with monosaccharides, *P. aeruginosa* biomass is concentrated in large surface-associated aggregates, whereas MUC5AC glycans suppress the formation of aggregates. The centre line indicates the median, the box limits indicate the upper and lower quartiles and the whiskers indicate 1.5 \times the interquartile range. Data are average aggregate sizes compiled from six separate z-stacks. Significance was assessed using the Kruskal–Wallis test followed by Dunn's multiple comparisons test. **h**, Low concentrations of MUC5AC glycans elicit a transcriptional response that positively correlates with transcriptional changes elicited by whole MUC5AC. Fold-change data are average measurements from three biologically independent replicates. Significance was assessed using a regression slope test. **i**, Free glycans suppress the same virulence pathways as whole mucin. The significance of enrichment was assessed using Mann–Whitney *U*-tests, for which ranking was calculated on the basis of mean \log_2 -transformed fold changes from three biologically independent replicates. **j**, Growth is not altered by the presence of the monosaccharide components in mucin glycans. Data are mean optical density at 600 nm (OD_{600}) \pm s.e.m.; $n = 3$ biologically independent replicates. **k**, Complex mucin glycans, but not their monosaccharide components, induce expression changes in signature virulence genes. Data are qPCR measurements of relative gene expression \pm s.e.m., $n = 3$ biologically independent replicates. **l**, Bacterial burden on porcine burn wounds decreases after treatment with 0.1% mucin glycans for 7 d. Symbols represent the burden of *P. aeruginosa* PAO1 on individual biopsies collected from burn wounds following no treatment (circle, $n = 6$), treatment with 0.1% MUC5AC glycans (square, $n = 3$) or treatment with 0.1% monosaccharides (triangle, $n = 3$). The centre bar indicates the mean bacterial burden. Significance was assessed in relation to the no-treatment control using Kruskal–Wallis tests followed by Dunn's multiple comparisons test.

Chapter 3: Mucin glycans signal through the sensor kinase RetS to inhibit virulence-associated traits in *Pseudomonas aeruginosa*

This chapter has been published in: Wang BX*, Wheeler KM*, Cady KC, Lehoux S, Cummings RD, Laub MT, Ribbeck K. Mucin glycans signal through the sensor kinase RetS to inhibit virulence-associated traits in *Pseudomonas aeruginosa*. *Current Biology*. 2020.

Supplementary information is provided in Appendix B.

Abstract

Mucus is a densely populated ecological niche that coats all non-keratinized epithelia, and plays a critical role in protecting the human body from infections. Although traditionally viewed as a physical barrier, emerging evidence suggests that mucus can directly suppress virulence-associated traits in opportunistic pathogens including *Pseudomonas aeruginosa*. However, the molecular mechanisms by which mucus affords this protection are unclear. Here, we show that mucins, and particularly their associated glycans, signal through the Dismed2 domain of the sensor kinase RetS in *P. aeruginosa*. We find that this RetS-dependent signaling leads to the direct inhibition of the GacS-GacA two-component system, the activity of which is associated with a chronic infection state. This signaling includes downregulation of the type VI secretion system (T6SS), and prevents T6SS-dependent bacterial killing by *P. aeruginosa*. Overall, these results shed light on how mucus impacts *P. aeruginosa* behavior in the human host, and may inspire novel approaches for controlling *P. aeruginosa* infections.

Introduction

Mucus, a viscous matrix that coats non-keratinized epithelial surfaces (Wagner et al. 2018), represents a critical interface for host-microbe interactions in the human body, serving as a home for trillions of our commensal microbes (Barko et al. 2018; Tropini et al. 2017), while simultaneously acting as the first line of defense against invading pathogens (Pelaseyed et al. 2014; Zanin et al. 2016). The ability of select pathogens to compromise the mucus barrier has been studied to some degree (Celli et al. 2009; Hews et al. 2017; In et al. 2016; Li et al. 2019; Liu et al. 2008). However, the mechanisms by which healthy mucus protects against unwanted invaders are poorly understood (Figure 3.1A).

While mucus has historically been viewed as a simple physical barrier, recent work has suggested that mucins, the major gel-forming components of mucus, may be potent regulators of microbial behavior that can attenuate virulence in a variety of pathogens without affecting viability (Frenkel & Ribbeck 2015; Kavanaugh et al. 2014; Wheeler et al. 2019). For example, the opportunistic pathogen *Pseudomonas aeruginosa* chronically colonizes certain diseased mucus environments such as the cystic fibrosis (CF) lung (Oliver et al. 2000), but is generally unable to infect the mucus barriers of healthy individuals. Recent work has shown that exposure of *P. aeruginosa* to purified mucins triggers the suppression of many virulence pathways including quorum sensing and the type III secretion system (T3SS) (Wheeler et al. 2019), but the molecular mechanisms underlying this response have not been identified.

Mucins are densely modified proteins with complex branched O-linked glycan structures, which represent up to 80% of the molecular mass of the mature glycoprotein (Brockhausen et al. 2009). These O-glycans are primarily built from five monosaccharide components (galactose, N-acetylglucosamine (GlcNAc), N-acetylgalactosamine (GalNAc), fucose, sialic acid) that are assembled on a core serine- or threonine-bound GalNAc. This assembly process leads to remarkable glycan heterogeneity and diversity, with over 200 distinct structures identified on mucins (Jin et al. 2017). Thus, mucins represent a rich source of potential regulatory signals for *P. aeruginosa* and other bacteria, but if, and how, *P. aeruginosa* senses and responds to these mucus-derived signals is unclear (Figure 3.1A).

One possibility is that *P. aeruginosa* may sense mucin glycans via one of its many two-component systems. Two-component systems are typically comprised of a histidine kinase that senses an environmental signal and a cognate response regulator that triggers changes in gene expression (Capra & Laub 2012). Although the signals that activate many of the two-component systems in *P. aeruginosa* are unknown, the histidine kinase RetS may respond to sugars (Anantharaman & Aravind 2003), making it a candidate for sensing mucin glycans. RetS has been extensively studied for its role in inhibiting the GacS-GacA two-component system (Heeb & Haas 2001; Lapouge et al. 2008), a master regulator of virulence that induces gene expression changes associated with a chronic infection state (Goodman et al. 2004). Among these GacS-activated pathways is the Hcp Secretion Island I-encoded Type VI Secretion System (H1-T6SS) (Goodman et al. 2004), a needle-like apparatus that directly injects proteinaceous toxic effectors into other bacteria (Hood et al. 2010) (Figure 3.1B), and may contribute to *P. aeruginosa* fitness during chronic infections (Hood

et al. 2010; Mougous et al. 2006). However, the signals that GacS and RetS respond to have remained elusive (Figure 3.1C).

Here, we identify mucin glycans as signals that promote the ability of RetS to directly inhibit GacS-GacA activity in the *P. aeruginosa* PA14 strain. We find that this signaling depends on both the signal-binding Dismed2 domain of RetS, as well as its cytoplasmic phosphorelay domains. In particular, we find that mucin glycan signaling downregulates the H1-T6SS and suppresses T6SS-dependent bacterial killing by PA14 in a RetS-dependent manner. Collectively, these results provide new insights into the mechanisms by which signals in healthy mucus are sensed by pathogens to suppress virulence-associated behaviors, and may guide the design of new molecules for mitigating infections by problematic pathogens like *P. aeruginosa*.

Results

Mucins downregulate the type VI secretion system

For *P. aeruginosa*, a chronic infection state is associated with activation of antagonistic factors such as the H1-T6SS (Goodman et al. 2004; Mougous et al. 2006; Wilton et al. 2016). However, it is unclear how the H1-T6SS is regulated in healthy mucus, in which *P. aeruginosa* is typically unable to establish chronic infections. To test how healthy mucus impacts the H1-T6SS, we cultured PA14, a hypervirulent strain, in a solution of whole mucus containing MUC5AC, an isoform of mucin found in mucosal niches exposed to *P. aeruginosa*, including the eyes, ears, and respiratory tracts (Demouveau et al. 2018). We used qRT-PCR to quantify the levels of *clpVI*, an ATPase involved in the secretion of type VI effectors, and *icmF1*, which encodes a structural component of the secretion apparatus (Figure 3.1B). The levels of these representative H1-T6SS transcripts, which are present on two different operons in this locus, were both lowered by ~4-fold in whole mucus relative to mucus depleted of its high molecular-weight components (>100 kDa) by ultrafiltration (Figure 3.1D).

These size-depleted components included mucin glycoproteins, the major structural and functional units of mucus, which are present at concentrations ranging from 0.2 – 5% w/v in various mucus samples (Leal et al. 2018). To determine if mucins are responsible for the H1-T6SS downregulation seen in whole mucus, we exogenously added natively purified MUC5AC back to mucin-depleted mucus, and then used qRT-PCR to measure the levels of *clpVI* and *icmF1*. For

these experiments, we used a concentration of 0.5% w/v MUC5AC, which is the total mucin concentration in respiratory mucus (Henderson et al. 2014). We found that this addition of purified mucin to depleted mucus also triggered H1-T6SS suppression (Figure 3.1D), indicating that mucins are sufficient to downregulate the H1-T6SS in native mucus. The magnitude of changes (~3-4 fold) seen here with mucin are similar to changes in H1-T6SS levels seen in response to *P. aeruginosa* lysate (Le Roux et al. 2015).

In addition to *clpVI* and *icmFI*, the H1-T6SS locus contains 25 other genes. To determine the extent to which mucin regulates the full H1-T6SS locus, we performed RNA-sequencing on PA14 exposed to 0.5% w/v purified MUC5AC for 5 hours in ABTGC medium (Chua et al. 2015). Isolated MUC5AC downregulated H1-T6SS genes by an average of 2.3-fold relative to a media control, with 18 of the 27 transcripts downregulated at least 2-fold (Figure 3.1E, Figure S3.1A). For comparison, five housekeeping genes were not substantially affected (>|2-fold|) by mucins (Figure 3.1E). To validate these RNA-seq results, we used qRT-PCR to measure the levels of *clpVI* and *icmFI* in cells exposed to purified mucins in ABTGC medium, and found that these transcripts were also downregulated at least 2-fold relative to a media control (Figure S3.1B). Taken together, these results suggest that mucins downregulate the majority of H1-T6SS genes in PA14.

Mucins act through the sensor kinase RetS, resulting in the inhibition of GacS and the downstream Rsm pathway

RetS is a sensor kinase that inhibits the H1-T6SS (Goodman et al. 2004) (Figure 3.1C). This protein contains an N-terminal periplasmic Dismed2 domain that has homology to carbohydrate-binding proteins (Anantharaman & Aravind 2003), and could potentially respond to mucin glycoproteins. To determine if RetS can sense mucins, we generated a strain lacking RetS ($\Delta retS$), and found the ability of mucins to downregulate *clpVI* and *icmFI* in this background was impaired (Figure 3.1F). Similarly, a variant of RetS lacking its periplasmic Dismed2 domain, which was as stable as full-length RetS protein (Figure S3.1C), failed to respond to mucin (Figure 3.1F).

RetS controls H1-T6SS activity by inhibiting the GacS-GacA two-component system and the downstream Rsm pathway (Figure 3.1C). To test if mucins act through the Gac/Rsm pathway, we deleted key components of the pathway, namely GacS ($\Delta gacS$), *rsmY/Z* ($\Delta rsmY/Z$), and RsmA/RsmF ($\Delta rsmA/F$), and exposed each of these strains to mucin. Mucin was unable to

downregulate H1-T6SS transcripts in any of these strains (Figure 3.1F), suggesting these components are essential to mucin-mediated suppression of the H1-T6SS. However, for the $\Delta gacS$ and $\Delta rsmY/Z$ strains, H1-T6SS levels may be low enough (Figure S3.1D) that mucin cannot further downregulate *clpVI* or *icmFI*. To circumvent this limitation, we complemented the $\Delta rsmY/Z$ strain with a plasmid expressing *rsmY* from the constitutive lacUV5 promoter ($\Delta rsmY/Z + P_{lacUV5-rsmY}$), which restored *clpVI* and *icmFI* to approximately wild-type levels (Figure S3.1D) but removed GacS/GacA control of *rsmY* expression. Mucins were unable to downregulate the H1-T6SS in the $\Delta rsmY/Z + P_{lacUV5-rsmY}$ strain (Figure 3.1F). By contrast, when the plasmid-borne copy of *rsmY* was expressed from its native promoter ($\Delta rsmY/Z + P_{rsmY-rsmY}$), mucin could still downregulate *clpVI* and *icmFI* (Figure 3.1F). Taken together, our results indicate that mucins act through RetS and the Gac/Rsm pathway to downregulate the H1-T6SS.

Mucin glycans downregulate the H1-T6SS

Given the homology of the RetS-Dismed2 domain to carbohydrate binding proteins, mucin-derived glycans may be the component of mucins that activates RetS. To test this possibility, we isolated mucin glycans from MUC5AC by alkaline β -elimination. Using mass spectrometry, we identified ~70 glycan structures (Figure 3.2A), not including possible isomeric forms. The diversity and complexity of our library is similar to that of previously published human respiratory and porcine gastric mucin profiles (Jin et al. 2017; Xia et al. 2005). Specifically, glycans were predominantly built on core 2 [Gal β 1-3(GlcNAc β 1-6)GalNAc α 1-] and core 1 (Gal β 1-3GalNAc α 1-) structures, with the most abundant species including the unmodified core 1 structure, the unmodified core 2 structure, the fucosylated core 1, galactose-extended core 1, fucosylated core 2, and galactose-extended core 2 (Jin et al. 2017; Xia et al. 2005). These glycans offer a rich source of potential signals that may activate RetS. Indeed, exposure to 0.1% w/v of this mucin glycan pool was sufficient to downregulate *clpVI* and *icmFI* (Figure 3.2B). We also measured T6SS transcript levels following exposure to a pool of 0.1% monosaccharides representing those present in mucin. The monosaccharide pool did not suppress *clpVI* or *icmFI* (Figure 3.2B), suggesting that the complex structures of mucin glycans are critical to their function.

To determine the extent to which free mucin glycans recapitulate the potency of intact mucins, we used RNA-seq to quantify the effects of 0.1% glycans on the full H1-T6SS locus. Similar to the suppression of H1-T6SS seen with intact mucins (Figure 3.1E), H1-T6SS genes were

downregulated by an average of 2.6-fold in the presence of glycans, with 18 of the 27 genes downregulated >2-fold (Figure 3.2C, Figure S3.2A). Beyond the H1-T6SS, there was also a significant correlation ($r = 0.66$, $p < 0.0001$) between the gene expression profiles in response to mucin and glycans, indicating that glycans are largely responsible for the gene expression changes induced by mucin (Figure 3.2D). Further, using p-nitrophenol (pNP) bound to the core monosaccharides GalNAc, GlcNAc, and Gal, we found PA14 possesses glycosidase activity that is strongly stimulated (>5-fold) by the presence of mucin (Figure S3.2B), suggesting that PA14 can, in principle, release glycans from the mucin backbone, as has been observed in other *P. aeruginosa* strains (Aristoteli & Willcox 2003).

To further characterize the response to mucin glycans, we measured *clpVI* and *icmFI* levels at multiple glycan concentrations, and found that serially diluted glycans downregulated these transcripts in a dose-dependent manner (Figure 3.3A). Further, glycans suppressed *clpVI* expression at multiple time points throughout exponential phase (Figure 3.3B), suggesting that the glycan response is prolonged and not an artifact of a particular time point.

PA14 is a lab-adapted strain, and may exhibit altered gene expression profiles compared to other *P. aeruginosa* isolates. To determine if other strains can also respond to mucin glycans, we measured *clpVI* and *icmFI* levels in a variety of *P. aeruginosa* isolates exposed to these signals. Mucin glycans downregulated these H1-T6SS transcripts in the majority of strains tested, specifically in another laboratory strain (PAO1), an environmental isolate (MSH1), a urinary tract infection isolate (S54485), and multiple CF isolates (FRD1, CEC73) (Figure 3.3C). By contrast, the ability of mucin glycans to downregulate *clpVI* and *icmFI* was partially impaired in the CF isolate CF127, and was completely ablated in the CF isolate C078C (Figure 3.3C), which harbors mutations in the GacS/RetS pathway that likely prevent this strain from responding to RetS-acting signals (Perault et al. 2020).

Signaling through RetS and GacS was previously found to trigger gene expression changes within 30 minutes (Le Roux et al. 2015). To determine how quickly the H1-T6SS is downregulated in response to mucin glycans, we performed RNA-seq on PA14 exposed to glycans for 15 minutes (Figure S3.2C) following growth to mid-exponential phase, when the H1-T6SS is maximally expressed in the absence of glycans (Figure 3.3B). We found that the H1-T6SS locus was downregulated by an average of ~2-fold after 15 minutes of glycan exposure (Figure 3.3D). To

confirm these RNA-seq results, we used qRT-PCR to measure *clpVI* and *icmFI* levels after incubation with glycans for 15 minutes, and also observed a ~2-fold downregulation (Figure S3.2D). These results indicate that mucin glycans rapidly downregulate the H1-T6SS.

Mucin glycans signal through the periplasmic Dismed2 and cytoplasmic phosphorelay domains of RetS

To confirm that liberated mucin glycans, like their intact mucin counterparts, also act through GacS and RetS, we incubated glycans with the $\Delta gacS$, $\Delta retS$, and signal-blind RetS($\Delta Dismed2$) strains, and measured H1-T6SS transcripts with qRT-PCR. As with intact mucins, soluble mucin glycans were no longer able to downregulate *clpVI* or *icmFI* in any of these mutants (Figure 3.4A), confirming that both GacS and the sensory domain of RetS are necessary for glycan signaling.

Although these results indicate that mucin glycans inhibit the GacS pathway by activating RetS, it is unclear how this signaling event is conveyed through these two histidine kinases at a molecular level. Because GacS activity depends on its phosphorylation state, we investigated the role of the three phosphorelay domains in RetS, which were described to modulate GacS activity in other *P. aeruginosa* strains (PA103, PAK, PAO1) to varying degrees (Francis et al. 2018; Goodman et al. 2009; Laskowski & Kazmierczak 2006), but have not been investigated in PA14. Specifically, we mutated a conserved residue of the DHp/CA domain to ablate potential phosphatase activity (T428R), and conserved residues in the two tandem receiver domains to prevent RetS from siphoning phosphoryl groups from GacS (D713/715A, D858A) (Figure 3.4B). After confirming that these mutations did not affect RetS stability (Figure S3.3A), we measured GacS activity in these mutants by using qRT-PCR to quantify H1-T6SS transcript levels (Figure S3.3B), and by using an *rsmY-lacZ* reporter (Figure S3.3C). These assays revealed that both the DHp/CA and second receiver domains of RetS are critical for GacS inhibition in PA14. Furthermore, the ability of RetS(D858) to siphon phosphate from GacS was confirmed using *in vitro* phosphorylation assays (Figure S3.3D).

Having confirmed the roles of the RetS phosphorelay domains in PA14, we then tested the involvement of these domains in glycan signaling. We found that the ability of mucin glycans to downregulate *clpVI* and *icmFI* was impaired in all three RetS point mutants to varying degrees, with the RetS(D858A) mutant displaying the strongest loss of glycan-induced T6SS suppression (Figure 3.4C). Overall, these results are consistent with a model in which glycans stimulate RetS

to directly siphon phosphate from GacS and to act as a phosphatase, which leads to decreased GacS activity and H1-T6SS suppression.

Mucin glycan signaling through RetS affects the RetS regulon

To confirm that glycans downregulate the full H1-T6SS locus in a RetS-dependent manner, we performed RNA-seq on the signal-blind RetS(Δ *Dismed2*) and RetS(D858A) strains following exposure to mucin glycans (Figure S3.4A-B). While glycans downregulated the H1-T6SS genes by ~2.6-fold on average in the wild type, this locus was no longer downregulated by glycans in either RetS mutant (Figure 3.4D, Figure S3.4C).

RetS controls the expression of dozens of other genes beyond the H1-T6SS, many of which are uncharacterized but may be associated with chronic infections (Goodman et al. 2004). To determine if the expression of these genes is also altered by mucin glycans, we compared gene expression profiles of glycan-exposed wild-type cells to the published expression profile of the Δ *retS* strain (Goodman et al. 2004). These two profiles were inversely correlated ($r = -0.57$, $p < 0.0001$), as glycans inhibit GacS, whereas a deletion of *retS* activates GacS (Figure S3.4D). To confirm that these glycan-induced changes were indeed RetS-dependent, we also compared the gene expression profiles of glycan-exposed RetS(Δ *Dismed2*) and RetS(D858A) cells to the published Δ *retS* regulon, and found that there was no longer a significant correlation (Figure S3.4E).

Previous work using *retS* and *rsmA* deletions has also suggested that activation of RetS and RsmA may upregulate the expression of genes associated with acute infections, including those that encode lipase (PA14_27100), rhamnolipids (PA14_19100-19110), and the T3SS (PA14_42250-42660) (Goodman et al. 2004; Heurlier et al. 2004). However, unlike the H1-T6SS, the mechanism by which RetS controls these acute infection genes is unclear, as these transcripts are not direct targets of RsmA/F binding (Brencic & Lory 2009). Further, our results indicate that RetS activation by mucin and mucin glycans does not substantially upregulate (>2-fold) these acute infection genes/operons on average, and may even downregulate some of these transcripts. This discrepancy suggests that completely deleting *retS* may indirectly alter the expression of some additional genes that are not strongly affected when stimulating RetS with a signal. In agreement with this model, RetS-signaling by *P. aeruginosa* lysate also triggered changes in H1-T6SS levels without altering the expression of acute infection genes (Le Roux et al. 2015).

A previous study reported that mucins regulate other pathways in addition to the H1-T6SS, many of which are virulence-associated (Wheeler et al. 2019). To determine if these pathways were also regulated via RetS, we performed gene set enrichment analysis on the glycan-regulated genes of the wild-type, RetS(Δ *Dismed2*), and RetS(D858A) strains. Of all the pathways significantly enriched in the wild-type strain following glycan exposure, the H1-T6SS was the only pathway not enriched in either RetS mutant (Figure 3.4E, Figure S3.5). By contrast, all other pathways were differentially expressed in the wild-type and both RetS mutants (Figure 3.4E, Figure S3.5).

Overall, these findings demonstrate that glycans act specifically through RetS to suppress H1-T6SS and the majority of the RetS regulon, but act through different pathways to control RetS-independent phenotypes.

A subset of mucin glycans that do not require fucose or sialic acid is sufficient to downregulate the H1-T6SS

We next sought to narrow down the active glycans that are responsible for H1-T6SS suppression. We first tested the small number of commercially-available sugar moieties present in mucin glycans, namely the core 1 structure, N-Acetyl-D-lactosamine (lacNAc), and the oligosaccharides (GlcNAc)₂ and (GlcNAc)₃. None of these di- or trisaccharides downregulated H1-T6SS transcripts when used in isolation (Figure S3.6A), which may indicate that these synthesized structures differ slightly from their purified counterparts, for example, due to differences in mutarotation and isomer formation (Collins & Ferrier 1995), that a combination of glycans is needed to downregulate the H1-T6SS, and/or that this small collection of commercial sugars does not include the active glycans responsible for H1-T6SS suppression.

To circumvent the limited availability of commercial glycans, we instead used chemical methods to fractionate our purified glycans. Mucin glycans are primarily built on either a linear core 1 (Gal β 1-3GalNAc α 1-) or branched core 2 (Gal β 1-3(GlcNAc β 1-6)(GalNAc α 1-) structure. Often, these glycans are further elongated with additional galactose or lactosamine units (Gal-GlcNAc) that are modified with terminal sialic acid and/or fucose. To determine if these terminal moieties are essential for signaling, we applied partial acid hydrolysis to the glycan pool. Sialic acid is removed by hydrolysis at 0.1 M trifluoroacetic acid (TFA) and fucose is removed by 1 M TFA, while the core structures are resistant to acid hydrolysis (Guttman 1997). We identified putative structures of the 1M TFA-treated glycans by mass spectrometry (Figure 3.5A-B). Acid treatment

generated shorter glycans, with the average number of monosaccharides per glycan decreasing from 4.46 in the untreated pool to 2.65 in the acid-treated sample (Figure 3.5C). Glycans in both the untreated and acid-treated pools retained high levels of the acid-resistant core 1 and core 2 structures (Figure 3.5D). By contrast, acid-treated glycans had substantially less fucose and sialic acid compared to the untreated pool (Figure 3.5E).

Notably, acid-treated glycans were at least as potent as the diverse pool, triggering a strong downregulation of *clpV1* and *icmF1* (Figure 3.5F). Thus, it is likely that glycans do not require fucosylation or sialylation to function as a signal. To confirm that the active signal is an intact glycan, and not an acid-released monosaccharide, we fractionated the 1 M TFA-treated glycans through a Hypercarb cartridge, which retains intact glycans but not monosaccharides or salts (Packer et al. 1998). The composition of the glycan pool before and after Hypercarb purification was similar, suggesting that most intact glycans were successfully retained by the column (Figure S3.6B). These Hypercarb-retained glycans downregulated *clpV1* and *icmF1* to the same extent as the unseparated glycans (Figure 3.5F), suggesting that the active signal is indeed an intact glycan. Overall, these results indicate that a small subset of mucin glycans enriched in core structures and lacking fucose and sialic acid is sufficient for H1-T6SS suppression.

Mucin glycans suppress T6SS-mediated killing by PA14 through RetS

Downregulation of the H1-T6SS by mucin glycans should lead to decreased bacterial killing by PA14. To test this prediction, we used an established T6SS killing assay involving the co-incubation of PA14 and *E. coli* (Le Roux et al. 2015). In the absence of glycans, co-incubation of PA14 and *E. coli* led to substantial killing of *E. coli* (Figure 3.6A, Figure S3.7A). Deleting a critical structural component of the H1-T6SS ($\Delta icmF1$) abrogated killing (Figure 3.6A, Figure S3.7A), confirming that *E. coli* killing was dependent on the H1-T6SS. Strikingly, the addition of mucin glycans abolished *E. coli* killing to a similar extent as the $\Delta icmF1$ mutant (Figure 3.6A, Figure S3.7A). To determine if this loss of killing was dependent on the T6SS or occurred through an independent pathway, we repeated the competition between *E. coli* and the $\Delta icmF1$ strain in the presence of glycans, and found that glycans did not further increase *E. coli* survival in this competition (Figure 3.6A, Figure S3.7A).

Because H1-T6SS downregulation by glycans was abolished in both the RetS($\Delta Dismed2$) and RetS(D858A) mutants (Figure 3.4D, Figure S3.4C), we reasoned that glycans would no longer be

able to rescue T6SS-mediated killing of *E. coli* by PA14 in these mutant strains. To test this hypothesis, we performed killing assays between *E. coli* and these PA14 mutants in the presence or absence of glycans. The RetS(D858A) mutation leads to hyper-activation of the T6SS (Figure S3.3B-C), and accordingly we observed a drastic loss in *E. coli* viability compared to competitions with wild-type PA14 (Figure S3.7B). Notably, glycans were no longer able to rescue *E. coli* survival when co-cultured with either RetS mutant (Figure 3.6B), confirming that glycans act through both the Dismed2 and second receiver domains of RetS to suppress T6SS-mediated killing.

To determine if mucin glycans can prevent *P. aeruginosa* from killing other lung-dwelling microbes, which may be more physiologically relevant than the *P. aeruginosa-E. coli* model system, we repeated the T6SS phenotypic assays with *Burkholderia cenocepacia*, an opportunistic pathogen that invades CF airways. As with the *E. coli* competitions, we found that PA14 could kill *B. cenocepacia* in a T6SS-dependent manner, as a deletion of *icmF1* in PA14 diminished killing (Figure 3.6C, Figure S3.7C). Strikingly, we found that mucin glycans also rescued *B. cenocepacia* from T6SS-mediated killing by *P. aeruginosa* (Figure 3.6C, Figure S3.7C). To confirm that this rescue was dependent upon RetS, we repeated the *P. aeruginosa-B. cenocepacia* competitions using the RetS(Δ Dismed2) and RetS(D858A) mutants. As with the *E. coli* competitions, we found that glycans were unable to protect *B. cenocepacia* from killing when this microbe was co-cultured with either RetS mutant (Figure 3.6D, Figure S3.7D). Together, these results suggest that mucin glycans prevent *P. aeruginosa* from killing other lung-dwelling microbes using its T6SS in a RetS-dependent manner.

Discussion

Recent work indicates that mucus contains potent signals that influence microbial gene expression and behavior (Frenkel & Ribbeck 2015; Kavanaugh et al. 2014; Wheeler et al. 2019). However, the molecules in mucus and the mechanisms by which bacteria sense and respond to these signals have remained unclear. Here, we demonstrate that mucin glycans signal through the sensor kinase RetS via its Dismed2 sensory domain in *P. aeruginosa*. This signaling promotes the ability of RetS to inhibit GacS, likely by siphoning phosphate from GacS and by acting as a phosphatase. Mucin glycans induce changes in the expression of the majority of the RetS regulon, with the exception of acute infection genes which are not directly regulated by the downstream Rsm pathway. This

signaling includes the downregulation of the H1-T6SS, which prevents T6SS-dependent bacterial killing by *P. aeruginosa* in a RetS-dependent manner.

While our results indicate that a small subset of mucin glycans suppresses the H1-T6SS, previous work has shown that *P. aeruginosa* releases an unidentified “danger signal” upon lysis that acts through RetS to instead activate the H1-T6SS in kin cells (Le Roux et al. 2015). One intriguing hypothesis is that the original purpose of RetS was to sense this self-produced signal to activate the virulence program of *P. aeruginosa*, but environmental signals, such as those found in mucus, can antagonize the activity of self-produced signals and suppress these same virulence-associated traits. In this way, perhaps mucin glycans can be considered host-produced “safety signals” that suppress bacterial antagonism and instead promote microbial co-existence (Figure 3.7). Indeed, our observation that mucin glycans reduce T6SS-dependent killing in phenotypic assays may help explain the inability of *P. aeruginosa* to invade and displace communities found in healthy mucus.

We expect that other environmental signals outside of mucus may also signal through RetS. Previous work has shown that Dismed2 homologs recognize multiple glycans including a variety of plant polysaccharides (Boraston et al. 2003; Ficko-Blean & Boraston 2009; Fouquaert & van Damme 2012; van Bueren & Boraston 2007). This may suggest that providing a source of competing signals is a general strategy employed by hosts to respond to the presence of problematic microbes like *P. aeruginosa*. Indeed, our finding that mucin glycans downregulate the H1-T6SS in a variety of *P. aeruginosa* isolates, including those that are never exposed to mucins, raises the possibility that this pathway is primed to respond to widespread environmental sugars that resemble mucin glycans.

Our observation that *P. aeruginosa* downregulates its T6SS in response to mucin is reminiscent of how *Vibrio* species modulate T6SS activity in response to chitin. Upon sensing chitin, *Vibrio* secretes chitinases that release smaller GlcNAc chains from this insoluble polymer (Li & Roseman 2004). These smaller species are imported across the outer membrane through a specific porin (ChiP) (Aunkham et al. 2018), and then bind to a soluble periplasmic carbohydrate binding protein (CBP) (Suginta et al. 2018), which in turn activates the ChiS histidine kinase and modulates T6SS activity (Chourashi et al. 2018). Whether *P. aeruginosa* responds to mucin in a similar way remains to be seen. In particular, a mechanistic understanding of if and how *P. aeruginosa* releases glycans from the mucin backbone and then transports them across the outer membrane will be an important

area of future research. In addition, while our results indicate that mucin glycan signaling is dependent upon the periplasmic RetS-Dismed2 domain, further experiments are needed to probe if the predicted glycan binding sites of Dismed2 bind to mucin glycans directly, or if mucin glycans activate RetS by a different mechanism. Intriguingly, RetS likely forms higher order oligomeric structures across the inner membrane with other histidine kinases including GacS (Mancl et al. 2019), LadS (Chambonnier et al. 2016) and PA1611 (Kong et al. 2013). How mucin glycans signal through RetS-Dismed2 in the context of these multiprotein membrane complexes to affect their structure and function remains to be seen.

P. aeruginosa is proficient at invading and displacing microbial communities in the CF lung, and previous work has suggested that CF lung mucin may promote biofilm formation, aggregation, and antibiotic resistance in this niche (Fung et al. 2010; Landry et al. 2006; Staudinger et al. 2014). Why CF mucus no longer retains the ability to attenuate virulence remains an open question. One possibility is that the partial dehydration of mucus (Mall et al. 2004) and increased concentrations of mucins or extracellular DNA found in CF lung mucus (Henderson et al. 2014; Henke et al. 2004) may create geometric constraints or trigger gene expression changes that induce aggregation (Secor et al. 2018). Alternatively, the extensive degradation of mucins associated with chronic airway disease (Henderson et al. 2014) may cause them to lose their virulence-suppressing function. Furthermore, changes to mucin glycosylation may hinder the virulence-suppressing response documented here. For example, some studies have reported increased sialylation and distinct glycosylation patterns in the mucus of individuals with CF (Davril et al. 1999; Scanlin & Glick 1999; Xia et al. 2005). In turn, terminal sugars may limit access to the T6SS-suppressing glycans observed in this work, which are enriched in core structures. In addition, the accumulation of RetS/GacS pathway mutations in CF clinical isolates may prevent these strains from responding to mucin glycans (Marvig et al. 2015; Perault et al. 2020).

Although we have shown that glycans suppress H1-T6SS through RetS, other virulence-associated pathways are also downregulated by mucins and glycans independently of RetS, including other secretion systems, quorum sensing, and phenazine biosynthesis (Figure 3.4E). As there are hundreds of distinct glycan structures, as well as dozens of known receptors in *P. aeruginosa*, further work is needed to identify the relevant glycans and receptors that may be involved in each of these responses.

The ability of mucin glycans to activate a bacterial receptor suggests that the host provides a rich source of signals that can be perceived by microbes. Consistent with this hypothesis, mucin glycans built on the core 2 structure prevent pathogenic *E. coli* invasion into a colonic cell line (Ye et al. 2015), suggesting that the virulence-attenuating effects of mucin glycans are not exclusive to *P. aeruginosa*. Furthermore, purified mucins attenuate virulence in the Gram-positive *Streptococcus mutans* (Frenkel & Ribbeck 2015) and the fungal pathogen *Candida albicans* (Kavanaugh et al. 2014), but specific mucin-sensing receptors have not been identified in these species. Ultimately, the large assortment of receptors across these phylogenetically distant species, combined with the rich diversity of mucin glycans, underscores the enormous signaling potential that is housed within mucus. An understanding of the molecular mechanisms driving these signaling events and identification of specific bioactive glycans may inspire the design of novel therapeutics. Further, unlike traditional antibiotic treatments that kill bacteria, glycan-inspired therapeutics may control infections by downregulating virulence pathways without affecting microbial viability, thus mitigating the selective pressure that drives antibiotic resistance.

Materials and Methods

Strains and growth conditions. *P. aeruginosa*, *E. coli*, and *B. cenocepacia* strains were all grown overnight in LB at 37 °C under shaking conditions. For all assays, strains were grown the next day in ABTGC medium (15.1 mM ammonium sulfate, 33.7 mM sodium phosphate dibasic, 22.0 mM potassium dihydrogen phosphate, 0.05 mM sodium chloride, 1 mM magnesium chloride, 100 µM calcium chloride, 1 µM iron (III) chloride, supplemented with 0.2% glucose, and 0.2% casamino acids) (Chua et al. 2015) at 37 °C, unless otherwise indicated. When applicable, antibiotics were added at the following concentrations: for *E. coli*, 10 µg/mL tetracycline, 20 µg/mL gentamycin, and 100 µg/mL carbenicillin, for *P. aeruginosa*, 100 µg/mL tetracycline, 75 µg/mL gentamycin, 45 µg/mL trimethoprim, and for *B. cenocepacia*, 1000 µg/mL kanamycin. Strains, plasmids, and primers used are listed in Tables S3.1-S3.3.

General cloning procedures. Chromosomal-based modifications in *P. aeruginosa* (deletions, insertions, and point mutations) were done with allelic exchange using the suicide vectors pEXG2 and pMQ30, which both confer gentamycin resistance and sucrose sensitivity. In general, vectors were made by Gibson assembly (N.E.B) and transformed into S17 *E. coli* on LB with appropriate antibiotics. S17 strains were then grown up to OD₆₀₀ ~ 0.6. At the same time, the relevant *P. aeruginosa* strains were incubated at 42 °C for at least 2 hours. Then, 1.5 mL of S17 and 0.5 mL of *P. aeruginosa* were mixed, spun down, and resuspended in 100 µL LB. This mixture was then pipetted onto the center of a plain LB plate and grown overnight at 30 °C for mating to occur. The mixture was then isolated and re-suspended in 1 mL PBS, with dilutions of this solution plated on *Pseudomonas* isolation agar (PIA) supplemented with the appropriate antibiotics. Single colonies were then streaked on LB plates supplemented with 15% sucrose for counter selection. Colonies from the sucrose plates were then patched onto plain LB plates and subjected to colony PCR; clones with the correct constructs were collected and stored at -80 °C.

Plasmid and reporter construction. The pEXG2 allelic exchange vector was used to generate the Rsm deletion strains, the *icmF1* mutant, as well as the RetS(Δ *Dismed2*) chromosomal construct. In this case, fragments corresponding to regions ~500-1000 bases upstream and downstream from each deleted sequence were PCR amplified from PA14 gDNA. Primers were designed so that the upstream and downstream fragments had ~20-30 bp overlap regions, and so that each fragment also overlapped by ~20-30 bp with the pEXG2 vector. Next, fragments were cloned into the

pEXG2 vector via Gibson assembly (N.E.B) using overlapping regions between the two fragments, and between each fragment and the vector. After sequence confirmation, assembled vectors were electroporated into S17 cells and mated with WT PA14. Colony PCR was performed on single colonies from the LB+15% sucrose plates, and those with the correct deletions were re-streaked onto plain LB plates. Complementation of the *rsmY/Z* deletion was done by expressing *rsmY* from either a constitutively active lacUV5 promoter or its native promoter on the pPSV38 plasmid. After sequence confirmation, the pPSV38-*rsmY* plasmid was electroporated into S17 cells and subjected to the same procedures described above, with the *rsmY/Z* deletion used during mating.

Deletions of *retS*, *gacS*, and *hptB* were made by allelic exchange using the suicide vector pMQ30. Briefly, regions corresponding to ~500-1000 bases upstream and downstream of these genes were amplified from PA14 gDNA. Primers were designed so that the two amplified fragments had ~20-30 bp of overlap, and so that both fragments had ~20-30 bp of overlap with the pMQ30 vector. Fragments were then assembled with linearized pMQ30 in yeast. Sequence verified plasmids were then transformed into S17 and subjected to the same procedures described above, with wild-type PA14 used during mating.

The pMQ30 allelic exchange vector was also used to generate chromosomal point mutations in *retS*. However, in this case, primers were designed so that the overlapping region between the upstream and downstream fragments contained the relevant point mutations. Fragments were then amplified from PA14 gDNA and combined with linearized pMQ30 in yeast. Subsequent steps were identical to that described above, except that plasmids were conjugated into a $\Delta retS$ strain to introduce mutant *retS* sequences at the native chromosomal locus.

The pEXG2 suicide vector was also used to add chromosomal 3x-FLAG tag to RetS variants. Briefly, an ~1.3 kb fragment comprising ~650 bases upstream and downstream of the desired 3x-FLAG integration site was amplified from PA14 gDNA and put into pEXG2 by Gibson assembly (N.E.B). Then, around-the-horn PCR was used to add the nucleotide sequence encoding a 3x-FLAG tag at the desired site in the assembled vector by putting each half of the 3x-FLAG tag region on the forward and reverse primers. The rest of the procedure was identical to that described above for construction of RetS($\Delta Dismed2$), except that the *P. aeruginosa* strains used for mating were different, depending on the desired background. Colony PCR was performed on individual clones from the LB+15% sucrose plates to check for integration of the 3x-FLAG tag.

For the RetS(D858A)-3xFLAG construct, the D858A mutation introduced was within the region used for recombination. As such, around-the-horn PCR was used to generate the D858A mutation on the assembled pEXG2-RetS-3xFLAG vector by designing a forward primer containing the mutation at the 5' end.

The *rsmY-lacZ* chromosomal reporters were made using the previously published pCTX-*rsmY-lacZ* plasmid (Hoang et al. 2000). Briefly, the plasmid was transformed into electrocompetent S17 *E. coli* cells and mated with the relevant *P. aeruginosa* strains. Single colonies that appeared on PIA supplemented with tetracycline were then picked, re-streaked on LB-tetracycline plates, and subjected to colony PCR to confirm integration of the *rsmY-lacZ* construct.

Expression vectors for protein purification were made using the pENTR-TOPO gateway cloning kit (ThermoFisher). Briefly, GacS_c and RetS_c sequences were amplified from PA14 gDNA, with a 'CACC' sequence added to the 5' end of each forward primer. PCR products were then incubated with the pENTR vector according to the Topo kit instructions, and then transformed into chemically competent DH5 α *E. coli* cells. After sequence verification, the correct pENTR vectors were subjected to a LR recombination reaction with either ML333 or ML310 destination vectors using the Gateway LR Clonase II enzyme mix (ThermoFisher). Sequence verified plasmids were transformed into BL21 *E. coli* cells for protein expression.

To generate point mutations of RetS for *in vitro* assays, primers were designed so that the mutation of interest was located near the middle of both forward and reverse primers. Mutations were then generated by using a Quikchange site-directed mutagenesis protocol (Agilent). Sequence verified plasmids were transformed into BL21 *E. coli* cells for protein expression.

Mucus experiments. Mucus was scraped from fresh pig stomachs and solubilized (1 g scrapings to 5 mL) in 10 mM phosphate buffer pH 7.0 with 0.2 M sodium chloride and protease inhibitors (5 mM Benzamidine HCl, 1 mM dibromoacetophenone, 1 mM phenylmethylsulfonylfluoride (PMSF), and 5mM EDTA at pH 7) and 0.04% sodium azide (Sigma). Cellular debris and food waste was removed via low-speed centrifugation, 8000 x g, (7,000 rpm Sorvall GS-3 rotor), for 30 minutes at 4 °C. Mucus was depleted of its high molecular weight components with Amicon ultra centrifugal 100 kDa filters (Sigma).

Batch cultivation of *Pseudomonas aeruginosa* PA14 was carried out shaking at 37 °C in LB (Difco). For whole-mucus experiments, overnight cultures of PA14 were diluted 150-fold into

ABTGC medium (Chua et al. 2015) and grown shaking at 37 °C for 3.5 h. Thirty microliters of these cultures were exposed to 30 µL of solubilized mucus, depleted mucus, or depleted mucus with purified mucin added back for 1.5 h at 37 °C in a static 96-well microtiter plate (Greiner).

Mucin purification. This study used native porcine gastric mucins (MUC5AC). Mucus was scraped from fresh pig stomachs, solubilized in sodium chloride buffer (described above), and insoluble material was removed by ultracentrifugation at 190,000 x g RCF for 1 hr at 4 °C (40,000 rpm, Beckman 50.2 Ti rotor with polycarbonate bottles). Mucus was then clarified and desalted with disposable PD-10 desalting columns (GE). Mucins were isolated using size-exclusion chromatography on a Sepharose CL-2B column. Mucin fractions were identified based on absorbance at 280 nm, then desalted and concentrated with an Amicon stirred cell pressure-based concentrator (Sigma) with an Omega ultrafiltration 100 kDa membrane disc filter (Pall). Purified mucins were then lyophilized for storage at -80 °C. Lyophilized mucins are reconstituted by shaking them gently at 4 °C overnight in the desired medium. Mass spectrometry is routinely used to monitor the composition of purified mucin extracts, which confirms that mucin extracts purified from porcine stomach mucus are composed predominantly of MUC5AC, with small quantities of MUC2, MUC5B, and MUC6, histones, actin, and albumin (Caldara et al. 2012).

Mucin glycan isolation. This study applied non-reductive alkaline β -elimination ammonolysis to dissociate non-reduced glycans from commercially available pig gastric mucins (Sigma). Mucins were added to 1x PBS at a ratio of 30 mg per mL and insoluble material was removed by low-speed centrifugation, 8000 x g, (7,000 rpm Sorvall GS-3 rotor), for 20 minutes at 4 °C. Mucins were then precipitated with 60% (v/v) ethanol, collected by centrifugation, and dissolved in 400 mL water. Dissolved mucin was then desalted and concentrated with an Amicon stirred cell pressure-based concentrator (Sigma) with 100 kDa membrane filter disc (Pall), and lyophilized. Lyophilized mucins were dissolved in 30-32% ammonium hydroxide solution (Sigma) saturated with 30% w/v ammonium carbonate and incubated at 60°C for 48 h to release oligosaccharide glycosylamines and partially deglycosylated mucins. For all steps, mucin and glycans are dissolved at a concentration of 30 mg per mL. Volatile salts were removed via repeated centrifugal evaporation from water. The resulting oligosaccharide glycosylamines were converted to reducing oligosaccharide hemiacetals via treatment with 0.5 M boric acid at 37°C for 1 h. Residual boric acid was removed via repeated centrifugal evaporation from methanol. Glycans were separated from residual deglycosylated mucins via centrifugal filtration through 10 kDa

molecular weight cut-off membranes in accordance with the manufacturer's instructions (Amicon Ultracel).

For each mucin glycan preparation, at least 5 μg of β -eliminated mucin glycans were analyzed using matrix-assisted laser desorption/ionization time-of-flight (MALDI-TOF). β -eliminated glycans were permethylated and analyzed at the Glycomics Core at Beth Israel Deaconess Medical Center. Mass spectrometry data were acquired on an UltraFlex II MALDI-TOF Mass Spectrometer (Bruker Daltonics). Reflective positive mode was used, and data were recorded between 500 m/z and 6000 m/z . The mass spectrometry O-glycan profile was acquired by aggregating at least 20,000 laser shots. Mass peaks were manually annotated and assigned to a particular O-glycan composition based on known core structures.

Glycans were quantified using the phenol-sulfuric method (Masuko et al. 2005). Briefly, up to 500 μg dried glycans were dissolved in 250 μL of water. 25 μL of glycans were added to a 96 well plate, following by 150 μL of concentrated sulfuric acid with rigorous pipetting. 30 μL of a 5% phenol solution was then added, which caused the solution to turn brown. Quantification of this color change was measured at 490 nm, and w/v measurements were made by comparing to a standard curve of serially diluted glucose.

Acid treatment of mucin glycans. 1 mg of mucin glycans per 400 μL 1 M TFA were incubated at 80 $^{\circ}\text{C}$ for 4 hours to remove sialic acid and fucose. Glycans were then dried using a speedvac, and washed repeatedly with methanol until all TFA was removed, as verified by pH testing.

For samples further purified through Hypercarb cartridges (ThermoFisher), acid-treated glycans were first neutralized with potassium hydroxide (KOH), incubated at room temperature for 10 minutes to allow salts to precipitate, and then spun at 16,000g for 10 minutes to remove any precipitant. The supernatant was then collected and dried using a speedvac. At the same time, the Hypercarb cartridges were first primed with 4 column volumes of 100% acetonitrile, then flushed with 4 column volumes of water. The 1 mg of dried TFA-treated glycans were resuspended in 500 μL of water, and loaded onto the cartridge. The Hypercarb cartridge was then washed with 2 column volumes of water and 1 column volume of 2% acetonitrile to remove salts and monosaccharides. Glycans were then eluted using 2 column volumes of 50% acetonitrile, and dried using a speedvac.

Set-up of sugar-signaling experiments. Cells were grown in ABTGC medium. Unless otherwise

indicated, all strains (WT and mutants) were grown in 96 well format for 5 hours (~30 μ L/well), or until reaching reached an OD of ~0.5-0.6.

For mucin experiments, mucin was reconstituted in ABTGC medium at 0.5% w/v overnight (4 degrees, with constant vortexing). The next morning, overnight cultures were diluted 1:100 into reconstituted mucin solutions and grown at 37 °C until OD~0.5-0.6 (typically ~5 hours). For glycan experiments, dried glycans were reconstituted to 0.1% w/v in ABTGC medium unless otherwise indicated, and overnight cultures were diluted 1:100 into these solutions and grown at 37 °C until OD~0.5-0.6 (typically ~5 hours). For monosaccharide experiments, the monomeric forms of each mucus sugar (GlcNAc, GalNAc, galactose, fucose, sialic acid), were purchased from Sigma and dissolved as a 0.1% w/v solution in ABTGC medium, and were then used in the same way as reconstituted mucins and glycans.

RNA preparation for qRT-PCR and RNA-seq experiments. 30 μ L of cells grown in ABTGC medium alone or with mucin or mucin glycans were pelleted at max speed in a table top centrifuge. Cell pellets were then resuspended in 300 μ L of Cell Lysis solution (Lucigen) with 2 μ L of 50 μ g/ μ L proteinase K and incubated at 65 °C for 30 minutes, with vortexing every 5 minutes. Samples were placed on ice for 5 minutes, and then mixed with 175 μ L of MPC Protein Precipitation Reagent (Lucigen). Next, samples were spun for 10 minutes at maximum speed in a tabletop centrifuge at 4 °C. The supernatant was then transferred to a clean tube and mixed with 500 μ L of isopropanol by inverting the tubes ~30 times. Tubes were spun for 10 minutes at maximum speed in a tabletop centrifuge at 4 °C again to pellet the RNA. After removal of the supernatant, the RNA pellet was mixed with 0.5 mL of 70% ethanol and centrifuged at 12,000 g for 15 minutes at 4 °C. The RNA pellet was washed again with 70% ethanol, and then air dried for 10 minutes at room temperature and resuspended in 30 μ L of nuclease free water.

To remove contaminating DNA from RNA preps, 5 μ L of Ambion RNA Turbo buffer + 1.5 μ L of Turbo DNase (ThermoFisher) were added to each RNA sample and incubated for 30 minutes at 37 °C. Following this incubation, 5 μ L of the Ambion reaction inactivator (ThermoFisher) were added to each sample and vortexed rigorously. After incubation at room temperature for 2 minutes, samples were spun down for 2 minutes at 10,000 g with a tabletop centrifuge. The supernatant containing purified RNA was then carefully collected and transferred to a new tube, before storing at -80 °C for long-term storage.

qRT-PCR. The SuperScript III kit (ThermoFisher) was used to prepare cDNA for qRT-PCR experiments. Briefly, 1 µg of purified RNA was combined with 1 µL of 50 ng/µL random hexamers, 1 µL of a 10 mM dNTP mix, and nuclease free water to a total volume of 10 µL. The samples were incubated at 65 °C for 5 minutes, and then placed on ice for 5 minutes. Next, 2 µL of 10X RT buffer, 4 µL of 25 mM MgCl₂, 2 µL of 0.1 M DTT, 1 µL of RNaseOUT™, and 1 µL of SuperScript III were added to each sample, and then incubated at 25 °C for 10 minutes, 50 °C for 50 minutes, and 85 °C for 5 minutes. Samples were then stored at -20 °C for long-term storage or used immediately for qRT-PCR.

qRT-PCR was performed with the Sybr Fast qPCR 2x Master Mix (Roche). Briefly, ~10 ng of cDNA was incubated with 5µL of 2x Sybr, 0.6 µL of 5 µM of each primer, for a final primer concentration of 300 nM, and nuclease free H₂O to a final volume of 10 µL. Samples were then placed onto 384 well white bottom plates, and qRT-PCR done in a LightCycler 480 system (Roche) with the following thermocycling program: 95 °C for 10 minutes, 95 °C for 15 seconds, 60 °C for 30 seconds, and 72 °C for 30 seconds, with 40 cycles of steps 2-4.

Data were analyzed by the ddCT method to determine the fold change of each relative to a housekeeping gene (*rpoD*). Primers were checked for efficiency by running serially diluted concentrations of cDNA, and only primers with efficiency of >90% were used.

RNA-seq. Purified RNA was depleted of rRNA using home-made biotinylated rRNA-specific probes (Culviner et al. 2020). Following ribo-depletion, 15 µL of depleted RNA was submitted to the MIT BioMicro center for strand-specific library preparation. Single-end sequencing was performed on a HiSeq2000, with a read length of 40 nucleotides. BWA was used to map the reads to the PA14 genome, and uniquely mapping reads were used. Any read that overlapped with a gene region was given a count of 1 read.

The RNA-seq data was processed as follows. Genes with an average of fewer than 10 counts were eliminated, as well as all rRNA reads. Next, the total number of reads across all genes was calculated for both the + and – glycan conditions. The normalized read count for each gene was calculated by dividing each raw read count by the total read count for each condition. Finally, the fold change of each gene was calculated as the ratio between the normalized read count of each gene in the + vs. –condition (i.e., +/- mucins, +/- glycans), for each respective strain and/or time point.

The RNA-seq datasets generated during this study are available at GEO with accession number GSE156995.

Western blotting. For Western blotting experiments, 50 mL of cells were grown up to $OD_{600} \sim 0.8$, and then spun down and washed three times in 50 mM KH_2PO_4 at pH 7.5. Cells were then resuspended in 1 mL of 50 mM KH_2PO_4 and lysed by sonication (2 minutes total time, 1 second on, 4 second off cycles at 30% power). Lysates were spun down for 10 minutes at 5,000 g to remove unlysed cells. As GacS and RetS are membrane proteins, proteins were not denatured by boiling, which can induce oligomerization of membrane proteins. Instead, lysates were incubated with 4x SB (200 mM Tris-HCl pH 6.8, 8% SDS, 0.4% bromophenol blue, 40% glycerol) for 30 minutes at room temperature to gently denature proteins and then sonicated in a Diagenode water bath sonicator for 5 seconds. Next, 20 μ g of lysate for each sample were loaded onto a 10% BioRad mini-protean TGX gel, along with a Chameleon Duo pre-stained ladder (Licor), and gels were run for 40 minutes at 200 V. Proteins on the gel were transferred to methanol-activated 0.45 μ m PVDF membranes in ice-cold transfer buffer (25 mM Tris-HCl at pH 7.6, 192 mM glycine, 20% methanol) at a constant current of 0.35 A for 60 minutes. Membranes were then blocked in a 4% milk solution for 2 hours, incubated in primary antibody solution (monoclonal anti-FLAG M2 from mouse (Sigma) diluted 1:5,000 in 4% milk) for 1 hour at room temperature, and then washed 3 times in TBST buffer for 5 minutes each. Following this wash step, membranes were incubated for 1 hour in secondary antibody solution (goat anti-mouse (ThermoFisher) diluted 1:5,000 in 4% milk) for another hour at room temperature, then washed 3 more times in TBST for 5 minutes each, followed by 1 wash in TBS for 10 minutes. Finally, 1 mL of working solution from the SuperSignal West Femto Maximum Sensitivity Substrate kit (ThermoFisher) was added to the membrane. Western blots were imaged using the 'chemiluminescent+markers' setting on a Protein Simple FluorChemR imager to visualize bands. Band intensity was quantified by ImageJ to determine relative ratios of proteins.

β -galactosidase assays. To measure *rsmY-lacZ* expression, cells (typically $\sim 25 \mu$ L) were added to 1 mL of Z buffer (0.06 M Na_2HPO_4 , 0.04 M $NaH_2PO_4 \cdot H_2O$, 0.01 M KCl, 0.001 M $MgSO_4$, adjusted to pH 7, and 135 μ L of β -mercaptoethanol added fresh to 50 mL of Z buffer). Next, 50 μ L of a 0.1% SDS solution and 100 μ L of chloroform were added to the mixture. Each sample was then vortexed for 8 seconds, followed by the addition of 200 μ L of a 4 mg/mL ONPG solution. Samples were then vortexed for another 8 seconds and then incubated at 30 °C for 30 minutes.

Following incubation, samples were spun at 21,000 *g* for 2 minutes in a tabletop centrifuge to pellet the chloroform. 250 μ L were then withdrawn from the top of each tube and pipetted into a clear bottom 96 well plate to measure both the OD₄₂₀ and OD₅₅₀ of each reaction using a BioTek Synergy H1 plate reader to calculate Miller Units.

Protein purification. To purify proteins for *in vitro* phosphorylation assays, BL21 cells were transformed with the appropriate ML333 or ML310 vectors, in which the expression of MBP-GacS_c or Trx-RetS_c variants are driven by IPTG. Next, 500 mL of each strain was grown up to OD₆₀₀ ~ 0.6 at 37 °C and induced with 1 mM IPTG for 4 hours at 30 °C. Cells were then spun down for 15 minutes at 5000 *g* and washed twice with lysis buffer (20 mM Tris-HCl, 20 mM imidazole, 0.5 M NaCl, 10% glycerol, 0.1% Triton X-100, adjusted to pH 8). Pellets were resuspended in 10 mL of lysis buffer, with the addition of 1 mg/mL lysozyme, 1 mM PMSF, and 5 μ L of benzonase, and incubated for 30 minutes at room temperature. Each sample was lysed by sonication (2 minutes total sonication time, 30 seconds on, 30 seconds off at 30% power). Lysed samples were spun down at 25,000 *g* for 1 hour at 4 degrees to separate the insoluble and soluble fractions. At the same time, Ni-NTA columns (Qiagen) were equilibrated with 10 mL of lysis buffer. Next, the soluble fractions were retained and run through the Ni-NTA columns. Columns were washed with 20 mL of wash buffer (20 mM HEPES, 20 mM imidazole, 0.5 M NaCl, 10% glycerol, 0.1% Triton X-100, adjusted to pH 8). Proteins were then eluted from the column with 2.5 mL of elution buffer (20 mM HEPES, 0.5 M NaCl, 10% glycerol, and 250 mM imidazole, adjusted to pH 8). Eluted proteins were immediately buffer exchanged through PD-10 columns (G.E.), which had been pre-equilibrated with 25 mL of HKEDG storage buffer (10 mM HEPES, 50 mM KCl, 10% glycerol, 0.1 mM EDTA, and 1 mM fresh DTT). Proteins were eluted in 3.5 mL of HKEDG storage buffer from the PD-10 columns and then concentrated using either 10K or 30K MWCO Amicon ultracel centrifugal filters for 30-60 minutes. Protein concentrations were quantified using a Nanodrop spectrophotometer.

***In vitro* phosphorylation assays.** An ATP regeneration system as used for phosphotransfer experiments. Gac Δ Rec Δ Hpt was used at a final concentration of 2.5 μ M in HKEDG storage buffer. Final concentrations of 0.5 mM ATP, 2.5 μ Ci of [γ -³²P]-ATP, 0.5 mM phosphoenolpyruvate (PEP), and 10 U/mL pyruvate kinase (PK) were first incubated together for 30 minutes at 30 °C to allow the γ -³²P to equilibrate between ATP and PEP. Gac Δ Rec Δ Hpt and MgCl₂ were diluted in HKEDG buffer and then added and used at final concentrations of 2.5 μ M and 5 mM, respectively.

Autophosphorylation reactions were performed at 30 °C.

For phosphotransfer assays, GacS Δ Rec Δ Hpt was first autophosphorylated using the above parameters at 30 °C for 60 minutes, and then spun through a Micro Bio-spin 6 column (Bio-rad) equilibrated with HKEDG buffer to remove unused nucleotide. The cleaned up GacS samples were then incubated with reactions containing RetS and MgCl₂ at final concentrations of 5 μ M and 5 mM, respectively. Phosphotransfer reactions were run at 30 °C. Reactions were stopped at the indicated time points with the addition of 4x SB (200 mM Tris-Cl at pH 6.8, 400 mM DTT, 8% SDS, 0.4% bromophenol blue, 40% glycerol).

Each sample was run on a 10% BioRad mini-protean TGX gel for 50 minutes at 150 V. Gels were then put into Ziploc bags and exposed to phosphor-screens for 4-5 hours so that phosphorylated protein bands could be observed. Screens were imaged using the Typhoon-FLA9500 imager with a “phosphor” setting and a resolution of 50 μ m.

Hydrolysis of pNP-linked sugars. To measure the hydrolysis of p-nitrophenol (pNP)-linked compounds (GoldBio), overnight cultures of PA14 were diluted 1:100 into ABTGC medium alone or with 0.5% mucin and grown for 4 hours at 37 °C. Bacterial cultures were then centrifuged at maximum speed for 3 minutes. 45 μ L of supernatant were mixed with 5 μ L of pNP-linked sugars (GalNAc, GlcNAc, or Galactose) made as 20 mg/ml stocks in DMSO. For a control, pNP sugars were mixed with medium not exposed to bacteria. Mixtures of pNP-sugars and bacterial supernatants were incubated for 3 hours at 37 °C. 100 μ L of 1M sodium carbonate (Sigma) was added to stop the reaction. Released pNP was determined by monitoring the absorbance at 405 nm (A405).

Type VI killing assays. For killing assays, overnight cultures of PA14 were diluted 1:100 into ABTGC (either with no glycans or 0.1% glycans) and grown for 5 hours at 37 °C until reaching an OD of ~0.5. At the same time, overnight cultures of *E. coli* S17 were diluted 1:500 into ABTGC and grown for 5 hours at 37 °C until reaching an OD of ~0.3. Overnight cultures of *B. cenocepacia* were diluted 1:1,000 into ABTGC and also grown for 5 hours at 37 °C until reaching an OD of ~0.3. For the PA14-S17 competitions, 100 μ L PA14 and S17 were then spun down at max speed for 2 minutes, and re-suspended in a total volume of 5 μ L to concentrate the cells. For the PA14-*B. cenocepacia* competitions, 50 μ L PA14 and 25 μ L *B. cenocepacia* were spun down at max speed for 2 minutes, and re-suspended in a total volume of 5 μ L to concentrate the cells. These

suspensions were then plated on ABTGC plates (3% agar), and incubated at 37 °C for 1.5 hours. The mixture was then scraped off the plates and re-suspended in 100 µL of ABTGC, and then serially diluted by 10x to count CFU. For *E. coli* based competitions, these serially diluted samples were plated on either LB-irgasan plates (to select for PA14) or LB-cefsulodin plates (to select for S17) overnight at 37 °C. Irgasan and cefsulodin were used at a concentration of 25 µg/mL. Competitive index was calculated as: $CI = E_o / E_t / P_t$, where E is the number of *E. coli* cells competed with or without *P. aeruginosa* (E_t and E_o , respectively) and P_t is the number of competing *P. aeruginosa* cells. For *B. cenocepacia* based competitions, these serially diluted samples were plated on either LB-Kanamycin plates (to select for *B. cenocepacia*, which harbored a kanamycin resistant cassette on the chromosome), or on LB-trimethoprim plates to select for *P. aeruginosa*. Kanamycin was used at a concentration of 1 mg/mL, and trimethoprim was used at 45 µg/mL. Competitive index was calculated in the same way as above, except E is the number of *B. cenocepacia*.

Quantification and statistical analysis. Where applicable, each figure shows each individual data point, as well as the mean and standard error, as specified in each figure caption. Statistical tests were performed where relevant by using a 2-way ANOVA on Prism, and corrected for multiple comparisons using Dunnett's test. All p-values are shown in Table S2.4. Linear regressions were also performed on Prism, with both the r-value and p-value reported. Pathway enrichment analysis was performed on differentially expressed gene sets using the hypergeometric test. Genes were classified as differentially expressed based on their log₂-transformed fold change. P-values were then adjusted for multiple comparisons with the Benjamini-Hochberg correction to obtain the false discovery rate.

References

- Anantharaman V, Aravind L. 2003. Application of comparative genomics in the identification and analysis of novel families of membrane-associated receptors in bacteria. *BMC Genomics*. 4(1):34
- Aristoteli LP, Willcox MDP. 2003. Mucin degradation mechanisms by distinct *Pseudomonas aeruginosa* isolates in vitro. *Infect. Immun.* 71(10):5565–75
- Aunkham A, Zahn M, Kesireddy A, Pothula KR, Schulte A, et al. 2018. Structural basis for chitin acquisition by marine *Vibrio* species. *Nat. Commun.* 9(1):1–13
- Barko PC, McMichael MA, Swanson KS, Williams DA. 2018. The Gastrointestinal Microbiome: A Review. *J. Vet. Intern. Med.* 32(1):9–25
- Boraston AB, Notenboom V, Warren RAJ, Kilburn DG, Rose DR, Davies G. 2003. Structure and ligand binding of carbohydrate-binding module CsCBM6-3 reveals similarities with fucose-specific lectins and “galactose-binding” domains. *J. Mol. Biol.* 327(3):659–69
- Brencic A, Lory S. 2009. Determination of the regulon and identification of novel mRNA targets of *Pseudomonas aeruginosa* RsmA. *Mol. Microbiol.* 72(3):612–32
- Brockhausen I, Schachter H, Stanley P. 2009. O-GalNAc Glycans. In A. Varki (Eds.) et. al., *Essentials of Glycobiology*. (2nd ed.). Cold Spring Harbor Laboratory Press.
- Caldara M, Friedlander RS, Kavanaugh NL, Aizenberg J, Foster KR, Ribbeck K. 2012. Mucin biopolymers prevent bacterial aggregation by retaining cells in the free-swimming state. *Curr. Biol.* 22(24):2325–30
- Capra EJ, Laub MT. 2012. Evolution of Two-Component Signal Transduction Systems. *Annu. Rev. Microbiol.* 66(1):325–47
- Celli JP, Turner BS, Afdhal NH, Keates S, Ghiran I, et al. 2009. *Helicobacter pylori* moves through mucus by reducing mucin viscoelasticity. *Proc. Natl. Acad. Sci. U. S. A.* 106(34):14321–26
- Chambonnier G, Roux L, Redelberger D, Fadel F, Filloux A, et al. 2016. The Hybrid Histidine Kinase LadS Forms a Multicomponent Signal Transduction System with the GacS/GacA Two-Component System in *Pseudomonas aeruginosa*. *PLoS Genet.* 12(5):1–30
- Chourashi R, Das S, Dhar D, Okamoto K, Mukhopadhyay AK, Chatterjee NS. 2018. Chitin-induced T6SS in *Vibrio cholerae* is dependent on ChiS activation. *Microbiol. (United Kingdom)*. 164(5):751–63
- Chua SL, Hultqvist LD, Yuan M, Rybtke M, Nielsen TE, et al. 2015. In vitro and in vivo generation and characterization of *Pseudomonas aeruginosa* biofilm-dispersed cells via c-di-GMP manipulation. *Nat. Protoc.* 10(8):1165–80
- Collins P, Ferrier R. 1995. *Monosaccharides: Their Chemistry and Their Roles in Natural Products*. John Wiley & Sons, Ltd
- Culviner PH, Guegler CK, Laub MT. 2020. A simple, cost-effective, and robust method for rRNA depletion in RNA-sequencing studies. *MBio.* 11(2):e00010-20
- Davril M, Degroote S, Humbert P, Galabert C, Dumur V, et al. 1999. The sialylation of bronchial mucins

- secreted by patients suffering from cystic fibrosis or from chronic bronchitis is related to the severity of airway infection. *Glycobiology*. 9(3):311–21
- Demouveau B, Gouyer V, Gottrand F, Narita T, Desseyn JL. 2018. Gel-forming mucin interactome drives mucus viscoelasticity. *Adv. Colloid Interface Sci.* 252:69–82
- Ficko-Blean E, Boraston AB. 2009. N-Acetylglucosamine Recognition by a Family 32 Carbohydrate-Binding Module from *Clostridium perfringens* NagH. *J. Mol. Biol.* 390(2):208–20
- Fouquaert E, van Damme EJM. 2012. Promiscuity of the *Euonymus* carbohydrate-binding domain. *Biomolecules*. 2(4):415–34
- Francis VI, Waters EM, Finton-James SE, Gori A, Kadioglu A, et al. 2018. Multiple communication mechanisms between sensor kinases are crucial for virulence in *Pseudomonas aeruginosa*. *Nat. Commun.* 9(1):2219
- Frenkel ES, Ribbeck K. 2015. Salivary mucins protect surfaces from colonization by cariogenic bacteria. *Appl. Environ. Microbiol.* 81(1):332–38
- Fung C, Naughton S, Turnbull L, Tingpej P, Rose B, et al. 2010. Gene expression of *Pseudomonas aeruginosa* in a mucin-containing synthetic growth medium mimicking cystic fibrosis lung sputum. *J Med Microbiol.* 59(Pt 9):1089–1100
- Goodman AL, Kulasekara B, Rietsch A, Boyd D, Smith RS, Lory S. 2004. A signaling network reciprocally regulates genes associated with acute infection and chronic persistence in *Pseudomonas aeruginosa*. *Dev. Cell.* 7(5):745–54
- Goodman AL, Merighi M, Hyodo M, Ventre I, Filloux A, Lory S. 2009. Direct interaction between sensor kinase proteins mediates acute and chronic disease phenotypes in a bacterial pathogen. *Genes Dev.* 23(2):249–59
- Guttman A. 1997. Analysis of monosaccharide composition by capillary electrophoresis. *J. Chromatogr. A.* 763(1–2):271–77
- Heeb S, Haas D. 2001. Regulatory Roles of the GacS/GacA Two-Component System in Plant-Associated and Other Gram-Negative Bacteria. *Mol Plant Microbe Interact.* 14(12):1351–63
- Henderson AG, Ehre C, Button B, Abdullah LH, Cai LH, et al. 2014. Cystic fibrosis airway secretions exhibit mucin hyperconcentration and increased osmotic pressure. *J. Clin. Invest.* 124(7):3047–60
- Henke MO, Renner A, Huber RM, Seeds MC, Rubin BK. 2004. MUC5AC and MUC5B Mucins Are Decreased in Cystic Fibrosis Airway Secretions. *Am. J. Respir. Cell Mol. Biol.* 31(1):86–91
- Heurlier K, Williams F, Heeb S, Dormond C, Pessi G, et al. 2004. Positive Control of Swarming, Rhamnolipid Synthesis, and Lipase Production by the Posttranscriptional RsmA/RsmZ System in *Pseudomonas aeruginosa* PAO1. *J. Bacteriol.* 186(10):2936–45
- Hews CL, Tran SL, Wegmann U, Brett B, Walsham ADS, et al. 2017. The StcE metalloprotease of enterohaemorrhagic *Escherichia coli* reduces the inner mucus layer and promotes adherence to human colonic epithelium ex vivo. *Cell. Microbiol.* 19(6):e12717
- Hoang TT, Kutchma AJ, Becher A, Schweizer HP. 2000. Integration-proficient plasmids for *Pseudomonas aeruginosa*: Site-specific integration and use for engineering of reporter and

- expression strains. *Plasmid*. 43(1):59–72
- Hood RD, Singh P, Hsu FS, Güvener T, Carl MA, et al. 2010. A Type VI Secretion System of *Pseudomonas aeruginosa* Targets a Toxin to Bacteria. *Cell Host Microbe*. 7(1):25–37
- In J, Foulke-Abel J, Zachos NC, Hansen AM, Kaper JB, et al. 2016. Enterohemorrhagic *Escherichia coli* Reduces Mucus and Intermicrovillar Bridges in Human Stem Cell-Derived Colonoids. *CMGH*. 2(1):48-62.e3
- Jin C, Kenny DT, Skoog EC, Padra M, Adamczyk B, et al. 2017. Structural diversity of human gastric mucin glycans. *Mol. Cell. Proteomics*. 16(5):743–58
- Kavanaugh NL, Zhang AQ, Nobile CJ, Johnson AD, Ribbeck K. 2014. Mucins suppress virulence traits of *Candida albicans*. *MBio*. 5(6):1–8
- Kong W, Chen L, Zhao J, Shen T, Surette MG, et al. 2013. Hybrid sensor kinase PA1611 in *Pseudomonas aeruginosa* regulates transitions between acute and chronic infection through direct interaction with RetS. *Mol. Microbiol*. 88(4):784–97
- Landry RM, An D, Hupp JT, Singh PK, Parsek MR. 2006. Mucin-*Pseudomonas aeruginosa* interactions promote biofilm formation and antibiotic resistance. *Mol. Microbiol*. 59(1):142–51
- Lapouge K, Schubert M, Allain FHT, Haas D. 2008. Gac/Rsm signal transduction pathway of γ -proteobacteria: From RNA recognition to regulation of social behaviour. *Mol Microbiol*. 67(2):241-53
- Laskowski MA, Kazmierczak BI. 2006. Mutational analysis of RetS, an unusual sensor kinase-response regulator hybrid required for *Pseudomonas aeruginosa* virulence. *Infect. Immun*. 74(8):4462–73
- Le Roux M, Kirkpatrick RL, Montauti EI, Tran BQ, Brook Peterson S, et al. 2015. Kin cell lysis is a danger signal that activates antibacterial pathways of *pseudomonas aeruginosa*. *Elife*. 2015(4):1–65
- Leal J, Dong T, Taylor A, Siegrist E, Gao F, et al. 2018. Mucus-penetrating phage-displayed peptides for improved transport across a mucus-like model. *Int. J. Pharm*. 553(1–2):57–64
- Li X, Bleumink-Pluym NMC, Luijckx YMCA, Wubbolts RW, van Putten JPM, Strijbis K. 2019. MUC1 is a receptor for the *Salmonella* SiiE adhesin that enables apical invasion into enterocytes. *PLOS Pathog*. 15(2):e1007566
- Li X, Roseman S. 2004. The chitinolytic cascade in *Vibrios* is regulated by chitin oligosaccharides and a two-component chitin catabolic sensor/kinase. *Proc. Natl. Acad. Sci. U. S. A*. 101(2):627–31
- Liu Z, Miyashiro T, Tsou A, Hsiao A, Goulian M, Zhu J. 2008. Mucosal penetration primes *Vibrio cholerae* for host colonization by repressing quorum sensing. *Proc. Natl. Acad. Sci. U. S. A*. 105(28):9769–74
- Mall M, Grubb BR, Harkema JR, O’Neal WK, Boucher RC. 2004. Increased airway epithelial Na⁺ absorption produces cystic fibrosis-like lung disease in mice. *Nat. Med*. 10(5):487–93
- Mancl JM, Ray WK, Helm RF, Schubot FD. 2019. Helix Cracking Regulates the Critical Interaction between RetS and GacS in *Pseudomonas aeruginosa*. *Structure*. 27(5):785-793.e5
- Marvig RL, Sommer LM, Molin S, Johansen HK. 2015. Convergent evolution and adaptation of *Pseudomonas aeruginosa* within patients with cystic fibrosis. *Nat Genet*. 47(1):57-64

- Masuko T, Minami A, Iwasaki N, Majima T, Nishimura SI, Lee YC. 2005. Carbohydrate analysis by a phenol-sulfuric acid method in microplate format. *Anal. Biochem.* 339(1):69-72
- Mougous JD, Cuff ME, Raunser S, Shen A, Zhou M, et al. 2006. A virulence locus of *Pseudomonas aeruginosa* encodes a protein secretion apparatus. *Science.* 312(5779):1526–30
- Oliver A, Cantón R, Campo P, Baquero F, Blázquez J. 2000. High frequency of hypermutable *Pseudomonas aeruginosa* in cystic fibrosis lung infection. *Science.* 288(5469):1251–53
- Packer NH, Lawson MA, Jardine DR, Redmond JW. 1998. A general approach to desalting oligosaccharides released from glycoproteins. *Glycoconj. J.* 15(8):737–47
- Pelaseyed T, Bergström JH, Gustafsson JK, Ermund A, Birchenough GMH, et al. 2014. The mucus and mucins of the goblet cells and enterocytes provide the first defense line of the gastrointestinal tract and interact with the immune system. *Immunol. Rev.* 260(1):8–20
- Perault AI, Chandler CE, Rasko DA, Ernst RK, Wolfgang MC, Cotter PA. 2020. Host Adaptation Predisposes *Pseudomonas aeruginosa* to Type VI Secretion System-Mediated Predation by the *Burkholderia cepacia* Complex. *Cell Host Microbe.* 28(4):534-547.e3
- Scanlin TF, Glick MC. 1999. Terminal glycosylation in cystic fibrosis. *Biochim. Biophys. Acta.* 1455(2–3):241–53
- Secor PR, Michaels LA, Ratjen A, Jennings LK, Singh PK. 2018. Entropically driven aggregation of bacteria by host polymers promotes antibiotic tolerance in *Pseudomonas aeruginosa*. *Proc. Natl. Acad. Sci.* 115(42):10780-85
- Staudinger BJ, Muller JF, Boles B, Angermeyer A, Nguyen D, et al. 2014. Conditions Associated with the Cystic Fibrosis Defect Promote Chronic *Pseudomonas aeruginosa* Infection. *Am J Respir Crit Care Med.* 189(7):812–24
- Suginta W, Sritho N, Ranok A, Bulmer DM, Kitaoku Y, et al. 2018. Structure and function of a novel periplasmic chitoooligosaccharide-binding protein from marine *Vibrio* bacteria. *J. Biol. Chem.* 293(14):5150–59
- Tropini C, Earle KA, Huang KC, Sonnenburg JL. 2017. The Gut Microbiome: Connecting Spatial Organization to Function. *Cell Host Microbe.* 21(4):433-42
- van Bueren AL, Boraston AB. 2007. The Structural Basis of α -Glucan Recognition by a Family 41 Carbohydrate-binding Module from *Thermotoga maritima*. *J. Mol. Biol.* 365(3):555–60
- Wagner CE, Wheeler KM, Ribbeck K. 2018. Mucins and Their Role in Shaping the Functions of Mucus Barriers. *Annu Rev Cell Dev Biol.* 34:189-215
- Wheeler KM, Cárcamo-Oyarce G, Turner BS, Dellos-Nolan S, Co JY, et al. 2019. Mucin glycans attenuate the virulence of *Pseudomonas aeruginosa* in infection. *Nat Microbiol.* 4(12):2146-54
- Wilton M, Wong MJQ, Tang L, Liang X, Moore R, et al. 2016. Chelation of membrane-bound cations by extracellular DNA activates the type VI secretion system in *pseudomonas aeruginosa*. *Infect. Immun.* 84(8):2355–61
- Xia B, Royall JA, Damera G, Sachdev GP, Cummings RD. 2005. Altered O-glycosylation and sulfation of airway mucins associated with cystic fibrosis. *Glycobiology.* 15(8):747–75

Ye J, Pan Q, Shang Y, Wei X, Peng Z, et al. 2015. Core 2 mucin-type O-glycan inhibits EPEC or EHEC O157:H7 invasion into HT-29 epithelial cells. *Gut Pathog.* 7(1):1–9

Zanin M, Baviskar P, Webster R, Webby R. 2016. The Interaction between Respiratory Pathogens and Mucus. *Cell Host Microbe.* 19(2):159-68

Acknowledgements

The authors thank M. LeRoux, M. Guzzo, K. Gozzi, and B. Imperiali for critical feedback during the preparation of this manuscript. This research was supported by NIBIB/NIH grant R01 EB017755-04 (OSP 6940725) (to K.R.), the MRSEC Program of the National Science Foundation under award DMR-1419807 (to K.R.), the National Science Foundation Career award PHY-1454673 (to K.R.), a CEHS grant (P30-ES002109) (to K.R.), the NSF GRFP under grant no. 1745302 (to B.X.W. and K.M.W.), the National Center for Functional Glycomics Grant P41GM103694 (to R.D.C.), and an NIH grant to M.T.L. (R01GM082899), who is also an Investigator of the Howard Hughes Medical Institute. The authors thank the Cotter lab for providing strains. Contributions: B.X.W., K.M.W, K.R., and M.T.L. designed the experiments. K.C.C performed preliminary experiments and constructed strains. B.X.W. and K.M.W. performed all experiments and analyses. S.L. and R.D.C. performed the glycan mass spectrometry.

Figures

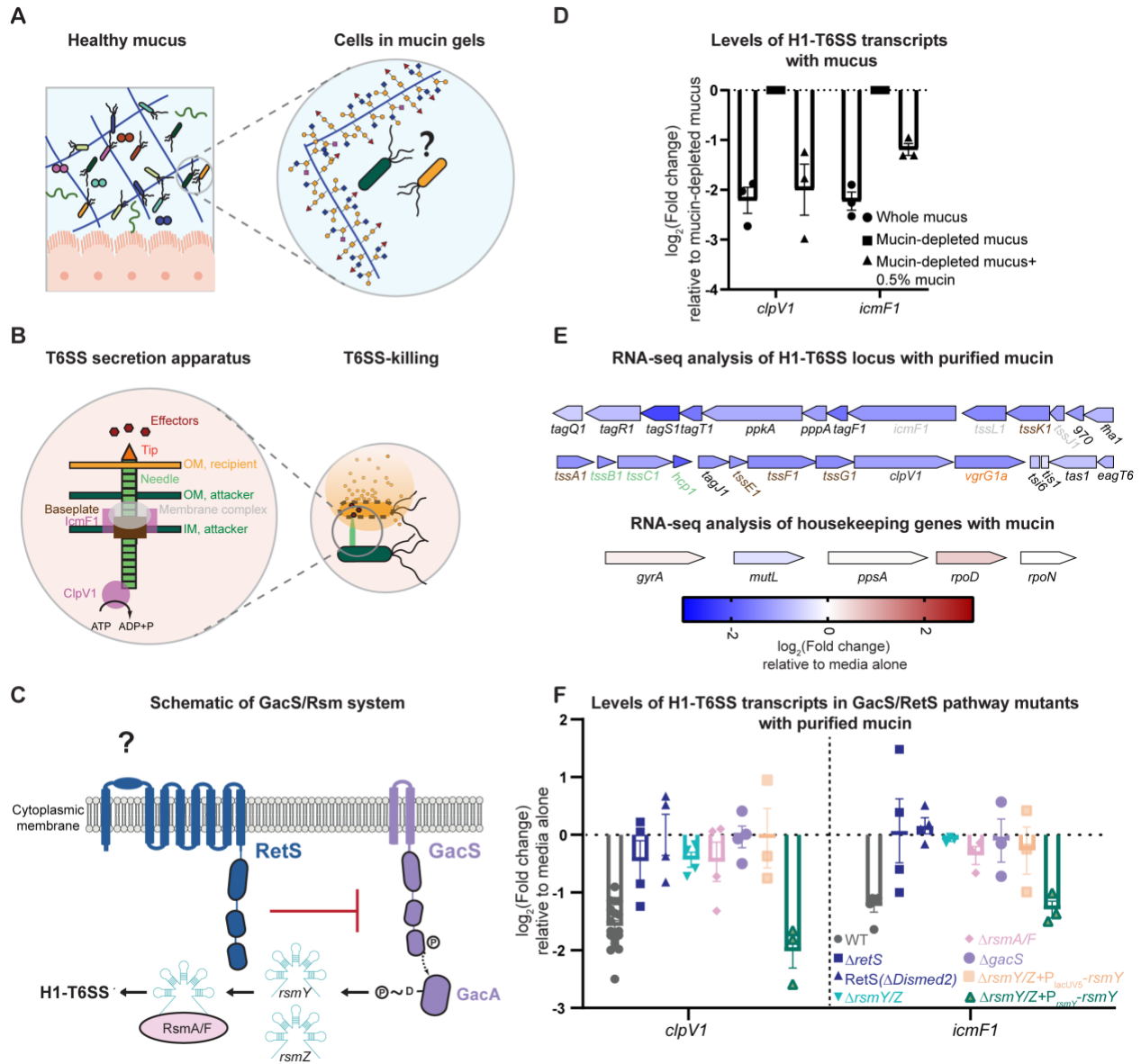


Figure 3.1. Mucin acts through the GacS/RetS/Rsm pathway to suppress the H1-T6SS. **A)** Healthy mucin suppresses bacterial virulence. The mechanisms by which mucin regulates bacterial behavior are unknown. **B)** Schematic representation of the H1-T6SS needle apparatus. Genes that were measured via qRT-PCR are shown in pink. Other key components of the T6SS are also highlighted: the baseplate in brown, the membrane complex in gray, the needle/sheath in green, the tip in orange, and the effectors in red. **C)** Schematic representation of the GacS/Rsm system, which controls H1-T6SS activation in response to unknown signals. GacS is a histidine kinase that phosphorylates GacA. Phosphorylated GacA activates transcription of the RNAs *rsmY* and *rsmZ*, which sequester the RNA-binding proteins, RsmA and RsmF. In the absence of *rsmY/Z*, RsmA and RsmF bind to H1-T6SS transcripts, which destabilizes them and also prevents their translation. By binding RsmA and RsmF,

rsmY/Z prevents these proteins from blocking H1-T6SS translation. Thus, activation of the GacS-GacA pathway upregulates the H1-T6SS, as well as dozens of other genes. RetS is an accessory histidine kinase that inhibits GacS activity. **D)** Levels of representative H1-T6SS transcripts following 1.5 hour exposure to whole mucus or mucin-depleted mucus with 0.5% MUC5AC added back, relative to mucin-depleted mucus. Transcript levels measured by qRT-PCR and normalized to a control gene (*rpoD*). Bars indicate the mean \pm SEM, with individual measurements shown (black dots). **E)** Diagram of the H1-T6SS operon and housekeeping genes representing the fold change of each gene following exposure to mucins for 5 hours relative to medium alone, measured by RNA-sequencing. The names of genes that encode key components of the T6SS apparatus are color coded according to **Figure 3.1B**. **F)** Levels of T6SS transcripts in wildtype and GacS/Rsm/RetS mutants following exposure to mucin relative to medium alone. Transcript levels measured by qRT-PCR and normalized to a control gene (*rpoD*). Bars indicate the mean \pm SEM, with individual measurements shown.

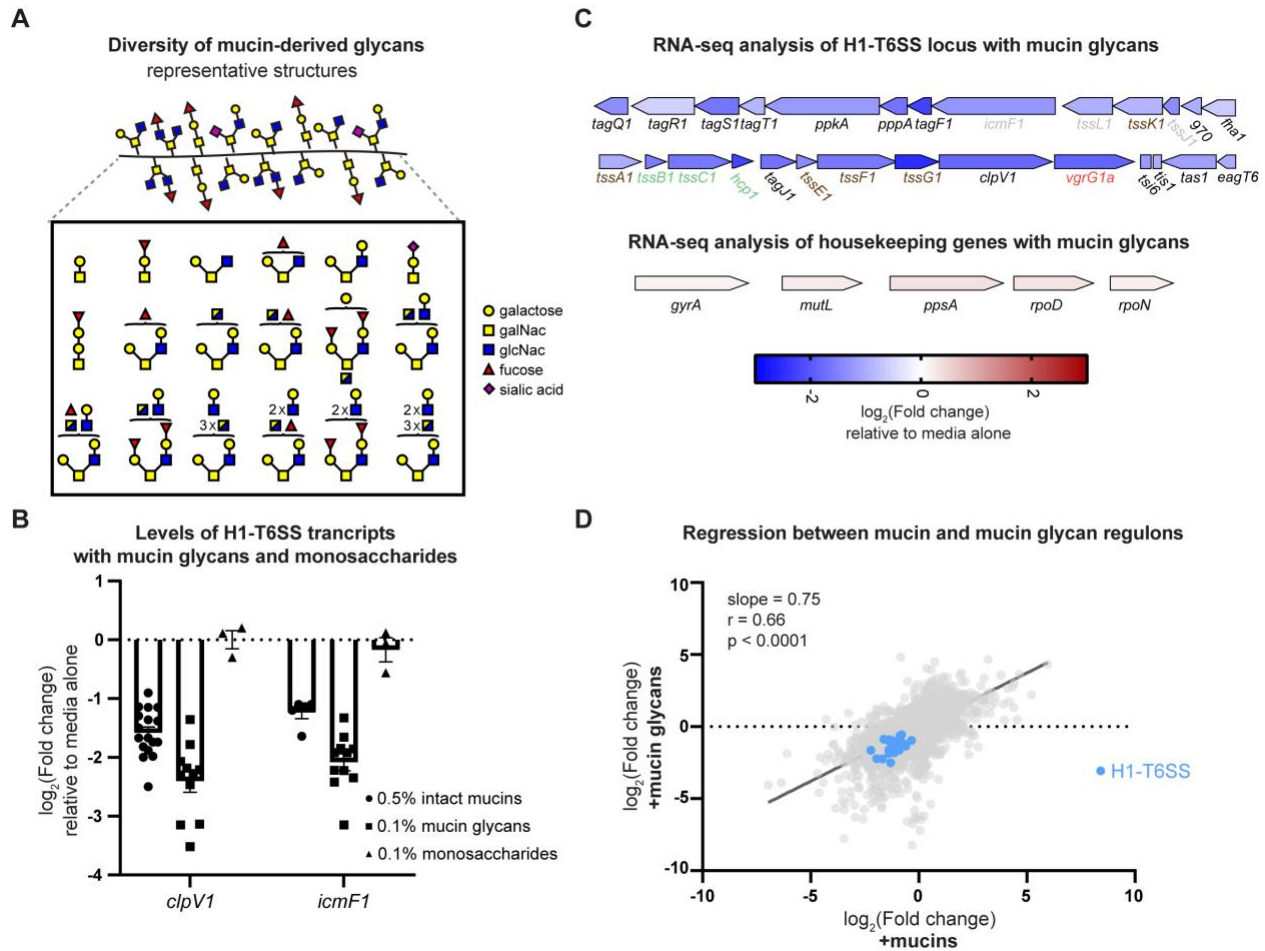


Figure 3.2. Mucin glycans are sufficient to suppress the T6SS. **A)** Representative glycan structures derived from MUC5AC, as identified by MALDI-TOF. **B)** Levels of T6SS transcripts in PA14 following exposure to the pool of mucin glycans or monosaccharides for 5 hours relative to medium alone. Transcript levels measured by qRT-PCR and normalized to a control gene (*rpoD*). Bars indicate the mean \pm SEM, with individual measurements shown (black dots). Mucin data are replicated from Figure 3.1F, for reference. **C)** Diagram of the H1-T6SS operon and housekeeping genes representing the fold change of each gene following exposure to glycans for 5 hours relative to medium alone, measured by RNA-sequencing. The names of genes that encode key components of the T6SS apparatus are color coded according to **Figure 3.1B**. **D)** Regression of glycan-induced gene expression changes against mucin-induced gene expression changes at 5 hours, as measured by RNA-sequencing. H1-T6SS genes are highlighted in blue.

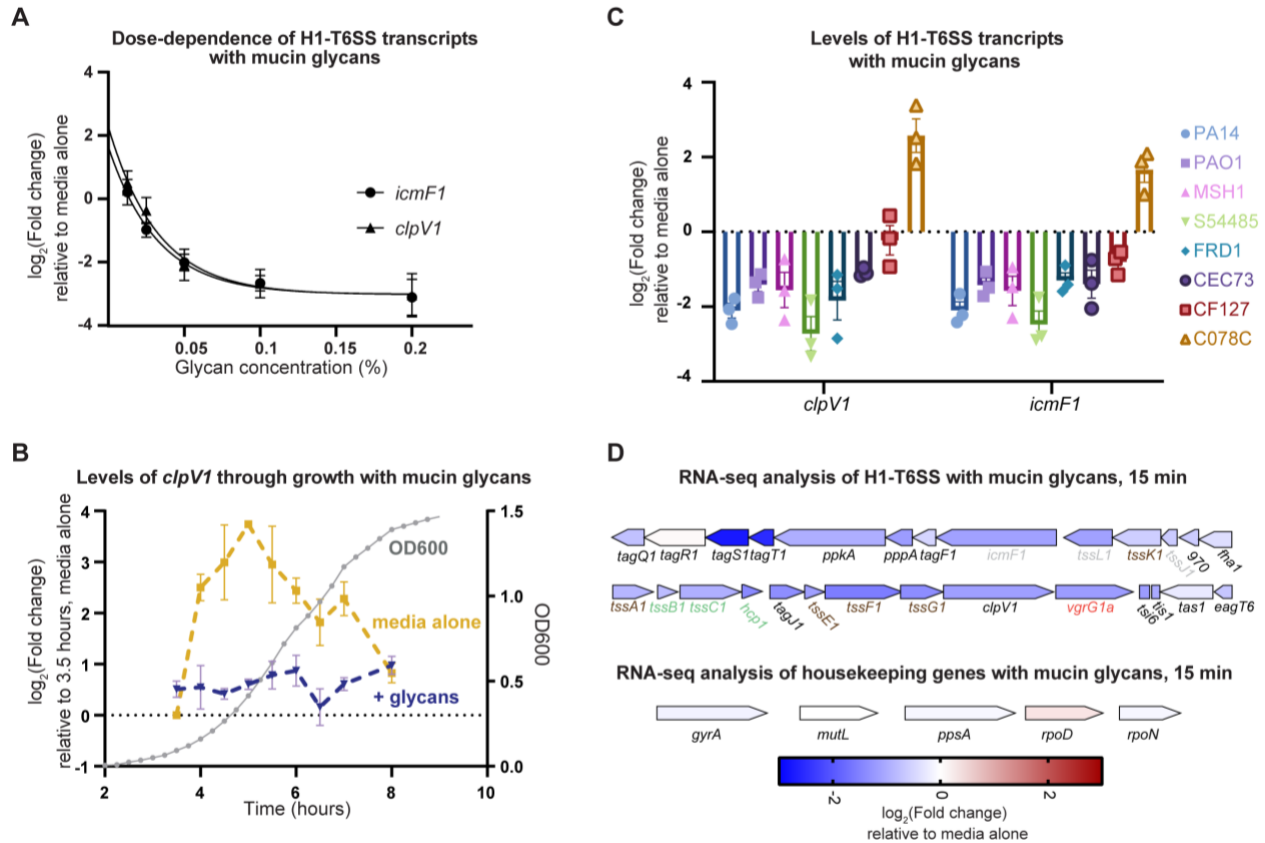


Figure 3.3. The signaling effects of mucin glycans are robust. **A)** Levels of T6SS transcripts in PA14 following 5-hour exposure to mucin glycans at different concentrations relative to medium alone. Transcript levels measured by qRT-PCR and normalized to a control gene (*rpoD*). Data points indicate the mean \pm SEM and are fitted to a one-site binding curve. **B)** Levels of T6SS transcripts in PA14 following exposure to the pool of mucin glycans (in blue) or medium alone (in yellow) at different time points, as measured by qRT-PCR and normalized to a control gene (*rpoD*). Transcript levels are measured relative to medium alone at 3.5 hours, and each point represents the mean \pm SEM (3 replicates). Grey data points indicate optical density of the culture at 600 nm. **C)** Levels of representative H1-T6SS transcripts following 5 hour exposure to 0.1% mucin glycans relative to ABTGC medium alone for different *P. aeruginosa* isolates. Transcript levels measured by qRT-PCR and normalized to a control gene (*rpoD*). Bars indicate the mean \pm SEM, with individual measurements shown. **D)** Diagram of the H1-T6SS operon and housekeeping genes representing the fold change of each gene following exposure to glycans for 15 minutes relative to medium alone, measured by RNA-sequencing. The names of genes that encode key components of the T6SS apparatus are color coded according to **Figure 3.1B**.

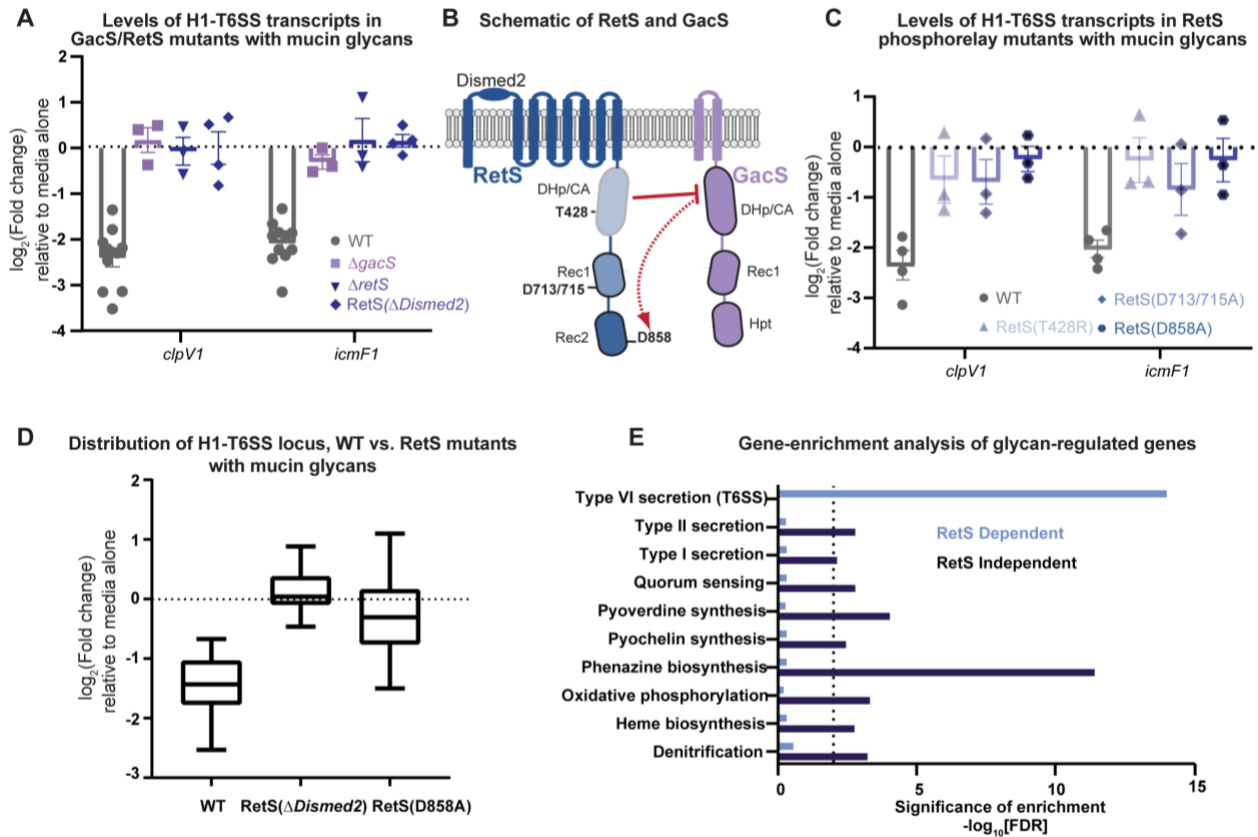


Figure 3.4. Mucin glycans promote RetS inhibition of GacS. **A)** Levels of T6SS transcripts in wild type and mutants following exposure to mucin glycans for 5 hours relative to medium alone. Transcript levels measured by qRT-PCR and normalized to a control gene (*rpoD*). Bars indicate the mean \pm SEM, with individual measurements shown. Wild type data are duplicated from **Figure 3.2B** for reference. **B)** Schematic of RetS phosphorelay domains (various shades of blue) and GacS/GacA (purple). **C)** Levels of T6SS transcripts in RetS phospho-mutants following exposure to mucin glycans for 5 hours relative to medium alone. Transcript levels measured by qRT-PCR and normalized to a control gene (*rpoD*). Bars indicate the mean \pm SEM, with individual measurements shown. **D)** Distribution of all H1-T6SS transcript levels following exposure to mucin glycans for 5 hours relative to a medium control in the wild type and RetS mutants, as measured by RNA-sequencing. Center bar represents the mean change in gene expression for all genes in the T6SS operon. **E)** Gene set enrichment analysis of RetS-dependent and RetS-independent gene sets. Bar length indicates false discovery rate for each enriched pathway. The dotted line indicates the threshold for significance.

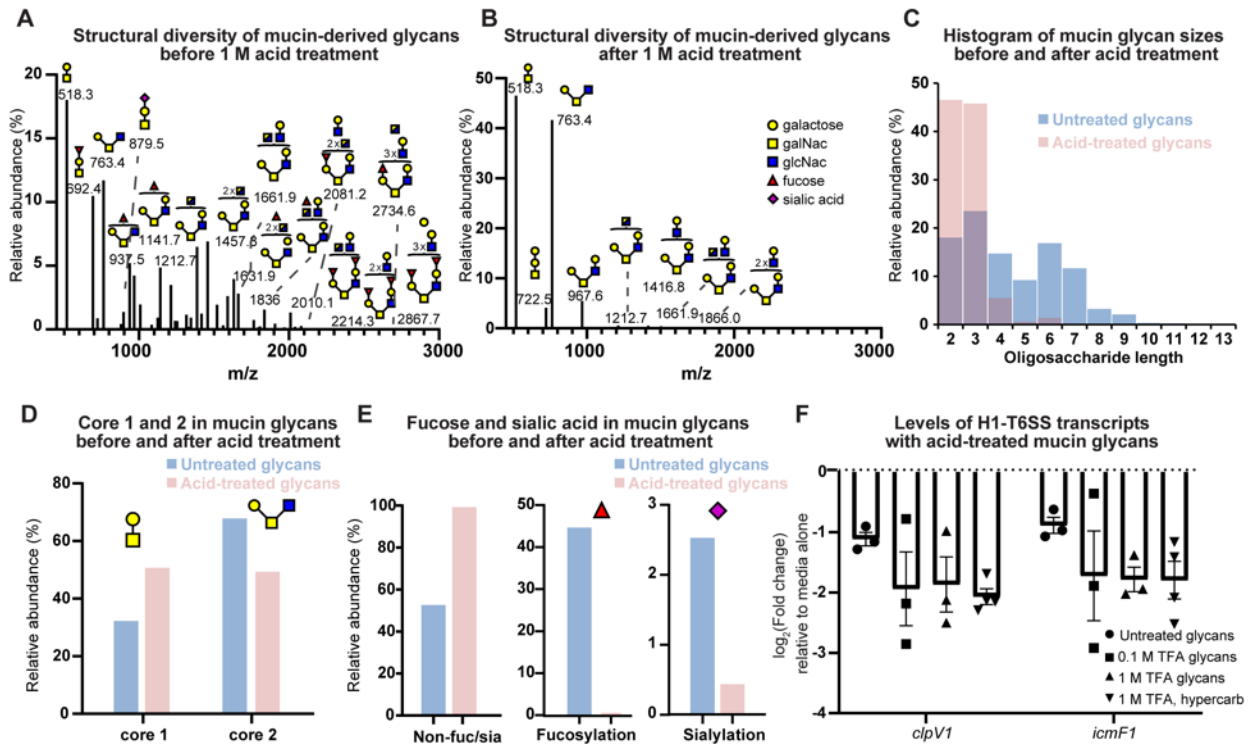


Figure 3.5. A subset of mucin glycans is sufficient for signaling. **A)** MALDI-TOF-MS spectrum of the MUC5AC glycan pool. Selected peaks labeled with monoisotopic masses and predicted structures. **B)** MALDI-TOF-MS spectrum of the MUC5AC glycan pool following partial acid hydrolysis (1 M TFA). Selected peaks labeled with monoisotopic masses and predicted structures. **C)** Distribution of glycan length in the untreated versus the acid-treated glycan pools. **D)** Relative abundance of core structures in the untreated versus the acid-treated glycan pools. **E)** Relative abundance of fucosylated, sialylated, and non-fucosylated/sialylated glycans in the untreated versus the acid-treated glycan pools. **F)** Levels of T6SS transcripts in PA14 following exposure to pools of acid-treated glycans for 5 hours relative to medium alone. Transcript levels measured by qRT-PCR and normalized to a control gene (*rpoD*). Bars indicate the mean \pm SEM, with individual measurements shown (black dots).

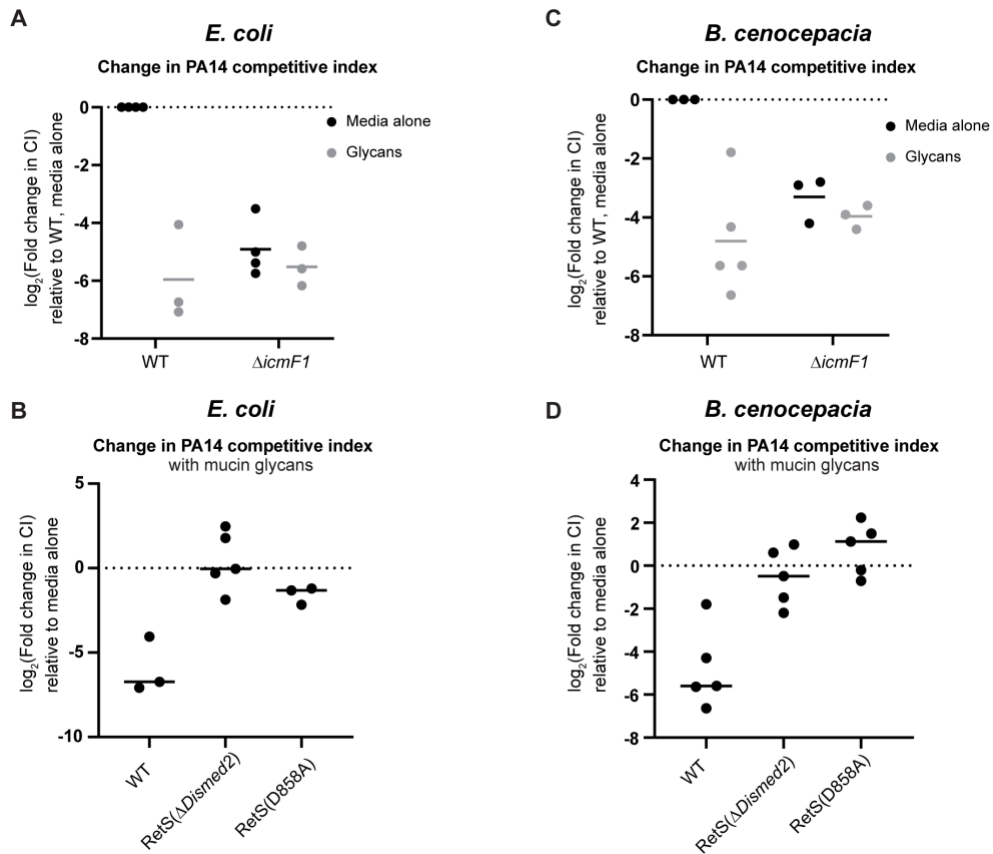


Figure 3.6. Mucin glycans suppress T6SS-mediated killing by PA14 in a RetS-dependent manner. **A,C**) Competition assay between *E. coli* (**A**) or *B. cenocepacia* (**C**) and the PA14 wild-type and T6SS mutant ($\Delta icmF1$) in the presence and absence of glycans. Center bar represents the mean change in *P. aeruginosa* competitive index relative to the wild type in medium alone, with individual measurements shown (black dots). **B,D**) Competition assay between *E. coli* (**B**) or *B. cenocepacia* (**D**) and the PA14 wild-type and RetS mutants in the presence and absence of glycans. Center bar represents the mean change in *P. aeruginosa* competitive index in the presence of glycans relative to medium alone, with individual measurements shown (black dots).

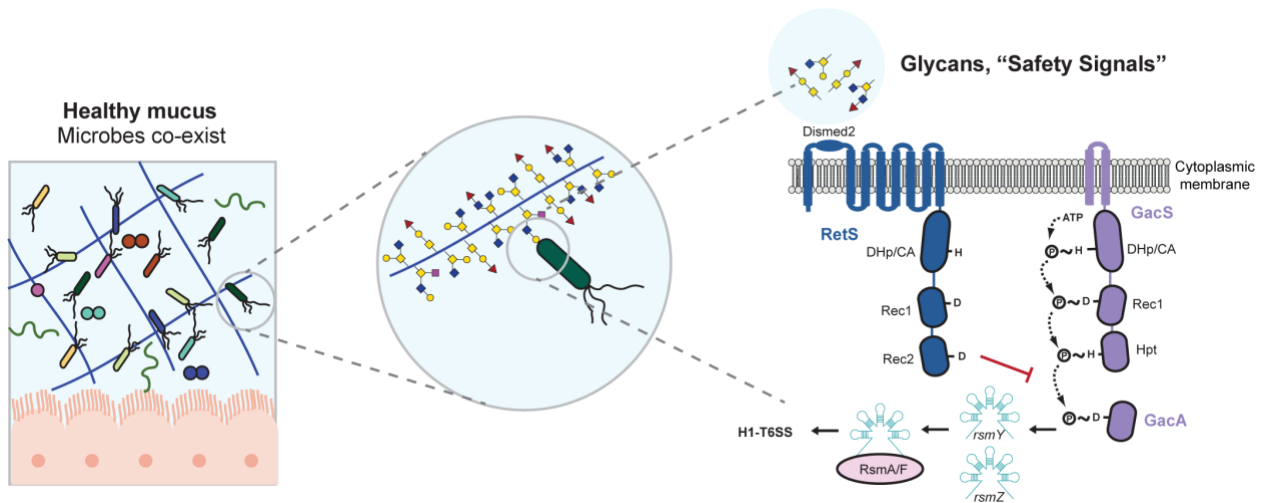


Figure 3.7. Model. Mucin glycans are host-produced “safety signals” that suppress the H1-T6SS by triggering RetS inhibition of GacS. This signaling may promote microbial co-existence in healthy mucus.

Chapter 4: Mucin glycans resist dysbiosis in complex microbial communities

Work in this chapter is in preparation for submission: Wheeler KM*, Wu CM*, Ribbeck K. Mucin glycans resist dysbiosis in complex microbial communities.

Supplementary information is provided in Appendix C.

Abstract

Mucus lines all wet epithelia in the human body and forms the first line of defense while housing dense microbial communities specific to different mucosal surfaces. Changes in microbial composition can cause disease, suggesting the presence of host mechanisms that select and stabilize these communities. Leveraging an *ex vivo* system to study human oral microbiota and libraries of mucin glycans purified from different body sites, we found that glycans specifically support growth of a wide range of health-associated microbes while resisting disease-associated compositional shifts. We uncovered that the complex glycans displayed on mucins interact with microbes by various mechanisms, serving as nutrients to recruit commensal microbes while also limiting antagonism between competing taxa. Specific glycan moieties drive the selection of certain microbes, suggesting that the unique glycosylation of mucosal tissues may tune microbial composition. Thus, mucin glycans represent potential therapeutic interventions to select and maintain a diverse, yet specialized microbiota.

Introduction

The human body hosts, in various locations, highly diverse microbial communities that have important functions in health and disease. However, dissecting the mechanisms underlying microbial community composition and function can be challenging due to their low culturability *in vitro*. This disconnect suggests that certain host factors may be important for the recruitment and retention of members in the healthy human microbiota and for the prevention of disease associated with dysbiosis, an imbalance in microbial communities.

Humans, and perhaps other hosts, have likely evolved several mechanisms to recruit beneficial microbes, maintain homeostasis, and prevent the collapse of microbial diversity. In particular,

microbial communities are embedded in a network of mucin glycoproteins (Figure 4.1A), the major gel-forming components of the mucus layer. Aberrant mucin production and changes in mucin glycosylation are associated with numerous pathologies and dysbiosis (Baughan et al. 2000; Bergstrom et al. 2020; Chaudhury et al. 2016; Einerhand et al. 2002; Fahy & Dickey 2010; Scanlin & Glick 1999; Szkaradkiewicz-Karpińska et al. 2019; Xia et al. 2005), highlighting the importance of the intact mucus barrier in health.

Mucins are comprised of a peptide backbone that is densely coated in hundreds of distinct branching sugar chains (glycans) (Figure 4.1A), which collectively represent up to 80% of mucin weight and thus offer a wealth of spatially concentrated biochemical information. Through this rich biochemistry, mucins may provide an alternative nutritional substrate for specific microbes or consortia of microbes that encode the machinery to degrade complex carbohydrates (Png et al. 2010; Sonnenburg et al. 2005; van der Hoeven et al. 1990; Wickström & Svensäter 2008). Additionally, mucins and their attached glycans can serve as virulence-attenuating signals with powerful abilities to influence microbial behavior, including the ability to swim (Caldara et al. 2012), settle (Frenkel & Ribbeck 2015), communicate (Wheeler et al. 2019), and compete (Frenkel & Ribbeck 2017; Wang et al. 2020). Based on these numerous functions, we hypothesized that mucins play a critical role in maintaining microbial homeostasis across the mucosal niches of the human body.

To date, no systematic studies exist that directly assess how mucins or their varied glycan structures interact with the microbiota to shape microbial community composition and structure. Testing how host factors or chemical interventions influence bacterial communities is challenging *in vivo* due to physiological differences between individuals and lack of experimental control. For these reasons, results are typically correlative and provide limited mechanistic insight. To bridge this gap, we cultured fully complex native microbiota obtained from the human oral cavity in a tightly controlled culture-based system to track how specific glycosylation patterns influence microbial composition. This approach enables the study of complex community dynamics in defined mucus environments that are physiologically relevant, and allows for the mechanistic dissection of mucin into its functional components. The salivary microbiota is an ideal model system for this work because these communities are easily accessible, highly diverse (Huttenhower et al. 2012), relatively stable over time (Costello et al. 2009), and seed other mucosal niches in the

gastrointestinal and respiratory tracts (Bassis et al. 2015; Ding & Schloss 2014; Schmidt et al. 2019).

We show that mucin-based medium better captures the diversity of complex oral communities found in health than a glucose-based medium. Moreover, we reveal that mucins isolated from different mucosal tissues throughout the body share a conserved function in resisting glucose-driven dysbiosis in a complex microbial community. Mucin glycans were the primary components responsible for this effect, capable of retaining health-associated bacteria and resisting dysbiosis by fundamentally shaping the metabolic landscape to support consortia of glycan-degraders and by limiting antagonism between competing taxa. The precise composition and arrangement of the sugar monomers influenced the potency and specificity of mucin glycan's effects, revealing that different mucosal tissues may tune the composition of the resident microbiota through the presentation of distinct glycosylation patterns. Taken together, these results suggest glycans as a potential therapeutic intervention for mitigating diseases related to dysbiosis.

Results

Culturing microbial communities in mucin-free medium leads to the exclusion of health-associated microbes

To assess changes in microbial ecology associated with the absence of host factors, we inoculated native microbial communities derived from human saliva in duplicate into a chemically defined high-glucose (0.5% w/v) medium developed for the cultivation of oral microbial flora. This medium mimicked the electrolyte balance of saliva (He et al. 2008), but lacked mucin as well as other host-derived factors. The inoculating salivary microbiota were highly diverse and taxonomically rich, containing at least 54 genera (range: 54-85 genera) across eight phyla (Figure 4.1B). Across the inoculating samples, 12 taxa classified to the genus level were detected at >1% average abundance (Figure 4.1B). In particular, there was a high abundance (range: 13.6 – 57.9%) of commensal Mitis group streptococci, including the species *Streptococcus mitis*, *Streptococcus oralis*, and *Streptococcus infantis*; this group is an indicator of oral health (Gross et al. 2012). The commensal bacteria *Streptococcus parasanguinis* and *Streptococcus australis* are most often included within the Mitis group (Jensen et al. 2016), but occasionally grouped with the closely related Sanguinis streptococci (Facklam 2002). Here, these species were classified as their own

independent group (as defined in Eren et al. 2014) to better understand if different, closely-related streptococci have distinct responses to their environment.

After inoculation into medium, *ex vivo* microbial communities were collected at 8, 16, 24, and 48 h of growth and 16S rRNA gene sequencing was used to quantitatively track microbial community composition over time. Beginning in the first 8 h, these *ex vivo* communities underwent a rapid loss of diversity (Figure 4.1C) and divergence from the starting community composition (Figure 4.1D) corresponding to significant reductions in abundance for nine of the dominant genera (>1% average abundance in starter culture), including *Haemophilus*, *Neisseria*, *Actinomyces*, *Gemella*, *Alloprevotella*, *Granulicatella*, *Fusobacterium*, *Rothia*, and *Leptotrichia* (Figure 4.1E). Moreover, the *Streptococcus* genus lost health-associated Mitis/Parasanguinis streptococci over time (Figure 4.1F). This loss in microbial diversity was associated with a concomitant outgrowth of the Salivarius streptococci (including the species *Streptococcus salivarius*, *Streptococcus vestibularis*, and *Streptococcus thermophilus*), which expanded from an average abundance of 3.8% (range: 0.7 – 6.9%) in the starting inoculum to 72% abundance (range: 47.9 – 90.6%) by 48 h of growth without host factors (Figure 4.1F). Intriguingly, lower diversity and shifts in the ratio of oral Mitis streptococci to Salivarius streptococci have been associated with disease, including the development of dental caries (Gross et al. 2012) and Crohn's disease (Goel et al. 2019), highlighting the biological relevance of our model.

Mucins isolated from different mucosal niches mitigate the collapse of microbial diversity

To evaluate how mucins from various tissues impact the composition of complex microbial communities, we leveraged our *ex vivo* model to test whether mucins from saliva (MUC5B), gastric mucus (MUC5AC), and intestinal mucus (MUC2) can preserve community diversity and retain health-associated community members that were lost in the absence of host factors. Critically, we gently purified mucins from native human or animal tissues in order to retain their fully complex glycan profiles (Figure 4.2A). Each mucin was then carefully reconstituted into a chemically defined medium at a physiologically relevant concentration of 0.25% (w/v) and exposed to salivary microbial communities for up to 48 h. Notably, each mucin partially mitigated the collapse in microbial diversity (Figure 4.2B) that we detected in cultures grown without mucins (Figure 4.1). In particular, the Shannon Diversity index, which accounts for both abundance and evenness of the species present in each community, was higher for cultures grown in the presence

of mucin than for communities cultured in medium without mucin (Figure 4.2B). Further, the compositions of communities cultured in medium with mucin more closely resembled the starting community than did those of cultures grown without mucin, as indicated by the Bray-Curtis dissimilarity (Figure 4.2C). These findings uncovered a conserved function across mucin types to maintain diverse communities that are more similar in composition to native microbiota.

To better understand the changes underlying the increased diversity observed with mucin, we examined the abundances of the health-associated *Mitis/Parasanguinis* streptococci. Strikingly, upon exposure to mucin, these commensal streptococci were strongly retained (Figure 4.2D, S4.1A, S4.1B). MUC2 had a particularly strong effect, as it retained these *Mitis* and *Parasanguinis* streptococci at nearly starting levels for the duration of the experiment (Figure 4.2D, S4.1A). Moreover, each mucin retained taxa that were lost in medium alone, including the commensal genus *Granulicatella* (Figure S4.1C), and limited the outgrowth of *Salivarius* streptococci to different extents (Figure 4.2E, S4.1D). Overall, these results highlight that mucins resist compositional shifts associated with disease (Goel et al. 2019; Gross et al. 2010, 2012).

In addition to compositional imbalance, changes in growth form and community structure can impact the competitive and cooperative interactions that maintain microbial homeostasis. In particular, the formation of bacterial community aggregates can create gradients in nutrients, chemical signals, and other small molecules, possibly disrupting competitive balances and driving disease progression (Parsek & Singh 2003). To assess how mucin influences the growth state of the community, we collected surface-attached biomass from the *ex vivo* cultures and compared this attached community to non-attached cells in medium with or without each mucin type. Consistent with previous work on mucin-microbe interactions (Caldara et al. 2012; Frenkel & Ribbeck 2015; Kavanaugh et al. 2014), all three mucins prevented surface attachment relative to medium alone (Figure S4.2A). In medium alone, the biofilm and planktonic communities had similar levels of diversity and similar compositions (Figure S4.2B-D). Taken together, these findings suggest that distinct mucin isoforms promote diversity, maintain commensal bacteria, and prevent surface attachment to different degrees.

Microbial community composition is shaped by mucins specific to different niches

Different mucosal tissues secrete unique mucin isoforms and also harbor distinct microbiota. Mucins from saliva (MUC5B), gastric mucus (MUC5AC), and intestinal mucus (MUC2) each

have overlapping but distinct glycan spectra (Figure 4.2A) that may have differential effects on the composition of microbial communities. For instance, while MUC5B glycans tend to have longer sugar chains and are more fucosylated and sialylated than MUC5AC and MUC2 glycans, all three mucins share a high abundance of fucosylated core structures (Figure 4.2A). To dissect the specific roles of these mucin isoforms, we applied hierarchical clustering to the sequencing data for each microbial community after 48 h of growth in medium with or without mucin. This algorithm recursively merged samples based on the similarity of the microbial community composition (pairwise distance: $1 - \text{Pearson coefficient}$), allowing for the discrimination of more subtle variations in microbial community structure. This approach identified three major sample clusters: a no-mucin cluster, a MUC2 cluster, and MUC5B cluster (Figure 4.3A). Communities cultured with MUC5AC did not form a distinct cluster, rather the communities derived from the less diverse microbiota (inoculum 1) clustered with communities cultured in MUC5B whereas communities derived from the more diverse microbiota (inoculum 2) clustered with communities cultured with MUC2. This finding may suggest that MUC5AC has an intermediate effect relative to MUC5B and MUC2. This clustering analysis suggests that the precise composition of the resulting community depends more strongly on the environment in which it was cultured than on the composition of the inoculating community. Since communities formed distinct clusters based on the particular mucin isoform in the medium (Figure 4.3A), the exact composition of the microbial community may depend on the specific structure and biochemistry of the mucin type secreted from a given body surface.

The individual taxa comprising each community were also clustered based on their relative abundances across samples (Figure 4.3B), highlighting signatures of cooccurring microbes associated with the mucin environment in general (Figure 4.3Bi), MUC2 specifically (Figure 4.3Bii), and starting inoculum 2 (Figure 4.3Biii). Signatures identified within the mucin clusters included a reduced abundance of *Salivarius* streptococci and a moderate increase in *Haemophilus*, *Gemella*, *Granulicatella*, *Prevotella*, *Veillonella*, and the *Mitis* and *Parasanguinis* streptococci relative to medium alone (Figure 4.3Bi). Differences in abundance relative to medium alone were more pronounced in the MUC2 cluster. Communities cultured in medium with MUC2 also harbored higher levels of *Pseudomonas*, *Aggregatibacter*, and *Leptotrichia* (Figure 4.3Bii). Overall, this clustering analysis reveals that community composition is driven by mucins specific

to different niches, and highlights microbial signatures corresponding to the different mucin environments.

Complex mucin glycans serve as a metabolic substrate to retain native genera

To better understand how mucins prevent the collapse of microbial communities, we began by testing one possible mechanism: that the highly abundant and diverse sugar chains on mucin promote diversity by serving as a complex nutrient source for host-adapted commensal organisms that encode glycan degradation machinery in their genomes (Figure S4.3A). For example, some strains of *S. mitis* and *S. oralis* that colonize mucosal surfaces produce neuraminidase (Figure S4.3A) and may utilize mucins as a carbon source (van der Hoeven et al. 1990). To assess whether mucins support the growth of diverse communities through nutritive mechanisms, we monitored the composition of oral communities cultured *ex vivo* in medium containing mucin, isolated mucin glycans, or a pool of the monosaccharides that comprise mucin glycans (containing equal amounts of galactose, N-acetyl glucosamine, N-acetyl galactosamine, fucose, sialic acid) as the sole carbon source. Including the pool of monosaccharides enabled us to assess the importance of their complex structural arrangement in mucin glycans, relative to the contribution from supplying diverse nutrient components.

Mucin and mucin glycans maintained higher levels of alpha diversity than the glucose-based medium (Figure 4.4A), and were each capable of supporting the growth of communities with diversity reaching levels comparable to that of the native salivary community (Figure 4.4A). Bray-Curtis dissimilarity further indicated that communities grown on mucin and mucin glycans more closely resemble the native oral microbiota than do communities grown in glucose (Figure 4.4B). Consistent with this finding, hierarchical clustering of the sequencing data revealed that the inoculating communities clustered most closely with communities cultured in medium with mucin as the sole carbon source, followed by mucin glycans (Figure 4.4C, S4.3B). By contrast, the pool of mucin-type monosaccharides only partially promoted alpha diversity (Figure 4.4A) and formed communities more divergent from the healthy starting microbiota (Figure 4.4B). Furthermore, communities cultured in medium with monosaccharides as the carbon source clustered with communities cultured in glucose-rich medium (Figure 4.4C, S4.3B). Taken together, these observations suggest that mucin glycans can shape community composition through nutritive mechanisms. Moreover, the inability of monosaccharide components to fully capture these effects

demonstrated that the complex configuration of mucin glycans is essential to maintain diverse communities that look more similar in composition to healthy starting microbiota.

We next sought to identify community members that specifically benefit from the presence of mucin glycans. Strikingly, mucin glycans maintained the majority of dominant genera from the native community (Figure 4.4D, S4.3C). In fact, the only dominant taxa significantly reduced when mucin glycans were supplied as the sole carbon source were the *Mitis*, *Parasanguinis*, and *Salivarius* streptococci (Figure 4.4D). This is in stark contrast to the glucose-based medium in which nine dominant genera were lost (Figure 4.1E). Additionally, mucin and mucin glycans each retained (i.e., log₂-transformed fold change > -1) many groups including several low-abundance genera (Figure 4.4E, S4.3C), highlighting the ability of mucin glycans to support taxonomically rich communities. In comparison, the pool of mucin-type monosaccharides only maintained a subset of the native taxa supported by mucin glycans (Figure 4.4E). Furthermore, in contrast to mucin glycans, the monosaccharides additionally enriched for *S. salivarius*, which similarly exhibited an outgrowth in glucose-based medium (Figure 4.1F). Collectively, these findings demonstrate that mucin glycans support the growth of communities as a metabolic substrate (Figure S4.3D) and specifically benefit a wide range of health-associated microbes, including a large portion of the oral microbiota that is lost in either glucose-based or monosaccharide-based medium.

Decomposing mucin glycans to their component monosaccharides revealed that the complex structural configuration of mucin glycans is essential for their role in retaining diverse genera in the community. This structural complexity may promote diversity by requiring cooperation between microbes producing different linkage-specific glycosidases to effectively break down and utilize mucin glycans. Indeed, many of the retained genera (Figure 4.4E) do not encode the putative mucin-targeting glycoside hydrolases needed for the complete degradation of glycans (Figure S4.3A), indicating that cooperative degradation may be one mechanism by which complex mucin glycans support diverse consortia of microbes. On the other hand, such cooperative degradation could also drive outgrowth of bacteria that more efficiently use free monosaccharide components, suggesting that mucin glycans may reduce competition between the microbes in addition to serving as nutritional substrates.

Complex mucin glycans suppress bacterial antagonism to promote diversity

To evaluate the possibility that mucin glycans influence community composition through a nutrient-independent mechanism, we assayed whether isolated mucin glycans are sufficient to resist the collapse of microbial diversity in the presence of high levels of glucose. Since glucose or its metabolic byproducts can be efficiently utilized by most microbes in the inoculating cultures, with the exception of the asaccharolytic bacteria *Prevotella*, *Fusobacterium*, and *Porphyromonas* (Takahashi 2005), this approach enabled us to assess the impact of mucin and its components on microbial interactions while limiting the nutritional contribution of mucin glycans and monosaccharides. By comparing fully intact mucin glycans to the pool of monosaccharides in glycans, we evaluated the impact of the complex arrangement of sugar monomers as well as the impact of adding additional non-glucose carbon to the culture (Figure 4.5Ai). In medium with high levels of glucose, a pool of monosaccharides did not retain the diversity of the oral community (Figure 4.5B, 4.5C) and did not impact the final composition of the microbial community (Figure 4.5D-H) relative to medium alone. Thus, the addition of other carbon sources that compose mucin glycans is not sufficient to promote diversity when glucose is abundant.

In contrast to the pool of monosaccharides, both MUC5B and MUC5AC glycans increased alpha diversity to approximately the same extent as whole intact MUC5AC and MUC5B (Figure 4.5B). Similarly, relative to communities grown in medium alone, communities cultured in medium with mucin glycans more closely resembled the starting communities in terms of composition (Figure 4.5C). Upon hierarchical clustering, communities cultured in medium containing mucin glycans clustered with communities cultured in medium with mucin (Figure S4.4A). Closer inspection of the microbial compositions of nodes in each cluster revealed groups of cooccurring taxa underlying the clustering patterns (Figure S4.4A). In particular, *Salivarius* streptococci were less abundant in medium with mucin or mucin glycans than in medium alone (Figure 4.5D). By contrast, commensal *Mitis* and *Parasanguinis* streptococci were enriched in medium with mucin glycans relative to medium alone (Figure 4.5E, 4.5F). Additionally, the glycan utilizers *Gemella* and *Granulicatella* were enriched in medium with mucin glycans versus medium alone (Figure 4.5G, 4.5H). In general, mucin glycans had a stronger effect on communities than whole mucin, suggesting that the peptide backbone is not essential to their ability to alter microbial community composition. Rather, mucin's associated glycans are the primary effector. Moreover, since monosaccharide components were unable to retain the abundance of these predominant

commensals (Figure 4.5E-H), it appears that the complex arrangement of monosaccharides is key to their function.

For each of these glycan signatures, we probed competitive dynamics by further examining the changes in abundance from the starting inoculum to 8 h, and from 8 h to 48 h (Figure S4.4B-F). This analysis revealed that the increases in the relative abundance of *Salivarius* streptococci occurred during the first 8 h of growth, after which point the abundance remained at approximately the same level for the remainder of the experiment, with glycans limiting the magnitude of outgrowth in the first 8 h (Figure S4.4B). This limited outgrowth corresponded with an increasing abundance of *Mitis* streptococci in the first 8 h (Figure S4.4C). Similarly, while the *Parasanguinis* streptococci, *Granulicatella*, and *Gemella* were each largely outcompeted in the first 8 h in medium alone (Figure S4.4D-F), in the presence of mucin glycans, *Parasanguinis* streptococci were retained at their initial abundance for the duration of the experiment (Figure S4.4D), and the loss of *Granulicatella* and *Gemella* was slowed by mucin glycans (Figure S4.4E, S4.4F). Taken together, these experiments showcase that loss of diversity in the absence of mucin glycans is likely the consequence of competition with *Salivarius* streptococci. By reducing bacterial antagonism or retaining less-competitive streptococci, mucin glycans may contribute to a more permissible environment for other taxa.

We gleaned further insights into the potential non-nutritive roles of mucin glycans by examining cases in which bacteria were differentially retained by mucin glycans in high-glucose medium versus when mucin glycans were provided as the sole carbon source. For example, when grown with glucose in the absence of mucin glycans, *Salivarius* streptococci outcompeted commensal *Mitis/Parasanguinis* streptococci, but when mucin glycans were included in the glucose medium, these two groups coexisted (Figure 4.5I). If the retention of *Mitis/Parasanguinis* streptococci were due to their ability to effectively utilize mucin glycans, then we would expect this group to be enriched in cultures where mucin glycans were the sole carbon source. On the contrary, neither the commensal *Mitis/Parasanguinis* streptococci nor the *Salivarius* streptococci were retained when mucin glycans were the sole carbon source (Figure 4.5I). Thus, mucin glycans support the coexistence of *Mitis/Parasanguinis* and the *Salivarius* streptococci, likely by suppressing competitive interactions rather than through a nutrient-dependent mechanism. Another informative comparison is of the glycan-utilizing bacteria *Gemella* and *Granulicatella* (Zhou et al. 2016). While both *Gemella* and *Granulicatella* were enriched in the presence of glycans alone, these two

genera were each present at lower levels In medium containing both glycans and glucose (Figure 4.5J), indicating that high nutrient conditions indeed mask the metabolic contribution(s) of mucin glycans. Taken together, these results illustrate how systematic comparisons between culturing environments can be leveraged to disentangle the multiple mechanisms underlying the composition of microbial communities. Moreover, these outcomes demonstrate that glycan-mediated suppression of competition likely plays a major role in facilitating microbial coexistence.

Mucin glycans promote the prolonged coexistence of competing microbes

To more closely monitor the interactions between mucin glycans and socially cohesive communities of bacteria over a prolonged period, we complemented our batch culturing approach with a serial passaging approach that facilitates the self-assembly of stable microbial communities (Goldford et al. 2018). Specifically, each community cultured in the defined glucose medium with or without mucin glycans (inocula 3 and 4, in duplicate) was further propagated every 48 hours for a total of 10 passages. Consistent with batch culturing, when *ex vivo* salivary communities were passaged in medium without mucin glycans, *Salivarius* streptococci rapidly increased in abundance, outgrowing the culture after two passages and remaining dominant (at >99% abundance) for the entirety of the experiment (Figure 4.6A).

In contrast to the *Salivarius*-dominated communities that assembled in medium alone, when passaged in medium supplemented with mucin glycans, the oral communities assembled into two distinct stable states, depending on the starting inoculum. Specifically, inoculum 3 assembled into a state in which a low abundance of *Lactobacillus* (range: 1.3% - 4.3%) coexisted with *Veillonella* (range: 89.8% - 98.4%), while inoculum 4 assembled into a state in which *Parasanguinis* streptococci (range: 35.7% - 58.0%) coexisted with *Veillonella* (range: 41.9% - 64.3%) (Figure 4.6B). *Veillonella* are unable to utilize glucose or mucin sugars as a carbon source and instead utilize lactate (Distler & Kröncke 1981), a byproduct of *Streptococcus* and *Lactobacillus* metabolism (Kandler 1983). Thus, while these findings suggest that the precise interaction networks present in the inoculating microbiota influence the final composition, the final states are functionally similar as we see coexistence of lactic acid-producing bacteria and lactic acid-utilizing bacteria in all four assemblages formed in the presence of mucin glycans.

Previous work has revealed that the collapse of communities competing for a single limiting nutrient may be stabilized through metabolic facilitation, which in turn leads to the coexistence of

multiple species (Goldford et al. 2018). The prolonged coexistence of *Veillonella* and Parasanguinis, but not Salivarius streptococci is therefore intriguing as both groups of Streptococci secrete metabolic by-products that should be utilizable by *Veillonella*. This suggests that the presence of metabolically cohesive bacteria is not always sufficient to promote stable coexistence, and that other host or environmental factors may be necessary to mitigate inhibitory interactions between species. For instance, *Veillonella* can be inhibited by certain metabolites produced during glucose fermentation by a range of oral streptococci, especially strains of *S. salivarius* (Doran et al. 2004). Since Parasanguinis streptococci were enriched by glycans in the presence of glucose (Figure 4.5F), but do not benefit from glycans as a sole carbon source (Figure 4.4D) (Zhou et al. 2016), the observed glycan-mediated coexistence of *Streptococcus* and *Veillonella* (Figure 4.6B) is likely not the result of changes to the available metabolic substrates, but rather reduced antagonism between Salivarius streptococci, Parasanguinis streptococci, and *Veillonella*. Overall, this experiment provides further support that mucin glycans play a role in maintaining microbial homeostasis, and it additionally reveals that mucin glycans influence competitive interactions between microbes over a prolonged period to support the stable assembly of diverse communities.

Mucin glycan structural patterns influence their potency and specificity

Building off our finding that community composition diverged with mucins isolated from different niches (Figure 4.3A), an intriguing hypothesis is that conserved glycan structures on mucin may have a role in recruiting and retaining specific microbes and that differences in mucin glycosylation may in turn impact the selectivity of mucus. To test this hypothesis, we created pools of glycans from MUC5AC and MUC5B and applied partial acid hydrolysis to MUC5AC glycans to obtain a glycan library of reduced complexity (Wang et al. 2020). Libraries of MUC5B and MUC5AC glycans tend to contain highly diverse, yet overlapping structures, with ~25% of the MUC5B glycan library being unique to MUC5B and only 4% of the MUC5AC glycan library unique to MUC5AC (unpublished data). In general, MUC5B glycans were longer and contained slightly more fucose and sialic acid than MUC5AC glycans (Figure 4.2A), while hydrolyzed glycans consisted almost entirely of unmodified core structures without fucosylation or sialylation (Wang et al. 2020). The most abundant structures on MUC5B and MUC5AC were present in both libraries at different relative abundances: fucosylated core-1 (26.0% and 17.3%, respectively), fucosylated core-2 (13.2% and 40.2%, respectively), core-2 glycans extended with both galactose and fucose (2.3% and 7.7%, respectively), and unmodified core-1 (2.6% and 3.7%, respectively). This library

of mucin glycans positioned us to test whether differences in structural complexity, glycan size, and/or modification with fucose or sialic acid influence the ability of mucin glycans to retain microbial diversity.

To determine whether different glycan profiles select for different microbes, we cultured native microbial communities in pools of complex MUC5B glycans, MUC5AC glycans, or partially hydrolyzed glycans and evaluated how specific glycosylation patterns impacted the composition of the microbial communities (Figure 4.5Aii). Communities grown in MUC5AC glycans and MUC5B glycans exhibited similar trends in diversity (Figure 4.5B, 4.5C) and membership (Figure 4.5D-H), providing evidence that glycan structures contribute to mucin's conserved ability to support characteristics of microbial communities associated with health. However, MUC5AC glycans generally had a stronger effect on the community composition than MUC5B glycans, particularly regarding the reduction of *Salivarius* streptococci (Figure 4.5D) and retention of *Mitis* streptococci (Figure 4.5E). The precise glycan patterns in each of the glycan pools therefore likely impact their function. In addition, the hydrolyzed glycan library (which had lower complexity) had an intermediate effect on diversity relative to mucin glycans and medium alone (Figure 4.5B). Intriguingly, this intermediate effect on diversity was not due to partial function across all bacterial groups, but rather due to changes in a subset of select taxa to an extent comparable to those prompted by the fully complex MUC5AC and MUC5B glycan pools. Specifically, relative to medium alone, hydrolyzed glycans increased the abundance of *Parasanguinis* streptococci and *Gemella* (Figure 4.5F, 4.5H) but not *Mitis* streptococci or *Granulicatella* (Figure 4.5E, 4.5G), suggesting that unmodified core structures may be sufficient to enrich certain bacteria, while the presence of fucose, sialic acid, and extended N-acetyl lactosamine chains may be important for maintaining others. Collectively, these findings reveal that mucin glycans maintain the diversity and composition of microbial communities, and that the potency and specificity of these effects vary with glycan pools with differing complexity and structures.

Discussion

Dietary sugar as well as changes in mucus production are associated with dysbiosis and the progression of various diseases (Baughan et al. 2000; Einerhand et al. 2002; Fahy & Dickey 2010; Marsh 1991; Szkaradkiewicz-Karpińska et al. 2019; Zhernakova et al. 2016). However, the underlying mechanisms by which the mucus layer impacts community composition and structure

to promote health was unclear. To address this gap, we developed a highly tractable and clinically-relevant mucin-based *ex vivo* culturing system with the ability to bridge *in vivo* and *in vitro* microbiome studies. The ability to culture highly diverse microbial communities *ex vivo* represents a valuable tool for the research community, allowing researchers to answer mechanistic questions about how the host mediates microbial community assembly. Here, we found that mucin glycans protected against compositional changes associated with disease. Specifically, mucin glycans resisted the collapse of microbial diversity and opposed microbial outgrowth in the presence of simple dietary sugars, rendering efficient glucose metabolizers less competitive. Furthermore, when nutrients were scarce, we found that mucin glycans could serve as a metabolic substrate to recruit microbes and foster diversity.

While many strains of bacteria retained by mucin, mucin glycans, or monosaccharides encode glycan degradation machinery, about half of the retained genera did not possess putative mucin-targeting glycoside hydrolases (Figure S4.3A) and are not known to utilize metabolic byproducts like lactic acid. This suggests that mucin glycan degradation may facilitate cooperativity and support the growth of certain bacteria (e.g., *Gemella*), but not others (e.g., *Streptococcus*). In combination with previous work (van der Hoeven et al. 1990; Wickström & Svensäter 2008), these findings underscore that mucin glycans can indeed influence community composition by serving as a nutritional substrate. However, it is unlikely that mucin glycans acting solely as a source of nutrition are sufficient to maintain diverse communities in the host. Several studies have demonstrated that bacteria with the ability to utilize mucin glycans actually prefer to consume dietary sugars when they are available (Schwalm et al. 2017; Sonnenburg et al. 2005). Consequently, the nutritive role of mucin glycans may be masked in native saliva or gastrointestinal mucus, where dietary polysaccharides and fermentable sugars are often abundant. Further, while commensals may benefit from diverse nutrient availability, so too can potentially harmful bacteria whose ability to utilize mucin glycans or byproducts of mucin metabolism could drive outgrowth (Flynn et al. 2016; Hall et al. 2017; MacMillan et al. 2019). Thus, while mucin's ability to serve as a substrate is important in certain contexts, it is also likely that mucin glycans act through additional mechanisms to maintain microbial homeostasis.

This possibility is supported by the experiments performed in the high-glucose medium, where the metabolic contributions of mucin glycans were masked (Figure 4.5J). In this high-glucose environment, mucin glycans promoted the coexistence of competing bacteria (Figure 4.5, 4.6) that

did not benefit from glycans supplied as a sole carbon source (Figure 4.4). Thus, in this condition, mucin glycans likely prevent the collapse of diversity through mechanisms beyond nutrition, such as modulating cooperative and antagonistic microbial interactions between bacteria. For instance, mucin glycans can suppress quorum sensing in certain bacteria (Wheeler et al. 2019), which controls the production and secretion of numerous inhibitory compounds (Mukherjee & Bassler 2019). Moreover, the salivary mucin MUC5B promotes the prolonged coexistence of the oral commensal *Streptococcus sanguinis* and the cariogenic *Streptococcus mutans* by preventing surface colonization (Frenkel & Ribbeck 2017), and MUC5AC glycans prevent killing of *Escherichia coli* and *Burkholderia cenocepacia* by *Pseudomonas aeruginosa* by suppressing the expression of its bactericidal type VI secretion system (Wang et al. 2020). Taken with the findings of this study, these dual species models further highlight how the attenuation of competitive interactions by mucins or mucin glycans can facilitate the coexistence of competing species to promote diversity.

Intriguingly, the degree to which mucin glycans resisted dysbiosis and the specific microbes retained by these glycans were influenced by the precise patterns present in each glycan library (Figure 4.5). In the living host, mucin glycosylation profiles vary across body sites (Holmen Larsson et al. 2013; Tailford et al. 2015). Thus, the presentation of characteristic mucin glycosylation patterns may be a mechanism by which the body recruits bacteria to a given mucosal niche and may contribute to the distinctive microbial profiles observed at each site. Changes to these characteristic mucin glycosylation patterns may, in turn, lead to dysbiosis. The ability to tune these glycosylation patterns would therefore represent a promising strategy for altering the composition and behavior of the microbiota in a manner that benefits host health.

Materials and Methods

Collection of inoculating microbial communities. Human saliva (5 mL) was collected from healthy subjects through gentle aspiration with a custom vacuum pump. Subjects were asked to refrain from any food or drink 2 h before donating saliva. Saliva samples were collected after explaining the nature and possible consequences of the studies, obtaining informed consent, and receiving approval from the institutional review board and Massachusetts Institute of Technology's Committee on the Use of Humans as Experimental Subjects under protocol #1312006096. For each inoculum, saliva samples from three donors were pooled.

Mucin purification. This study used native porcine gastric mucins (MUC5AC), porcine intestinal mucins (MUC2), and human salivary mucins (MUC5B). Native mucins were purified as previously reported (Caldara et al. 2012; Frenkel & Ribbeck 2015; Kavanaugh et al. 2014). Briefly, mucus was scraped from fresh pig stomachs and intestines, solubilized in sodium chloride with protease inhibitors, and insoluble material was removed by ultracentrifugation at 190,000 x *g* for 1 h at 4 °C (40,000 rpm, Beckman 50.2 Ti rotor with polycarbonate bottles). Submandibular saliva was collected in bulk (50 mL/sample) from human volunteers using a custom vacuum pump, pooled, centrifuged, and protease inhibitors were added. Mucins were purified using size-exclusion chromatography on separate Sepharose CL-2B columns. Mucin fractions were then desalted, concentrated, and lyophilized for storage at -80 °C. Lyophilized mucins were reconstituted by shaking them gently at 4 °C overnight in the desired medium. Mass spectrometry was used to monitor the composition of purified mucin extracts, as is routine (Caldara et al. 2012).

Isolation of mucin O-glycans. This study applied non-reductive alkaline β -elimination ammonolysis to dissociate non-reduced glycans from mucins as described previously (Wang et al. 2020; Wheeler et al. 2019). Purified mucins were dissolved in ammonium hydroxide saturated with ammonium carbonate and incubated at 60 °C for 40 h to release oligosaccharide glycosylamines and partially deglycosylated mucins. Volatile salts were removed via repeated centrifugal evaporation and the oligosaccharide glycosylamines were separated from residual deglycosylated mucins via centrifugal filtration through 3-5 kDa molecular weight cut-off membranes in accordance with the manufacturer's instructions (Amicon Ultracel). The resulting oligosaccharide glycosylamines were converted to reducing oligosaccharide hemiacetals via treatment with boric acid. Residual boric acid was removed via repeated centrifugal evaporation

from methanol. Glycans were further purified via solid-phase extraction through Hypercarb mini-columns (ThermoFisher) and residual solvents were removed through centrifugal evaporation. MALDI-TOF mass spectrometry is routinely used to monitor the composition of the isolated mucin glycans (Wang et al. 2020; Wheeler et al. 2019).

Partial acid hydrolysis of released mucin O-glycans. For isolation of core glycan structures, we used partial acid hydrolysis (Wang et al. 2020) in which different monosaccharides were hydrolyzed from intact glycans. To remove terminal sialic acid and fucose, glycans were incubated in 1 M trifluoroacetic acid at 80 °C for 4 h. Glycans were then neutralized with KOH, incubated at room temperature for 10 min to allow salts to precipitate, and then centrifuged at 16,000 x g for 10 min to remove precipitant. Soluble glycans were purified through Hypercarb cartridges primed with 4 column volumes of 100% acetonitrile, then flushed with 4 column volumes of water. Hypercarb cartridges were washed with 2 column volumes of water and 1 column volume of 2% acetonitrile to remove salts and monosaccharides. Glycans were then eluted using 2 column volumes of 50% acetonitrile and dried via centrifugal evaporation.

Batch culture. Native bacterial communities from healthy individuals were grown in various controlled environments consisting of chemically defined medium (He et al. 2008) with glucose as the carbon source or without the addition of a carbon source. Pooled saliva samples were inoculated into 100 µL of culture medium with or without mucin, a pool of free monosaccharides present on mucin (including N-acetyl glucosamine, N-acetyl galactosamine, galactose, fucose, and sialic acid in equal concentrations; each monosaccharide purchased from Sigma), or a pool of isolated mucin glycans. Cultures were incubated under anaerobic conditions for up to 48 h at 37 °C, and then collected via centrifugation for total DNA extraction.

Serial passaging. To assess the membership of stabilized communities cultured with or without mucin glycans, we sequentially passaged healthy microbial communities. Aliquots (5 µL) of the starting saliva pool were inoculated into 100 µL of the chemically-defined glucose medium. In addition to medium alone, culture medium was supplemented with a pool of isolated mucin glycans. Cultures were grown anaerobically for 48 h at 37 °C. Each culture was homogenized by pipetting up and down 10 times before passaging. Passaging was performed by taking 2 µL from each culture as inocula for 100 µL of fresh medium. This process was repeated every 48 h for a

total of 10 passages. Samples were collected after each passage, flash frozen, and stored at -80 °C prior to DNA extraction and sequencing.

Community membership analysis. Total genomic DNA from bacterial samples was isolated at multiple time points from 0 to 48 h with an initial lysozyme treatment (Thermo Fisher) and bead beating step with lysing matrix B (MP Biomedicals), followed by extraction with the MasterPure DNA Purification Kit (EPICENTRE) in accordance with the manufacturer's instructions. The V4 region of the 16S rRNA gene was PCR amplified and the resulting amplicons were cleaned, quantified, and sequenced on the Illumina MiSeq platform by the MIT BioMicro Center as previously described (Preheim et al. 2013). Raw sequences (300 bp paired end reads) were processed and taxonomic assignments were determined using QIIME2 (Quantitative Insights Into Microbial Ecology) (Estaki et al. 2020) and the Human Oral Microbe Database (Chen et al. 2010). QIIME2 was also used to quantify diversity metrics. Prior to calculating fold changes, a pseudocount of 0.001% was added (corresponding to < 1 read) to each taxa to ensure the generation of real numbers. Hierarchical clustering was performed and visualized using Morpheus (<https://software.broadinstitute.org/morpheus>). Specifically, unless otherwise noted, communities were clustered based on the relative abundance of each genera present at >0.1% average abundance in at least one condition using the 1-Pearson distance metric, and average linkage.

Validation of *Streptococcus* group annotations. Since streptococci have highly similar 16S regions (Facklam 2002; Kawamura et al. 1995), we sequenced the variable ribosomal intergenic spacer region of streptococci isolated from the saliva samples to further verify these assignments. Following growth in medium with or without mucin glycans, microbial communities were homogenized by pipetting up and down and then 1 µL of medium was used to isolate individual bacteria on Brucella blood agar plates with hemin, and vitamin K (VWR). After growth for 48 h in an anaerobic box at 37 °C, single colonies were picked and re-streaked onto Mitis-Salivarius agar (VWR), a selective medium that facilitates the growth and phenotypic identification of streptococci. After growth for 48 h in an anaerobic box at 37 °C, single colonies were picked and cultured in liquid medium. Once turbid, bacterial DNA was extracted, purified, and quantified by nanodrop. The intergenic spacer region between the large and the small subunit of ribosomal sequences (RIS) was then PCR amplified using the Phusion high fidelity polymerase Master Mix (NEB), purified template DNA, and the following primers: Forward (5'-TGCGGCTGGATCCCCTCCTT-3') and Reverse (5'-CCGGGTTTCCCCATTCGG-3')

(Cardinale et al. 2004). To amplify the gene product, the following cycling parameters were used: Initial denaturation, 98°C for 3 m. 35 cycles: Denaturation, 98°C for 10 s; Annealing, 56°C for 30 s; Extension, 72°C for 45 s. Final extension, 72°C for 10 m. In total, 7 isolates were successfully obtained and sequenced. Alignment with BLAST identified 4 isolates as *Streptococcus salivarius*, and 3 isolates as *Streptococcus oralis*. Sequences aligning to the *Streptococcus oralis* RIS region also aligned at >99% identity to the *Streptococcus mitis* and *Streptococcus infantis* RIS regions.

Statistical analysis. Unless otherwise noted, significant changes in diversity relative to medium alone were assessed using the repeated measures one-way ANOVA with Dunnett's multiple comparison test. Significant changes in taxa abundance were identified with one-way, two-sided t-tests. Significance threshold was adjusted with Bonferroni correction for multiple comparisons.

References

- Bassis CM, Erb-Downward JR, Dickson RP, Freeman CM, Schmidt TM, et al. 2015. Analysis of the upper respiratory tract microbiotas as the source of the lung and gastric microbiotas in healthy individuals. *MBio*. 6(2):e00037
- Baughan LW, Robertello FJ, Sarrett DC, Denny PA, Denny PC. 2000. Salivary mucin as related to oral *Streptococcus mutans* in elderly people. *Oral Microbiol. Immunol.* 15(1):10–14
- Bergstrom K, Shan X, Casero D, Batushansky A, Lagishetty V, et al. 2020. Proximal colon–derived O-glycosylated mucus encapsulates and modulates the microbiota. *Science (80-.)*. 370(6515):467–72
- Caldara M, Friedlander RS, Kavanaugh NL, Aizenberg J, Foster KR, Ribbeck K. 2012. Mucin biopolymers prevent bacterial aggregation by retaining cells in the free-swimming state. *Curr. Biol.* 22(24):2325–30
- Cardinale M, Brusetti L, Quatrini P, Borin S, Puglia AM, et al. 2004. Comparison of different primer sets for use in automated ribosomal intergenic spacer analysis of complex bacterial communities. *Appl. Environ. Microbiol.* 70(10):6147–56
- Chaudhury NMA, Proctor GB, Karlsson NG, Carpenter GH, Flowers SA. 2016. Reduced mucin-7 (MUC7) sialylation and altered saliva rheology in Sjögren’s syndrome associated oral dryness. *Mol. Cell. Proteomics.* 15(3):1048–59
- Chen T, Yu WH, Izard J, Baranova O V., Lakshmanan A, Dewhirst FE. 2010. The Human Oral Microbiome Database: a web accessible resource for investigating oral microbe taxonomic and genomic information. *Database (Oxford)*. baq013
- Costello EK, Lauber CL, Hamady M, Fierer N, Gordon JI, Knight R. 2009. Bacterial community variation in human body habitats across space and time. *Science (80-.)*. 326(5960):1694–97
- Ding T, Schloss PD. 2014. Dynamics and associations of microbial community types across the human body. *Nature*. 509(7500):357–60
- Distler W, Kröncke A. 1981. The lactate metabolism of the oral bacterium *Veillonella* from human saliva. *Arch. Oral Biol.* 26(8):657–61
- Doran A, Kneist S, Verran J. 2004. Ecological Control: In Vitro Inhibition of Anaerobic Bacteria by Oral *Streptococci*. *Microb. Ecol. Health Dis.* 16(1):23–27
- Einerhand AWC, Renes IB, Makkink MK, Van Der Sluis M, Büller HA, Dekker J. 2002. Role of mucins in inflammatory bowel disease: Important lessons from experimental models. *Eur. J. Gastroenterol. Hepatol.* 14(7):757–65
- Eren AM, Borisy GG, Huse SM, Mark Welch JL. 2014. Oligotyping analysis of the human oral microbiome. *Proc. Natl. Acad. Sci. U. S. A.* 111(28):E2875-84
- Estaki M, Jiang L, Bokulich NA, McDonald D, González A, et al. 2020. QIIME 2 Enables Comprehensive End-to-End Analysis of Diverse Microbiome Data and Comparative Studies with Publicly Available Data. *Curr. Protoc. Bioinforma.* 70(1):e100
- Facklam R. 2002. What happened to the streptococci: Overview of taxonomic and nomenclature changes. *Clin. Microbiol. Rev.* 15(4):613–30
- Fahy J V., Dickey BF. 2010. Airway Mucus Function and Dysfunction. *N. Engl. J. Med.* 363(23):2233–47
- Flynn JM, Niccum D, Dunitz JM, Hunter RC. 2016. Evidence and Role for Bacterial Mucin Degradation in Cystic Fibrosis Airway Disease. *PLoS Pathog.* 12(8):e1005846

- Frenkel ES, Ribbeck K. 2015. Salivary mucins protect surfaces from colonization by cariogenic bacteria. *Appl. Environ. Microbiol.* 81(1):332–38
- Frenkel ES, Ribbeck K. 2017. Salivary mucins promote the coexistence of competing oral bacterial species. *ISME J.* 11(5):1286–90
- Goel RM, Prosdocimi EM, Amar A, Omar Y, Escudier MP, et al. 2019. Streptococcus salivarius: A potential salivary biomarker for orofacial granulomatosis and Crohn’s disease? *Inflamm. Bowel Dis.* 25(8):1367–74
- Goldford JE, Lu N, Bajić D, Estrela S, Tikhonov M, et al. 2018. Emergent simplicity in microbial community assembly. *Science (80-)*. 361(6401):469–74
- Gross EL, Beall CJ, Kutsch SR, Firestone ND, Leys EJ, Griffen AL. 2012. Beyond Streptococcus mutans: Dental Caries Onset Linked to Multiple Species by 16S rRNA Community Analysis. *PLoS One.* 7(10):e47722
- Gross EL, Leys EJ, Gasparovich SR, Firestone ND, Schwartzbaum JA, et al. 2010. Bacterial 16S sequence analysis of severe caries in young permanent teeth. *J. Clin. Microbiol.*
- Hall AB, Yassour M, Sauk J, Garner A, Jiang X, et al. 2017. A novel Ruminococcus gnavus clade enriched in inflammatory bowel disease patients. *Genome Med.* 9(1):103
- He X, Wu C, Yarbrough D, Sim L, Niu G, et al. 2008. The cia operon of Streptococcus mutans encodes a unique component required for calcium-mediated autoregulation. *Mol. Microbiol.* 70(1):112–26
- Holmen Larsson JM, Thomsson KA, Rodriguez-Pineiro AM, Karlsson H, Hansson GC. 2013. Studies of mucus in mouse stomach, small intestine, and colon. III. Gastrointestinal Muc5ac and Muc2 mucin O-glycan patterns reveal a regiospecific distribution. *AJP Gastrointest. Liver Physiol.* 305(5):G357–63
- Huttenhower C, Gevers D, Knight R, Abubucker S, Badger JH, et al. 2012. Structure, function and diversity of the healthy human microbiome. *Nature.* 486(7402):207–14
- Jensen A, Scholz CFP, Kilian M. 2016. Re-evaluation of the taxonomy of the mitis group of the genus Streptococcus based on whole genome phylogenetic analyses, and proposed reclassification of Streptococcus dentisani as Streptococcus oralis subsp. dentisani comb. nov., Streptococcus tigurinus. *Int. J. Syst. Evol. Microbiol.*
- Kandler O. 1983. Carbohydrate metabolism in lactic acid bacteria. *Antonie Van Leeuwenhoek.* 49(3):209–24
- Kavanaugh NL, Zhang AQ, Nobile CJ, Johnson AD, Ribbeck K. 2014. Mucins suppress virulence traits of Candida albicans. *MBio.* 5(6):1–8
- Kawamura Y, Hou XG, Sultana F, Miura H, Ezaki T. 1995. Determination of 16S rRNA sequences of Streptococcus mitis and Streptococcus gordonii and phylogenetic relationships among members of the genus Streptococcus. *Int. J. Syst. Bacteriol.* 45(2):406–8
- MacMillan JL, Vicaretti SD, Noyovitz B, Xing X, Low KE, et al. 2019. Structural analysis of broiler chicken small intestinal mucin O-glycan modification by Clostridium perfringens. *Poult. Sci.* 98(10):5074–88
- Marsh PD. 1991. Sugar, fluoride, pH and microbial homeostasis in dental plaque. *Proc. Finnish Dent. Soc.* 87(4):515–25
- Mukherjee S, Bassler BL. 2019. Bacterial quorum sensing in complex and dynamically changing environments. *Nat. Rev. Microbiol.* 17(6):371–82
- Parsek MR, Singh PK. 2003. Bacterial Biofilms: An Emerging Link to Disease Pathogenesis. *Annu. Rev.*

Microbiol. 57(1):677–701

- Png CW, Lindén SK, Gilshenan KS, Zoetendal EG, McSweeney CS, et al. 2010. Mucolytic bacteria with increased prevalence in IBD mucosa augment in vitro utilization of mucin by other bacteria. *Am. J. Gastroenterol.* 105(11):2420–28
- Preheim SP, Perrott AR, Martin-Platero AM, Gupta A, Alm EJ. 2013. Distribution-based clustering: Using ecology to refine the operational taxonomic unit. *Appl. Environ. Microbiol.* 79(21):6593–6602
- Scanlin TF, Glick MC. 1999. Terminal glycosylation in cystic fibrosis. *Biochim. Biophys. Acta.* 1455(2–3):241–53
- Schmidt TSB, Hayward MR, Coelho LP, Li SS, Costea PI, et al. 2019. Extensive transmission of microbes along the gastrointestinal tract. *Elife.* 8:e42693
- Schwalm ND, Townsend GE, Groisman EA. 2017. Prioritization of polysaccharide utilization and control of regulator activation in *Bacteroides thetaiotaomicron*. *Mol. Microbiol.* 104(1):32–45
- Sonnenburg JL, Xu J, Leip DD, Chen C-H, Westover BP, et al. 2005. Glycan Foraging in Vivo by an Intestine-Adapted Bacterial Symbiont. *Science (80-).* 307(5717):1955–59
- Szkaradkiewicz-Karpińska AK, Ronij A, Goślińska-Kuźniarek O, Przybyłek I, Szkaradkiewicz A. 2019. MUC7 level as a new saliva risk factor for dental caries in adult patients. *Int. J. Med. Sci.* 16(2):241–46
- Tailford LE, Crost EH, Kavanaugh D, Juge N. 2015. Mucin glycan foraging in the human gut microbiome. *Front. Genet.* 6:81
- Takahashi N. 2005. Microbial ecosystem in the oral cavity: Metabolic diversity in an ecological niche and its relationship with oral diseases. In: Watanabe M, Takahashi N, Takada H, editors. *Interface Oral Health Science. Int. Congr. Ser.* 1984:103–12
- van der Hoeven JS, van den Kieboom CWA, Camp PJM. 1990. Utilization of mucin by oral *Streptococcus* species. *Antonie Van Leeuwenhoek.* 57(3):165–72
- Wang BX, Wheeler KM, Cady KC, Lehoux SD, Cummings RD, et al. 2020. Mucin glycans signal through the sensor kinase RetS to inhibit virulence-associated traits in *Pseudomonas aeruginosa*. *Curr. Biol.* 31:1–13
- Wheeler KM, Cárcamo-Oyarce G, Turner BS, Dellos-Nolan S, Co JY, et al. 2019. Mucin glycans attenuate the virulence of *Pseudomonas aeruginosa* in infection. *Nat. Microbiol.* 4(12):
- Wickström C, Svensäter G. 2008. Salivary gel-forming mucin MUC5B - A nutrient for dental plaque bacteria. *Oral Microbiol. Immunol.* 23(3):177–82
- Xia B, Royall JA, Damera G, Sachdev GP, Cummings RD. 2005. Altered O-glycosylation and sulfation of airway mucins associated with cystic fibrosis. *Glycobiology.* 15(8):747–75
- Zhernakova A, Kurilshikov A, Bonder MJ, Tigchelaar EF, Schirmer M, et al. 2016. Population-based metagenomics analysis reveals markers for gut microbiome composition and diversity. *Science (80-).* 352(6285):565–69
- Zhou Y, Yang J, Zhang L, Zhou X, Cisar JO, Palmer RJ. 2016. Differential utilization of basic proline-rich glycoproteins during growth of oral bacteria in saliva. *Appl. Environ. Microbiol.* 82(17):5249–58

Acknowledgements

We thank Bayana Science for editing assistance. This research was supported by NIBIB/NIH grant R01 EB017755-04 (to K.R.), the National Science Foundation Career award PHY-1454673 (to K.R.), the U.S. Army Research Office under cooperative agreement W911NF-19-2-0026 for the Institute for Collaborative Biotechnologies, the NIEHS/NIH grant P30-ES002109 (to the MIT BioMicro Center), and the NSF GRFP under grant no. 1745302 (to K.M.W. and C.M.W.). Contributions: K.M.W., C.M.W, and K.R. designed the experiments. K.M.W. and C.M.W. performed all experiments and analyses. K.M.W., C.M.W, and K.R. wrote the paper.

Figures

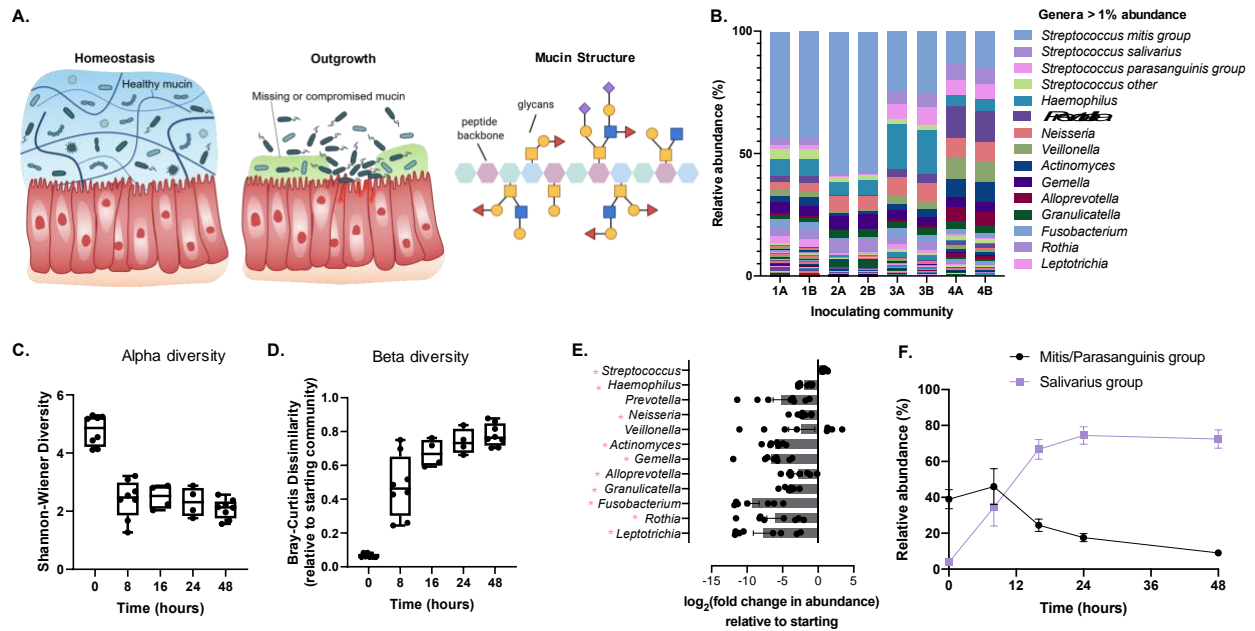


Figure 4.1. Culturing oral microbial communities in mucin-free medium leads to a collapse of diversity associated with the outgrowth of *Salivarius* streptococci. (A) Schematic of the relationship between mucus production and microbial communities. Symbols: yellow square, N-acetyl galactosamine; yellow circle, galactose; blue square, N-acetyl glucosamine; red triangle, fucose; purple diamond, sialic acid. (B) Inoculating communities derived from human saliva were taxonomically rich. The labels A and B following each number denote replicate communities derived from the same human subjects. (C) Alpha diversity of microbial communities decreased following growth in glucose medium over time. Time points 0, 8, 48 h (n=8); time points 16 and 24 h (n=4). The center line indicates the median, the box limits indicate the upper and lower quartiles and the whiskers indicate the minimum and maximum values. Each point represents an independent replicate. (D) Microbial communities became increasingly dissimilar to the starting inoculum following growth in the presence of glucose and absence of host factors. Time points and n as in (C). The center line indicates the median, the box limits indicate the upper and lower quartiles and the whiskers indicate the minimum and maximum values. Each point represents an independent replicate. (E) The majority of genera that were dominant in the native oral microbiota had reduced abundances following growth in glucose medium for 48 h. Bar length represents the mean change in abundance, each point represents the change for an independent replicate, and error bars indicate standard error of the mean (SEM). Significant changes in taxa abundance were identified with one-way, two-sided t-tests. Significance threshold was adjusted with Bonferroni correction for multiple comparisons * $p < 0.0042$. (F) *Salivarius* streptococci relative abundance increased, while *Mitis/Parasanguinis* streptococci abundance decreased following growth in glucose medium. Each point represents the average relative abundance, and bars represent SEM. Time points and n as in (C).

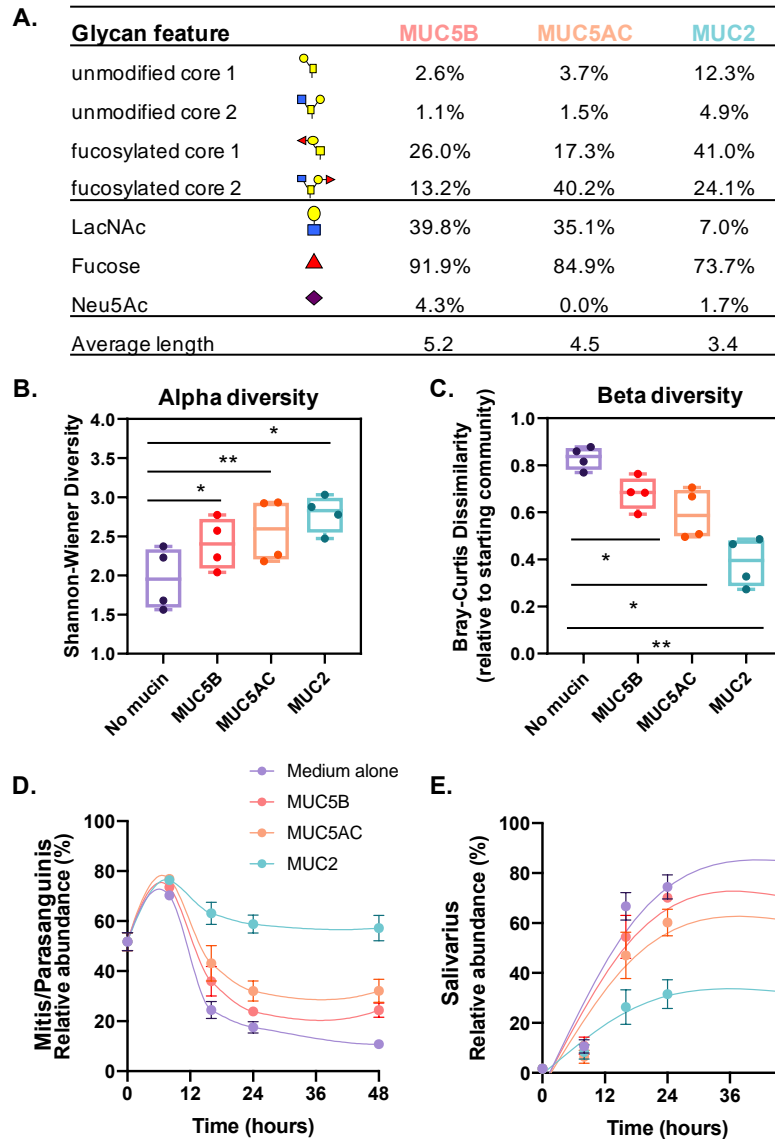


Figure 4.2. Mucins isolated from saliva (MUC5B), gastric mucus (MUC5AC), or intestinal mucus (MUC2) promote microbial diversity. (A) Comparison of mucin isoforms utilized in this study. Mucin glycosylation patterns are adapted from unpublished data. Abbreviations: LacNAc, N-acetyl lactosamine; Neu5Ac, sialic acid. Symbols: yellow square, N-acetyl galactosamine; yellow circle, galactose; blue square, N-acetyl glucosamine; red triangle, fucose; purple diamond, sialic acid. (B) Microbial communities cultured in medium with mucins for 48 h had higher alpha diversity relative to communities cultured in medium alone (n=4). The center line indicates the median, the box limits indicate the upper and lower quartiles and the whiskers indicate the minimum and maximum values. Each point represents an independent replicate. Significant differences relative to medium without mucin were assessed using the repeated measures one-way ANOVA with Dunnett's multiple comparison test, * $p < 0.05$, ** $p < 0.01$. (C) Microbial communities cultured in medium without mucins were more dissimilar to the native microbiota (starting inoculum) than communities cultured in medium with

mucins (48 h, n=4). The center line indicates the median, the box limits indicate the upper and lower quartiles and the whiskers indicate the minimum and maximum values. Each point represents an independent replicate. Significance assessed as in **(B)**, * p < 0.05, ** p < 0.01. **(D,E)** Communities grown in medium with mucin had **(D)** higher relative abundance of Mitis/Parasanguinis streptococci and **(E)** lower abundance of Salivarius streptococci than communities cultured in medium alone (n=4). Each point represents the average relative abundance, and bars represent SEM. All experiments were performed using inoculating communities 1 and 2, as depicted in **Figure 4.1B**. See also **Figure S4.1** and **Figure S4.2**.

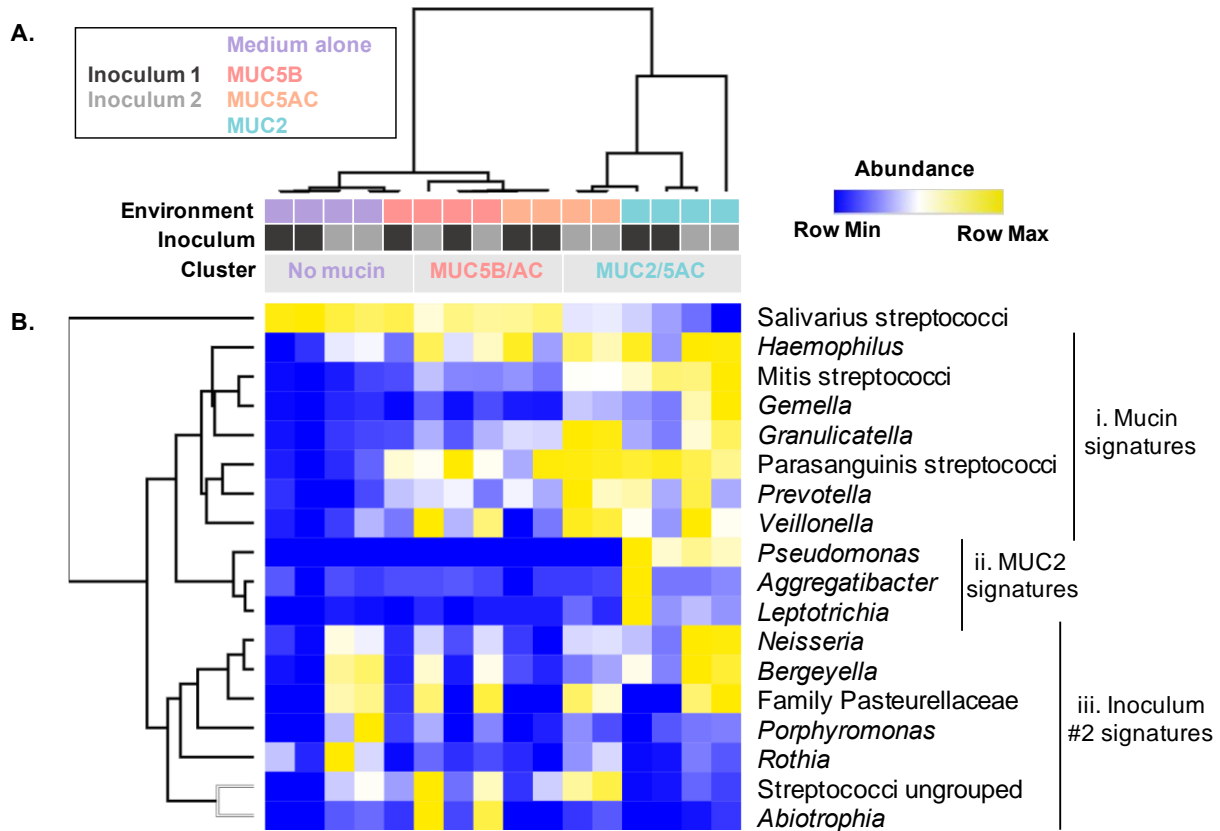


Figure 4.3. Microbial communities cluster according to the environments in which they were cultured.

(A) Dendrograms represent average linkage clustering (1-Pearson distance metric) of *ex vivo* communities based on the microbial composition (48 h). (B) Dendrograms represent average linkage clustering of taxa based on their abundance profiles across samples. Heatmap shows the relative abundance of microbial taxa present at >0.1% abundance (48 h), and the color key is indicated in the upper right corner. (i-iii) Groups of microbes that cooccur within communities cultured in a particular environment or within communities derived from the same microbiota. (i) Taxa with a relatively high abundance in the mucin clusters compared to the no mucin cluster. (ii) Taxa with a relatively high abundance in medium with MUC2 compared to medium alone or medium with other mucins. (iii) Taxa with a relatively high abundance in inoculum 2 compared to inoculum 1.

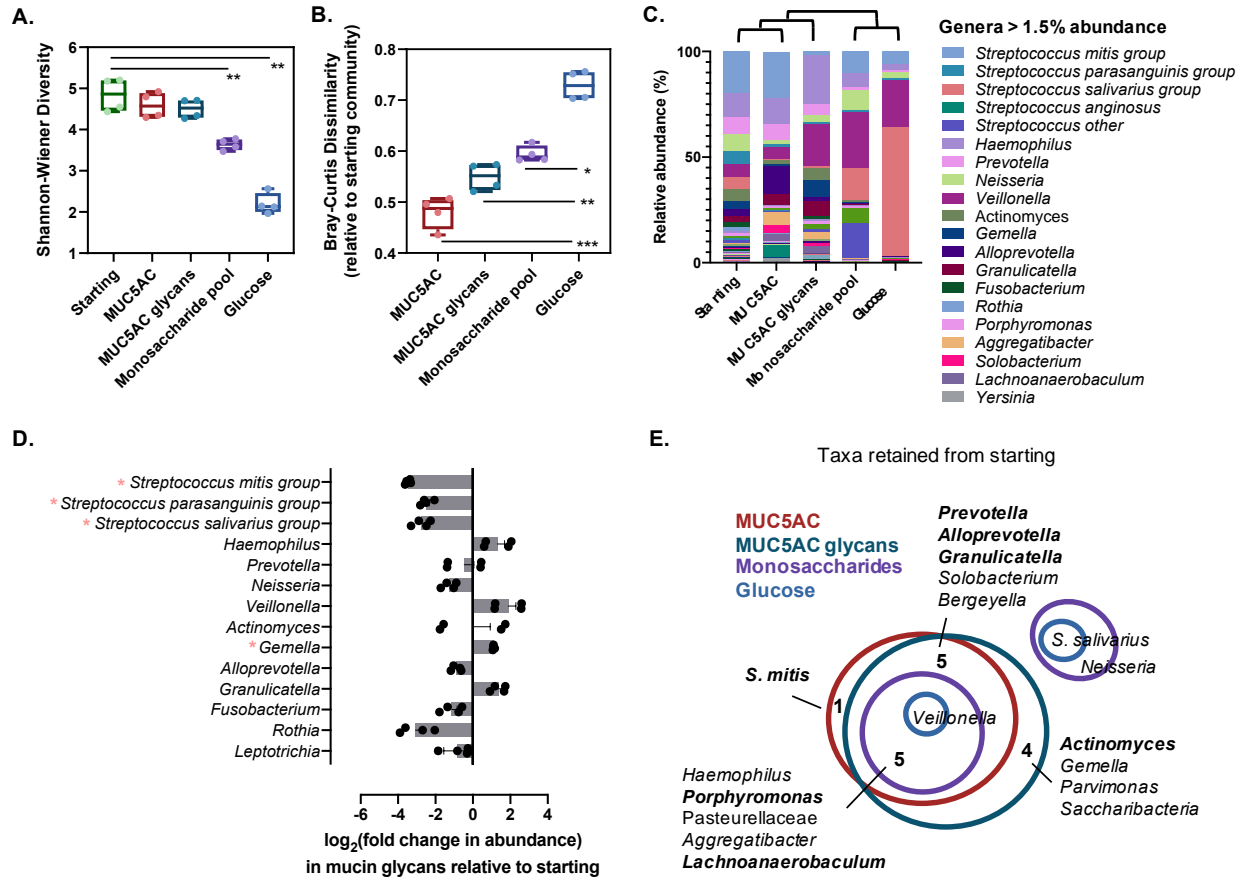


Figure 4.4. Mucins and mucin glycans provided as the sole carbon source promote the culturability of native microbial communities. (A) Microbial communities cultured for 48 h in medium with 0.25% mucins or 0.25% mucin glycans as the sole carbon source had higher alpha diversity relative to communities cultured in medium with 0.5% glucose as the carbon source (n=4). The center line indicates the median, the box limits indicate the upper and lower quartiles and the whiskers indicate the minimum and maximum values. Each point represents an independent replicate. Significant differences relative to the native microbiota (starting) were assessed using the repeated measures one-way ANOVA with Dunnett's multiple comparison test, ** p < 0.01. (B) Microbial communities cultured in medium with glucose as the carbon source were more dissimilar to the native microbiota (starting inoculum) than communities cultured in medium with mucins, mucin glycans, or mucin monosaccharides as the sole carbon source (48 h, n=4). The center line indicates the median, the box limits indicate the upper and lower quartiles and the whiskers indicate the minimum and maximum values. Each point represents an independent replicate. Significant differences relative to medium with glucose were assessed using the repeated measures one-way ANOVA with Dunnett's multiple comparison test, * p < 0.05, ** p < 0.01, *** p < 0.001. (C) Microbial communities cultured for 48 h with mucin or mucin glycans as the sole carbon source clustered with native microbiota (starting); communities cultured with monosaccharides or glucose formed a separate cluster. Bars show the average composition of microbial communities. Relative abundance of each genus is the average of four independent replicates. Overlaying tree is based on results

of the hierarchical clustering presented in **Figure S4.3B**. **(D)** The majority of genera that were dominant in the native oral microbiota were not significantly altered following growth in medium with mucin glycans as the sole carbon source for 48 h. Bar length represents the mean change in abundance, each point represents the change for an independent replicate, and error bars indicate standard error of the mean (SEM). Significant changes in taxa abundance were identified with one-way, two-sided t-tests. Significance threshold was adjusted with Bonferroni correction for multiple comparisons * $p < 0.0036$. **(E)** Venn diagram of genera and groups of streptococci retained (\log_2 fold change > -1) in cultures with different carbon sources. Bolded genera likely encode putative mucin glycan degradation machinery according to the CAZy database. All experiments in **Figure 4.4** were performed using inoculating communities 3 and 4, as depicted in **Figure 4.1B**. See also **Figure S4.3**.

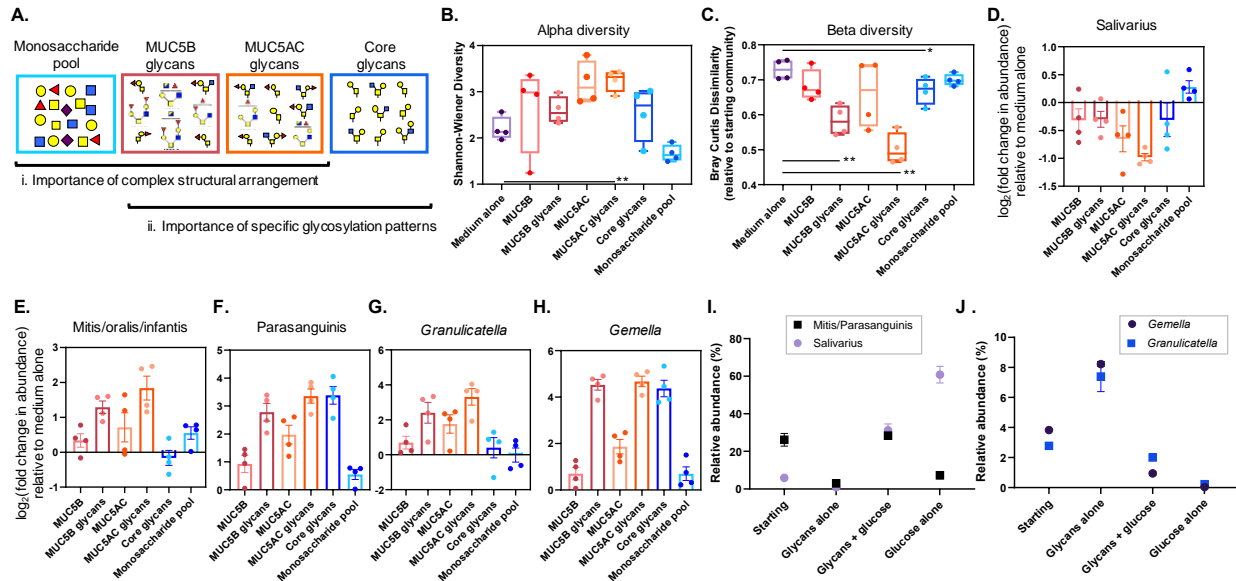


Figure 4.5. Complex mucin glycans support microbial diversity and promote the assembly of multispecies communities. (A) Summary of experimental batch culture conditions. Monosaccharide symbols: yellow square, N-acetyl galactosamine; yellow circle, galactose; blue square, N-acetyl glucosamine; red triangle, fucose; purple diamond, sialic acid. (B) Microbial communities cultured in medium with mucin glycans for 48 h had higher alpha diversity relative to communities cultured in medium alone (n=4). The center line indicates the median, the box limits indicate the upper and lower quartiles and the whiskers indicate the minimum and maximum values. Each point represents an independent replicate. Significant differences relative to medium alone were assessed using the repeated measures one-way ANOVA with Dunnett’s multiple comparison test, ** p < 0.01. (C) Microbial communities cultured in medium alone were more dissimilar to the native microbiota (starting inoculum) than communities cultured in medium with mucin glycans (48 h, n=4). The center line indicates the median, the box limits indicate the upper and lower quartiles and the whiskers indicate the minimum and maximum values. Each point represents an independent replicate. Significance was assessed as in (B), * p < 0.05, ** p < 0.01. Note: Medium alone diversity measurements in panels (B) and (C) are duplicated from **Figures 4.4B** and **4.4C** (glucose) for comparison. (D-H) Communities grown for 48 h in medium with mucin glycans had a lower relative abundance of (D) *Salivarius* streptococci, and a higher relative abundance of (E) *Mitis* streptococci, (F) *Parasanguinis* streptococci, (G) *Granulicatella*, and (H) *Gemella* relative to communities grown in medium alone. (D-H) Bar length represents the mean change in abundance, each point represents the change for an independent replicate (n=4), and error bars indicate SEM. (I) *Salivarius* streptococci increased in relative abundance compared to the native microbiota (starting) following growth in medium with glucose for 48 h. *Mitis/Parasanguinis* streptococci decreased in relative abundance compared to the native microbiota (starting) following growth in medium with mucin glycans or glucose as a sole carbon source for 48 h, but coexisted with *Salivarius* streptococci when glucose and glycans were both present in the medium. (J) *Gemella* and *Granulicatella* increased in abundance relative to the native microbiota (starting) after

being cultured with mucin glycans as a sole carbon source for 48 h, but decreased in relative abundance when glucose was supplied as a carbon source. **(I, J)** Points represent the mean relative abundance for 4 independent replicates, and error bars indicate SEM. All experiments were performed with inoculating communities 3 and 4, as depicted in **Figure 4.1B**. See also **Figure S4.4**.

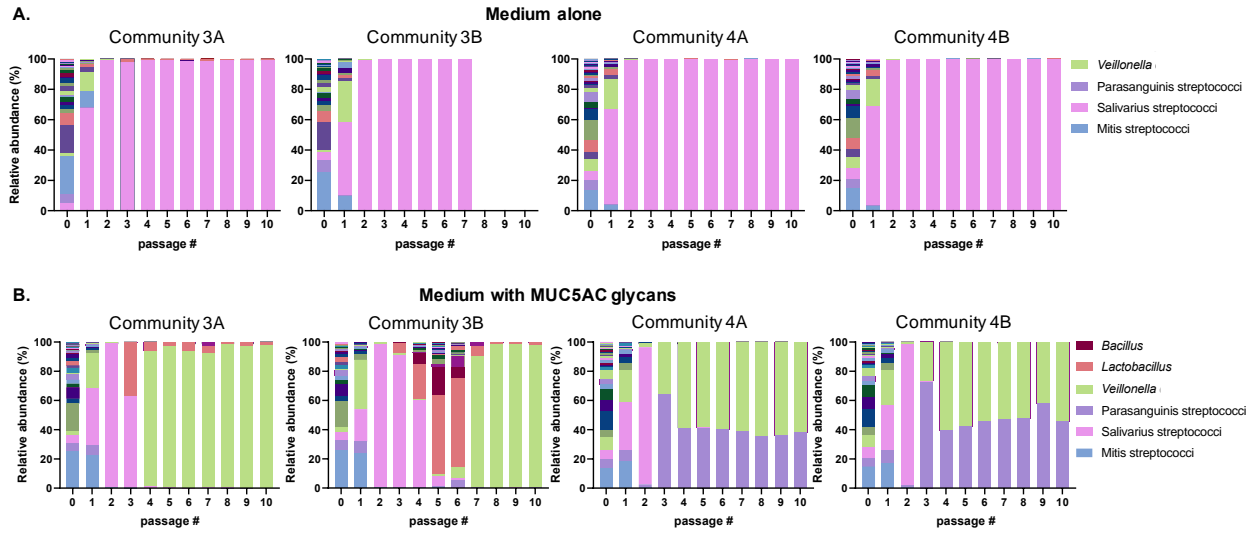


Figure 4.6. Mucin glycan promote the prolonged coexistence of competing microbes. Relative abundance of taxa in microbial communities after serial passaging in (A) medium alone or in (B) medium with mucin glycan. Each graph represents an independent serial passaging experiment with inoculating community 3 or 4, as indicated. (A) Community 3B, passages #8-10 contained insufficient sequencing reads, and were excluded from analysis.

Chapter 5: Conclusions

In this thesis, I present three projects that explore how mucins, and specifically their attached glycans, influence bacterial virulence, host-pathogen interactions, and interspecies competition. In Chapter 2, I identified a previously unrecognized role for mucin glycans as potent host-derived regulators of bacterial phenotype. In particular, I discovered that mucin glycans suppress a range of acute and chronic virulence traits in the opportunistic pathogen *P. aeruginosa*, which is associated with a reduction in its ability to kill epithelial cells and proliferate in burn wounds. In Chapter 3, I further uncovered an underlying mechanism by which *P. aeruginosa* senses its presence in the mucus environment. I identified that a subset of core mucin glycans activate the histidine kinase RetS through its carbohydrate-binding Dismed2 domain, triggering the downregulation of the H1-T6SS. This glycan-mediated signaling prevents T6SS-dependent bacterial killing of neighboring bacterial cells by *P. aeruginosa*. In Chapter 4, I broaden the scope of this work to investigate how mucin glycans influence the culturability and composition of fully complex, naturally-derived bacterial communities. By combining 16S rRNA gene sequencing with a series of well-controlled culture based experiments, I show that mucin glycans resist the collapse of microbial diversity by retaining health-associated bacteria that would otherwise be outcompeted. In a carbon-deplete environment, mucin glycans serve as a complex metabolic substrate to recruit microbes and foster diversity. Whereas in a glucose-replete environment, mucin glycans retain diversity by rendering effective glucose metabolizers less competitive. Overall, the projects in this thesis reveal the broad functions of mucin glycans in preserving host health, and thus open many avenues of future research that I detail in this chapter.

Limitations and Extensions

Bulk mucin and glycan preparation

A major obstacle encountered throughout this work is the limited commercial availability of intact mucins. To circumvent this limitation, the Ribbeck lab has developed protocols to purify the major gel-forming mucins from native sources (Caldara et al. 2012; Frenkel & Ribbeck 2015; Kavanaugh et al. 2014; Lieleg et al. 2010). This purification protocol is relatively gentle and leaves mucins in their native form (Wagner et al. 2018). Similarly, free mucin glycans are not commercially available, are difficult to synthesize, and therefore must be isolated from purified mucin. Unlike

N-linked glycans, which can be released enzymatically from tissues, the *O*-linked glycans present on mucin are released from the mucin backbone chemically through the process of alkaline β -elimination (Cummings & Pierce 2014). In the past, this isolation process from native tissue to purified glycans yielded only analytical quantities of material. Although the scope of experiments that were feasible at the onset of this work were limited by the technical challenges of purifying mucin glycans, over the course of this thesis, we have optimized these protocols to facilitate bulk preparation of mucin glycans for some of the first functional studies with bacteria. In building off this work, it is now possible to obtain milligrams of highly pure glycans from various mucin types. Thus, I anticipate it will soon be feasible to screen individual glycans for function as well as develop genome-wide screens for glycan-sensing pathways in mucin-responsive microbes.

Testing for individual mucin glycan effectors

The complexity of mucin glycans makes them ideal for encoding biological information with a high degree of specificity. In this thesis, I identified dozens of complex glycan structures on just the mucin MUC5AC alone. When isomeric forms and modifications like sulfation are taken into account, the diversity of *O*-linked glycans on a single mucin can increase to several hundred structures (Cummings & Pierce 2014). In this way, mucins present and retain a diversity of potential regulatory cues. Separation of individual glycans in high enough quantity for functional studies is technically challenging with standard column-based chromatographic methods. The studies in this thesis circumvented this limitation by isolating a subset of core glycans through the application of partial acid hydrolysis and separation on a porous graphitic carbon (PGC) cartridge. In chapter 3, this approach enabled the identification of the core mucin glycan structures as signals for the sensor kinase RetS in *P. aeruginosa*. However, this approach does not permit the study of larger, branching structures.

Ideally, future work will further optimize procedures for the preparative separation of mucin glycans using a combination of mixed-mode hydrophilic interaction liquid chromatography/anion-exchange chromatography (HILIC/AEX), which separates glycans based on length and number of negative charges (Deguchi et al. 2008), and PGC chromatography, which separates glycans based on hydrophobic interactions and hydroxyl orientations (Melmer et al. 2011). After separation, glycan fractions can be used in functional studies to identify specific bioactive structures. Since mucin glycosylation is often altered in different tissues and in disease states, the ability to

systematically test individual glycans may reveal specific changes associated with altered mucin function and thus identify therapeutic targets for restoring a healthy mucus barrier.

Glycan-responsive pathways beyond RetS/GacS

In Chapter 3, I report the first identified mucin glycan sensor in *P. aeruginosa* as RetS, a well-characterized histidine kinase with a putative carbohydrate-binding Dismed2 domain. I report that glycan sensing through RetS leads to the suppression of the H1-T6SS as well as the majority of the RetS regulon, but not RetS-independent phenotypes like quorum sensing, biofilm dispersal, and siderophore production. It is therefore likely that glycans act through different pathways to control these virulence traits. Additional research will be required to identify the pathways mediating these changes in virulence in response to mucin glycans as well as the underlying mechanism of action. For example, mucin glycans may signal directly through these pathways by binding to receptors with carbohydrate-binding Dismed2 domains, such as RetS as well as the sensory proteins LadS and NicD (Basu Roy & Sauer 2014), or indirectly by titrating away other exogenous signals in the environment. In the case of a direct interaction with the periplasmic Dismed2, further research will also be required to determine how mucin glycans are released from the mucin backbone and traverse the outer membrane of *P. aeruginosa*.

Another key question is whether the observed reduction in bacterial virulence in response to mucin glycans is a general response in other microbes with conserved regulatory pathways or structurally related sensory proteins. Previous work in the Ribbeck lab indicates that mucins indeed inhibit virulence in a range of cross-kingdom pathogens beyond *P. aeruginosa* including *Candida albicans* (Kavanaugh et al. 2014) and *Streptococcus mutans* (Frenkel & Ribbeck 2015). It is interesting to note that biofilm formation is reduced in all three of these pathogens. This raises the question of whether glycans suppress surface attachment through a conserved mechanism or through a convergent one. In either case, the ability of mucins to target group behaviors suggests that these molecules may be able to broadly alter the function of microbial communities.

Glycan-mediated changes to community function

In Chapter 4, I focus on how mucin glycans resist ecological imbalance of native microbial communities following growth *ex vivo*. While compositional changes in oral microbial communities are certainly important for health (De Paiva et al. 2016; Goel et al. 2019; Kumar et al. 2006; Sudhakara et al. 2018), the collective function of these communities is also a critical and

understudied driver of health and disease. For this reason, in future studies it will be informative to couple gene sequencing studies with metatranscriptomics and metabolomics, which will provide an overview of how community function and resource use are altered in the presence of mucin glycans.

Variations of the culturing conditions

In all three projects discussed in this thesis, I focus on how mucin glycans influence bacteria following growth in batch culture over a relatively short period of time. This approach maximizes throughput, allows for direct comparisons between experimental conditions, and tests the initial response of a bacteria or community to a new environment. However, relying solely on batch culturing limits the ecological questions that can be addressed in Chapter 4. For example, stable states can only be identified in an open culturing system after dozens of generations. To address this limitation, I included experiments that allowed complex bacterial communities to undergo multiple-dilution regrowth cycles and tracked how diversity within the communities change over time. In Chapter 4, I perform this experiment in glucose medium with or without mucin glycans; however, it would also be informative to repeat these passaging experiments with mucin glycans as a sole carbon source. Ideally, I could also utilize this same approach to assess the stability and resilience of communities in response to perturbations or exposure to a pathogen or probiotic spike-in.

In addition to varying the duration of the experiment, it would be interesting to expand our inoculum sampling to include microbial communities derived from other niches such as the nasal cavity, stool, or the environment. This would allow us to better assess how the initial composition and the precise interaction network of the community impacts the final composition. Sampling dysbiotic communities from certain disease states would further allow us to assess whether mucin glycans can shift these communities back to a more commensal state.

Another potentially informative variation of our culturing system is to test other metabolic substrates beyond glucose. Using a glucose polymer like starch, another dietary monosaccharide like fructose, or a chemically distinct carbon source like succinate, citrate, or leucine would help us to systematically assess how the primary metabolic substrate in the culture medium affects glycan function. Additionally, by comparing the final compositions of communities grown on each

of these substrates, I may begin to answer fundamental questions about the relative contributions of competition, facilitation, and metabolism on microbial community assembly.

Tractable mucin-based models of the host environment for *ex vivo* bacterial studies

Over the past two decades, 16S and metagenomic sequencing studies have revealed an important link between microbial community composition and human health; however systematically testing how host factors or chemical interventions influence bacterial communities is challenging. *In vitro* culturing systems are widely available and represent one of the most controllable environments for mechanistic and molecular profiling; however, these systems often become dominated by a few competitive organisms and are therefore less physiologically relevant for the complex microbial communities found in mucosal niches of the human body. On the other hand, it can also be challenging to study the factors influencing bacterial behavior and community assembly *in vivo* due to physiological differences between individuals and lack of experimental control. For this reason, the resulting associations are typically correlative rather than clearly causal.

In this thesis, I tackled this problem by building tractable models for studying host-associated microbes in a native mucus-like environment, while reducing environmental heterogeneity. I show that mucin-based medium better captures the diversity of complex oral communities found in health than a glucose-based medium. Based on these studies, I can now layer on complexity by adding in additional factors within the mucosal environment including immune factors, host-produced proteins, or extracellular DNA. In doing so, I have not only developed a tractable model bridging *in vitro* and *in vivo* studies, but also detailed an experimental system that can be used to address how other host factors in mucus influence individual microbes or communities of microbes.

Mucin glycans as therapeutic molecules

Antibiotic resistance is a growing global concern that presents a clear danger and urges the development of treatment strategies that do not drive resistance. Targeting virulence to treat and prevent infections without killing the microbes would have significant advantage over existing strategies to combat infections because it would avoid the selective pressure that drives resistance (Maura et al. 2016). Additionally, antibiotics can have off-target consequences on the composition and function of the human microbiota (Xu et al. 2020). By developing a therapeutic based on

human biology, I anticipate soluble mucin glycans will have fewer off-target side-effects than traditional antibiotics and, based on the results of Chapter 4, may actually promote a healthy microbiota.

In Chapter 2, I demonstrate that topical application of mucin glycans to burn wounds aids in the clearance of *P. aeruginosa*, highlighting the therapeutic potential of mucin glycans in treating opportunistic infections without antibiotics. Since mucins prevent or reverse biofilm formation in a wide range of cross-kingdom pathogens (Caldara et al. 2012; Co et al. 2018; Frenkel & Ribbeck 2015; Kavanaugh et al. 2014; Wheeler et al. 2019), mucin glycans could also potentially be supplied as an antibiofouling coating on in-dwelling devices. Thus, mucin glycans represent a class of versatile and broad-spectrum anti-virulence molecules with the potential to treat microbial infections or dysbiosis without contributing to the growing problem of antibiotic resistance.

References

- Basu Roy A, Sauer K. 2014. Diguanylate cyclase NicD-based signalling mechanism of nutrient-induced dispersion by *Pseudomonas aeruginosa*. *Mol. Microbiol.* 94(4):771-93
- Caldara M, Friedlander RS, Kavanaugh NL, Aizenberg J, Foster KR, Ribbeck K. 2012. Mucin biopolymers prevent bacterial aggregation by retaining cells in the free-swimming state. *Curr. Biol.* 22(24):2325–30
- Co JY, Cárcamo-Oyarce G, Billings N, Wheeler KM, Grindy SC, et al. 2018. Mucins trigger dispersal of *Pseudomonas aeruginosa* biofilms. *npj Biofilms Microbiomes.* 4(23)
- Cummings RD, Pierce JM. 2014. The challenge and promise of glycomics. *Chem. Biol.* 21(1):1–15
- De Paiva CS, Jones DB, Stern ME, Bian F, Moore QL, et al. 2016. Altered Mucosal Microbiome Diversity and Disease Severity in Sjögren Syndrome. *Sci. Rep.* 6:23561
- Deguchi K, Keira T, Yamada K, Ito H, Takegawa Y, et al. 2008. Two-dimensional hydrophilic interaction chromatography coupling anion-exchange and hydrophilic interaction columns for separation of 2-pyridylamino derivatives of neutral and sialylated N-glycans. *J. Chromatogr. A.* 1189(1-2):169-74
- Frenkel ES, Ribbeck K. 2015. Salivary mucins protect surfaces from colonization by cariogenic bacteria. *Appl. Environ. Microbiol.* 81(1):332–38
- Goel RM, Prosdocimi EM, Amar A, Omar Y, Escudier MP, et al. 2019. *Streptococcus salivarius*: A potential salivary biomarker for orofacial granulomatosis and Crohn’s disease? *Inflamm. Bowel Dis.* 25(8):1367-74
- Kavanaugh NL, Zhang AQ, Nobile CJ, Johnson AD, Ribbeck K. 2014. Mucins suppress virulence traits of *Candida albicans*. *MBio.* 5(6):1–8
- Kumar PS, Leys EJ, Bryk JM, Martinez FJ, Moeschberger ML, Griffen AL. 2006. Changes in periodontal health status are associated with bacterial community shifts as assessed by quantitative 16S cloning and sequencing. *J. Clin. Microbiol.* 44(10):3665-73
- Lieleg O, Vladescu I, Ribbeck K. 2010. Characterization of particle translocation through mucin hydrogels. *Biophys. J.* 98(9):1782–89
- Maura D, Ballok AE, Rahme LG. 2016. Considerations and caveats in anti-virulence drug development. *Curr Opin Microbiol.* 33:41-46
- Melmer M, Stangler T, Premstaller A, Lindner W. 2011. Comparison of hydrophilic-interaction, reversed-phase and porous graphitic carbon chromatography for glycan analysis. *J. Chromatogr. A.* 1218(1):118-23
- Sudhakara P, Gupta A, Bhardwaj A, Wilson A. 2018. Oral dysbiotic communities and their implications in systemic diseases. *Dent J (Basel).* 6(2):10
- Wagner CE, Wheeler KM, Ribbeck K. 2018. Mucins and Their Role in Shaping the Functions of Mucus Barriers. *Annu Rev Cell Dev Biol.* 34(1):189-215
- Wheeler KM, Cárcamo-Oyarce G, Turner BS, Dellos-Nolan S, Co JY, et al. 2019. Mucin glycans attenuate the virulence of *Pseudomonas aeruginosa* in infection. *Nat Microbiol.* 4(12):2146-54

Xu L, Surathu A, Raplee I, Chockalingam A, Stewart S, et al. 2020. The effect of antibiotics on the gut microbiome: A metagenomics analysis of microbial shift and gut antibiotic resistance in antibiotic treated mice. *BMC Genomics*. 21(1):263

Appendix A: Supplementary Information for Chapter 2

Supplementary materials include:

Figures S2.1 to S2.14

Tables S2.1 to S2.3

References

Supplementary Figures

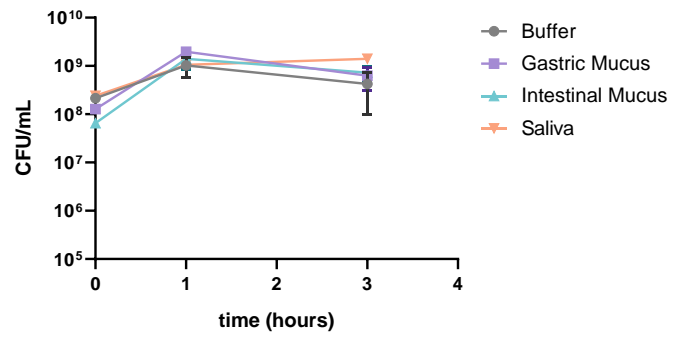
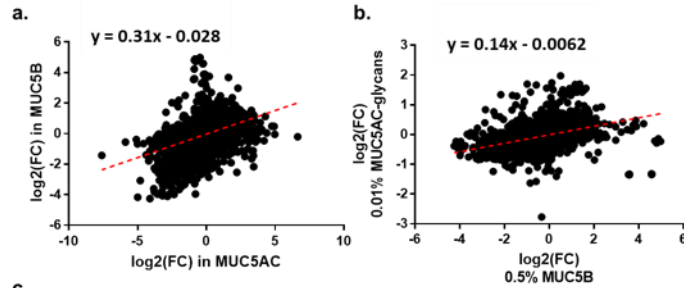


Figure S2.1. *P. aeruginosa* viability is not altered in the presence of native mucus solutions relative to the solubilization buffer. Data are mean CFU, colony-forming units, \pm standard error, $n = 3$ biologically independent replicates.



c.

Pathways represented in the non-overlapping regions of the Venn Diagram (Fig 2c)

Downregulated by MUC5AC	FDR
biofilm formation	2.5E-08
quorum sensing	7.6E-06
hcp secretion island i (hsi-i) type vi secretion system	1.5E-05
bacterial secretion system	3.2E-04
psl exopolysaccharide biosynthesis	1.3E-03
Downregulated by MUC5B	
sulfur metabolism	5.4E-16
tyrosine metabolism	3.0E-04
polyamine catabolism	3.1E-04
type iii secretion	3.1E-04
abc transporters	8.5E-04
synthesis and degradation of ketone bodies	2.3E-03
butanoate metabolism	3.0E-03
apr type i secretion system	3.1E-03
novobiocin biosynthesis	3.1E-03
styrene degradation	3.1E-03
phenylalanine metabolism	6.9E-03

Figure S2.2. Shared and distinct responses of *P. aeruginosa* to MUC5AC and MUC5B. Correspondence of expression changes in response to MUC5AC vs MUC5B (a) and MUC5B vs. MUC5AC glycans (b). Fold-change data are average measurements from 3 biologically independent replicates. c, Pathway analysis of non-overlapping regions of Figure 2.2C indicates that similar virulence pathways are differentially regulated by these mucins, there are differences in the specific genes in these pathways. There are additional metabolic pathways unique to the response to MUC5B, including downregulation of sulfur metabolism. Significance of enrichment was assessed using the one-sided Mann-Whitney U test, where ranking was based on mean log₂-transformed fold changes from 3 biologically independent replicates.

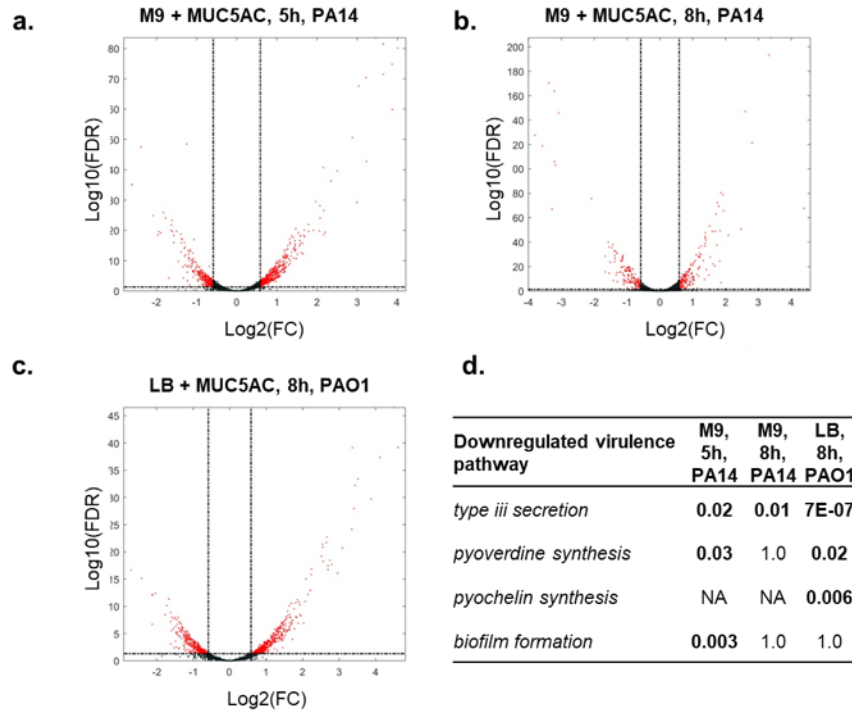


Figure S2.3. Mucin-mediated suppression of virulence pathways is independent of specific experimental conditions including media, time point, and strain. Volcano plots of the RNA-seq profiles of *P. aeruginosa* PA14 grown in M9 minimal media with or without MUC5AC for 5 hours (a) or 8 hours (b) and of *P. aeruginosa* PAO1 grown in LB rich medium with or without MUC5AC for 8 hours (c) under shaking conditions. Fold-change data are average measurements. FDR was determined using the Benjamini Hochberg *p*-value adjustment method. Data are biologically independent replicates: LB (*n* = 3), M9 (*n* = 2). **d.** Gene list enrichment analysis identified *type iii secretion*, *pyochelin* and *pyoverdine* biosynthesis, and *biofilm formation* as significantly enriched among the downregulated gene sets. FDR < 0.05 are bolded. Significance of enrichment was assessed using the one-sided Mann-Whitney U test, where ranking was based on mean log2-transformed fold changes from biologically independent replicates: M9, 5h, PA14 (*n* = 2); M9, 8h, PA14 (*n* = 2); LB, 8h, PAO1 (*n* = 3).

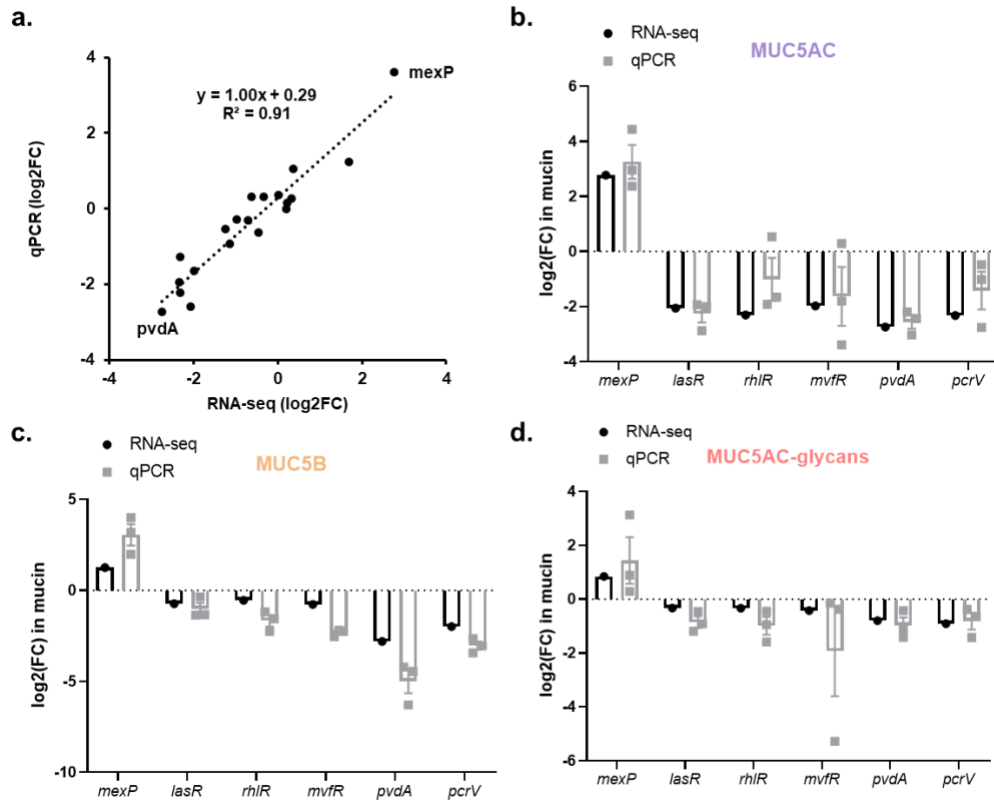


Figure S2.4. qRT-PCR confirms that mucins downregulate the expression of key virulence genes. **a**, Linear regression of the log₂-transformed fold changes (FC) in gene expression for 20 genes following 0.5% MUC5AC exposure measured by qPCR and RNA-seq revealed good correlation between the two techniques. Data are means, $n = 3$ biologically independent replicates. **b-d**, qPCR was used to validate the downregulation of key virulence genes by 0.5% MUC5AC (**b**), 0.5% MUC5B (**c**), and 0.01% MUC5AC glycans (**d**). Data are fold change measurements of gene expression based on mean change in qPCR cycle threshold (dCt) \pm standard error, $n = 3$ biologically independent replicates.

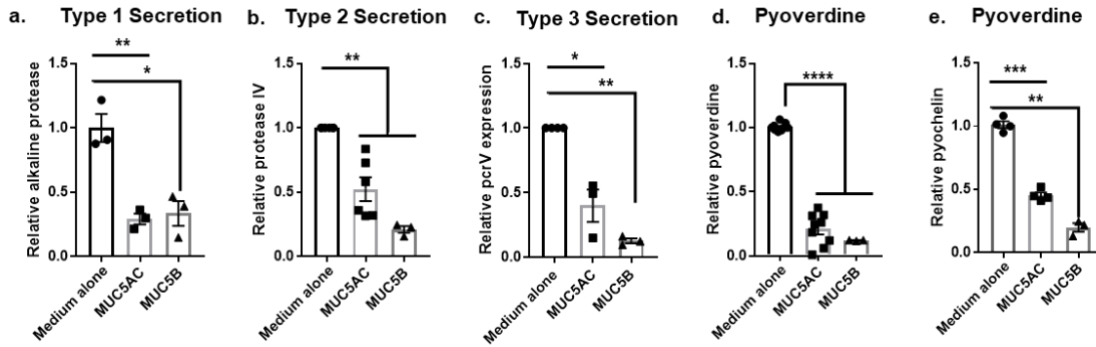


Figure S2.5. Validation of differentially expressed virulence pathways. **(a)** Alkaline protease (encoded by *aprA*) and **(b)** protease IV (*piv*) activities were reduced in the presence of MUC5AC or MUC5B relative to medium alone. **a**, $n = 3$ biologically independent replicates. **b**, $n = 6$ (Medium alone, MUC5AC) or 3 (MUC5B) biologically independent replicates. **c**, Exotoxin translocator *pcrV* expression as determined by qPCR was suppressed in mucin relative to medium alone, $n = 3$ biologically independent replicates. **(d)** Pyoverdine and **(e)** pyochelin production as determined by fluorescence were reduced in the presence of either mucin. **d**, $n = 9$ (Medium alone, MUC5AC) or 3 (MUC5B) biologically independent replicates. **e**, $n = 4$ (Medium alone, MUC5AC) or 3 (MUC5B) biologically independent replicates. **a-e**, Data indicate mean \pm standard error. Significance tested in relation to the medium alone control with one-sample two-sided t-test, followed by Bonferroni correction for multiple comparisons. * $p < 0.05$, ** $p < 0.01$, *** $p < 0.001$, **** $p < 0.0001$.

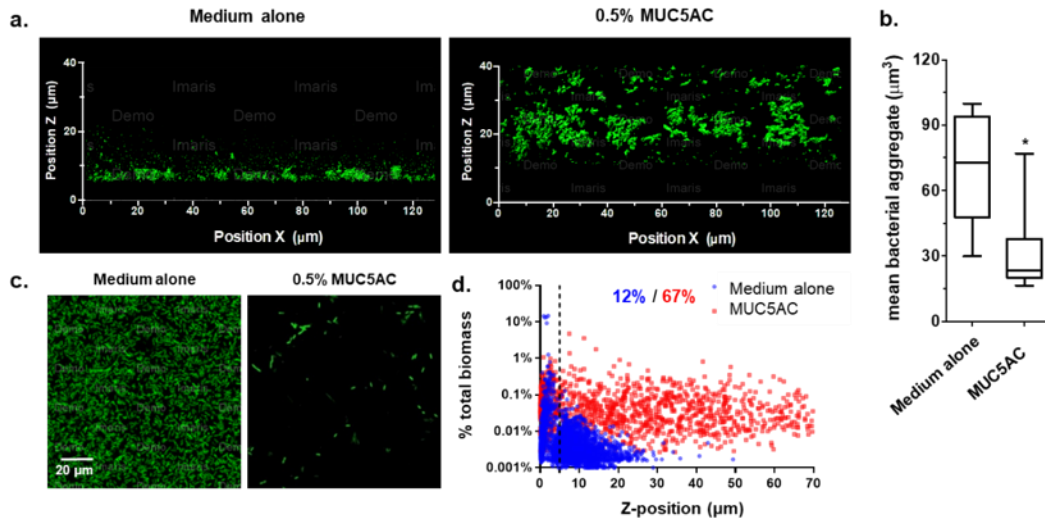


Figure S2.6. Mucins prevent surface attachment and aggregation of *P. aeruginosa*. **a**, MUC5AC influences localization and aggregation of *P. aeruginosa* PAO1. Representative Z-stacks of GFP-expressing *P. aeruginosa* PAO1 cells (green) after exposure to MUC5AC for 5 hours show that mucin reduces surface attachment. Similar results were observed in different fields of view across three independent replicates. **b**, MUC5AC reduces the average bacterial aggregate size. Confocal images of PAO1 aggregates were analyzed using COMSTAT to quantify average aggregate volumes after 5 h of exposure to MUC5AC across six separate Z-stacks. Center line, median; box limits, upper and lower quartiles; whiskers, 1.5x interquartile range. Significance tested with two-sided student t-test, $*p < 0.05$. **c**, MUC5AC prevents *P. aeruginosa* attachment to glass. Representative confocal microscopy of GFP-expressing *P. aeruginosa* PAO1 cells (green) after exposure to MUC5AC for 5 hours. **d**, MUC5AC promotes suspended growth of *P. aeruginosa*. Each point represents a distinct aggregate identified via live 3-dimensional confocal microscopy; Z-position refers to distance from glass bottom. Data compiled from six separate z-stacks: no mucin ($n = 3526$ aggregates), MUC5AC ($n = 1289$). *P. aeruginosa* in media alone tended to grow in aggregates, with a few very large colonies each representing more than 10% of the total biomass, near to the bottom of the well. *P. aeruginosa* in media with MUC5AC exhibited a more vertically distributed mode of growth, with relatively small aggregates suspended at higher positions in the well. For media alone, nearly all the biomass is found within 20µm of the surface. Percentages represent the total biomass found at more than 5µm (indicated with dashed lines) from the surface. Similar results were observed in different fields of view across three independent replicates.

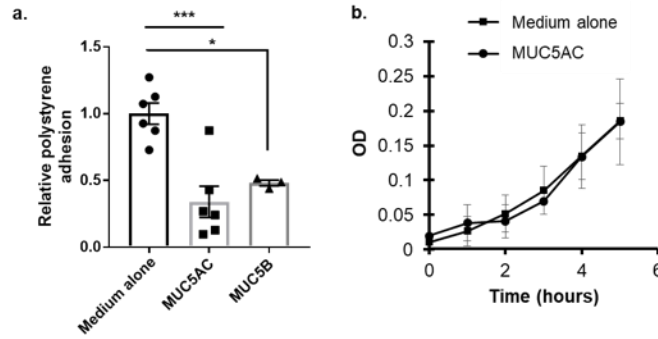


Figure S2.7. Mucins suppress surface attachment without inhibiting bacterial viability. **a**, Microbial adhesion to plastic based on crystal violet staining. Mucin prevents surface attachment by *P. aeruginosa* at the 5 hour time point. Center bar = mean \pm standard error. Data points are biologically independent replicates: medium alone ($n = 6$), MUC5AC ($n = 6$), MUC5B ($n = 3$). Significance tested in relation to the medium alone control with one-way ANOVA, followed by Dunnett's multiple comparisons correction. * $p < 0.05$, *** $p < 0.001$. **b**, Bacterial growth assay. Mucin does not have a bactericidal effect on *P. aeruginosa* based on optical density (OD) at 600 nm. Data points are mean \pm standard error, $n = 3$ biologically independent replicates.

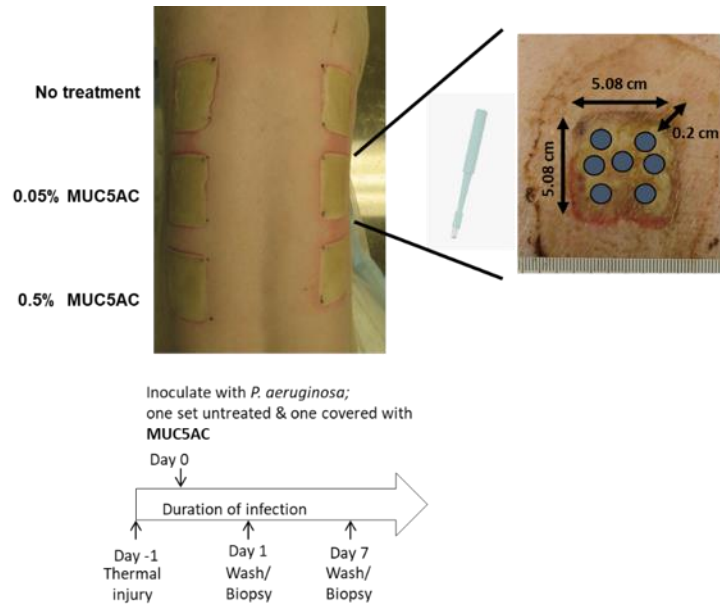


Figure S2.8. Porcine thermal injury model. Six 2"x2" full thickness burn wounds were created on the back of pigs. At specified time points, full thickness wound tissue biopsies were collected using a 6 mm sterile disposable punch biopsy tool (shown above) for microbiological analysis.

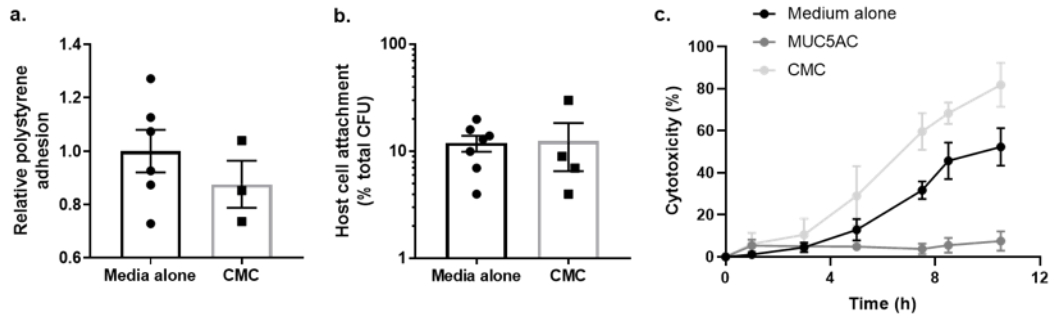


Figure S2.9. A synthetic polymer solution (carboxymethylcellulose, CMC) does not replicate the mucin-triggered response. **a**, CMC does not reduce surface attachment after 5 hours, $n = 6$ (Medium alone) and 3 (CMC) biologically independent replicates. **b**, CMC does not prevent HT-29 epithelial cell adhesion, $n = 7$ (Medium alone) and 4 (CMC) biologically independent replicates. **c**, Treatment with 0.5% CMC results in enhanced killing of HT-29 cells by *P. aeruginosa*. Data are mean \pm standard error (SEM), $n = 3$ biologically independent replicates.

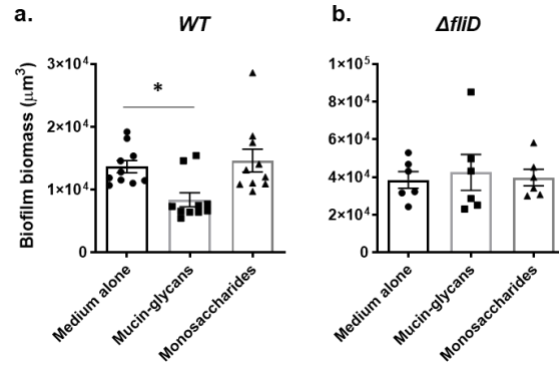


Figure S2.10. Mucin (MUC5AC) glycans trigger the disruption of *P. aeruginosa* biofilms. Confocal images of PAO1 WT ($n = 10$) (a) and PAO1 ΔfliD ($n = 6$) (b) biofilms were analyzed using COMSTAT to quantify biomass after 3 h of exposure to glycans. Center bars are mean \pm standard error (SEM). Significance tested in relation to the medium alone control with an ordinary one-way ANOVA, followed by Bonferroni correction for multiple comparisons. * $p \leq 0.05$

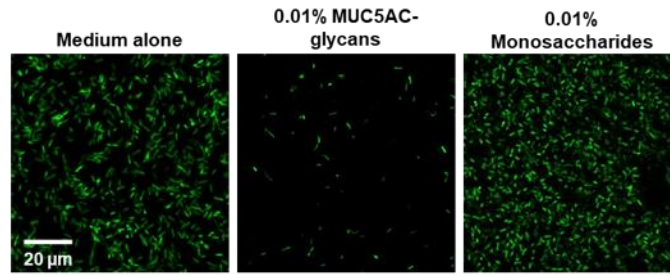


Figure S2.11. Mucin glycans, but not monosaccharides, prevent *P. aeruginosa* attachment to glass. Representative confocal microscopy of GFP-expressing *P. aeruginosa* PAO1 cells (green) after exposure to MUC5AC glycans for 5 hours. Similar results were observed in different fields of view across three independent replicates.

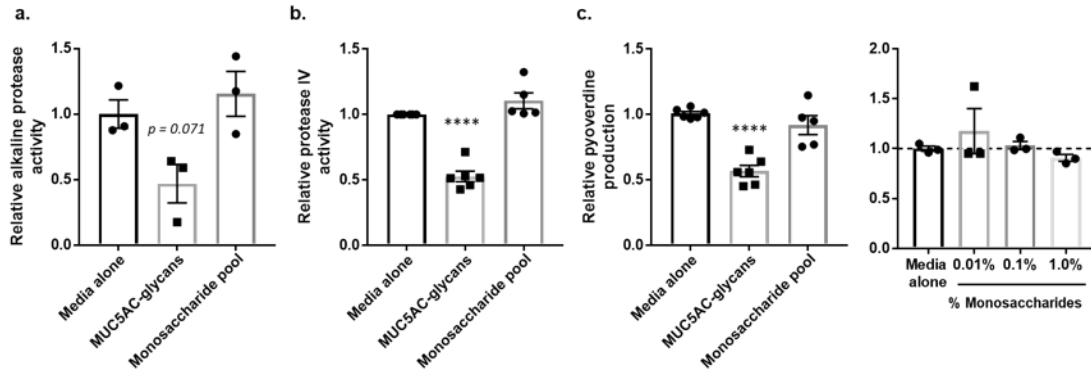


Figure S2.12. Mucin glycans, but not their monosaccharide components, reduce virulence factor production. 0.01% (w/v) mucin glycans, but not a 0.01% (w/v) pool of the monosaccharide components, reduced alkaline protease activity ($n = 3$) (a), protease IV activity ($n = 5$) (b), and pyoverdine production ($n = 5$) (c). Increasing concentrations of the monosaccharide pool does not reduce siderophore production by *P. aeruginosa*. Center bars are mean \pm standard error (SEM). Significance tested in relation to the medium alone control with a one-sample t-test followed by Bonferroni correction for multiple comparisons. **** $p < 0.0001$.

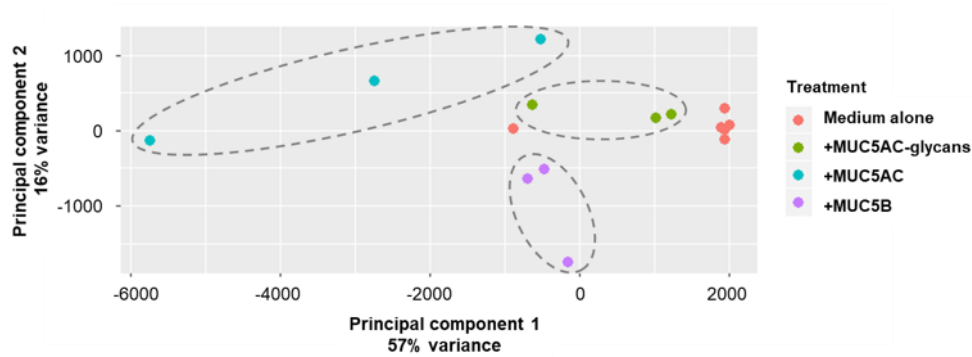


Figure S2.13. Exposure to mucin or mucin glycans induces a distinct transcriptional profile in *P. aeruginosa* relative to growth in media alone. Principal component analysis of the transcriptional profiles of *P. aeruginosa* cells grown in ABTGC minimal media ($n = 6$) with or without mucins ($n = 3$) or mucin glycans ($n = 3$). Raw data of RNA-seq were normalized using the DESeq2 package. Dashed lines circle the three treatment groups.

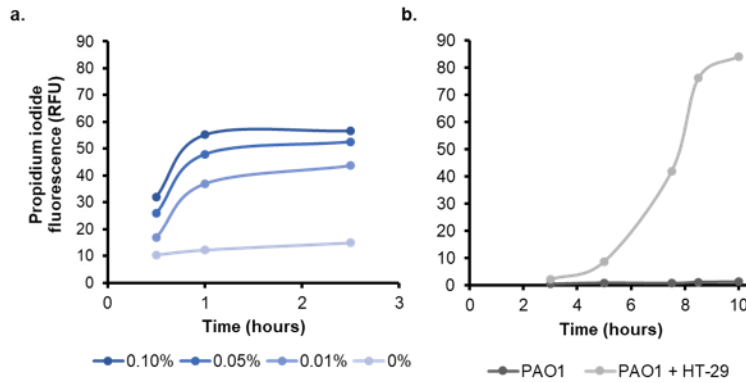


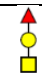
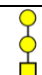

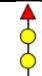




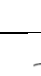




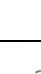
Figure S2.14. Propidium iodide (PI) can detect cytotoxicity of HT-29 cells. **(a)** PI can detect dose dependent differences in cytotoxicity by Triton-X. Legend: Percentage Triton-X added to cell culture medium. **(b)** PI can detect host cell death caused by *P. aeruginosa* over time, without background from bacterial cell death. Representative plots, similar results were observed in six biologically independent replicates.

Supplementary Tables

Locus	Gene	MUC5AC	MUC5B	Pathway annotation
PA0263	<i>hcpC</i>	0.34	2.25	Type 6 Secretion
PA1512	<i>hcpA</i>	0.31	2.08	Type 6 Secretion
PA1894	<i>PA1894</i>	0.34	5.65	Hypothetical
PA3118	<i>leuB</i>	0.24	3.40	Amino acid biosynthesis
PA3119	<i>PA3119</i>	0.25	4.57	Hypothetical
PA3120	<i>leuD</i>	0.18	4.07	Amino acid biosynthesis
PA3121	<i>leuC</i>	0.13	2.63	Amino acid biosynthesis
PA3792	<i>leuA</i>	0.21	3.97	Amino acid biosynthesis
PA4888	<i>desB</i>	0.30	2.10	Fatty acid and phospholipid metabolism
PA5267	<i>hcpB</i>	0.32	2.28	Type 6 Secretion
PA0049	<i>PA0049</i>	6.60	0.44	Hypothetical
PA2019	<i>mexX</i>	4.32	0.48	Antibiotic resistance, Transport, Two-component systems
PA2050	<i>PA2050</i>	2.30	0.38	Transcriptional regulators
PA2109	<i>PA2109</i>	6.03	0.46	Hypothetical
PA2110	<i>PA2110</i>	10.70	0.37	Hypothetical
PA2111	<i>PA2111</i>	10.52	0.46	Hypothetical
PA2112	<i>PA2112</i>	9.79	0.32	Hypothetical
PA2113	<i>opdO</i>	10.85	0.22	Transport
PA2114	<i>PA2114</i>	6.94	0.35	Transport
PA2116	<i>PA2116</i>	9.56	0.46	Hypothetical
PA2445	<i>gcvP2</i>	3.58	0.41	Amino acid metabolism
PA2523	<i>czcR</i>	4.89	0.43	Transcriptional regulators, Two-component systems
PA3372	<i>PA3372</i>	2.59	0.50	Phosphonate and phosphinate metabolism
PA3412	<i>PA3412</i>	8.01	0.50	Hypothetical
PA3443	<i>PA3443</i>	3.06	0.37	Sulfur metabolism, Transport

PA3444	<i>PA3444</i>	4.34	0.45	Sulfur metabolism
PA3445	<i>PA3445</i>	3.46	0.27	Sulfur metabolism, Transport
PA3446	<i>PA3446</i>	4.64	0.17	Hypothetical
PA3936	<i>PA3936</i>	2.41	0.28	Sulfur metabolism, Transport

Table S2.1. Fold changes and pathway annotations for the 29 genes inversely regulated by MUC5AC and MUC5B. FC are all relative to *P. aeruginosa* grown in media alone. Experiments were performed in ABTGC media supplemented with 0.5% MUC5AC or MUC5B at 5h with the PAO1 strain grown under static conditions. Notable transcriptional differences are in the *hcp* type 6 secretion pathway, which is upregulated by MUC5B, Leucine biosynthesis, which is upregulated by MUC5B, and sulfur metabolism, which is upregulated by MUC5AC, and may be related to differences in mucin-glycan sulfation.

Mass (m/z)		Composition	Proposed Structure
Theoretical	Observed		
692.4	692.3	Hex1HexNAc1Fuc1	
722.4	722.4	Hex2HexNAc1	
763.4	763.4	Hex1HexNAc2	
896.5	896.5	Hex2HexNAc1Fuc1	
937.5	937.5	Hex1HexNAc2Fuc1	
967.6	967.5	Hex2HexNAc2	
1008.6	1008.6	Hex1HexNAc3	
1141.7	1141.7	Hex2HexNAc2Fuc1	
1171.7	1171.7	Hex3HexNAc2	
1212.7	1212.7	Hex2HexNAc3	
1315.8	1315.8	Hex2HexNAc2Fuc2	
1345.8	1345.8	Hex3HexNAc2Fuc1	
1386.8	1386.8	Hex2HexNAc3Fuc1	
1416.8	1416.8	Hex3HexNAc3	

1907.1	1907.1	Hex3HexNAc5	
1969.1	1969.1	Hex4HexNAc3Fuc2	
2010.1	2010.1	Hex3HexNAc4Fuc2	
2040.2	2040.1	Hex4HexNAc4Fuc1	
2070.2	2070.2	Hex5HexNAc4	
2081.2	2081.2	Hex3HexNAc5Fuc1	
2111.2	2111.2	Hex4HexNAc5	
2214.3	2214.2	Hex4HexNAc4Fuc2	
2244.3	2244.3	Hex5HexNAc4Fuc1	
2255.3	2255.3	Hex3HexNAc5Fuc2	

2560.5	2560.4	Hex5HexNAc6	
2592.5	2592.4	Hex5HexNAc4Fuc3	
2633.5	2633.5	Hex4HexNAc5Fuc3	
2663.5	2663.5	Hex5HexNAc5Fuc2	
2693.5	2693.5	Hex6HexNAc5Fuc1	
2704.5	2704.5	Hex4HexNAc6Fuc2	
2734.5	2734.5	Hex5HexNAc6Fuc1	
2764.6	2764.6	Hex6HexNAc6	
2805.6	2805.6	Hex5HexNAc7	

2837.6	2837.6	Hex5HexNAc5Fuc3	<p>3x</p>
2867.6	2867.6	Hex6HexNAc5Fuc2	<p>3x</p>
2878.6	2878.6	Hex4HexNAc6Fuc3	<p>2x 2x</p>
2908.6	2908.6	Hex5HexNAc6Fuc2	<p>3x</p>
2938.7	2938.7	Hex6HexNAc6Fuc1	<p>4x</p>
2968.7	2968.7	Hex7HexNAc6	<p>4x</p>
2979.7	2979.7	Hex5HexNAc7Fuc1	<p>3x 2x</p>
3009.7	3009.7	Hex6HexNAc7	<p>4x</p>
3041.7	3041.7	Hex6HexNAc5Fuc3	<p>3x</p>

3082.7	3082.8	Hex5HexNAc6Fuc3	
3112.8	3112.8	Hex6HexNAc6Fuc2	
3142.8	3142.8	Hex7HexNAc6Fuc1	
3153.8	3153.8	Hex5HexNAc7Fuc2	
3183.8	3183.8	Hex6HexNAc7Fuc1	
3213.8	3213.8	Hex7HexNAc7	
3254.8	3254.9	Hex6HexNAc8	
3286.9	3286.9	Hex6HexNAc6Fuc3	
3316.9	3316.9	Hex7HexNAc6Fuc2	

3837.2	3837.3	Hex8HexNAc8Fuc1	
3910.2	3910.4	Hex7HexNAc7Fuc4	
3940.2	3940.4	Hex8HexNAc7Fuc3	
3981.2	3981.5	Hex7HexNAc8Fuc3	
4011.3	4011.5	Hex8HexNAc8Fuc2	

Table S2.2. Complete list of O-glycans identified by MADLI-TOF. Galactose (●), N-acetylglucosamine (■), N-acetylgalactosamine (■), Hexosamine (■), Fucose (▲). Hex: Hexose, HexNAc: Hexosamine, Fuc: Fucose

Strains	
<i>P. aeruginosa</i>	NCBI Taxonomy ID/Reference
PAO1	208964
PAO1 Δ <i>fliD</i>	Co et al. 2018
PAO1 Δ <i>motABCD</i>	Co et al. 2018
PAO1 Δ <i>pelpsI</i>	Borlee et al. 2010
PA14	208963
Plasmid	
pBBR1(MCS5)-Plac- <i>gfp</i>	Co et al. 2018
Primers for qPCR	
Gene	Sequence
lasR-F	TCTACCAGACGCGAAAGCA
lasR-R	GCGTAGTCCTTGAGCATCCA
rhlR-F	CGCCACACGATTCCCTTCA
rhlR-R	TCCAGACCACCATTTCCGAG
mvfR-F	CCTCCGGTTTCGATTTCTCC
mvfR-R	GCATGTAAGGGATCAGGCGA
pvdA-F	GGCCTTCATCGACCTCAAC
pvdA-R	CGGTATCCACCACCGAATAG
pcrV-F	GTCAACGAGAAGACCACCCT
pcrV-R	TAGATCGCGCTGAGAATGTCTG
proC-F	CAGGCCGGGCAGTTGCTGTC
proC-R	GGTCAGGCGCGAGGCTGTCT
rpoD-F	GGGCGAAGAAGGAAATGGTC
rpoD-R	CAGGTGGCGTAGGTGGAGAA

Table S2.3. Strains and primers used in this study.

Supplementary References.

Borlee, B. R. et al. 2010. *Pseudomonas aeruginosa* uses a cyclic-di-GMP-regulated adhesin to reinforce the biofilm extracellular matrix. *Mol. Microbiol.* 75:827–842

Co, J. Y. et al. 2018. Mucins trigger dispersal of *Pseudomonas aeruginosa* biofilms. *NPJ Biofilms Microbiomes.* 4(23)

Appendix B: Supplementary Information for Chapter 3

Supplementary materials include:

Figures S3.1 to S3.7

Table S3.1 to S3.4

References

Supplementary Figures

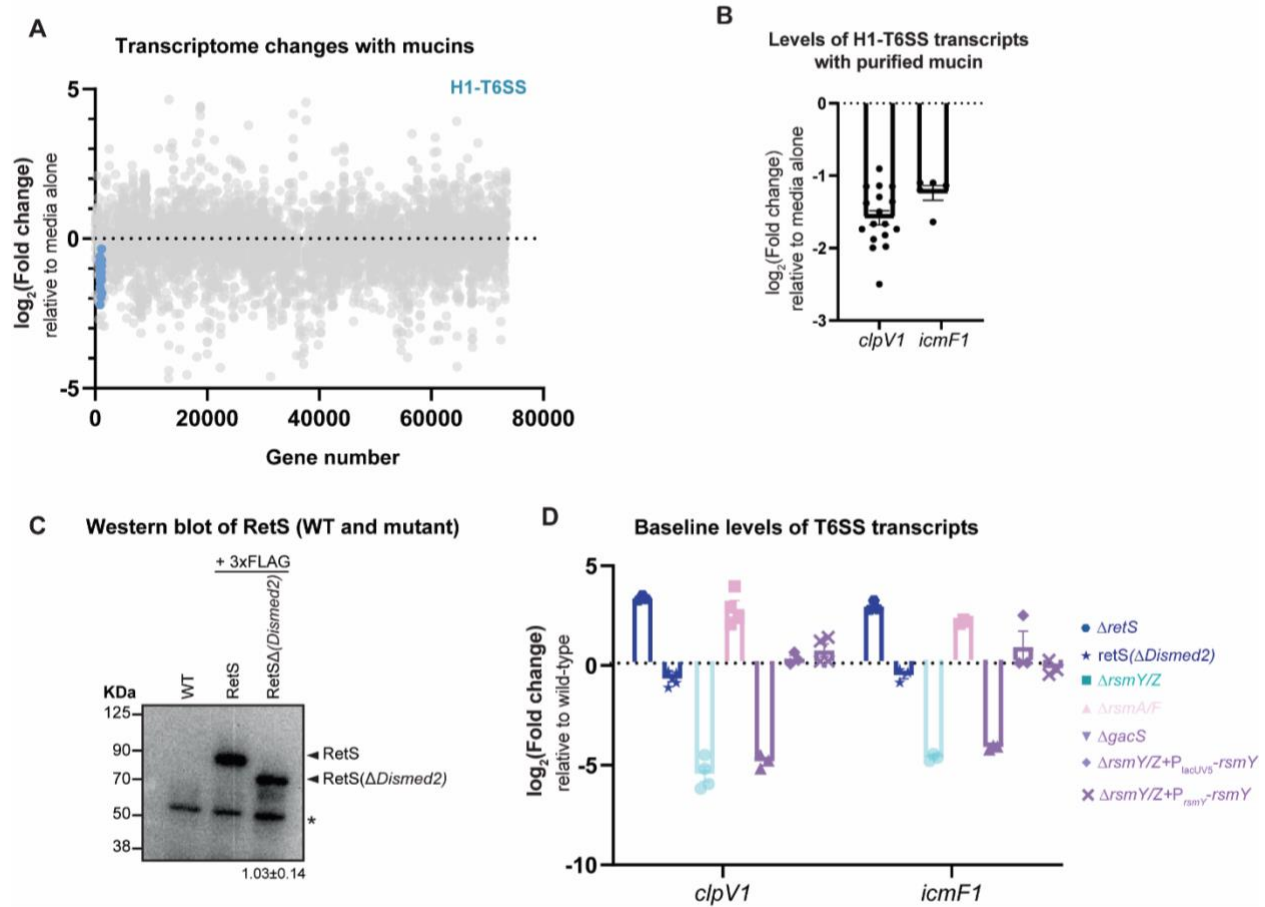


Figure S3.1. Gene expression analysis of differentially regulated genes in response to mucin in the wild type, and baseline levels of H1-T6SS transcripts in different mutant backgrounds. A) RNA-seq analysis of gene expression changes in response to 0.5% mucin, relative to a media control. RNA-seq data are plotted as a function of genomic position (denoted by gene number), with each circle representing an individual gene. The H1-T6SS operon is shown with blue circles. B) Levels of T6SS transcripts in following exposure to isolated mucin glycoproteins relative to medium alone. Transcript levels measured by qRT-PCR and normalized to a control gene (*rpoD*). Bars indicate the mean \pm SEM, with individual measurements shown. C) Representative Western blot of WT RetS-3xFLAG and RetS(Δ Dismed2)-3xFLAG. The quantification (mean \pm SD, n=4) of RetS(Δ Dismed2)-3xFLAG levels relative to WT RetS-3xFLAG levels is indicated below. * indicates a non-specific band also present in the WT strain. D) Baseline levels of *clpV1* and *icmF1* in each GacS/Rsm/RetS mutant relative to the WT. Transcript levels measured by qRT-PCR and normalized to a control gene (*rpoD*). Bars indicate the mean \pm SEM, with individual measurements shown (dots).

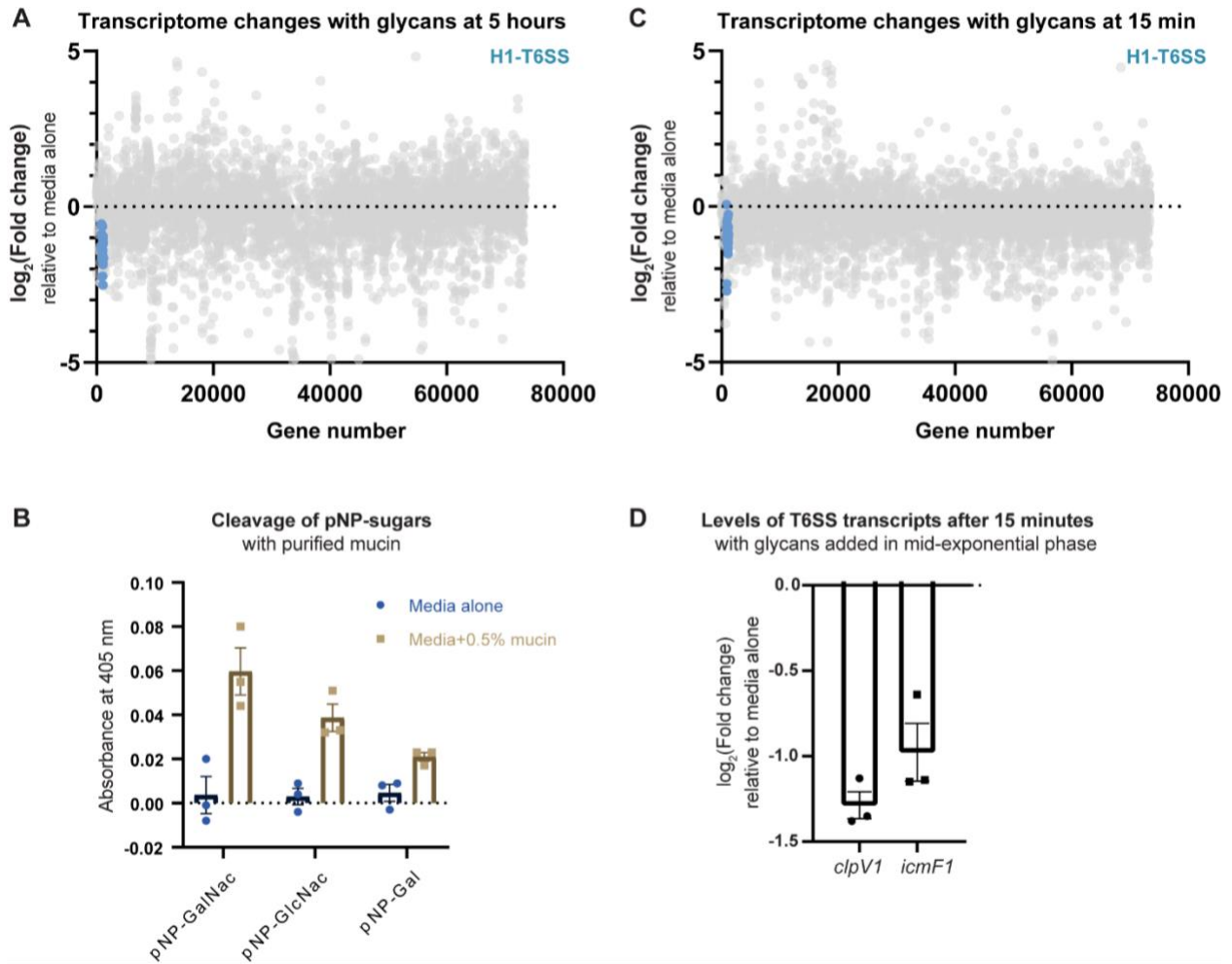


Figure S3.2. Mucin glycans downregulate the H1-T6SS at both 5 hours and 15 minutes after exposure. A) RNA-seq analysis of gene expression changes in response to 0.1% glycans after 5 hours of exposure, relative to a media control. RNA-seq data are plotted as a function of genomic position (denoted by gene number), with each circle representing an individual gene. The H1-T6SS operon is shown with blue circles. B) Cleavage of pNP-sugars by *P. aeruginosa* supernatants following growth in ABTGC medium with or without 0.5% mucin. Bars indicate the mean absorbance at 405 nm \pm SEM, with individual measurements shown. C) RNA-seq analysis of gene expression changes in response to 0.1% glycans after 15 minutes of exposure, relative to a media control. RNA-seq data are plotted as a function of genomic position (denoted by gene number), with each circle representing an individual gene. The H1-T6SS operon is shown with blue circles. D) Levels of T6SS transcripts in PA14 following exposure to the pool of mucin glycans for 15 minutes relative to medium alone. Transcript levels measured by qRT-PCR and normalized to a control gene (*rpoD*). Bars indicate the mean \pm SEM, with individual measurements shown (black dots).

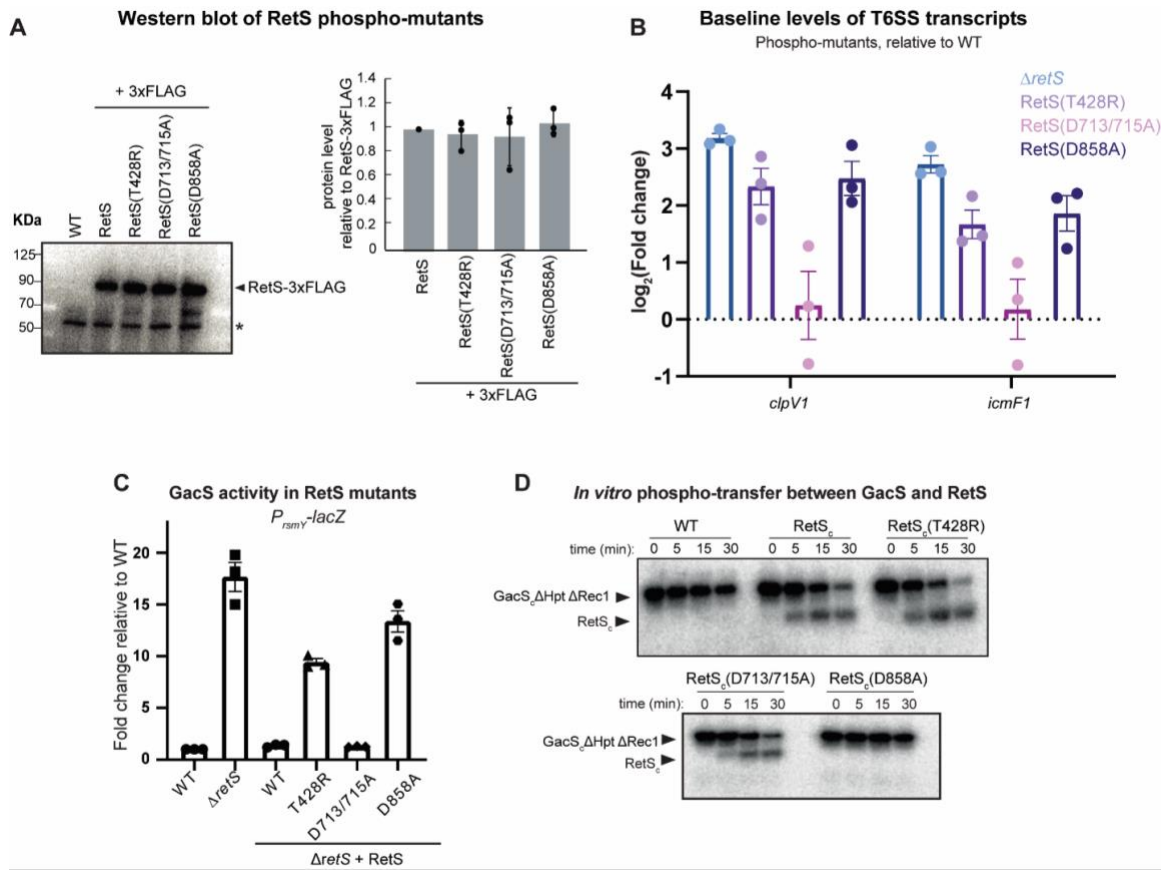


Figure S3.3. Measurement of GacS activity and RetS stability in RetS phospho-mutants. A) Western blot of 3x-FLAG tagged versions of chromosomal RetS point mutants. A quantification from three independent blots is shown on the right, indicating mean \pm SD, with individual values indicated (black dots). * indicates a non-specific band also present in the WT strain. B) Baseline levels of *clpV1* and *icmF1* in each RetS mutant relative to the WT. Transcript levels measured by qRT-PCR and normalized to a control gene (*rpoD*). Bars indicate the mean \pm SEM, with individual measurements shown (dots). C) *rsmY-lacZ* expression, quantified by β -galactosidase assays, in WT and $\Delta retS$ strains and a series of strains in which *retS* was deleted and then replaced, at the native locus, with the mutant variant of *retS* indicated (or a wild-type control). Data shown are mean \pm SEM, with individual values indicated. D) Phosphotransfer from GacS_cΔRec1ΔHpt (the GacS kinase core) to RetS_c. GacS_cΔRec1ΔHpt was autophosphorylated and then examined for phosphotransfer to wild-type RetS_c, the RetS_c point mutants indicated, or a buffer control. Reaction times (in minutes) are indicated above each gel. Bands corresponding to various phosphorylated proteins are labeled on the left of each gel. GacS is able to phosphorylate RetS, except in the RetS(D858A) mutant, indicating that the second receiver domain of RetS is responsible for siphoning phosphate from GacS.

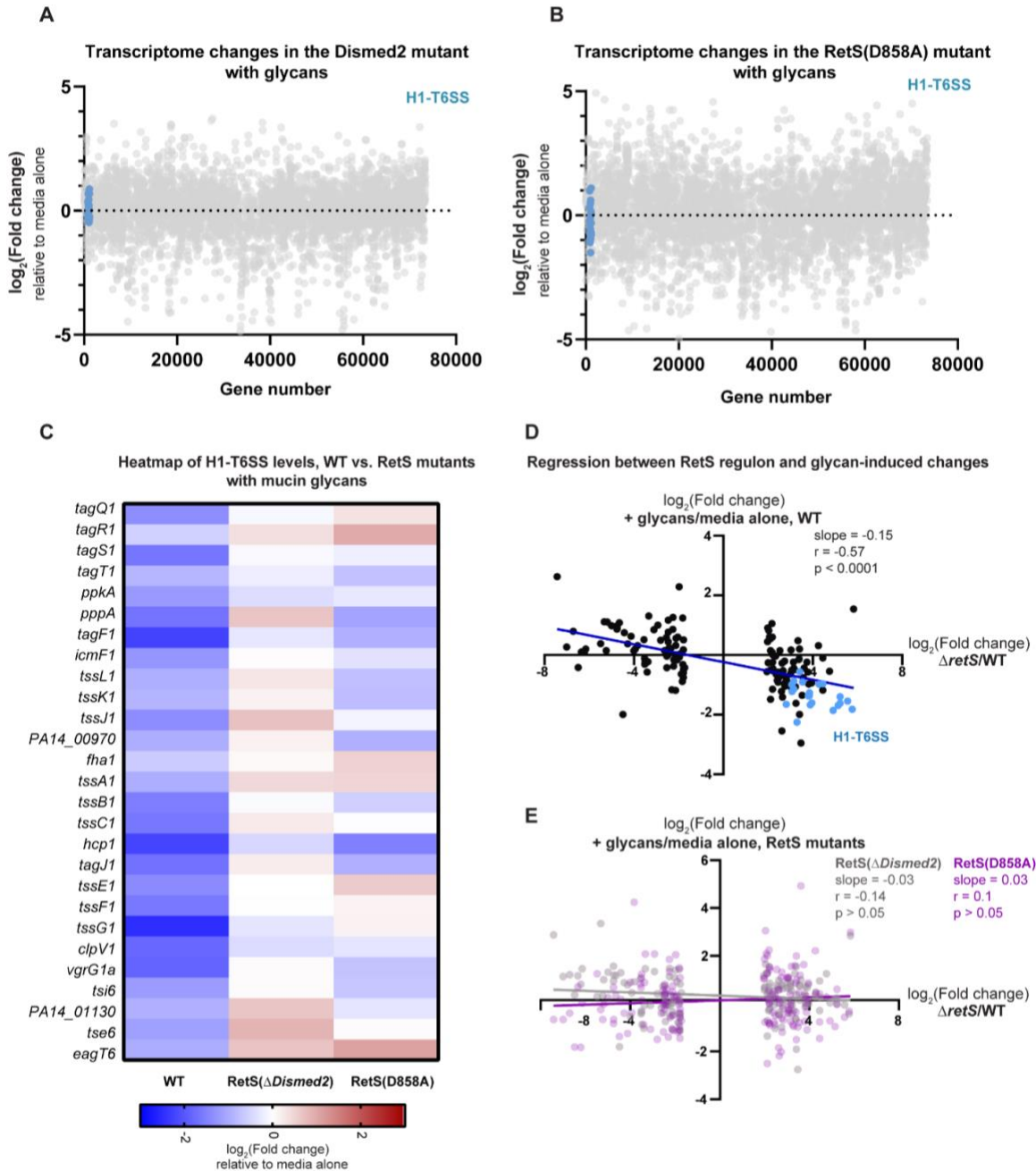


Figure S3.4. Mucin glycans differentially regulate the *RetS* regulon in a *RetS*-dependent manner. A) RNA-seq analysis of gene expression changes in response to 0.1% glycans in the *RetS*(Δ *Dismed2*) strain 5 hours after exposure, relative to a media control. RNA-seq data are plotted as a function of genomic position (denoted by gene number), with each circle representing an individual gene. The H1-T6SS operon is shown with blue circles. B) RNA-seq analysis of gene expression changes in response to 0.1% glycans in the *RetS*(D858A) strain 5 hours after exposure, relative to a media control. RNA-seq data are plotted as a function of genomic position (denoted

by gene number), with each circle representing an individual gene. The H1-T6SS operon is shown with blue circles. C) Heatmap of all H1-T6SS transcript levels following exposure to mucin glycans for 5 hours relative to a medium control in the wild type, *RetS*(Δ *Dismed2*), and *RetS*(D858A) strains, as measured by RNA-sequencing. D,E) Regression of glycan-induced transcript-level changes in the wild-type (D) or *RetS* mutants (E) against the top 50% of differentially expressed genes in the *RetS* regulon (Δ *retS*/WT) [S1], that were also present and expressed in the PA14 RNA-seq datasets. Genome-wide transcript changes were measured by RNA-sequencing. H1-T6SS genes are highlighted in blue in the top panel. In the bottom panel, *RetS*(Δ *Dismed2*) is highlighted in gray, and *RetS*(D858A) in purple. Linear regression fits and statistics were calculated on Prism.

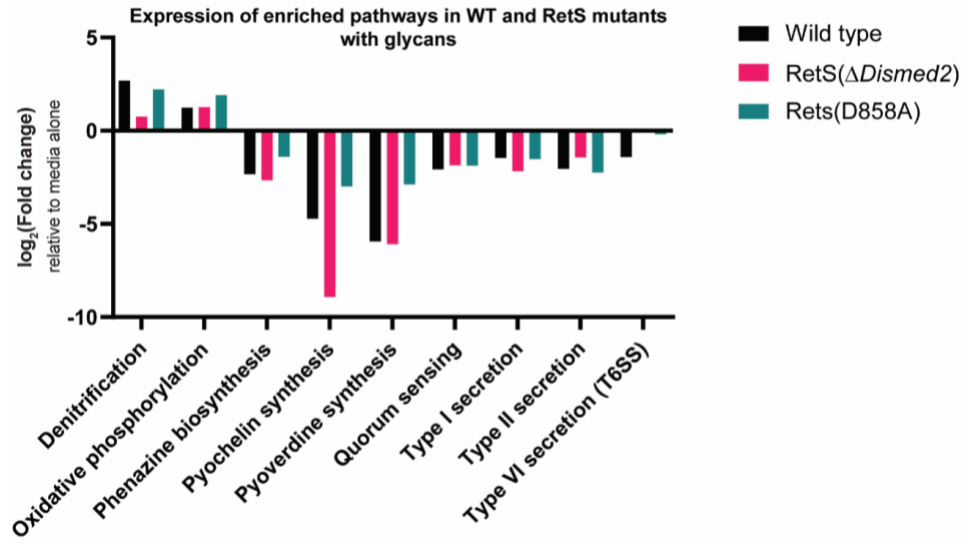


Figure S3.5. Mucin glycans regulate other pathways independently of RetS. Average expression of each enriched pathway upon exposure to 0.1% glycans in the WT (black), RetS(Δ Dismed2) (red), and RetS(D858A) (green) strains. Fold changes are derived from each respective RNA-seq dataset.

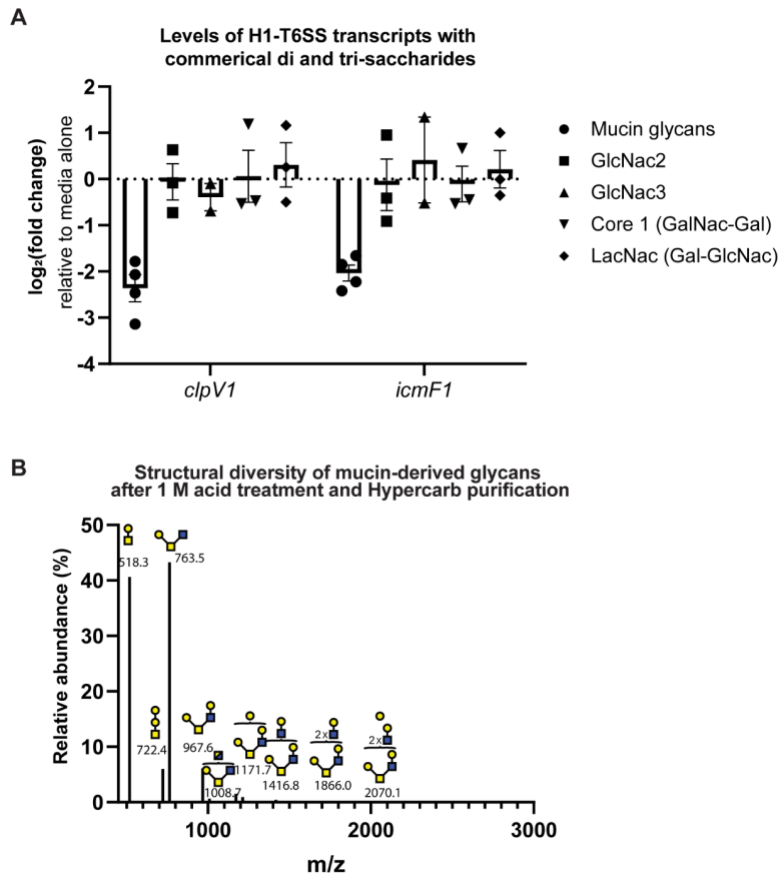


Figure S3.6. Commercially available synthetic moieties present on mucin glycans do not downregulate H1-T6SS transcripts, and acid-treated mucin glycans are retained on Hypercarb columns. A) Levels of T6SS transcripts in PA14 following exposure to commercially available di and tri-saccharides. Transcript levels measured by qRT-PCR and normalized to a control gene (*rpoD*). Bars indicate the mean \pm SEM, with individual measurements shown (black dots). Mucin glycan data duplicated from Figure 4C, for reference. B) MALDI-TOF-MS spectrum of MUC5AC glycans following 1 M TFA treatment and Hypercarb purification. Selected peaks labeled with monoisotopic masses and predicted structures.

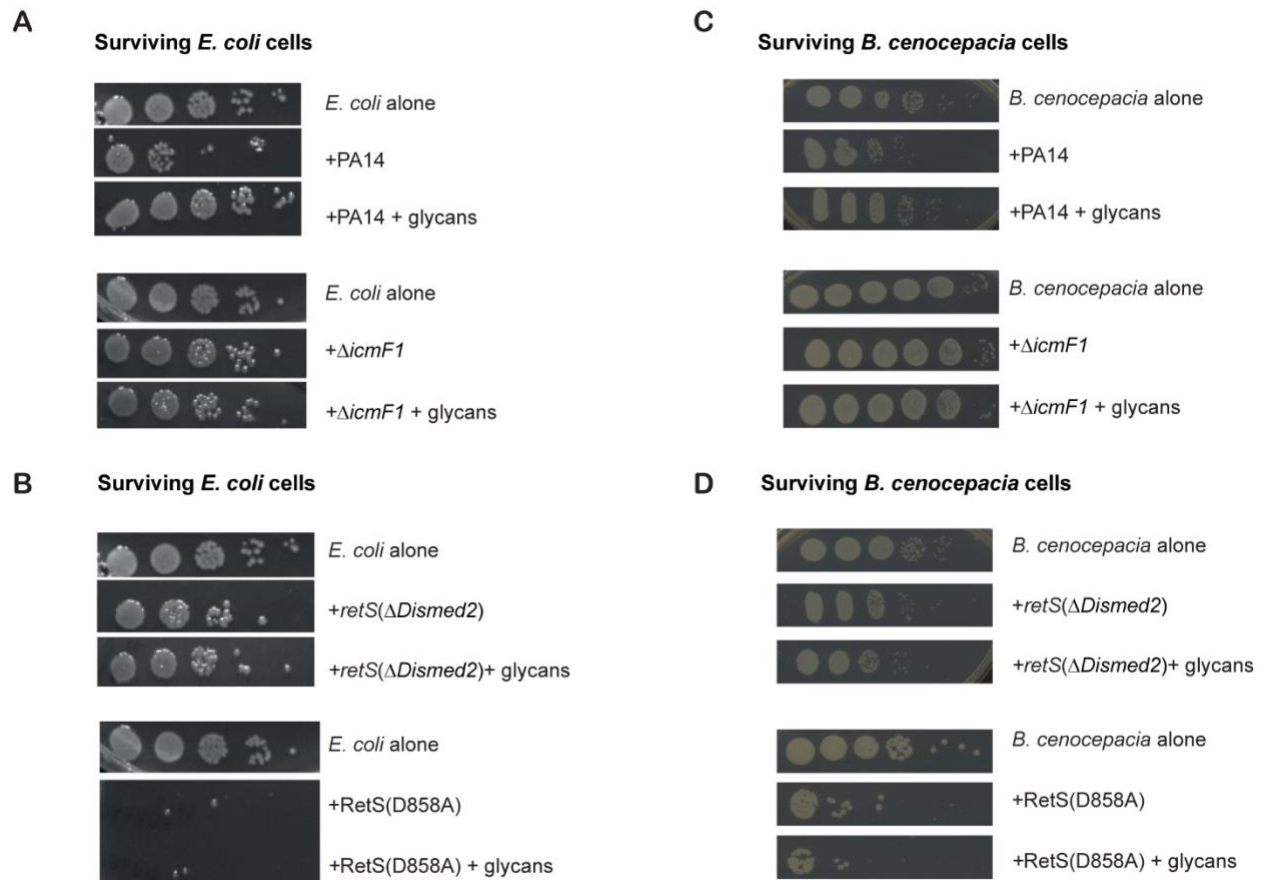


Figure S3.7. Mucin glycans suppress T6SS-mediated killing of *E. coli* and *B. cenocepacia* by PA14 in a RetS-dependent manner. A) Representative images of serial dilutions of viable *E. coli* cells following competition with PA14 wild type and T6SS mutant ($\Delta icmF1$) in the presence and absence of glycans. B) Representative images of serial dilutions of viable *E. coli* cells following competition with PA14 RetS mutants in the presence and absence of glycans. A,B) Experiments performed on the same plate were compared to same *E. coli* alone control. In turn, note that the *E. coli* alone data panels are identical for Figure S3.7A, top panel and S3.7B, top panel, as well as for Figure S3.7A, bottom panel and Figure S3.7B, bottom panel. C) Representative images of serial dilutions of viable *B. cenocepacia* cells following competition with PA14 wild type and T6SS mutant ($\Delta icmF1$) in the presence and absence of glycans. D) Representative images of serial dilutions of viable *B. cenocepacia* cells following competition with PA14 RetS mutants in the presence and absence of glycans.

Supplementary Tables

Description	Reference
WT PA14	lab collection
$\Delta retS$	This study
$\Delta gacS$	This study
WT PA14 + <i>rsmY-lacZ</i>	This study
RetS($\Delta Dismed2$) + <i>rsmY-lacZ</i>	This study
RetS($\Delta Dismed2$) + -3x-FLAG + <i>rsmY-lacZ</i>	This study
RetS-3x-FLAG + <i>rsmY-lacZ</i>	This study
$\Delta retS$ + RetS	This study
$\Delta retS$ + RetS(T428R)	This study
$\Delta retS$ + RetS(D713/715A)	This study
$\Delta retS$ + RetS(D858A)	This study
$\Delta retS$ + RetS + <i>rsmY-lacZ</i>	This study
$\Delta retS$ + RetS(T428R) + <i>rsmY-lacZ</i>	This study
$\Delta retS$ + RetS(D713/715A) + <i>rsmY-lacZ</i>	This study
$\Delta retS$ + RetS(D858A) + <i>rsmY-lacZ</i>	This study
$\Delta retS$ + RetS(T428R)-3xFLAG + <i>rsmY-lacZ</i>	This study
$\Delta retS$ + RetS(D713/715A)-3xFLAG + <i>rsmY-lacZ</i>	This study
$\Delta retS$ + RetS(D858A)-3xFLAG + <i>rsmY-lacZ</i>	This study
$\Delta rsmY/Z$	This study
$\Delta rsmA/F$	This study
$\Delta rsmY/Z + P_{lacUV5-rsmY}$	This study
$\Delta rsmY/Z + P_{rsmY-rsmY}$	This study
$\Delta icmF1$	This study
PAO1	lab collection
MSH1	[S2]
S54485	[S3]
FRD1	[S4]
CEC73	[S5]
CF127	[S5]
C078C	[S5]
<i>E. coli</i> S17	Lab collection

<i>E. coli</i> Dh5 α	Lab collection
<i>B. cenocepacia</i> AU1054- <i>pecG10</i> - constitutive <i>lacZ</i>	[S5]

Table S3.1. Bacterial strains used in this study.

Plasmid	Description	Reference
Mini-CTX-lacZ	For chromosomal integration of genes in <i>P. aeruginosa</i>	[S6]
pCTX-rsmY-lacZ	Chromosomal integration of <i>rsmY-lacZ</i>	[S7]
pexG2	Suicide vector for allelic exchange	[S8]
pMQ30	Suicide vector for allelic exchange	[S9]
pPSV38	Plasmid-borne expression of genes	[S10]
pEXG2-RetS(ΔDismed2)	Chromosomal deletion of Dismed2 domain of RetS	This study
pEXG2-RetS-3xFLAG	Chromosomal integration of 3x-FLAG tag onto the C terminus of RetS	This study
pEXG2-RetS(D858A)-3xFLAG	Chromosomal integration of 3x-FLAG onto the C terminus of RetS(D858A) mutant	This study
pMQ30-RetS(T428R)	Integrate mutant RetS at native RetS locus on chromosome	This study
pMQ30-RetS(D713/715A)	Integrate mutant RetS at native RetS locus on chromosome	This study
pMQ30-RetS(D858A)	Integrate mutant RetS at native RetS locus on chromosome	This study
pEXG2-rsmY	Chromosomal deletion of <i>rsmY</i>	This study
pEXG2-rsmZ	Chromosomal deletion of <i>rsmZ</i>	This study
pEXG2-rsmA	Chromosomal deletion of <i>rsmA</i>	This study
pEXG2-rsmF	Chromosomal deletion of <i>rsmF</i>	This study
pEXG2-icmF1	Chromosomal deletion of <i>icmF1</i>	This study
pPSV38-lacUV5-rsmY	Express <i>rsmY</i> from constitutive lacUV5 promoter	This study
pPSV38-rsmY-rsmY	Express <i>rsmY</i> from native <i>rsmY</i> promoter	This study
pMQ30-GacS	Chromosomal deletion of GacS	This study
ML310	IPTG-driven expression of Trx-tagged proteins	Lab collection
ML333	IPTG-driven expression of MBP-tagged proteins	Lab collection
ML333-GacSAHpt ΔRec1	Expression of GacS _c DHP/CA only	This study

ML310-RetS	Expression of RetS _c	This study
ML310-RetS(T428R)	Expression of putatively phosphatase dead RetS	This study
ML310-RetS(D713/715A)	Expression of receiver one dead RetS	This study
ML310-RetS(D858A)	Expression of receiver two dead RetS	This study

Table S3.2. Plasmids used in this study.

#	Description	Sequence
1	pEXG2_vector_ΔDISMED2_F	GGCTGATCCAGCAGCTCAACCTGCAACAGCTGCTTT ACATTTATGCTTCCGGCTCGTA
2	pEXG2_vector_ΔDISMED2_R	AGGACCAGGGAGGACTCCAGGCGGACCATGCTTAAT TAATTTCCACGGGTGCGCATG
3	pEXG2_DISMED2_frag1_F	GATCATGCGCACCCGTGGAAATTAATTAAGCATGGT CCGCCTGGAGTCTCCCTGGTCCT
4	pEXG2_DISMED2_frag1_R	GAGCAGCATGCCGAAGGCGTAGGCGGGCTTGGCGCT GGGAGTAGTGGCGGTGGTTTGCAG
5	pEXG2_DISMED2_frag2_F	CTGCAAACCACCGCCACTACTCCCAGCGCCAAGCCC GCCTACGCCTTCGGCATGCTGCTC
6	pEXG2_DISMED2_frag2_R	TATACGAGCCGGAAGCATAAATGTAAAGCAGCTGTT GCAGGTTGAGCTGCTGGATCAGCC
7	pEXG2-RetS-3xFLAG_vec_F	CGGCCGCTACATCTTCATCCTCTTCGGTATTGCTTTA CATTTATGCTTCCGGCTCGTATA
8	pEXG2-RetS-3xFLAG_vec_R	TCGCCGCCAGTTGCATGCCGGTCATGCCGCTTAATTA ATTTCCACGGGTGCGCATGATC
9	pEXG2-RetS-3xFLAG_insert_F	GATCATGCGCACCCGTGGAAATTAATTAAGCGGCAT GACCGGCATGCAACTGGCGGCGA
10	pEXG2-RetS-3xFLAG_insert_R	TATACGAGCCGGAAGCATAAATGTAAAGCAATACCG AAGAGGATGAAGATGTAGCGGCCG
11	pEXG2-RetS-3xFLAG_RTH_F	AGATCATGACATCGACTACAAGGATGACGATGACAA GTGAGGGCAGCGACGTGCTCCGGC
12	pEXG2-RetS-3xFLAG_RTH_R	TTATAATCACCGTCATGGTCTTTGTAGTCGCCGCTAC CGCCGGAGGGCAGGGCGTCGCC
13	pEXG2-GacS-3xFLAG_vec_F	GAAACCCGGCGCGATGCTGATCAATACCGGTGCTTT ACATTTATGCTTCCGGCTCGTATA
14	pEXG2-GacS-3xFLAG_vec_R	CGACGCAGAGCAGCCGTGGCGGCCGTCCGGCTTAAT TAATTTCCACGGGTGCGCATGATC
15	pEXG2-GacS-3xFLAG_insert_F	GATCATGCGCACCCGTGGAAATTAATTAAGCCGGAC GGCCGCCACGGCTGCTCTGCGTCG
16	pEXG2-GacS-3xFLAG_insert_R	TATACGAGCCGGAAGCATAAATGTAAAGCACCGGTA TTGATCAGCATCGCGCCGGGTTTC
17	pEXG2-GacS-3xFLAG_RTH_F	AGATCATGACATCGACTACAAGGATGACGATGACAA GTGACCATGCGCATCCTGTTCTTC
18	pEXG2-GacS-3xFLAG_RTH_R	TTATAATCACCGTCATGGTCTTTGTAGTCGCCGCTAC CGCCGAGTTCGCTGGAGTCGAGG
19	pEXG2-RetS(D858A)-3xFLAG-RTH_F	GCCTGCGAGATGCCGGTGCTCGACGGC
20	pEXG2-RetS(D858A)-3xFLAG-RTH_R	CATCAGCACCAGGTCGTACTIONGGTTC
21	RetS(T428R)_F	ACGAGATCCGCAGGCCCATGAACGGCG

22	RetS(T428R)_R	CGCCGTTTCATGGGCCTGCGGATCTCGT
23	RetS(D713/715A)_F	CCTGCTCGCCCAGGCCATGCCCCG
24	RetS(D713/715A)_R	CCGGGCATGGCCTGGGCGAGCAGG
25	RetS(D858A)_F	GGTGCTGATGGCCTGCGAGATGCCGGT
26	RetS(D858A)_R	ACCGGCATCTCGCAGGCCATCAGCACC
27	pENTR-RetS_F	caccATCCAGCAGCTCAACCTGCAACAGCGCAC
28	pENTR-RetS_R	TCAGGAGGGCAGGGCGTCGCCCTGG
29	pENTR-GacS_F	caccGGCAGCAACGAGCTGGACGAACTGGCCTCC
30	pENTR-GacS_R	TCAGAGTTCGCTGGAGTCGAGGCTGGTGGAA
31	pENTR-GacS Δ RecI Δ Hpt_R	TCATGGCGGCCGTCCGAAACCATGGCGTG
32	Δ retS_primer1	caggctgaaaatcttctcatccgcaaaGCCTACCTGCGCGAGCAG GGCGC
33	Δ retS_primer2	TCGCCCTGGCGGCGGCGATCGATCCGAAGCCGTACC ACGGCGAAGTCCCTTC
34	Δ retS_primer3	CCGTGGTACGGCTTCGGATCGATCGCCGCCGCCAGG GCGACG
35	Δ retS_primer4	GCGGATAACAATTTACACAGGAAACAGCTCGCCAG CGCGCAGACGAACAGACCC
35	Δ gacS_primer1	caggctgaaaatcttctcatccgcaaaACTACGTCCCAGGTCCA GGACAGCCATACCGATAG
36	Δ gacS_primer2	TCG AGG CTG GTG GAA GAC AGG CCG AGA TCC TTG AAC ACA CGT CTC TCC GTC G
38	Δ gacS_primer3	GTGTGTTCAAGGATCTCGGCCTGTCTTCCACCAGCCT CGACTCCAGCGAAC
39	Δ gacS_primer4	GCG GAT AAC AAT TTC ACA CAG GAA ACA GCT TGC TAC CAC GCC ATC AGG CCC GGA CCC G
40	Δ rsmY_primer1	GATCATGCGCACCCGTGGAAATTAATTAAGCGGTGG CCACGTAGTTCGGGG
42	Δ rsmY_primer2	CGACGCGGTTTTCTCGGGCAATAAGGTTTGAAGAT TACGCATCTCTGCGAGGG
43	Δ rsmY_primer3	CCCTCGCAGAGATGCGTAATCTTCAAACCTTATTGCC CGAGGAAAACCGCGTCG
44	Δ rsmY_primer4	TATACGAGCCGGAAGCATAAATGTAAAGCACTGCTC ACCGGCAACCTGGATATCG
45	Δ rsmZ_primer1	GATCATGCGCACCCGTGGAAATTAATTAAGCATGCT CGGCCTGAACGAACGGG

46	$\Delta rsmZ$ _primer2	GGCGACGAGTAAAACGGCAGGCAAACGCAGGAGTG ATATTAGCGATTCCCTG
47	$\Delta rsmZ$ _primer3	CAGGGAATCGCTAATATCACTCCTGCGTTTGCCTGCC GTTTTACTCGTCGCC
48	$\Delta rsmZ$ _primer4	TATACGAGCCGGAAGCATAAATGTAAAGCAGCACG AGATGCCGAGCCAGCAG
49	$\Delta rsmA$ _primer1	GATCATGCGCACCCGTGGAAATTAATTAAGCCTTCA AGATCCTCGGGCCGATC
50	$\Delta rsmA$ _primer2	TCGGCGCGTTGACGCCGAAATCAGCATTCTTTCTCC TCACGCGAATATTTT
51	$\Delta rsmA$ _primer3	GAAATATTCGCGTGAGGAGAAAGGAATGCTGATTTC GGCGTCAACGCGCCGA
52	$\Delta rsmA$ _primer4	TATACGAGCCGGAAGCATAAATGTAAAGCAGCAACT GTCGATCCTTCGTCCGTC
53	$\Delta rsmF$ _primer1	GATCATGCGCACCCGTGGAAATTAATTAAGGCTCCA GGTTGAGCTGATTGAGGC
54	$\Delta rsmF$ _primer2	CTTTCGGTGCCGTCTTCAACTCGTCGAAACCCATGTT CCGCGTCTTGC
55	$\Delta rsmF$ _primer3	GCAAGGACGCGGAACATGGGTTTTCGACGAGTTGAAG ACGGCACCGAAAG
56	$\Delta rsmF$ _primer4	TATACGAGCCGGAAGCATAAATGTAAAGCATAATCG CGTTCGGCCTGCTGG
57	$\Delta icmF1$ _primer1	GATCATGCGCACCCGTGGAAATTAATTAAGATCGCC GACGCCCTGCGCAAGGTCAAGG
58	$\Delta icmF1$ _primer2	GGCCAGCTTGCCGTAGAAACCGACGCTGTGACCTTC GCCGCGTTGCGCCGGGCCT
59	$\Delta icmF1$ _primer3	AGGCCCGGCGCAACGCGGCGAAGGTCACAGCGTCG GTTTCTACGGCAAGCTGGCC
60	$\Delta icmF1$ _primer4	TATACGAGCCGGAAGCATAAATGTAAAGCAGCGCTG CGCCGGGGTCACCGCTTC
61	$P_{lacUV5-rsmY}$ primer 1	GCTTCCGGCTCGTATAATGTGTGGGTCAGGACATTG CGCAGGAAG
62	$P_{lacUV5-rsmY}$ primer 2	GTTTAGAGGCCCAAGGGTTATGCTAAAAGGCGTG GTCTGAGCGAC
63	$P_{rsmY-rsmY}$ primer 1	CGGTACCCGGGGATCCTCTAGAGCGAGCGGAACTAT TACAGCGTGT
64	$P_{rsmY-rsmY}$ primer 2	GTTTAGAGGCCCAAGGGTTATGCTAAAAGGCGTG GTCTGAGCGACG
65	$clpVI$ _F (qPCR)	CACAAGGTGCCGTTTCGAGTT
66	$clpVI$ _R (qPCR)	GTTGTGCGGGCTACTGATAC
67	$icmF1$ _F (qPCR)	CAACCCTACGTCGACACCTC

68	<i>icmF1_R</i> (qPCR)	CATGGTCACCGGCTTGAGTT
69	<i>rpoD_F</i> (qPCR)	GGGCGAAGAAGGAAATGGTC
70	<i>rpoD_R</i> (qPCR)	CAGGTGGCGTAGGTAGAGAA

Table S3.3. Primers used in this study.

Figure 3.1F

<i>clpVI</i>	p value
WT vs. $\Delta retS$	0.0028
WT vs. $retS(\Delta Dismed2)$	<0.0001
WT vs. $\Delta rsmY/Z$	0.0022
WT vs. $\Delta rsmA/F$	0.0033
WT vs. $\Delta gacS$	<0.0001
WT vs. $\Delta rsmY/Z + lacUV5-rsmY$	0.0002
WT vs. $\Delta rsmY/Z + native promoter-rsmY$	0.7561

icmFI

WT vs. $\Delta retS$	0.0044
WT vs. $retS(\Delta Dismed2)$	0.002
WT vs. $\Delta rsmY/Z$	0.0307
WT vs. $\Delta rsmA/F$	0.1567
WT vs. $\Delta gacS$	0.0338
WT vs. $\Delta rsmY/Z + lacUV5-rsmY$	0.0985
WT vs. $\Delta rsmY/Z + native promoter-rsmY$	0.9998

Figure 3.2B***clpVI***

0.5% native mucins vs. 0.1% glycans	<0.0001
0.5% native mucins vs. 0.1% monosaccharides	<0.0001

icmFI

0.5% native mucins vs. 0.1% glycans	0.0046
0.5% native mucins vs. 0.1% monosaccharides	0.0496

Figure 3.3C***clpVI***

PA14 vs. PAO1	0.5569
PA14 vs. MSH3	0.7617
PA14 vs. S54485	0.6638
PA14 vs. FDR1	0.9919
PA14 vs. CEC73	0.1835
PA14 vs. CF127	0.0026

PA14 vs. C078C	<0.0001
----------------	---------

icmF1

PA14 vs. PAO1	0.5798
PA14 vs. MSH3	0.8007
PA14 vs. S54485	0.9445
PA14 vs. FDR1	0.4086
PA14 vs. CEC73	0.5408
PA14 vs. CF127	0.0567
PA14 vs. C078C	<0.0001

Figure 3.4A

clpV1

WT vs. Δ <i>gacS</i>	<0.0001
WT vs. Δ <i>retS</i>	<0.0001
WT vs. <i>retS</i> (Δ <i>Dismed2</i>)	<0.0001

icmF1

WT vs. Δ <i>gacS</i>	<0.0001
WT vs. Δ <i>retS</i>	<0.0001
WT vs. <i>retS</i> (Δ <i>Dismed2</i>)	<0.0001

Figure 3.4C

clpV1

WT vs. <i>RetS</i> (T428R)	0.01
WT vs. <i>RetS</i> (D713/715A)	0.0122
WT vs. <i>RetS</i> (D858A)	0.0018

icmF1

WT vs. <i>RetS</i> (T428R)	0.0078
WT vs. <i>RetS</i> (D713/715A)	0.0829
WT vs. <i>RetS</i> (D858A)	0.0078

Figure 3.4D

Strains comparison

WT vs. <i>RetS</i> (Δ <i>Dismed2</i>)	<0.0001
--	---------

WT vs. RetS(D858A)	<0.0001
Figure 3.5F	
<i>clpVI</i>	
0.1% glycans vs. 0.1 M TFA treated glycans	0.3496
0.1% glycans vs. 1 M TFA treated glycans	0.4179
0.1% glycans vs. 1 M TFA, hypercarb	0.2022
<i>icmF1</i>	
0.1% glycans vs. 0.1 M TFA treated glycans	0.3377
0.1% glycans vs. 1 M TFA treated glycans	0.2883
0.1% glycans vs. 1 M TFA, hypercarb	0.2327
Figure 3.6A	
Medium alone - Glycans	
WT	0.0014
$\Delta icmF1$	0.6158
Figure 3.6B	
Strains comparison	
WT vs. $\Delta retS$ (Dismed2)	0.0008
WT vs. RetS(D858A)	0.0129
Figure 3.6C	
Medium alone - Glycans	
WT	0.0007
$\Delta icmF1$	0.7777
Figure 3.6D	
Strains comparison	
WT vs. retS($\Delta Dismed2$)	0.0053
WT vs. RetS(D858A)	0.0098

Table S3.4. Statistical analyses.

Supplementary References

- S1. Goodman, A.L., Kulasekara, B., Rietsch, A., Boyd, D., Smith, R.S., and Lory, S. 2004. A signaling network reciprocally regulates genes associated with acute infection and chronic persistence in *Pseudomonas aeruginosa*. *Dev. Cell.* 7:745–754
- S2. Spencer, D.H., Kas, A., Smith, E.E., Raymond, C.K., Sims, E.H., Hastings, M., Burns, J.L., Kaul, R., and Olson, M. V. 2003. Whole-genome sequence variation among multiple isolates of *Pseudomonas aeruginosa*. *J. Bacteriol.* 185:1316–1325. Available at: <https://pubmed.ncbi.nlm.nih.gov/12562802>.
- S3. Kulasekara, B.R., Kulasekara, H.D., Wolfgang, M.C., Stevens, L., Frank, D.W., and Lory, S. 2006. Acquisition and Evolution of the *exoU* Locus in *Pseudomonas aeruginosa*; *J. Bacteriol.* 188:4037-50. Available at: <http://jb.asm.org/content/188/11/4037.abstract>.
- S4. Silo-Suh, L.A., Suh, S.-J., Ohman, D.E., Wozniak, D.J., and Pridgeon, J.W. 2015. Complete Genome Sequence of *Pseudomonas aeruginosa* Mucoid Strain FRD1, Isolated from a Cystic Fibrosis Patient. *Genome Announc.* 3:e00153-15. Available at: <https://pubmed.ncbi.nlm.nih.gov/25792066>.
- S5. P erault AI, Chandler CE, Rasko DA, Ernst RK, Wolfgang MC, Cotter PA. 2020. Host Adaptation Predisposes *Pseudomonas aeruginosa* to Type VI Secretion System-Mediated Predation by the *Burkholderia cepacia* Complex. *Cell Host Microbe.* 28(4):534-547.e3
- S6. Hoang, T.T., Kutchma, A.J., Becher, A., and Schweizer, H.P. 2000. Integration-proficient plasmids for *Pseudomonas aeruginosa*: Site- specific integration and use for engineering of reporter and expression strains. *Plasmid.* 43:59–72
- S7. Brencic, A., and Lory, S. 2009. Determination of the regulon and identification of novel mRNA targets of *Pseudomonas aeruginosa* RsmA. *Mol. Microbiol.* 72:612–632
- S8. Castang, S., and Dove, S.L. 2012. Basis for the essentiality of H-NS family members in *Pseudomonas aeruginosa*. *J. Bacteriol.* 194:5101–9
- S9. Shanks, R.M.Q., Caiazza, N.C., Hinsa, S.M., Toutain, C.M., and O’Toole, G.A. 2006. *Saccharomyces cerevisiae*-based molecular tool kit for manipulation of genes from gram-negative bacteria. *Appl. Environ. Microbiol.* 72:5027–36
- S10. McFarland, K.A., Dolben, E.L., LeRoux, M., Kambara, T.K., Ramsey, K.M., Kirkpatrick, R.L., Mougous, J.D., Hogan, D.A., and Dove, S.L. 2015. A self-lysis pathway that enhances the virulence of a pathogenic bacterium. *Proc. Natl. Acad. Sci. U. S. A.* 112: 8433–38

Appendix C: Supplementary Information for Chapter 4

Supplementary materials include:

Supplementary Information

Figures S4.1 to S4.4

References

Supplementary Information

Planktonic and biofilm biomass. To monitor the ability of communities to form biofilms on plastic, wells were washed with phosphate-buffered saline to remove loosely adherent cells and then biofilm cells were isolated from the surface by scraping. Total bacterial load in the culture and bacterial load in the biofilm were quantified based on the total DNA content (Allison et al. 2013; Jaysree et al. 2013) via nanodrop.

Quantification of putative mucin-targeting glycoside hydrolases (GH). For each representative bacterial strain corresponding to a dominant genus in the inoculum, a GH profile was obtained from the carbohydrate-active enzyme (CAZy) database (Lombard et al. 2014). The total number of GHs targeting linkages present in mucin were enumerated. The specific GH families of interest were GH2 [β -gal], 18 [β -glcNAc], 20 [β -glcNAc, lacNAc, β -SO₃-glcNAc], 27 [α -galNAc], 29 [α -fuc], 31 [α -galNAc], 33 [neu5Ac], 35 [β -gal], 36 [α -galNAc], 42 [β -gal], 95 [α -fuc], 98 [β -gal], 101 [α -galNAc], 109 [α -galNAc], 112 [lacNAc], and 151 [α -fuc], where the target linkages are indicated in brackets.

Supplementary Figures

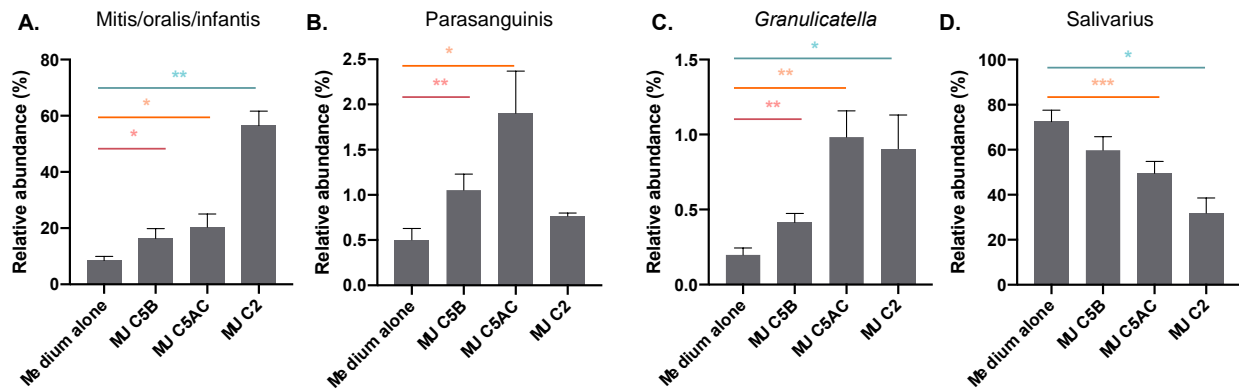


Figure S4.1, related to Figure 4.2. Mucins isolated from saliva (MUC5B), gastric mucus (MUC5AC), or intestinal mucus (MUC2) retained (A) Mitis group streptococci, (B) Parasanguinis streptococci, and (C) *Granulicatella* to different degrees, while restricting the outgrowth of Salivarius streptococci (D) after 48 h. Salivarius data are duplicated from the 48 h time point in **Figure 4.2E**. All experiments were performed using inoculating communities 1 & 2, $n = 4$. Significant differences relative to medium alone were assessed using the repeated measures one-way ANOVA with Dunnett's multiple comparison test, * $p < 0.05$, ** $p < 0.01$. * p -value < 0.05 , ** p -value < 0.01 , *** p -value < 0.001 .

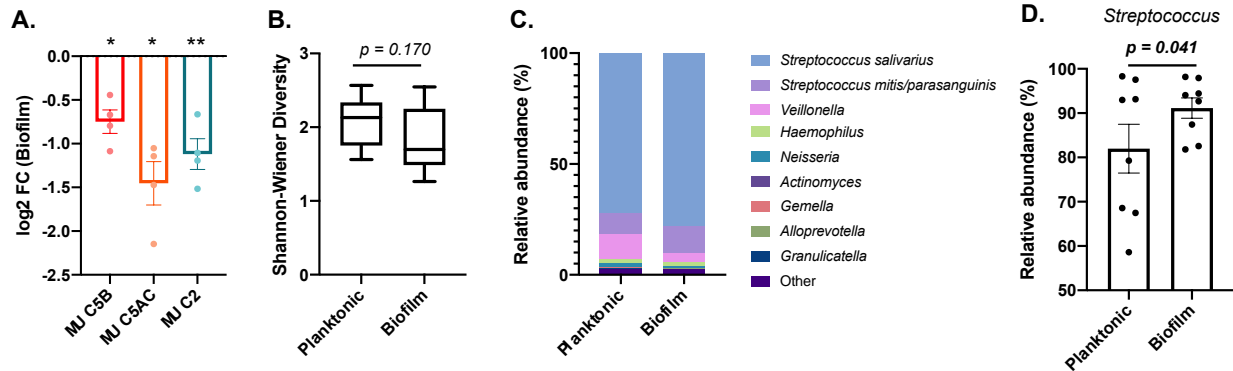


Figure S4.2, related to Figure 4.2. Comparison of the planktonic and biofilm fractions of microbial communities cultured for 48 h in glucose medium. (A) Biofilm formation was reduced at 48 hours following growth in medium with mucins relative to medium alone. Bar length represents the mean change in biofilm formation, each point represents the change for an independent replicate ($n = 4$, inoculating communities 1 and 2), and error bars indicate standard error of the mean (SEM). Significant changes in biofilm formation were identified with one-way, two-sided t-tests, * $p < 0.05$, ** $p < 0.01$. (B) Biofilm and planktonic communities had similar levels of alpha diversity. The center line indicates the median, the box limits indicate the upper and lower quartiles and the whiskers indicate the minimum and maximum values. Significance was assessed using a two-sided t-test. Planktonic community diversity is duplicated from **Figure 4.1C** (48 h) for comparison to the biofilm community. (C) The biofilm and planktonic fractions had similar microbial compositions. (D) Biofilm communities were significantly enriched in *Streptococcus*. Bar length represents the mean *Streptococcus* abundance, and each point represents the abundance for an independent replicate. Significance was assessed using a two-sided t-test. (B-D) Experiments were performed using inoculating communities 1 – 4, $n = 8$, time = 48 h.

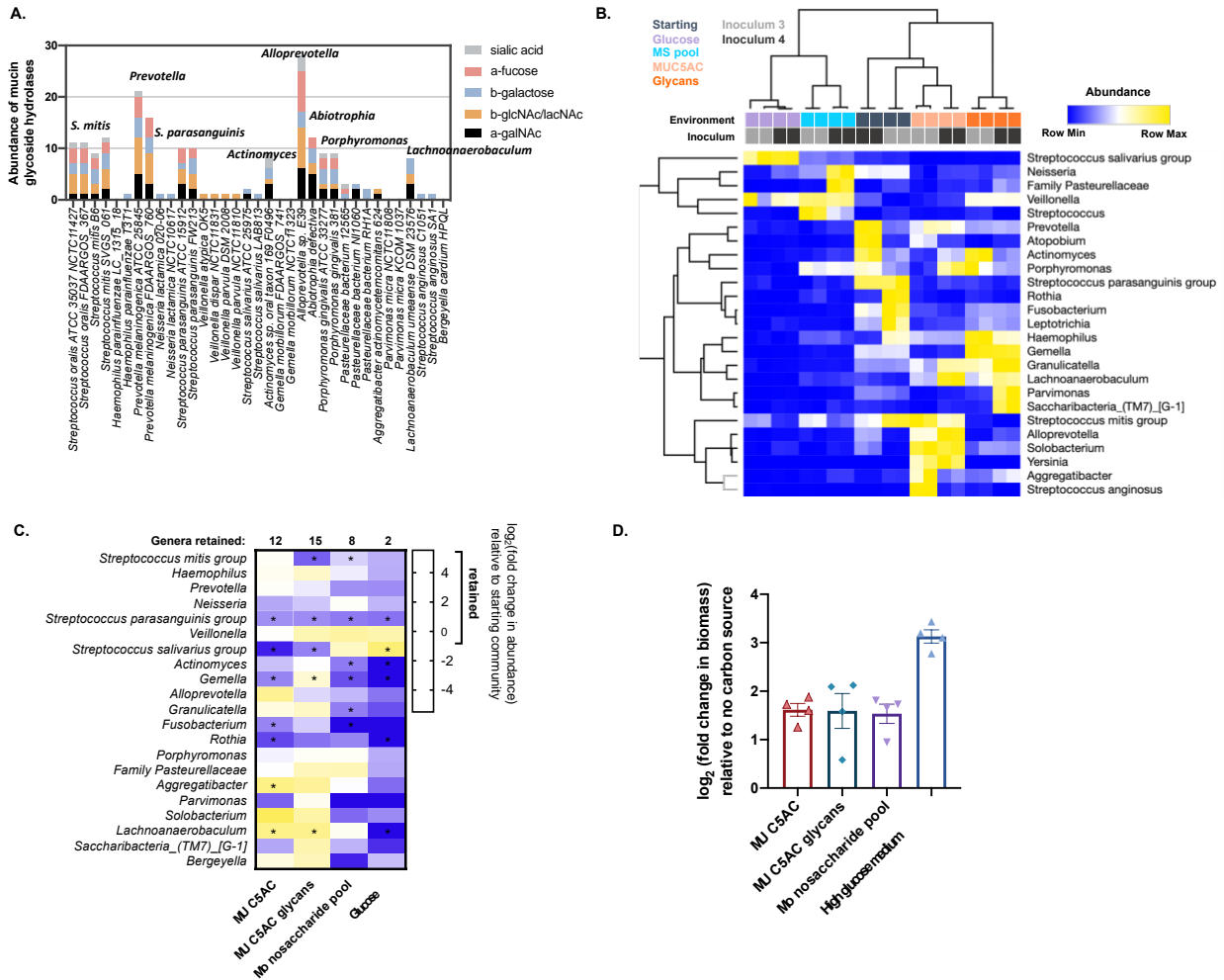


Figure S4.3, related to Figure 4.4. Mucin glycan can serve as the sole carbon source to promote the culturability of microbial communities containing putative glycan-degraders. (A) Abundance of putative mucin-targeting glycoside hydrolases in representative oral bacteria. **(B)** Microbial communities clustered according to sole carbon source (48 h). Heatmap shows the relative abundance of microbial taxa present at >1.5% abundance, and the color key is indicated in the upper right corner. Dendrograms represent average linkage clustering (1-Pearson distance metric) of **(top)** *ex vivo* communities based on the microbial composition and **(left)** taxa based on their abundance profiles across samples. **(C)** Heatmap of log₂-transformed fold change in abundance of dominant genera following 48 hours growth in medium with 0.25% mucin, 0.25% mucin glycans, 0.25% mucin monosaccharides, or 0.5% glucose as a sole carbon source relative to the starting community (n = 4). Significant changes in abundance were identified with one-way, two-sided t-tests. Significance threshold was adjusted with Bonferroni correction for multiple comparisons * p < 0.0024. **(D)** Log₂-transformed fold change in biomass after 48 hours following growth in medium with 0.25% mucin, 0.25% mucin glycans, 0.25% mucin monosaccharides, or 0.5% glucose as a sole carbon source relative to medium without a carbon source. Each dot represents an independent replicate. Experiments in **Figure S4.3** were performed using inoculating communities 3 & 4.

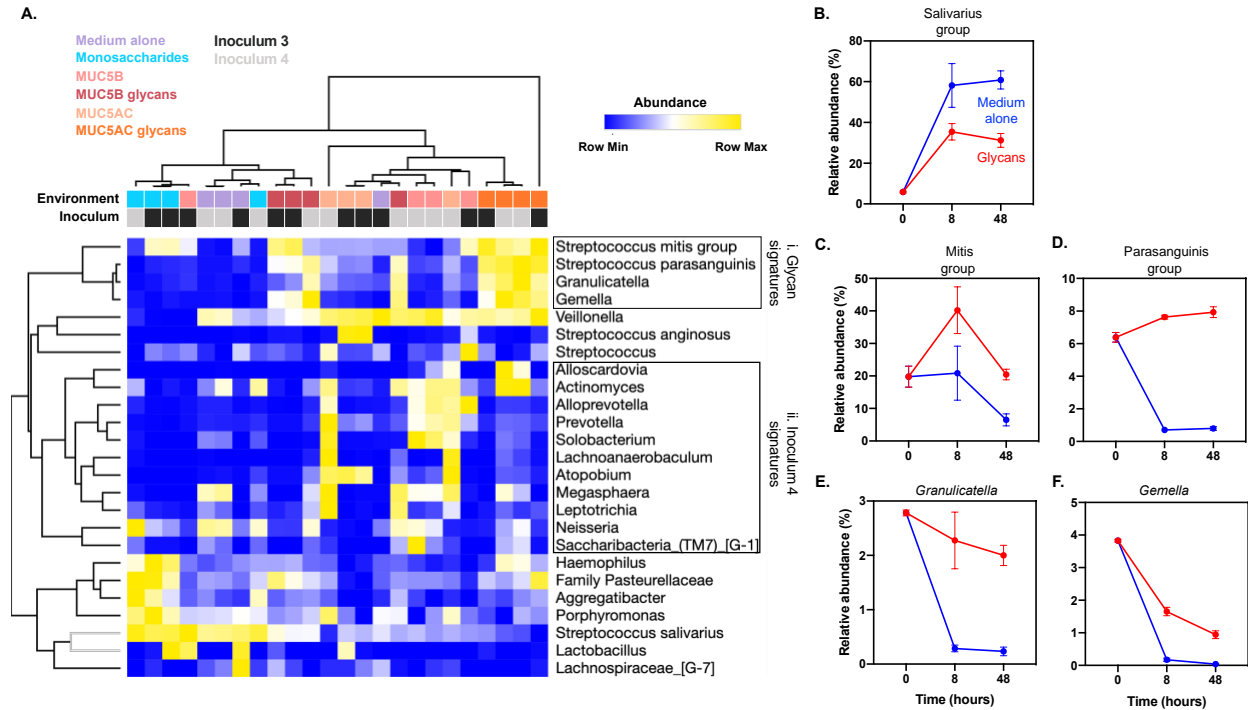


Figure S4.4, related to Figure 4.5. Mucin glycans promote the prolonged coexistence of multiple genera.

(A) Microbial communities clustered according to the environments in which they were cultured (48 h). Heatmap shows the relative abundance of microbial taxa present at >0.1% abundance, and the color key is indicated in the upper right corner. Dendrograms represent average linkage clustering (1-Pearson distance metric) of (top) *ex vivo* communities based on the microbial composition and (left) taxa based on their abundance profiles across samples. (i,ii) Groups of microbes that cooccur within communities cultured in a particular environment or within communities derived from the same microbiota. (i) Taxa with a relatively high abundance in mucin glycans. (ii) Taxa with a relatively high abundance in inoculum 4 compared to inoculum 3. (B-F) Change in abundance over time in medium alone or medium with glycans (n = 4) for Salivarius streptococci (B), Mitis streptococci (C), Parasanguinis streptococci (D), *Granulicatella* (E), and *Gemella* (F). All experiments in Figure S4.4 were performed using inoculating communities 3 & 4.

Supplementary References

- Allison SD, Lu Y, Weihe C, Goulden ML, Martiny AC, et al. 2013. Microbial abundance and composition influence litter decomposition response to environmental change. *Ecology*. 96(1):154-63
- Jaysree RC, Das A, Priya I, Shivani, Rajam C, Rajendran N. 2013. Quantification of bacterial biomass by DNA analysis. *J. Chem. Pharm. Res.* 5(10):332-6
- Lombard V, Golaconda Ramulu H, Drula E, Coutinho PM, Henrissat B. 2014. The carbohydrate-active enzymes database (CAZy) in 2013. *Nucleic Acids Res.* 42(Database issue):D490–5